AN EXPERIMENTAL DEMONSTRATION OF CONVERTING ORGANIC LIQUIDS AND THEIR AQUEOUS SOLUTIONS IN A FILM BOILING REACTOR

by John William Evangelista

AN EXPERIMENTAL DEMONSTRATION OF CONVERTING ORGANIC LIQUIDS AND THEIR AQUEOUS SOLUTIONS IN A FILM BOILING REACTOR

A Thesis

Presented to the Faculty of the Graduate School

of Cornell University

In Partial Fulfillment of the Requirements for the Degree of

Master of Science

by

John William Evangelista

August 2010

ABSTRACT

This thesis presents an experimental demonstration of a chemical reactor design based on film boiling using aqueous mixtures of ethylene glycol. Termed a Film Boiling Reactor (FIBOR), the reactor volume is established around a horizontal heater tube (Nickel Alloy-Inconel 600) that is immersed in the aqueous bulk liquid. Chemical reactions are promoted within the vapor layer due to large temperature gradients inherent to film boiling. Product gas flow rates and chemical composition are analyzed to assess the extent that the FIBOR can promote chemical change of the reactant liquid mixture.

Catalytic reaction and thermal decomposition (pyrolysis) in the FIBOR are investigated by using a catalyst coated tube and a bare tube respectively. The heater tube surface temperature is the central operating parameter. Pure ethylene glycol is examined and compared to previously reported results to assess the role of the heater diameter. This work extends the FIBOR concept to aqueous mixtures of ethylene glycol to explore if the FIBOR is capable of promoting steam reforming chemistry.

The results show that the FIBOR has the potential to support both catalytic and thermal decomposition of aqueous ethylene glycol mixtures. Diluting ethylene glycol with water decreases the reaction of ethylene glycol but it also reduces the effects of carbon deposition or "coking." Peak product yields for thermal decomposition of pure ethylene glycol and aqueous mixtures of 90% (vol) and 80% (vol) ethylene glycol reached 4.5, 1.8 and 0.8 LPM/min·m^2 respectively at an operating temperature of 1475K. Results for platinum and nickel based coatings converting an 80% (vol) ethylene glycol aqueous mixture achieved product yields approximately 3-4 times higher than the case for a bare tube, however platinum showed slightly better overall performance with respect to product yields and resistance to deactivation.

Thermochemical and gas chromatography analysis revealed the FIBOR's capability to convert organic aqueous mixtures through steam reforming. An upward shift in the boiling curve for the catalyst coated tubes was determined to be due to the endothermic nature of the chemical mechanism. Conversion of aqueous mixtures with a bare tube produced synthesis gas (syngas) with a lower ratio of H_2:CO (1:1) compared to catalytic conversion which resulted in a significant enrichment of syngas products with hydrogen (H_2:CO=3). This difference is attributed to the FIBOR's ability to promote steam reforming of ethylene glycol.

BIOGRAPHICAL SKETCH

The author was born on December 24, 1978 to John and Celeste Evangelista in Geneva, NY. After graduating from Geneva High School in 1997, he attended the United States Military Academy at West Point where he studied Mechanical Engineering. He graduated from West Point in 2001 and was commissioned as a Second Lieutenant in the United States Army Corps of Engineers.

Following graduation from West Point, the author served in numerous military assignments and positions to include the 101st Airborne Division as a Combat Sapper Platoon Leader in support of Operation IRAQI FREEDOM, Company Executive Officer, Battalion Staff Officer and Company Commander. While receiving advanced military engineering training, the author continued to pursue his passion for academia through earning a Master of Science in Engineering Management at the Missouri University of Science and Technology in 2005. Shortly after, the author was selected as a junior faculty member candidate for the Department of Civil and Mechanical Engineering at West Point and given the opportunity to pursue a fully funded advanced technical degree from Cornell University. Following graduation from Cornell, the author will serve as a Mechanical Engineering Instructor at West Point. The author currently holds the rank of Major and has received numerous military awards and decorations to include the Bronze Star Medal for meritorious service in combat.

The author married the former Alison Sheahan of Endicott, NY on June 11, 2005.

ACKNOWLEDGMENTS

This work holds the name of only one author, yet reflects the impact and assistance of many. I am truly humbled to be in the position that I am and to have had the opportunity to study at such a revered institution as Cornell.

First and foremost, I would like to thank my Professor, C. Thomas Avedisian for the opportunity to study under his tutelage. Professor Avedisian will always be remembered as the one who taught me how to conduct scholarly work. It has been a tremendous experience that I will undoubtedly build upon in the future and one that I will never forget. I would also like to thank my special committee member, Professor Brian Kirby for reaching out to me and going above and beyond in terms of offering help and advice. His impressive intellect and perspectives on my work have been a tremendous help.

I would like to acknowledge the Army as well as the Cornell Graduate School for the financial support to pursue fully funded studies here at Cornell. Additionally, I would not have had this opportunity if it wasn't for the guidance and support of my various supervisors and leaders that I have encountered throughout my career in the Army.

This research has been made possible by the funding under the National Science Foundation (NSF) (#CTS-05-00015; CTS-09-02549). It has truly been an amazing experience to conduct research in an environment with the resources made available through NSF.

Several individuals provided me with technical advice and expertise that made this research possible. My thanks go to Dr. William Retallick who provided advanced catalyst coating techniques, Mr. Tim Brock for advice and machining expertise related to the electrode clamp design, Mr. John Hunt of the Cornell Center for Materials

Research (CCMR) for assistance with SEM images and Dr. Xia Zeng of the Cornell Department of Food Science for assistance with GC-MS analysis for determining liquid reactant concentration. I would also like to thank Dr. Wing Tsang of the National Institute of Science and Technology (NIST). It has been a privilege to collaborate with such a distinguished scientist. Dr. Tsang's help, particularly with understanding the chemical kinetics of the FIBOR has been extremely helpful.

A colleague and friend I would like to recognize is Frank Liu. I learned that it is always an advantage to have extremely kind and smart people around you in graduate school willing to offer advice and help. Frank always provided both-thank you.

Much of my work extends upon the original ideas and work of Sung Ryel Choi. Sung also provided daily assistance, answered my seemingly never-ending questions and after two years, taught me how to conduct experimental research. Perhaps what I will always cherish, miss and value most however is our friendship.

Having the opportunity to spend time close to home is often a rarity in the military. This time has been special as it has brought me closer to my parents in Geneva, NY. Any accomplishment I take credit for is a direct reflection upon the fortune of being raised at 423 William St. Those special years that embodied love, discipline, nurture, passion, encouragement, support, integrity, knowing when to have fun, and knowing when to "make believe your life depends on it" has made me into the person I am today and I can only hope that I may pass it all on someday-thank you.

The final acknowledgement is for the one closest to my heart and who I dedicate everything it is that I do-my wife, Ally. We welcomed this time at graduate school as a respite from the grind of military life. These years however have brought unique challenges that we have both endured, ultimately bringing us closer. I want to thank Ally for her patience and understanding-for the times I was physically absent

and also for the times I was present, but mentally absent. I can't imagine what life would be like without her and can't wait to start our next chapter, along with many others.

TABLE OF CONTENTS

LIST OF FIGURES

LIST OF TABLES

LIST OF ABBREVIATIONS

APR	Aqueous Phase Reforming
CHF	Critical Heat Flux
CV	Control Volume
DAQ	Data Acquisition
EG	Ethylene Glycol
EBS	Electron Backscatter
EDS	Energy Dispersion X-Raw Spectroscopy
EROEI	Energy Return on Energy Invested
FIBOR	Film Boiling Reactor
GC	Gas Chromatography
GC-MS	Gas Chromatograph Mass Spectrometer
ID	Inside Diameter
LPM	Liter Per Minute
NEB	Net Energy Balance
NEG	Net Energy Gain
NIST	National Institute of Standards and Technology
OD	Outside Diameter
SEM	Scanning Electron Microscope
TC	Thermocouple
TCD	Thermal Conductivity Detector

LIST OF SYMBOLS

A_c	Cross Section Area
A_1	Pre-Exponential Factor, Reaction Rate Equation
$A_{s,c}$	Condenser Surface Area
$A_{s,f}$	FIBOR Heater Tube Surface Area
$c_{p,l}$	Specific Heat at Constant Pressure, Liquid Phase
d	Condenser Diameter
d_i	Inconel Heater Tube Outside Diameter
d_c	Ceramic Tube Outside Diameter
d_a	Air Space Within Heater Tube Assembly Outside Diameter
E_a	Activation Energy
F	Actual Volumetric Flow Rate
g	Acceleration Due to Gravity
$\bar{h}$	Average Heat Transfer Coefficient
h_{fg}	Latent Heat of Vaporization
I	Current
Ja	Jakob Number
k	Thermal Conductivity; Rate of Chemical Reaction
k_l	Thermal Conductivity, Liquid Phase
L	Condenser Length; Axial Heater Length
$\dot{m}$	Mass Flow Rate
N	Moles
$\dot{N}$	Molar Flow Rate
P	Power
Pr	Prandtl Number

q	Heat Transfer Rate, Power
q”	Heat Flux
$\dot{q}$	Volumetric Heat Generation
r	Heater Tube Radius
R	Heater Radius
R_g	Gas Constant
R_e	Electrical Resistance
Re	Reynolds Number
t	Time
T	Temperature
T_w	Wall Temperature
T_i	Liquid/Vapor Interface Temperature
T_s	Surface Temperature, Condenser
T_{sat}	Saturation Temperature
T_∞	Temperature of Bulk Liquid
T(1-4)	Temperature Read Acquired by Thermocouple #1-#4
V	Voltage
$\dot{V}$	Volumetric Flow Rate
w	Mass Fraction of Less Volatile Component
w_i	Liquid Mass Fraction and Liquid/Vapor Interface
w_v	Vapor Mass Fraction
w_∞	Mass Fraction of Bulk Liquid
x	Power Reference Point for Data Organization
X	Mole Fraction
y	Temperature Reference Point for Data Organization

Greek Symbols

ϕ	Heater Geometry Angular Coordinate
δ	Vapor Film Thickness
ρ	Electrical Resistivity
μ_l	Viscosity, Liquid Phase
ν_l	Kinematic Viscosity, Liquid Phase
ν	Stoichiometric Coefficient
Δh°	Heat of Chemical Reaction

CHAPTER 1

INTRODUCTION

1.1 Film Boiling Background and Theory

This research is motivated by the potential of a film boiling process to convert heavy organics into useful products. This could apply to the growing need to develop alternative techniques to extract sources of energy from materials otherwise considered to be waste. For example the bio-fuels industry produces several "heavy" byproducts, one in particular being glycerol ($C_3H_5(OH)_3$). In fact, if just 2% of the nation's diesel were converted to bio-diesel, an additional 325,000 tons of crude glycerol would be produced annually. Since the annual demand for glycerol averages a steady 350,000 tons, many researchers believe a "glut" of glycerol could quickly develop. (Biodiesel Magazine, Aug/Sep 2005) Finding a new method to process such byproducts could possibly add energy efficiency to the biofuels industry and even decrease the nation's dependence on fossil fuels.

Most practical engineering applications that involve either boiling or condensation are motivated by the large rates of heat transfer associated with the latent heat effects of phase change, along with the turbulent mixing action of the bubbles produced. Common applications include power and refrigeration cycles. Boiling, however, has rarely been considered as a mode to promote chemical change of a liquid.

The aim of this study is to explore experimentally the extent that film boiling can support chemical change of an organic aqueous mixture. Ethylene glycol ($C_2H_4(OH)_2$) and water (H_2O) is chosen as the model organic reactant mixture to be examined in order to build upon previous research of converting pure ethylene glycol (Choi 2010) and because the decomposition of other heavier, related organics may not

be that different (e.g. propylene glycol-$C_3H_6(OH)_2$, glycerol- $C_3H_5(OH)_3$). It is also expected that the thermophysical properties of ethylene glycol aqueous mixtures (boiling point, vapor-liquid equilibrium, viscosity) provides for a reasonable operating range compared to challenges posed by other heavier organics (e.g. aforementioned glycerol). In order to investigate a possible operating domain in which boiling can support chemical change, examining the different regimes of boiling serves as the starting point of analysis.

1.1.1 Boiling Regimes and the Boiling Curve

The boiling curve (Figure 1.1) shows the dependency of the heated surface wall temperature, T_w (abscissa) to the respective heat flux, q" applied (ordinate). Boiling curves are typically derived empirically often from laboratory scale experiments. While generalized boiling curve correlations do exist, their reliability is limited to select geometries and often result in significant sources of error up to approximately 20%. (Lienhard 2008)

Point A in Figure 1.1 depicts the wall temperature at which nucleate boiling starts. For the case of water, a wall temperature of typically 5-10 degrees above the liquid's saturation point is usually suitable to initiate nucleate boiling (Incropera et al. 2007). Within this region, liquid is in direct contact with the heater surface where vapor bubbles are formed inside tiny crevices, or nucleation sites. The nucleate boiling regime is bounded to the right by point B, the Critical Heat Flux (CHF). Estimating the CHF is important for many applications and has been the subject of many studies. (Dhir et al. 1974; Katto 1994) Operating as close as possible to the CHF is often desired to exploit maximum rates of heat transfer. However exceeding this point can lead to a rapid transition to the film boiling regime (dotted line) resulting in extremely high surface temperatures and possibly a meltdown scenario.

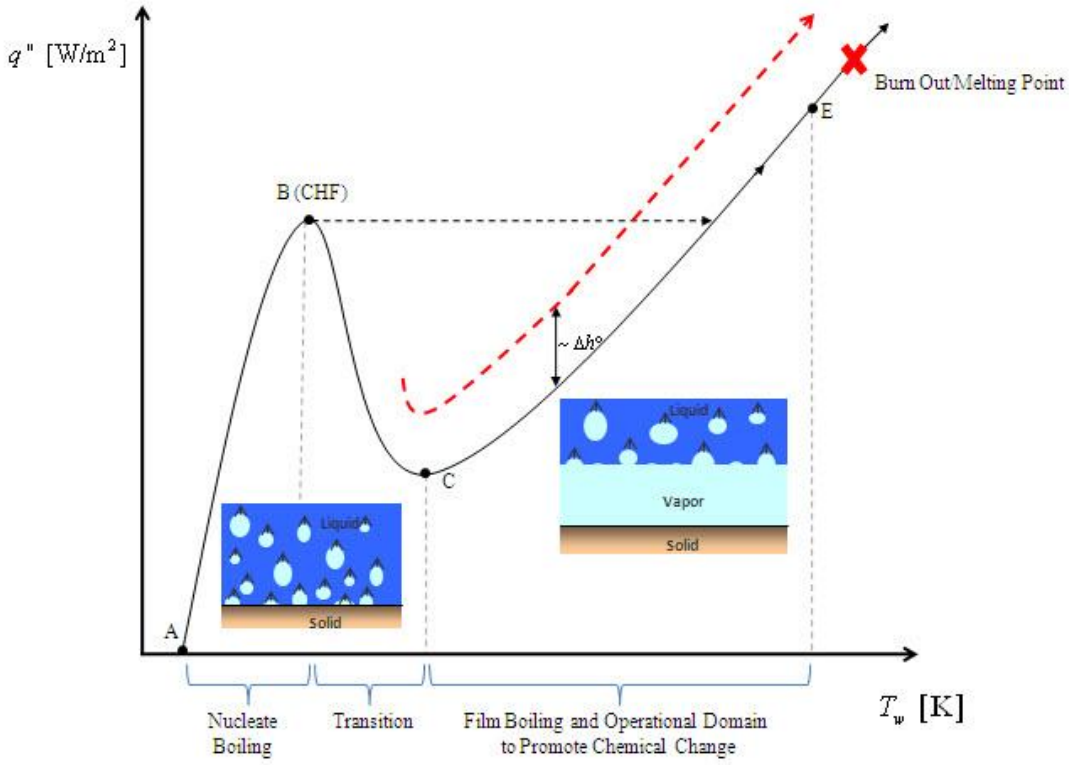

Figure 1.1: Boiling Curve

The section of the boiling curve between points B and C is termed the "transition regime." Transition between nucleate and film boiling, however, does not follow the idealized smooth trend shown in Figure 1.1. Experimental results show that the actual transition between points B and C is unstable and highly non-linear until a vapor film blankets the heater surface and stable film boiling ensues. (Bromley 1950) Traversing the boiling curve by starting in the nucleate boiling regime and raising the heat input to transition with a flux-controlled variation to the film boiling regime is very difficult. For certain liquids and boiling surfaces, controlling the transition zone is also extremely difficult. A temperature controlled heating process provides greater control of the transition zone heater surface temperature above point C and "quenching" it into the liquid is a more experimentally proven technique to safely operate in the transition and film boiling regime. (Ede and Siviour 1975)

Point C is known as the minimum film boiling or "Leidenfrost" point. (Incropera 2007) This point serves as the lower limit for film boiling. The surface melting temperature (point D) serves as the upper limit. Within this regime, a thin vapor film blankets the heater surface (e.g. see inset of Figure 1.1 for a flat plate and Figure 1.3 for a horizontal tube). The liquid is never in direct contact with the heater surface. Liquid vaporizes at the vapor/liquid interface and is further expelled from the liquid in the form of bubbles under the action of buoyancy. It is within this realm that chemical change is possible. The vapor film forms the "reactor" volume and is termed a Film Boiling Reactor (FIBOR). (Urban et al. 2006)

The physics that govern film boiling and the transport phenomena within the vapor film suggests a potential for supporting chemical change through using the bulk liquid as a reactant. Some of the essential features include: 1) The vapor layer forms automatically as a result of the governing physics of film boiling which results in a "self-forming" reactor; 2) the natural transport of vapors prevents the need for any

pumping or pressurization when carried out in a gravitational field (i.e. Earth's normal gravity); 3) high temperature gradients, along with the absence of air within the thin vapor film that separates the heater wall from the relatively cool bulk liquid can promote thermal decomposition (pyrolysis) within the vapor layer; and 4) catalytic reaction is possible when coating the heater surface with a suitable catalyst. This latter process will promote reaction at lower temperatures than thermal decomposition.

Comparing boiling curves with and without chemical reaction provides insight into the overall heat needed to support chemical reaction, or the "heat of reaction." This effect is depicted in Figure 1.1 which shows the red dashed curve (chemical reaction) shifted above the black curve (no chemical reaction). The upward shift reveals the presence of an endothermic chemical mechanism and for decomposition of simple organics (e.g. methanol-CH_3OH) the actual space between the curves is approximately equal to the heat of reaction. (Okuyama and Iida 1994; Choi 2010)

` *1.1.2 Film Boiling of Binary Mixtures and Vapor Liquid Equilibrium*

Considering liquid mixtures adds complexity to the film boiling process due to several factors. Mass diffusion effects and the role of vapor-liquid equilibrium are two central factors that influence the physics of boiling mixtures. (Liu 1996) Preferential vaporization is another consideration that will enrich the vapor with the volatile species. At the same time, the non-volatile species (here being ethylene glycol) is the reactant species so that there could be a liquid concentration threshold for the volatile species above which reaction will not occur. These aspects are investigated here.

An important, yet subtle assumption of this study is that the concentration of reactants (ethylene glycol and water) within the FIBOR is in vapor-liquid equilibrium (VLE). This means that the rate of vaporization is equal to the rate of condensation

causing no net change in conversion from liquid to vapor. For a binary mixture (here being ethylene glycol and water), each component's vapor concentration is directly related to its vapor pressure which also depends on the corresponding liquid component concentration and temperature. Such VLE concentration data can be determined experimentally and is available for many different mixtures. (Othmer 1943) Assuming VLE serves as an engineering approximation used for this study in terms of estimating amounts of vaporized ethylene glycol (reactant) and water in relation to the liquid composition.

Figure 1.2 is a VLE plot for an ethylene glycol aqueous mixture (by volume) compiled from published experimental data (MEGlobal 2008). Vapor-liquid equilibrium plots are useful because one can determine both the boiling temperature and vapor composition for a given liquid composition. The gray dotted line in Figure 1.2 depicts how data from a typical VLE plot is interpreted. Starting at a given liquid mixture composition, the boiling point of the mixture is found by drawing a vertical line until it intersects with the lower curve, or bubble point curve. The corresponding composition of the vapor is determined by drawing a horizontal line along the bubble point temperature until it intersects with the dew point curve. The abscissa value gives the composition of the vapor. For example an 85% ethylene glycol-water (by volume) liquid solution has a boiling temperature of approximately 405K and the equilibrium vapor composition is approximately 20% (by volume) ethylene glycol. Hence, the vapor is substantially enriched by water compared to the liquid. This further demonstrates that a liquid threshold concentration of the volatile species (water) likely exists above which reaction is not possible.

Figure 1.3 is an idealized physical schematic model for film boiling a binary mixture. A more in-depth analysis of the physics of film boiling mixtures can be found in the literature (Liu 1997). Far from the vapor-liquid interface, the bulk liquid

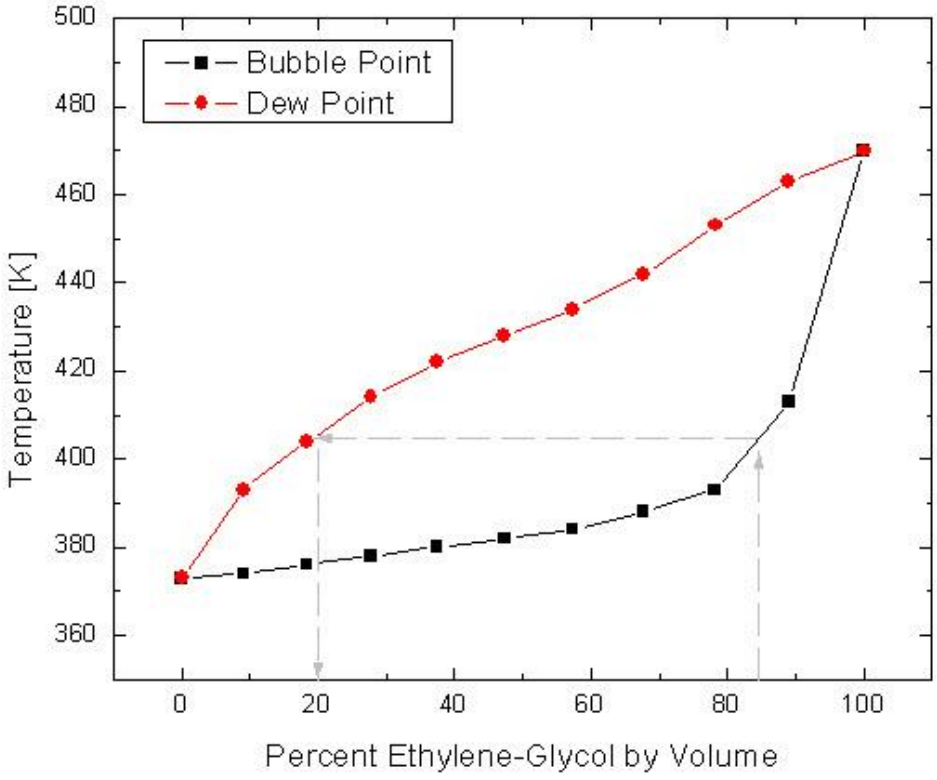

Figure 1.2: Ethylene Glycol/Water Vapor Liquid Equilibrium (MEGlobal, 2008)

contains a mass fraction (w_∞) of the more volatile component. The mixture is also at the saturation temperature (T_∞) according to VLE (Figure 1.2). Due to preferential evaporation and diffusion, the mass fraction (w_i) and temperature (T_i) at the vapor-liquid interface are not equal to that of the bulk liquid. The more volatile component will evaporate first, thus lowering its mass fraction at the vapor-liquid interface ($w_i<w_\infty$). The depletion of the volatile component at the vapor-liquid interface will raise the saturation temperature there ($T_i>T_\infty$). The temperature gradient in the liquid at the vapor-liquid interface can cause conduction heat losses into the bulk. An increase in wall superheat can raise the vapor-liquid interface temperature and assuming vapor-liquid equilibrium, the mass fraction of the volatile component (water) decreases. The relative volatility of the mixture will impact the vapor-liquid interface temperature and composition due to diffusion effects. Additional analysis and supporting literature for film boiling mixtures can be found in Section 1.2.1.

1.1.3 Physics of a Film Boiling Reactor (FIBOR)

Figure 1.4 illustrates the processes involved for a cylindrical FIBOR. An outline will be given here for general operation. More details can be found in Urban et al. (2006). The chemical reactor occupies the physical space created by the vapor film around the heater. It is within this volume that chemical change is possible. Reactants vaporize ($\dot{N}_{R,in}$) at the vapor-liquid interface and are transported around the heater tube under the action of buoyancy. When exposed to high enough heater surface temperatures, reactants turn to products ($\dot{N}_{P,out}$). If the heater is coated with a suitable catalyst, reactants will convert at the surface by catalytic (heterogeneous) reaction. Joule heating provides the heat necessary to support the vaporization and establishment of a vapor film with thickness, $\delta(\phi)$ in Figure 1.4. If the surrounding

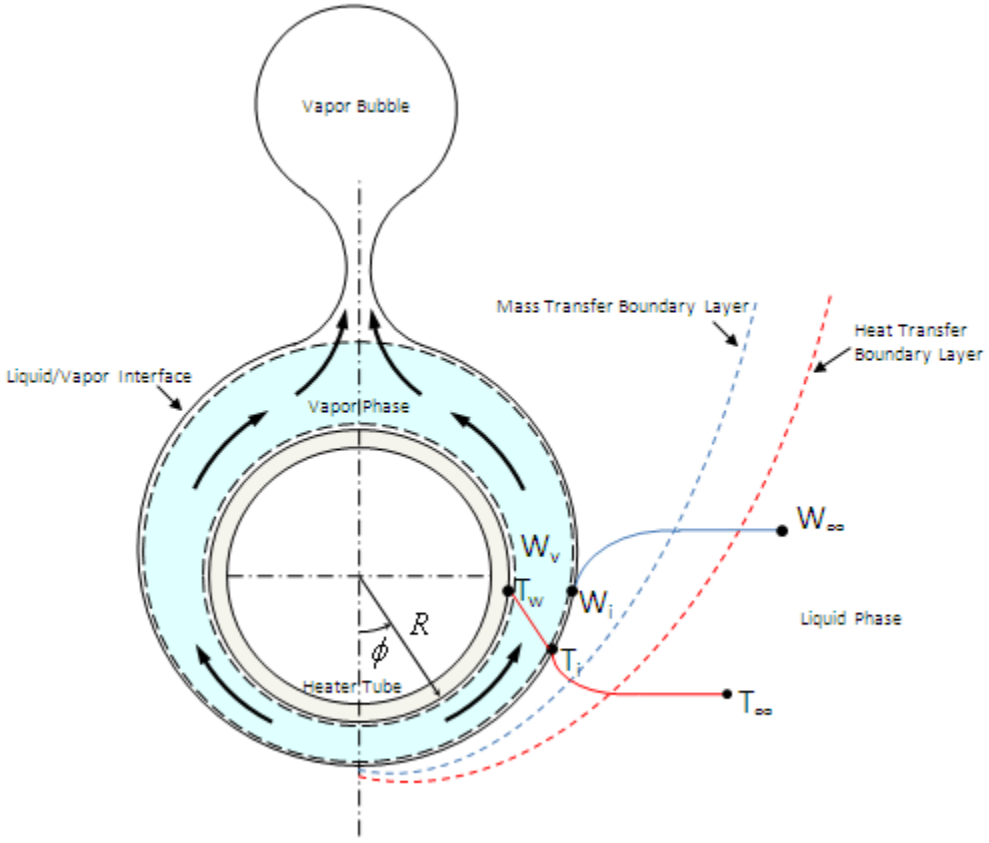

Figure 1.3: Mixture Film Boiling Physical Model

bulk liquid temperature is below its saturation point, heat losses ($\dot{Q}_{sub}$) to the bulk can destabilize film boiling. The inset of Figure 1.4 provides even additional detail of the transport paths within the vapor film (for a catalyst coated heater). The inflow of reactants is created by vaporization at the vapor-liquid interface (a). Some of the reactant diffuses all the way to the surface and reacts (b), while the rest flows around the tube (c). A buoyancy induced vapor flow (e) consists of both product species (d) and non-converted reactant vapors (c). The vapor flows in a radial direction around the heater and accumulates at the top of the tube where bubbles are formed. Bubbles carry away both product species and un-converted reactant vapors where they are eventually expelled at the surface of the bulk liquid.

1.1.4 Chemistry

An understanding of the relevant chemical reactions that can occur within the FIBOR is critical to examining its overall ability to promote chemical change. In addition to analysis of product species through gas chromatography, the FIBOR's effectiveness can also be assessed by comparing boiling curves with and without catalytic reaction. The difference in these curves provides an estimate for the chemical mechanism's overall heat of reaction. As a result, it is important to identify both the primary and anticipated secondary chemical reactions and their heats of reaction. Pure ethylene glycol thermally decomposes according to the primary reaction (Yaws 2003), (heat of reaction is in parentheses)

$$C_2H_4(OH)_2 \rightarrow 2CO + 3H_2 \quad (\Delta h^\circ = 173 \text{ kJ/mol}) \qquad 1.1$$

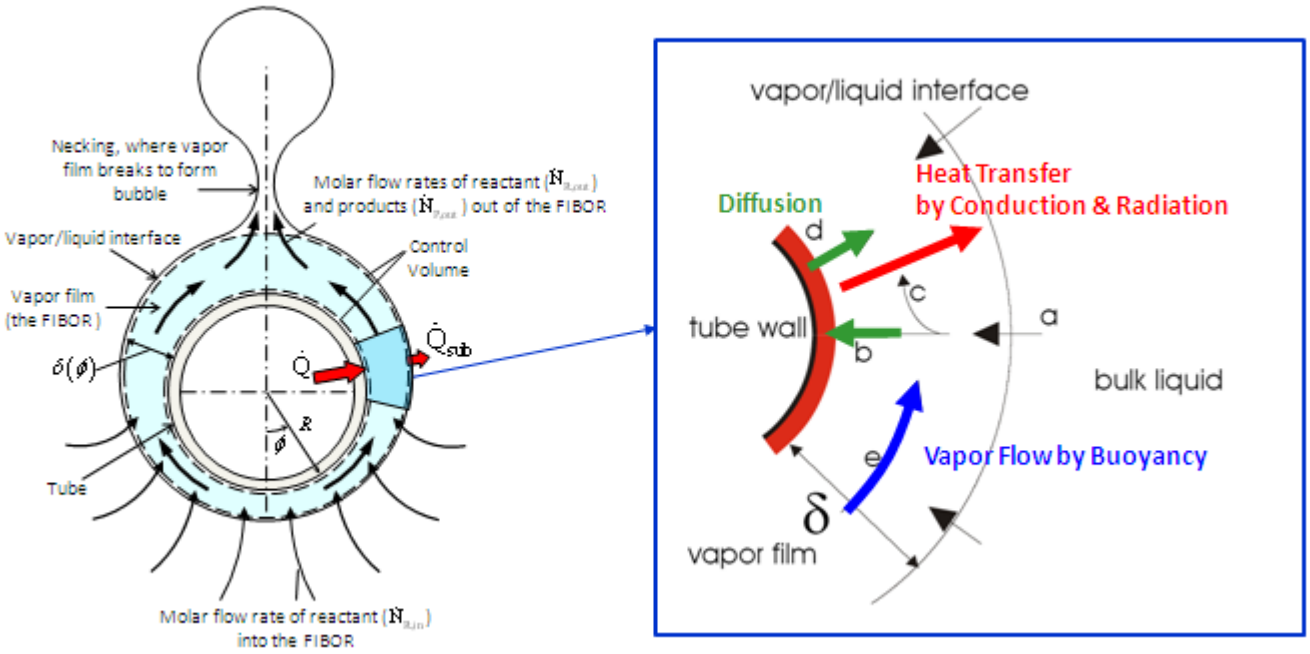

Figure 1.4: Physics of a Film Boiling Reactor (cylindrical heater)

Steam reforming ethylene glycol follows the primary reaction (Hu 2009),

$$C_2H_4(OH)_2 + 2H_2O \rightarrow 2CO_2 + 5H_2 \quad (\Delta h° = 86 \text{ kJ/mol}) \qquad 1.2$$

Important secondary reactions include the water-gas shift reaction (Hu 2009),

$$CO_2 + H_2 \rightarrow CO + H_2O \quad (\Delta h° = 41 \text{ kJ/mol}) \qquad 1.3$$

and the methanation reaction,

$$CO + 3H_2 \rightarrow CH_4 + H_2O \quad (\Delta h° = -206 \text{ kJ/mol}) \qquad 1.4$$

Reactions 1.3 and 1.4 play critical roles, particularly in the formation (or elimination) of carbon monoxide and methane depending on the operating conditions since their directions are sensitive to temperature.

Carbon deposits or “coke” can also form during operation of the FIBOR, which can be detrimental to catalyst performance. The following reactions are possible pathways for coke formation that can accumulate on the catalyst surface (Hu 2009),

$$2CO \rightarrow C + CO_2 \quad (\Delta h° = -172.4 \text{ kJ/mol}) \qquad 1.5$$

$$CH_4 \rightarrow C + 2H_2 \quad (\Delta h° = -74.9 \text{ kJ/mol}) \qquad 1.6$$

$$CO + H_2 \rightarrow C + H_2O \quad (\Delta h° = -131.3 \text{ kJ/mol}) \qquad 1.7$$

$$CO_2 + 2H_2 \rightarrow C + 2H_2O \quad (\Delta h° = -90.1 \text{ kJ/mol}) \qquad 1.8$$

Carbon can also be eliminated with the presence of steam according to,

$$C + H_2O \rightarrow CO + H_2 \ (\Delta h° = 131.3 \text{ kJ/mol}) \quad 1.9$$

or the presence of carbon dioxide,

$$C + CO_2 \rightarrow 2CO \ (\Delta h° = 172.4 \text{ kJ/mol}) \quad 1.10$$

The last secondary reaction includes dehydration of ethylene glycol (Shabaker 2003),

$$C_2H_6O_2 + H_2 \rightarrow C_2H_5OH + H_2O \quad 1.11$$

which through reaction of hydrogen product with un-reacted ethylene glycol can create ethanol and water. The formation of ethanol formed by Equation 1.1 can contaminate the bulk liquid because it is soluble with ethylene glycol and water. Over time, a mixture with changing concentration will form that in turn can affect the bulk liquid temperature. This effect is described in Section 5.1.2.

The above reactions are not all inclusive and the actual chemical reactions for the FIBOR are likely more complicated with even more pathways for generation of product species. For example steam reforming studies of ethylene glycol from both Kechagiopoulos (2007) and Hu (2009) found that for certain operating conditions, traces of other product species such as acetylene (C_2H_2), ethylene (C_2H_4) and ethane (C_2H_6) can be formed. Indeed, we find such species reported in our work reported in this thesis. The intent of this study however is to estimate the extent that the primary reactions occur with given operating parameters (bulk concentration and heater wall

temperature), while evidence for secondary reactions is reported. A rigorous treatment of the FIBOR's chemical mechanism is beyond the scope of this study.

Coating the heater's surface with a suitable heterogeneous catalyst lowers the activation energy by increasing the effective surface area for chemical reactions to take place, thereby increasing the rate of chemical reaction. The rate of chemical reaction typically has an exponential dependence on temperature evidenced by the common Arrhenius form. (Turns 2000)

$$k = A_1 e^{\frac{-E_a}{R_g T}} \qquad 1.12$$

By selecting a suitable catalyst, higher product flow rates can be promoted at lower temperatures. Therefore the efficacy of the FIBOR is then determined in part by catalyst selection and fabrication. The challenge is to find an appropriate catalyst capable of enduring the FIBOR's operating conditions, namely the high heater surface temperatures as well as resisting other deactivation mechanisms. Catalyst performance may degrade during operation due to fusion of the catalyst crystal structure at high temperatures, otherwise known as sintering (Fogler 2006). The catalyst surface can also become fouled with carbon deposits through the chemistry of Equations 1.5 through 1.8, known as coking (Hu 2009). Lastly, the catalyst surface can detach or delaminate from the heater surface due to differential thermal expansion of Inconel 600 (heater material) and the adhesion material of the catalyst. While these concerns can affect the practical implementation of a FIBOR, our main interest here is to simply show the extent to which reactions can be driven and not to design new catalysts or optimize performance of existing catalyst structures.

1.2 Literature Review

The literature review is organized into three parts, with an initial focus on studies related to film boiling. A particular emphasis is given to the establishment of the physics that govern film boiling of mixtures. These concepts are then extended to studies that consider the complexities of film boiling with chemical reaction. Finally a brief review of contemporary reactor designs (e.g. packed bed) is given to provide a measure of performance for comparison and useful insights into reactor engineering such as relevant chemistry and assessments of different catalysts.

1.2.1 Film Boiling Pure Components and Mixtures without Chemical Reaction

Few works have considered film boiling as a practical means to promote chemical reaction. Most research related to film boiling has rather explored and developed the physics as it relates to boiling heat transfer. Nukiyama's (1934) pioneering experimental work revealed the regimes of boiling heat transfer depicted by the boiling curve. After numerous experiments (and melting several platinum wire heating elements) Nukiyama predicted "maximum values of heat, Q" or CHF's for water much higher than previously reported. He also reported data and an explanation of the transition to what he named the "spheroidal state," or what we now term the film boiling regime. His experimental apparatus has become a classical method to study boiling heat transfer. Bromley (1950) was the first to provide a theoretical analysis of film boiling and a correlation to estimate the heat transfer coefficient for film boiling on horizontal cylinders. Bromley's equation is reasonably accurate for heater diameters between 0.6cm (0.25in) to 1.9cm (0.75in). Breen and Westwater (1962) later examined the effect of heater diameter and provided a modified treatment of Bromley's equation to account for a wide range of cylinder diameters. Interestingly it was determined that for small heater diameters (less than 0.6cm) the heat transfer

rate is independent of the heater diameter. In addition to the effect of heater geometry on film boiling, Lee (1998) reported the effect of liquid subcooling for both the nucleate and film boiling regimes of the boiling curve. Methanol was boiled on an electrically heated tungsten wire which revealed that as the liquid subcooling increases, the critical heat flux increases and the film boiling curve is shifted upward. However a negligible effect on the film boiling curve was found at either very high liquid subcoolings (>50K) or high wall superheats (>800K).

Water has been the most common liquid used in boiling applications because of its natural abundance and safe handling. Boiling curve data for water are readily available and found in most engineering heat transfer textbooks (Incroprera et al., 2007; Lienhard et al., 2008). Comprehensive studies on boiling heat transfer often classify data as either pool or flow boiling data. Pool boiling data apply to conditions where the bulk liquid is stagnant relative to the heating surface. Flow boiling relates to conditions where the liquid is forced over or through the heater surface. Most studies available for ethylene glycol provide flow boiling data because of its common use as an engine coolant mixed with water (e.g. anti-freeze) (Frea, 1977). Limited data are available for ethylene glycol in pool boiling, especially for the film boiling regime. Even fewer data are available for film boiling aqueous mixtures.

Several studies in the 1970's addressed the problem of film boiling binary mixtures. Van Stralen et al. (1972) revealed the effects of mass diffusion in the bulk liquid when film boiling a binary mixture. It was determined that the local depletion of the more volatile component at the vapor-liquid interface causes a concentration gradient in the bulk. This therefore creates a liquid mass transfer boundary layer with the concentration of the more volatile component always being less at the vapor-liquid interface than in the bulk far from it. This in turn creates a liquid heat transfer boundary layer, where the temperature of the vapor-liquid interface is higher than that

of the bulk. This phenomenon causes conduction heat loss to the bulk and a decrease in vaporization. Figure 1.3 provides a depiction of the physics described above.

Yue and Weber (1973) conducted a theoretical analysis by solving the two phase boundary layer problem postulated by Van Stralen (1972). In the vapor phase, Yue provided appropriate boundary conditions and solved conservation equations for mass, momentum and energy while conservation equations for mass, momentum, energy and diffusion were solved in the liquid phase. Equations were resolved by a similarity transformation and the resulting ordinary differential equations were solved numerically. Yue's experimental results agreed well with his theoretical analysis for a horizontal heated cylinder and indicated that mass diffusion affects the vapor-liquid interface temperature. Neglecting this aspect could lead to erroneous results. Marschall and Moresco (1977) conducted a similar analysis as Yue and Weber for the case of a heated vertical plate.

More recent research (Liu et al. 1997) attempted to provide a correlation to predict the mass diffusion effect on heat transfer for various binary mixtures. Liu examined various mixtures ranging from very high to low relative volatilities and introduced a correlation to account for mass diffusion for a given binary mixture composition to predict the film boiling heat transfer coefficient. This correlation was shown to agree satisfactorily with experimental data.

1.2.2 Film Boiling with Chemical Reaction

Few works have considered the problem of film boiling with chemical reaction and even fewer are known to exist that consider the case of film boiling of aqueous mixtures as a method to intentionally promote chemical conversion by steam reforming. Several early studies (Ruebsamen et al. 1952; Lustman 1955; Higgins 1955) of film boiling with chemical reaction were motivated by nuclear reactor safety

and limited from the perspective of considering film boiling as a useful chemical reactor process. Satterfield (1966) was one of the first to examine the complexities of heat transfer, mass transfer and chemical reaction associated with the decomposition of hydrogen peroxide (an exothermic reaction) undergoing film boiling on a horizontal tube. Epstein et al. (1984) considered the problem of surface reactions in film boiling on a flat plate in the context of molten metal/water interactions, also commonly encountered in nuclear meltdown scenarios. Although this study demonstrated the ability to produce hydrogen gas, implementing a molten metal industrial process lacks practicality because of high operating temperatures and liquid containment issues.

Film boiling with catalytic decomposition was first analyzed by Okuyama and Iida (1994) who studied film boiling with chemical reaction on a tube. They examined the effect of reactivity of methanol in film boiling on the heat transfer coefficient which was conjectured to be due to an enhancement of the heat flux associated with the input heat flux needed to drive the endothermic reaction and the heat needed to sustain the vapor film. Many of the physics of film boiling were missing in the analysis, such as radiation across the vapor film and motion in the liquid as the result of non-zero shear at the vapor/liquid interface caused by vapor transport in the film. Product species were not actually measured. Furthermore, there was no attempt to examine the influence of parameters (one surface temperature and tube diameter was tested), to extract a rate expression appropriate for the catalyst examined (carbon-black on a platinum tube), to optimize the experimental design for production of hydrogen or to determine the parameters that influence it.

Zhukov et al. (2003) analyzed film boiling as a method for promoting chemical reaction with some results directly applicable to previous FIBOR studies (Urban et al. 2007; Avedisian et al. 2008) and the findings of this thesis. Most notable are the

experimental findings that included thermal decomposition of carbon tetrachloride (CCl_4) and various alcohols (C1-C5) through film boiling on a heated wire. The results included measuring product flow rates with respect to heater temperature and detecting chemical species that consisted mainly of hydrogen (H_2), methane (CH_4), ethane (C_2H_6), ethylene (C_2H_4) and carbon monoxide (CO). The observations also included the existence of surface reactions that created graphite-like compounds on the heater surface. These substances were analyzed further and determined to consist mainly of carbon and small amounts of hydrogen (less than 1%). Additional X-ray analysis found that the structure was similar to that of meteoric graphite. The liquid phase was observed to undergo chemical change through diffusion of contaminants consisting of aldehydes (mainly formaldehyde-CH_2O), various alcohols and ketones. Zhukov also reported that surface carbon forming reactions could be inhibited by adding water (10-15% by volume) to pure alcohols, carbon tetrachloride, benzene (C_6H_6), toluene (C_7H_8) and hexane (C_6H_{14}) to principally dissolve carbon deposits. For the case of aqueous alcoholic solutions, the heater surface remained pure.

These results (Zhukov 2003) serve as direct evidence that film boiling of an aqueous mixture can promote chemical reactions involving water vapor, in this case having the chemical effect of removing carbon from the heated surface. This therefore suggests the possibility that the action of film boiling on a suitable catalyst may promote steam reforming reactions (Equation 1.2) of an organic liquid by using an aqueous mixture as the feedstock-the primary objective of this study.

Urban et al. (2006) provided a theoretical framework and analysis for a FIBOR. The model considered film boiling of pure organics as a platform for catalytic chemical reaction, with methanol serving as the reactant and platinum black as a catalyst coated on a horizontal tube. This was one of the first rigorous analyses of film boiling as a means for chemical reaction. It was determined that as both the heater

tube surface temperature and diameter increase, so does the hydrogen (product specie) throughput. This was explained as a consequence of the strong reaction rate dependence on temperature (Equation 1.12) combined with the physics of increasing the vapor velocity (See Figure 1.3) as the tube diameter increases. An optimum operating range was predicted to exist for 1.5mm < tube diameter < 1.5cm and wall temperatures between 1080 and 1225K. These results suggested that the FIBOR could serve as a new chemical reactor platform because of its simplicity, scalability and potential to be used as a tool to study catalytic conversion. Avedisian et al. (2008) extended the FIBOR's analysis to include the effects of radiation. Results indicated that volumetric emission was not an important factor, however surface emission played a role above temperatures of 1000K resulting in a larger vapor film thickness and higher product yields than previously reported.

Choi (2010) was the first to develop an experimental apparatus of a laboratory scale FIBOR. Both thermal decomposition and catalytic conversion (Pt with Al_2O_3) of pure methanol and ethylene glycol as reactants was investigated. Product flow rates were reported similar to those found by Zhukov (2003), consisting mainly of hydrogen (H_2) and carbon monoxide (CO) along with smaller amounts of methane (CH_4), acetylene (C_2H_2) and ethylene (C_2H_4). When the heater was coated with a catalyst, appreciably higher product flow rates were achieved at lower operating temperatures. However the catalyst's performance degraded with prolonged periods of exposure in the FIBOR as shown by lower product yields over time and SEM photographs before and after use. It was postulated that the catalyst may be susceptible to deactivation at high temperatures (e.g., by sintering, de-lamination due to differential thermal expansion) or may become fouled from carbon build up or "coking." Boiling curves were also reported for each reactant to reveal the FIBOR's operating domain, as well as the overall endothermic nature of the mechanism for chemical conversion.

1.2.3 Conventional Reactor Designs

Reviewing literature based on more common chemical reactors is valuable in that it establishes a baseline to measure the FIBOR's performance. These related studies also provide useful information with regards to chemistry for a given reactant liquid as well as insights into the catalyst design and fabrication. For example, aqueous phase reforming (APR) has received recent attention as a mode to generate hydrogen from bio-mass derived hydrocarbons. Because of relatively mild operating conditions (225ºC-300ºC), the energy efficient APR process can produce high yields of hydrogen (low concentrations of carbon monoxide) because of the favorable water-gas shift (Equation 1.3) thermodynamics. (Pagliaro 2008) The drawback of APR is that it requires operating pressures often ranging between 2.2 and 2.9 MPa. Cortright et al. (2002) and Shabaker et al. (2003) have reported extensively on the APR of ethylene glycol and its aqueous mixtures. Detailed analysis of the relevant chemical reaction pathways are reported along with analysis of products formed over platinum based catalysts and optimum carbon to water ratios (concentration of ethylene glycol/water reactant mixture).

Traditional packed bed reactor designs used for steam reforming are more relevant to the FIBOR since operating temperatures are higher and reactants (e.g. ethylene glycol and aqueous mixture) are vaporized before entering a heated reactor. Such reactors are often characterized by their "conversion," or the effectiveness to completely convert reactants to products. Kechagiopoulos et al. (2007) reported results for steam reforming ethylene glycol in a bed reactor at operating temperatures similar to those in the FIBOR. Results included achieving 80% conversion at an operating temperature of 850°C with the main gaseous products including carbon monoxide (CO), carbon dioxide (CO_2), methane (CH_4), hydrogen (H_2) and ethane (C_2H_6) along with a very small trace of ethylene (C_2H_4). Additionally, minimal coking was

observed and a nickel/olivine based catalyst yielded optimum results. Hu (2009) also reported results for steam reforming of ethylene glycol, along with several other model compounds, using a nickel (Ni) / alumina (Al_2O_3) based catalyst to demonstrate the capability of producing hydrogen from bio-oil. Notable results included achieving 100% conversion at a reaction temperature of 500°C with the main products species including hydrogen (H_2), carbon dioxide (CO_2), methane (CH_4), carbon monoxide (CO) and some ethylene (C_2H_4). The effect of steam in the reactant was also analyzed. Results showed that carbon formation occurred at a rate three times higher when converting pure ethylene glycol in the reactor compared to converting ethylene glycol in the presence of steam at stoichiometric ratios (stoichiometric steam to carbon ratio is 1:1). High reactor temperatures (above 800°C) also showed the tendency for CO concentration to increase significantly due the reverse water gas shift reaction being favored.

1.3 Objectives

The broad objective of this study is to seek a better understanding of chemically converting heavy organic liquids and their aqueous mixtures through a film boiling process using ethylene glycol as the model organic compound. Measured product specie flow rates with respect to heater wall temperature and gas chromatography will serve as the primary evidence for chemical conversion. Boiling curves will outline possible operational domains as well as provide an estimate for the overall heat transfer to support the anticipated endothermic chemical mechanism.

More specifically, supporting objectives will include the following:

a) Experimental Apparatus

An experimental apparatus must be designed that is capable of processing aqueous mixtures. Details relating to the design and setup of an experimental apparatus capable of processing ethylene glycol aqueous mixtures will be reported. All relevant procedural steps, to include raw data and analysis will also be reported.

b) Tube Diameter

The effect of tube diameter on reactor performance will be investigated. This study utilizes a 2.4mm-diameter/76.2mm-length heater tube as the support structure for a FIBOR. Results will be compared to to Choi's (2010) study using a larger size tube (4.8mm-OD/100mm-length) for the case of pure ethylene glycol thermal decomposition (bare tube).

c) Catalyst Performance

A platinum based catalyst and a nickel based catalyst will be examined. Possible degradation of catalyst performance as a result of FIBOR operating conditions will also be investigated.

d) Wall Temperature

Wall temperature is a controllable parameter in the FIBOR and will be studied as it relates to the product flow rate and product specie concentrations. This is an important aspect of the FIBOR because the rate of chemical reaction has an exponential dependence on temperature shown by equation 1.12. Additionally, chemical reactions (Equations 1.3 and 1.4) are sensitive to temperature which can affect product concentrations.

e) Feedstock Concentration

In order to assess the effect of the steam to carbon reactant ratio, feedstock concentrations will include pure ethylene glycol and aqueous mixtures (80% and 90% by volume ethylene glycol). This relates to the FIBOR's performance because varying the feedstock concentration alters the vapor concentration that is fed into the vapor volume that constitutes the FIBOR.

f) Evidence of Specific Conversion Process

The additional heat flux needed to support chemical reaction will be reported. Individual product species and their concentrations will also be determined through gas chromatography to provide further evidence that the FIBOR is capable of promoting steam reforming of organic compounds.

CHAPTER 2

FIBOR DESIGN AND FABRICATION

2.1 Design Considerations

The FIBOR's design is centered on the construction of an experimental apparatus capable of accommodating binary mixtures. A liquid mixture must be drawn into a chamber where it is heated to its saturation point (Figure 1.2) under atmospheric conditions, and a heating element to support the FIBOR is immersed at high enough temperatures to promote film boiling. Product gases that are contained in the percolating bubbles must be separated and analyzed to determine overall volumetric product flow rates and composition. All relevant operating parameters such as bulk liquid temperature, heating element surface temperature and power supplied to the heating element must be controlled by the user and digitally stored for analysis. Product gas flow rates, to include gas chromatography (GC) analysis of extracted product samples must also be stored. The experimental apparatus design concept is mainly based on Choi's (2010) work, yet designed in a manner to support testing of mixtures. A suitable laboratory scale FIBOR design has the following considerations:

a) Heater Length

In order to fit within pre-existing hardware (power supply electrode buses and liquid chamber), the length of the heater cannot exceed 140mm.

b) Heater Geometry

A cylindrical heater geometry is considered for ease of scalability and analysis.

d) Heater Temperature Monitoring/Control System

Heater surface temperature must be monitored, such as by using thermocouples inserted (and electrically isolated) inside of the heater tube and digitally stored. The temperature is controlled manually by adjusting power input for joule heating through a Labview user interface.

e) Constant Liquid Composition

A constantly changing bulk liquid adds significant complexity in analyzing experimental data. Composition changes can result from both evaporation and chemical reaction. The former is caused by preferential evaporation of the volatile species (water) which can lead to considerable composition differences between the liquid and vapor phases for a given mixture over time. For example, boiling a water/ethylene glycol mixture that is open to the surroundings leads to a rapid depletion of water since the vapor is enriched with steam (see figure 1.2). This therefore motivates a design that returns reactant vapors into the bulk liquid, or a "reflux" condensing design. Composition changes due to chemical reaction can also occur and depend on the reaction rate and chemical mechanism. For example if steam reforming is the primary chemical reaction (Equation 1.2) and is assumed to be the dominant reaction pathway, two moles of water will be consumed for every mole of ethylene glycol, leading to an eventual depletion of water. Composition change due to chemical reaction therefore suggests that the volume of the bulk liquid should be much larger than that of the FIBOR so that for a given period of time (average length of an experiment) the change in bulk composition due to chemical reaction is negligible. This therefore suggests that the heater tube size relative to the bulk liquid chamber volume is a critical design parameter.

f) Power Supply Requirements

The available power supply is a programmable 580A/8V DC (Agilent, 34980A) power supply. Joule heating is accomplished by manually controlling direct current which is passed through a heating element with sufficient electrical resistance to raise the surface temperature high enough to support film boiling. This will serve as the technique to traverse boiling curves for respective liquid mixtures in this study, due to consideration being given to the inability of joule heating the tube to access the transition zone in Figure 1.1 (i.e. from points B-C). Hence control is required from C to D (Figure 1.1) to avoid burnout.

g) Heater Electrode Clamps

Electrode clamps must hold the heater tube in place while it is submerged in the bulk liquid in such a way as to allow a good seal between the electrode and heater tube surface. It must also attach to existing electrode buses. Figure 2.1 is a general design schematic that shows this arrangement.

h) Reactants

The primary compound of interest includes pure and aqueous mixtures of ethylene glycol. Considerations for accommodating glycerol are also included in anticipation for future research.

i) Product Flow Rates

Product species must be separated and their flow rates measured on a volumetric basis. Since anticipated product species of interest from Equations 1.1-1.10 are non-condensable gases, the remaining flow of gases after all reactant vapors are condensed and returned into the bulk liquid would be proof of chemical reaction.

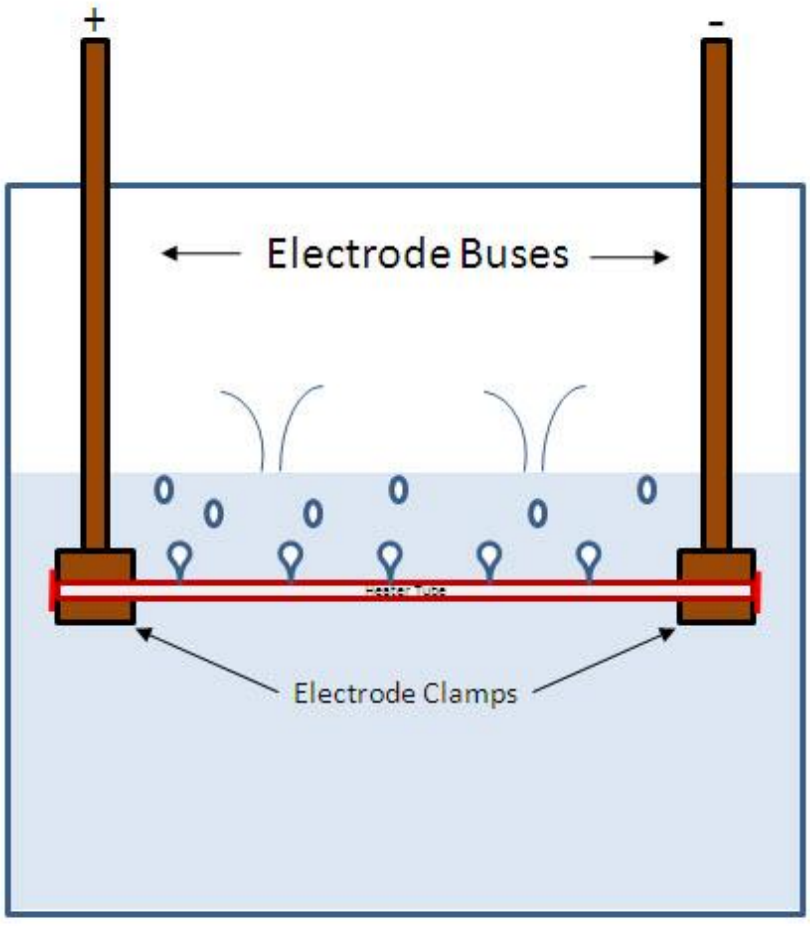

Figure 2.1: Electrode Clamp/Heater Arrangement

j) Gas Chromatography (GC)

The GC used in this study is a GOW-MAC 600 Series. The GC must be upgraded and configured to detect all anticipated product species outlined in Equations 1.1-1.10.

k) Catalytic Reaction and Thermal Decomposition

The FIBOR must demonstrate the ability to convert reactant mixtures through both catalytic conversion and thermal decomposition. At least two different catalysts must be evaluated, one being Platinum and the other Nickel based. Thermal decomposition must be demonstrated through use of a bare tube.

l) Data Acquisition

All relevant parameters must be digitally stored in real time, including power input, heater temperatures, bulk liquid temperatures, product flow rate and gas chromatograms.

2.2 Required Tasks to Generate Final Design Concept

In order to generate the final design, the most critical task is determining a suitable heater tube size and material. This task is coupled to several other intermediate tasks and once the heater size is determined, several remaining intermediate tasks generate a large portion of the final design. Figure 2.2 is a mind-mapping diagram that depicts how tasks are related to one another. There are four key tasks (depicted by ovals): heater size and material, gas chromatography, data acquisition and the catalyst. The heater size and material are

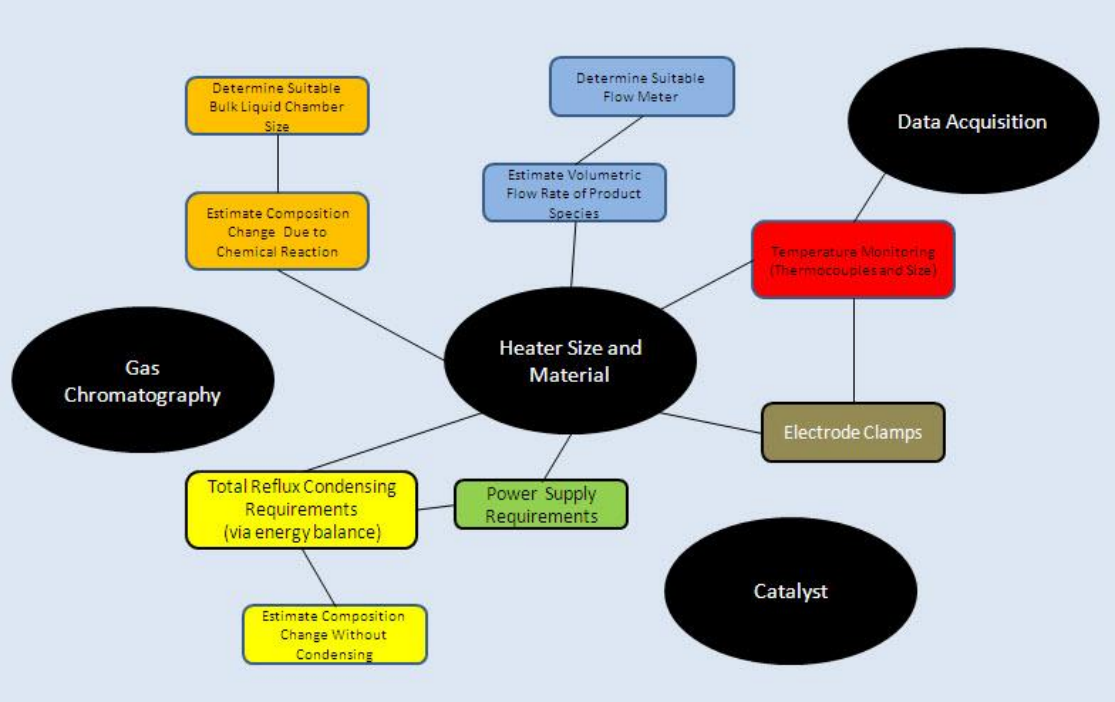

Figure 2.2: FIBOR Design Mind-Map

directly related to several other intermediate tasks, while upgrading and configuring the GC, and selecting and fabricating a catalyst, are stand-alone, independent tasks. A brief description of each design task follows and concludes with the final design concept sketch.

a) Heater Size and Material

Figure 2.2 shows the interdependence of several other secondary tasks with the heater size and material design (center oval). Starting in the top/left corner of Figure 2.2 and traversing in a clockwise fashion, perhaps the most critical task is estimating the liquid composition change as a result of chemical reaction. This task is performed through a species balance on the primary steam reforming reaction for a chosen heater size and an initial bulk liquid volume using an assumed rate of reaction which is based on experimental results reported by Choi (2010) for catalytic conversion of pure ethylene glycol. The rates of product specie generation are assumed to scale linearly with heater surface area and used to estimate the time rate of change of the bulk liquid composition with respect to heater surface area. In conjunction with this calculation, product flow rates are also estimated when varying heater surface area. Details of this analysis and results are discussed in Section 2.3.1.

Thermocouples are used to monitor the temperature of the heater surface by inserting them inside of the heater tube. The heater geometry determines the maximum size of the thermocouples and the number that can be inserted respectively.

The design of the electrode clamps (Figure 2.1) considers several factors, yet the most critical is to accommodate the chosen heater geometry and thermocouple arrangement. Ensuring a proper fit around the heater tube requires advanced machining techniques that consider precise allowances and tolerances. The clamps must also fit within existing hardware mentioned in Section 2.1 and depicted in Figure

2.1. Detailed technical drawings and machining procedures are outlined in Section 2.3.2.

Power supply requirements are determined by the electrical resistance of the heater tube. The electrical resistance is determined by equation 2.1 where the resistivity of the chosen material is temperature dependent and the heater's cross sectional area and length depict the geometry through which current passes.

$$R_e = \rho \cdot \frac{L}{A_c} \qquad 2.1$$

Inconel 600 is chosen as a heater material because of its high electrical resistivity and melting point (Special Metals 2008). Since this study utilizes a joule heating technique, Inconel 600 possesses appropriate properties for the expected range of operating conditions. A 6th order polynomial is used to determine the electrical resistivity,

$$\rho(T) = 0.4763 + 5.27 \cdot 10^{-3} T - 1.95 \cdot 10^{-5} T^2 + 3.56 \cdot 10^{-8} T^3 - 3.23 \cdot 10^{-11} * T^4 + 1.35 \cdot 10^{-14} T^5 - 1.89 \cdot 10^{-18} T^6 \qquad 2.2$$

Applying Equations 2.1 and 2.2 to available boiling curve data for pure ethylene glycol (Choi 2010) estimates the power supply requirements for a given geometry design. Details are given in Section 2.3.3.

The condensing requirements include condenser surface area and temperature, and are estimated through an energy balance around the FIBOR and condensing module. In order to ensure that all reactant vapors are condensed and returned into the bulk liquid, the heat supplied to the FIBOR ($P=I^2R$) to vaporize reactants must balance the amount of heat that the condenser can remove. The heat that the condenser is able to remove from the vapor flow must be large enough to condense the entire vapor flow

to the liquid phase, allowing for a return to the bulk liquid under gravity flow. Further details of this calculation are provided in Section 2.3.4.

b) Gas Chromatography

A Gas Chromatograph (GC) detects individual product species and their concentrations from the product gas stream that the FIBOR produces. At a minimum, the GC must be capable of detecting hydrogen (H_2), carbon monoxide (CO), methane (CH_4) and carbon dioxide (CO_2) because these are the main anticipated product species outlined in Equations 1.1-1.10 respectively. It is also possible however that traces of higher hydrocarbons can exist in the gas stream such as acetylene (C_2H_2), ethylene (C_2H_4) and ethane (C_2H_6).

The GC's capability to detect product species is largely dependent on the column(s) installed. A GC column is a narrow tube filled with packing material. Product species flow through the column with the aid of a carrier gas such as helium. Gases travel through certain columns in specific amounts of time, otherwise known as the retention times. The retention time is related to the molecular weight of the gas and thus the composition of a gas mixture can be determined.

Columns are limited to how many different species they can simultaneously detect. One column may facilitate detection of species such as H_2, CO and CH_4 while a separate column would be required to detect heavier species such as CO_2 and higher hydrocarbons. These considerations suggest that the GC requires two columns to be installed in parallel to detect all product species of interest.

Two separate samples must be extracted after all reactant vapors are condensed and separated. The first sample is injected into the column capable of detecting H_2, CO and CH_4. A second sample is then injected into the column capable of detecting CO_2, C_2H_2, C_2H_4 and C_2H_6.

The GC is programmed with data acquisition software (ChromPerfect, versopm 5.4.1) to generate a chromatogram for each column. A separate "calibration gas" with a known gas composition that contains all species of interest must be analyzed under the same GC settings used in testing product gases generated by the FIBOR. This allows for a reference chromatogram to be generated for further analysis to ultimately determine specific species and concentrations of the actual FIBOR product gas stream. Details regarding the GC's programming and configuration will be provided in Sections 2.3.5, 4.3, and B.3.4.

c) Data Acquisition

Five operating parameters must be monitored and controlled: bulk liquid temperature; immersion heater power supply setting to the bulk liquid; heater tube temperature; power supply settings to the heater tube; and product gas flow rates. The GC must also have an integrated data acquisition system to generate and save chromatograms. This function can be performed separately under the internal settings of the GC. Immersion heaters, connected to a manually adjusting AC/DC transformer (Staco Energy Products, Type 3PN1010) allow for manual control of the power input to maintain the bulk liquid at its saturation point. A programmable DC power supply allows the user to manually control the heater tube temperature through "joule heating" or adjusting the current passed through the heater tube. The product gas flow rate is monitored by a digital flow meter positioned downstream of the condensers so that the only gases that reach the flow meter are non-condensable and therefore products of interest. A Labview program must acquire and store all temperature outputs from thermocouples, flow meter readings and allow the user to control power supply settings. Further details are provided in Section 2.3.6.

d) Catalyst

Higher product yields can be promoted by a suitable catalyst that would coat the heater tube. (bottom right, Figure 2.2) The coating must be uniform to prevent both uneven thermal resistance and catalyst loading along the tube. The coating's adhesion must also be able to endure some surface agitation by bubbles and the high operating temperatures required for film boiling. Additionally, catalyst coating procedures are commonly held as proprietary information.

Catalyst coatings used in this study were professionally applied by Catacel Corp. (Garrettsville, OH). More detailed coating procedures are provided in Section 2.3.7.

e) Final Design Schematic

Figure 2.3 is a schematic of the final design for the experimental apparatus used in this study. It is labeled alphabetically in the general order that follows the liquid reactant as it is first introduced into the FIBOR, then converted to the gas phase and finally analyzed. The labeling also corresponds to the final design bill of materials (BOM) presented in Section 2.5.

The liquid mixture is manually fed into the bulk liquid reactant chamber through both gravity and an in-line peristaltic pump (a-h). Immersion heaters (j) heat and maintain the bulk liquid at its saturation point inside of a glass bulk liquid chamber (k). The heater tube (l) is mounted to copper electrode buses and clamps (m) through which direct current is passed to provide joule heating. Thermocouples are inserted inside of the heater tube (n) as well as immersed into the bulk liquid (o) to

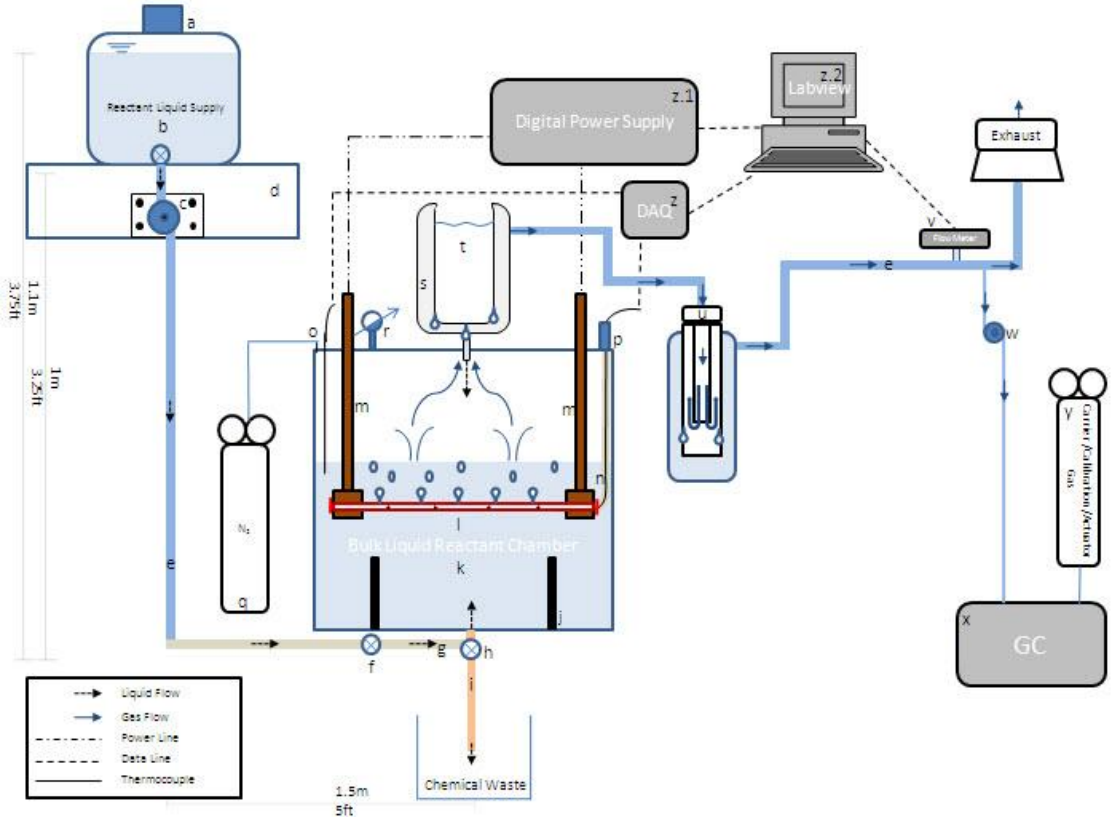

Figure 2.3: Final Design Concept

monitor their temperatures. Packing glands (p) with Teflon seals provide an air-tight seal for inserting the thermocouples into the bulk liquid reactant chamber. Nitrogen (q) is passed through the system for safety reasons to prevent possible ignition. A pressure gage (r) is also installed to safely ensure the entire system remains at atmospheric conditions. Gases created by the FIBOR consisting of both products and non-converted reactant vapors travel out of the chamber and through a condenser (s) which is filled with a heat transfer coolant (t) such as ice water or dry ice and acetone. Unconverted reactant vapors are condensed and return to the liquid chamber. Products (non-condensable gases) then travel through an additional cold trap (u). Any liquid that accumulates in the cold trap suggests that the condenser (s) is insufficient and reactant vapors are therefore passing through. Product gases then flow through a digital flow meter that records volumetric flow rate data. Since the condenser is designed to return all reactant vapors into the bulk liquid chamber, any flow reading at (v) is therefore evidence of chemical reaction. Before products are exhausted to the atmosphere, a mini-pump (w) extracts a gas sample and sends it through the GC (x-y) for analysis. A Labview user controlled program interface (z.2) allows the user to adjust the power supply settings (z.1), while also monitoring the heater tube temperature (n,z), bulk liquid temperature (o,z) and product flow rates (v). All information is digitally stored for further analysis.

2.3 Detailed Design Process and Fabrication

The following sections provide a systematic and detailed approach to design a FIBOR capable of processing liquid mixtures. The remainder of this chapter is written to a level of detail that one could follow in order to design and re-construct an experimental apparatus similar to the one used in this study.

2.3.1 Heater Tube Size

Figure 2.4 is a model that depicts how the heater tube design, condenser(s) design, power supply settings and electrode clamp design are related. This model is a recommended procedure to design a FIBOR intended for mixture analysis. The first step is to identify a suitable heater tube size that prevents composition change in the bulk liquid mixture (Figure 2.3a) as a result of chemical reaction. This is estimated by applying an assumed peak flow rate (7270 LPM/m^2) (experimentally determined by Choi 2010) for catalytic conversion of pure ethylene glycol to the stoichiometric steam reforming reaction (Equation 1.2). This assumes that products formed through the steam reforming reaction will progress at nearly the same rate as catalytic conversion of pure ethylene glycol. Further assuming single step chemistry (Equation 1.2), products behave as ideal gases (1 mol = 22.4 liters) and that product flow rates scale linearly with heater surface area, the composition change as a result of chemical reaction can be estimated for prolonged periods of operation in the FIBOR. A derivation of this calculation follows.

The volumetric product flow rate is assumed to be constant (7270 LPM/m^2) and can be converted to a molar basis,

$$\dot{N}_p = \dot{V} \cdot \frac{1\ mol}{22.4\ liters} \qquad 2.3$$

Equation 1.2 indicates that for every 7 moles of products converted, 1 mole of ethylene glycol is consumed while at the same time, 2 moles of water are also consumed. Since Equation 2.2 provides the rate at which moles of products are created, the depletion of ethylene glycol can be expressed as,

$$N_{eg}(t) = \frac{1}{7}\dot{N}_p t \qquad 2.4$$

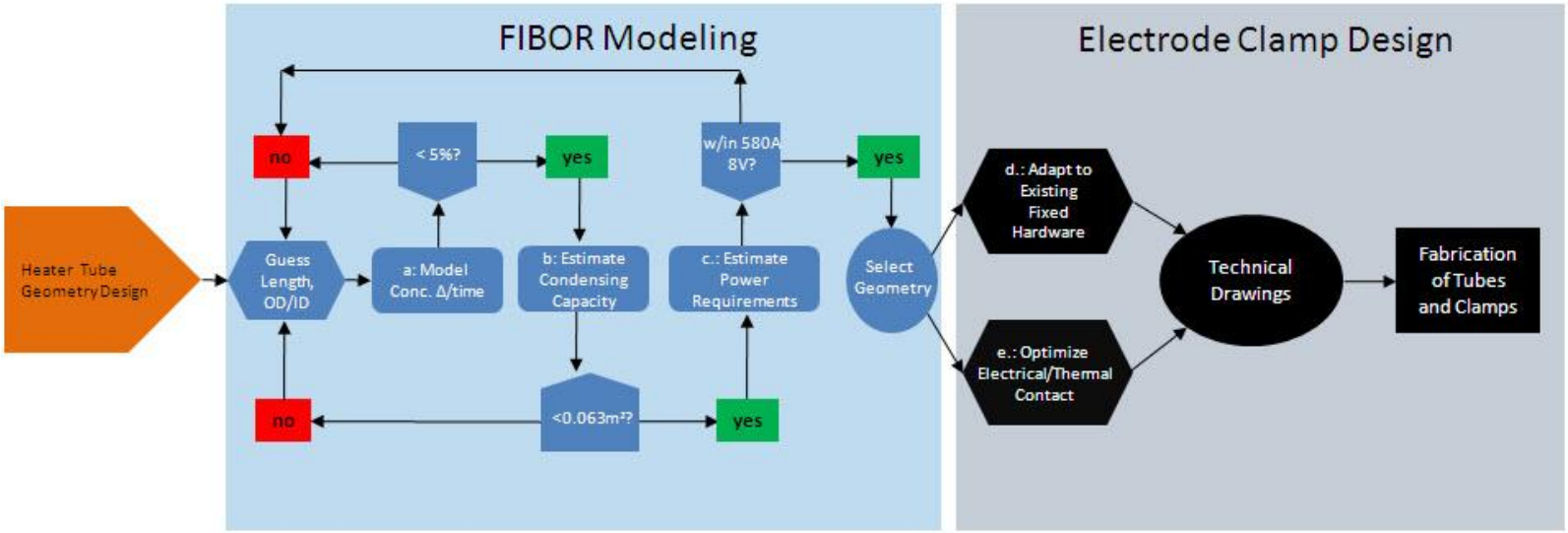

Figure 2.4: FIBOR Design Model

and the depletion of water is similarly expressed as,

$$N_w(t) = \frac{2}{7}\dot{N}_p t \tag{2.5}$$

The mole fraction is defined as,

$$X_i = \frac{\text{Moles of i}}{\text{Total Moles}} \tag{2.6}$$

The initial mole fraction of the i^{th} component is known (e.g. 80% ethylene glycol/20% water by volume converts to a 0.57 ethylene glycol/0.43 water mole fraction by applying known values of density and molecular weight respectively) as well as the total volume of liquid that the bulk liquid reactant chamber can hold (for our case 3 liters) and is expressed as,

$$N_i = X_i N_R \tag{2.7}$$

Combining equations 2.2-2.6, it follows that the depletion of water with respect to time can be expressed as,

$$X_w(t) = \frac{X_{w,0}N_r - \frac{2}{7}\dot{N}_p t}{\left(X_{w,0}N_r - \frac{2}{7}\dot{N}_p t\right) + \left(X_{eg,0}N_r - \frac{1}{7}\dot{N}_p t\right)} \tag{2.8}$$

Figure 2.5 shows results of varying the heater tube length and diameter respectively to minimize the mixture's composition change due to chemical reaction

alone. Details of this calculation can be found in the Matlab code provided in Appendix C.1.

As the surface area of the heater decreases (sample dimensions given in inset of Figure 2.5) so does the rate of composition change until there is a negligible effect at surface areas comparable to using a wire heating element (OD<1mm) immersed in a 3 liter chamber.

A design of 2.4mm x 60mm is chosen because a) ease of fabricating a standard size (3/32in); b) it is the smallest diameter that can reasonably support a tubular heating element design that allows for insertion of multiple thermocouples; and c) changes of bulk composition are small (by approximately 3% over a four hour period according to Figure 2.5).

It should be noted that this is a very simplified approach to modeling composition change due to chemical reaction and serves as only a conservative engineering estimate. Two significant assumptions include single step chemistry and assuming product flow rates match that of catalytic conversion of pure ethylene glycol. A rigorous analysis of the actual chemical mechanism is likely more complex and beyond the scope of this study.

2.3.2 Total Reflux Condensation

The goal is to design the condenser with enough surface area held at a sufficiently low temperature (T_s) to completely condense the saturated vapor creating an equal and opposite mass flow of condensed saturated liquid back into the bulk liquid chamber. An energy balance is performed around the condenser as depicted by Figure 2.6 to estimate the enthalpy transported into the control volume by the saturated vapor mass flow (small red arrow) and balanced by energy transferred into

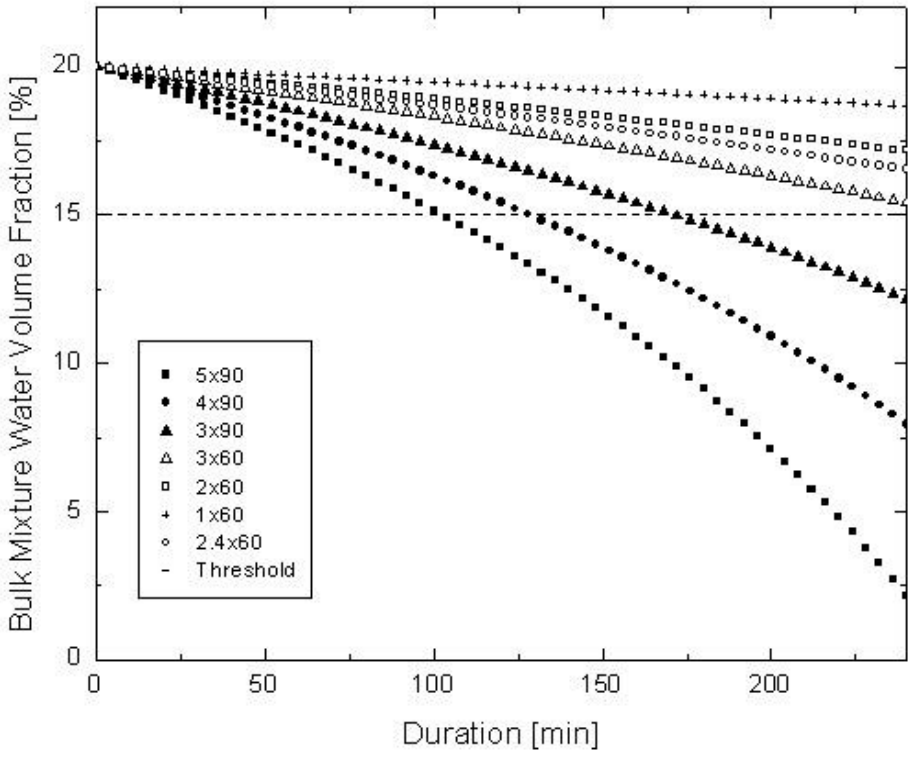

Figure 2.5: Rate of Bulk Liquid Composition Change Due to Chemical Reaction

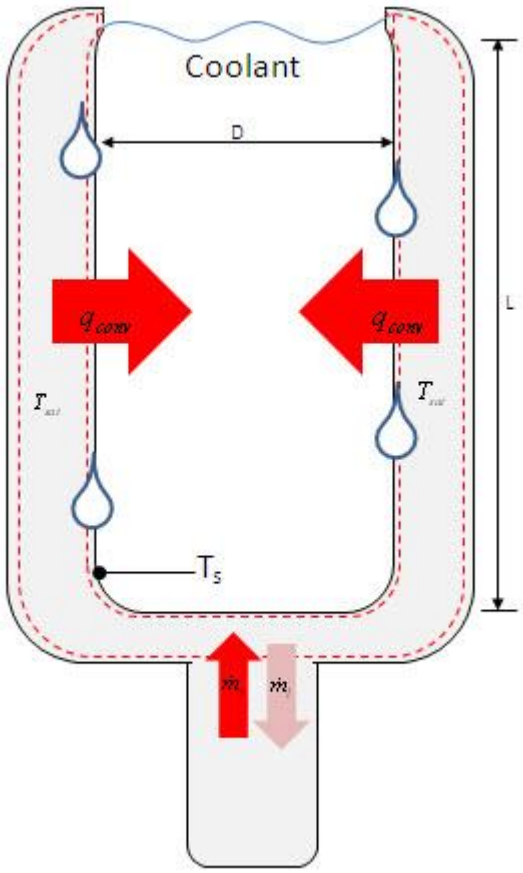

Figure 2.6: Condenser Energy Balance

the condenser coolant ($q_{conv,}$ large red arrows). The heat transfer to the coolant is represented as,

$$q_{conv} = \bar{h} A_{s,c} (T_{sat} - T_s) = \dot{m} h_{fg} = I^2 R \qquad 2.9$$

$$A_{s,c} = \pi D L \qquad 2.10$$

Equation 2.9 is valid with the assumption that all of the heat supplied to the FIBOR is consumed by vaporizing the liquid and thus creating a vapor mass flow. In order to ensure that no vapor is able to pass the condenser, the heat transferred into the condenser coolant must balance with enthalpy transported into the condenser. The heat transfer coefficient is estimated from correlations for film condensation on a vertical plate (Incropera 2007),

$$\bar{h} = \frac{\mathrm{Re}\, \mu_l h_{fg}^{'}}{4L(T_{sat} - T_s)} \qquad 2.11$$

with the Reynolds number approximated by,

$$\mathrm{Re} = \left[\frac{3.70 k_l L (T_{sat} - T_s)}{\mu_l h_{fg}^{'} (v_l^2 / g)^{1/3}} + 4.82 \right]^{.82} \qquad 2.12$$

Figure 2.7 shows results for the amount of heat the condenser can absorb by varying its surface area with two coolants of interest-ice water and an acetone/dry-ice bath. A threshold of 2000W is chosen based on reported FIBOR boiling curve data (Choi 2010). Results indicate that a condenser with 275 cm^2 of surface area ($A_{s,c}$ from Eqn 2.10, Figure 2.6) is required if using acetone/dry-ice while ice water requires

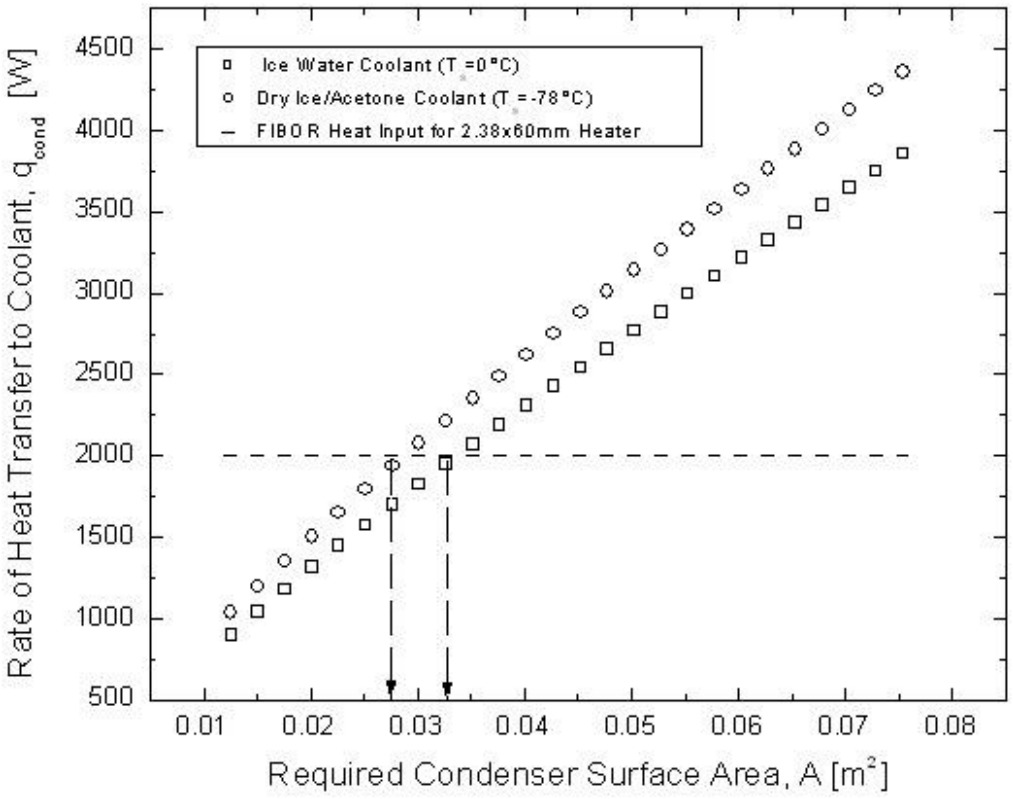

Figure 2.7: Condenser Modeling Results

approximately 325 cm^2. Further details of this calculation can be found in the Matlab code provided in Appendix C.2.

2.3.3 Power Supply Requirements

The final step (Figure 2.4c) before selecting a final heater tube size is to estimate the power supply requirements to ensure they fall within the equipment specifications (8V/580A DC Power Supply, Agilent 34980A) available for this study. The inside diameter is a critical parameter in this step as it relates directly to the cross sectional area of the heater tube and thus the overall electrical resistance (Equation 2.1).

Estimating power requirements is quite straight forward and only requires boiling curve data and the material's resistivity dependence on temperature both being readily available. The critical assumption in this estimate is that the boiling curve data for pure ethylene glycol is a reasonable estimate for various ethylene glycol aqueous mixtures. This assumption will be evaluated in a preliminary design test and presented at the end of this chapter.

Table 2.1 shows the power requirements over the anticipated operating range in the film boiling regime. Wall temperature and heat flux data are taken from experimental data. (Choi 2010) The power can be estimated by

$$P = q'' A_{s,F} \tag{2.13}$$

Table 2.1: Power Supply Requirements

Tube Design [ODxIDXLength]	Wall Temperature[K] [Boiling Curve Data (Choi, 2010)]	Heat Flux [W/m^2] [Boiling Curve Data (Choi,2010)]	Power [W] [Eqn 2.11]	Resistivity[μ·Ω·m] [Material Data (Table 2.2)]	Resistance[Ohm] [Eqn2.1]	Current[A] [Eqn 2.12]	Voltage[V] [Eqn 2.13]
1.57mmx1.32mmx92.05mm (1/16inx.0525inx3&5/8in)	1083.00	350532.46	157.26	1.13	0.04	64.08	2.45
	1198.00	414351.23	185.89	1.16	0.04	68.66	2.71
	1306.00	576787.99	258.76	1.29	0.04	76.97	3.36
	1393.00	739234.88	331.64	1.51	0.05	80.42	4.12
	1483.00	952085.87	427.12	1.92	0.07	80.93	5.28

where q'' is the heat flux and $A_{s,F}$ is the surface area of the FIBOR. The material (Inconel 600) electrical resistivity is dependent on temperature and shown by Equation 2.2 (Special Metals 2008). The electrical resistance is given by Equation 2.1, thus the current is estimated by,

$$I = \sqrt{\frac{P}{R_e}} \tag{2.14}$$

so that the voltage,

$$V = IR_e \tag{2.15}$$

Results tabulated in Table 2.1 show that a final heater tube design of 2.38x1.85x60mm with Inconel 600 as the chosen material falls well within the available power supply settings (8V/580A).

2.3.4 Heater Tube Electrode Clamps

As shown in the Electrode Clamp Design portion of Figure 2.4, once a satisfactory heater size is found, the remaining steps are rather broad and open to design creativity. Existing copper electrode buses with threaded ends are considered to be permanent hardware fixtures that the electrode clamp design must adapt to (Figure 2.1). This arrangement could be modified, yet would have added significant work beyond the scope of this study. In order to optimize thermal and electrical contact, a cylindrical precision fit design is used. Additionally a ceramic heater tube insert is used to both prevent anticipated heater tube sagging due to material softening

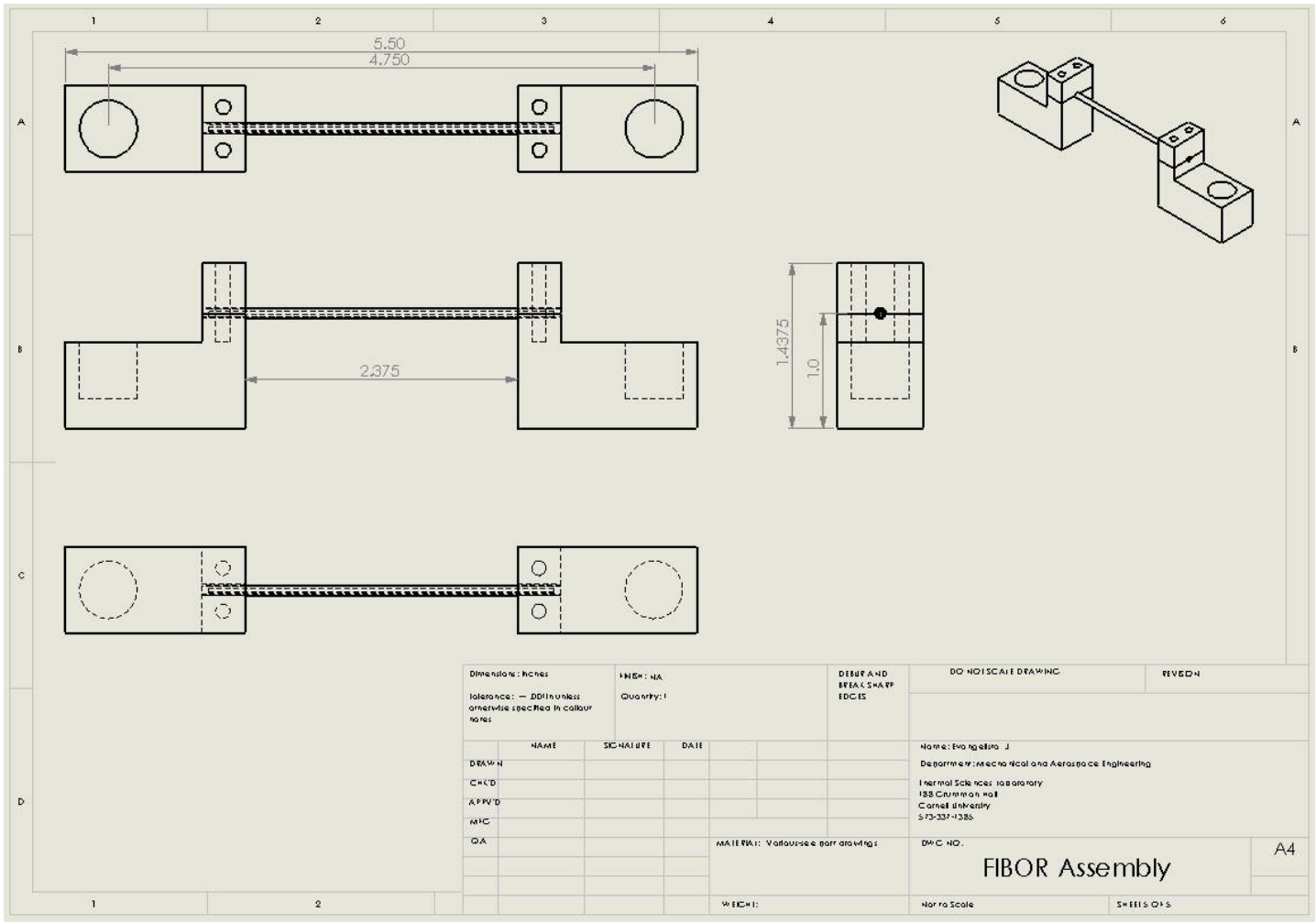

Figure 2.8: Heater Tube Clamp Design

at high operating temperatures and also provide electrical insulation for inserted thermocouples. Detailed technical drawings are provided in Appendix A. Figure 2.8 shows the assembled technical drawing view. Figure 2.9a is an isometric assembled view of the electrode clamp design drawn with Solidworks software along with a zoomed in cross sectional view (Figure 2.9b) of fitting tolerances around the heater tube. The following machining steps were followed to fabricate the final design:

a) Inconel heater tubes are manufactured and cut to length by Microgroup, Inc. (Microgroup, 600F10093X010SL). Details of the heater tube to include dimensions and material characteristics are listed in Table 2.2.

b) Top and bottom components (x2) are machined from Copper Alloy 110 according to technical drawings found in Appendix A without the feed-through hole for the Inconel heater tube. The large hole in each bottom clamp is threaded (1/2”-20) in order to assemble into existing electrode buses. Two smaller threaded holes (#6-32) through the top and bottom clamps (x2) provide for assembly with four #6-32 hex screws.

c) The actual OD of the Inconel Tubes (3/32 +/- .001in) acquired in step 1 are measured to the nearest .00001 in.

d) The top and bottom components (x2) are clamped together and the heater tube feed-through hole is reamed to within 0.00025in(min)/.00045in(max) clearance of OD measured in step 3 to achieve a Close Sliding Fit, RC1 (Oberg 2008).

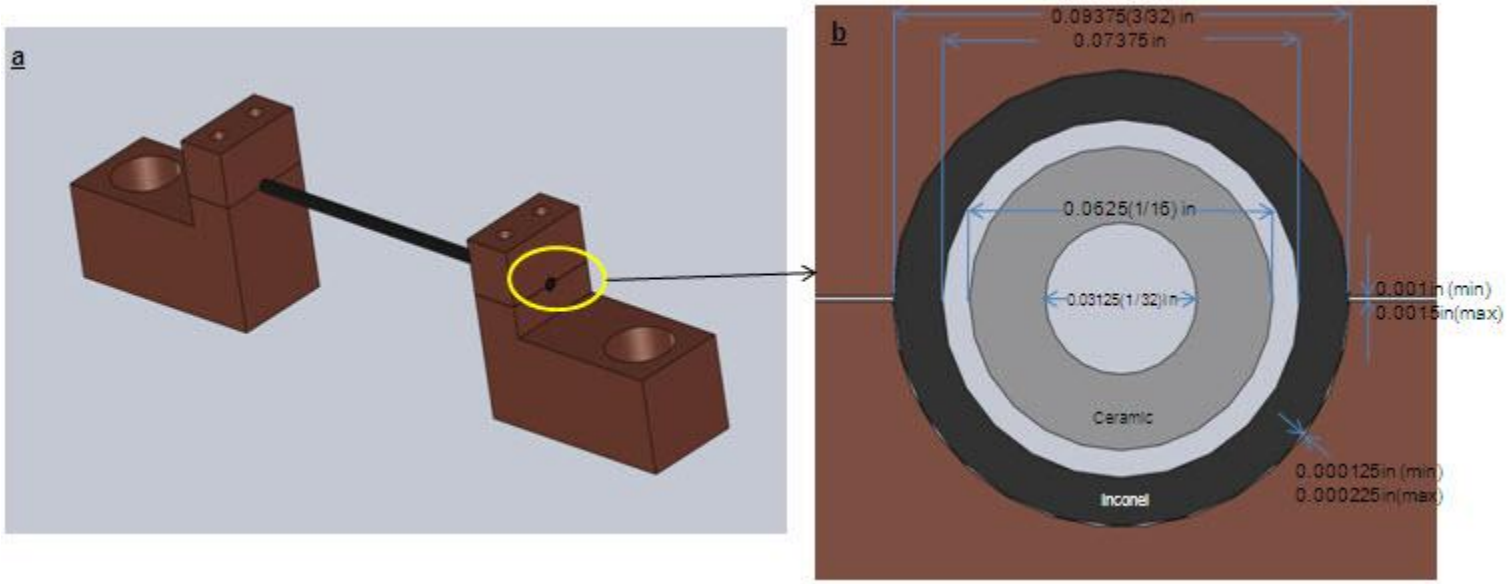

Figure 2.9: Heater Tube Clamp Design Tolerances

Table 2.2: Heater Tube Properties

Physical Properties (Microgroup 2009)						
Material	Grade	Mfg Type	OD Max/Min [in]	ID Max/Min [in]	Length [in]	Melting Rg [ºC]
Nickel Alloy	600(Inconel)	Seamless	0.0936/.0935	.073/.0728	3.1245	1354-1413
Chemical Properties (Microgroup 2009)						
C%	Mn%	S%	Si%	Ni%	Cr%	Cu%
0.023	0.77	0.001	0.32	72.4	16.27	0.01
Ti%	Cb%	Co%	Al%	N%	Fe%	Other%
0.31	0.01	0.02	0.18	0.023	9.49	0.173

Thermophysical Properties (Special Metals Corporation 2008)			
Temperature [ºC]	Electrical Resistivity [μΩ·m]	Thermal Conductivity [W/m·ºC]	Specific Heat [J/kg·ºC]
20	1.03	14.9	444
100	1.04	15.9	465
200	1.05	17.3	486
300	1.07	19	502
400	1.09	20.5	519
500	1.12	22.1	536
600	1.13	23.9	578
700	1.13	25.7	595
800	1.13	27.5	611
900	1.15	-	628

5. Remove material (0.127mm (0.0005in) (min)/0.019mm (0.00075in) (max) from mating surfaces of the top and bottom components to achieve a clearance of 0.00254mm (0.0001in) (min)/0.00381mm (0.00015in) (max) as depicted in Figure 2.7b. A Light Drive Fit (FN1) (Oberg 2008) is achieved when assembled.

2.3.5 Gas Chromatography

This section reports specifications to the existing GC (GOW-MAC Series 600) to facilitate mixture testing. Figure 2.10 is a flow diagram that depicts the installation of two columns, two gas sample valves and two liquid injection ports. Column A is an 8ft. x 1/8in Molesieve 13x, 1ml Loop Column and can be used for detecting H_2, O_2, N_2, CO and CH_4. Column B is an 8ft. x 1/8in Haysep Q 13x, 1ml Loop Column and can be used for detecting CO_2 and hydrocarbons up to C5 (for this study used to detect C_2H_2, C_2H_4, C_2H_6). The GC is retrofitted with liquid injection ports for liquid chromatography. Liquid mixtures of interest are injected directly into Column B with a syringe holding a 10mL sample. The Column must be held at a temperature (GC oven temperature setting) above the highest individual component boiling temperature to prevent condensation inside of the column. To first ensure accurate results, actual liquid testing for this study utilized a GC-MS (Agilent Technologies 6890N/5973 High Performance Combination). Future research however can utilize the GOW-MAC 600 Series GC for liquid testing.

The configuration shown in Figure 2.11 allows for the extraction of a sample from the FIBOR product gas for GC analysis. FIBOR product gas flow ranges

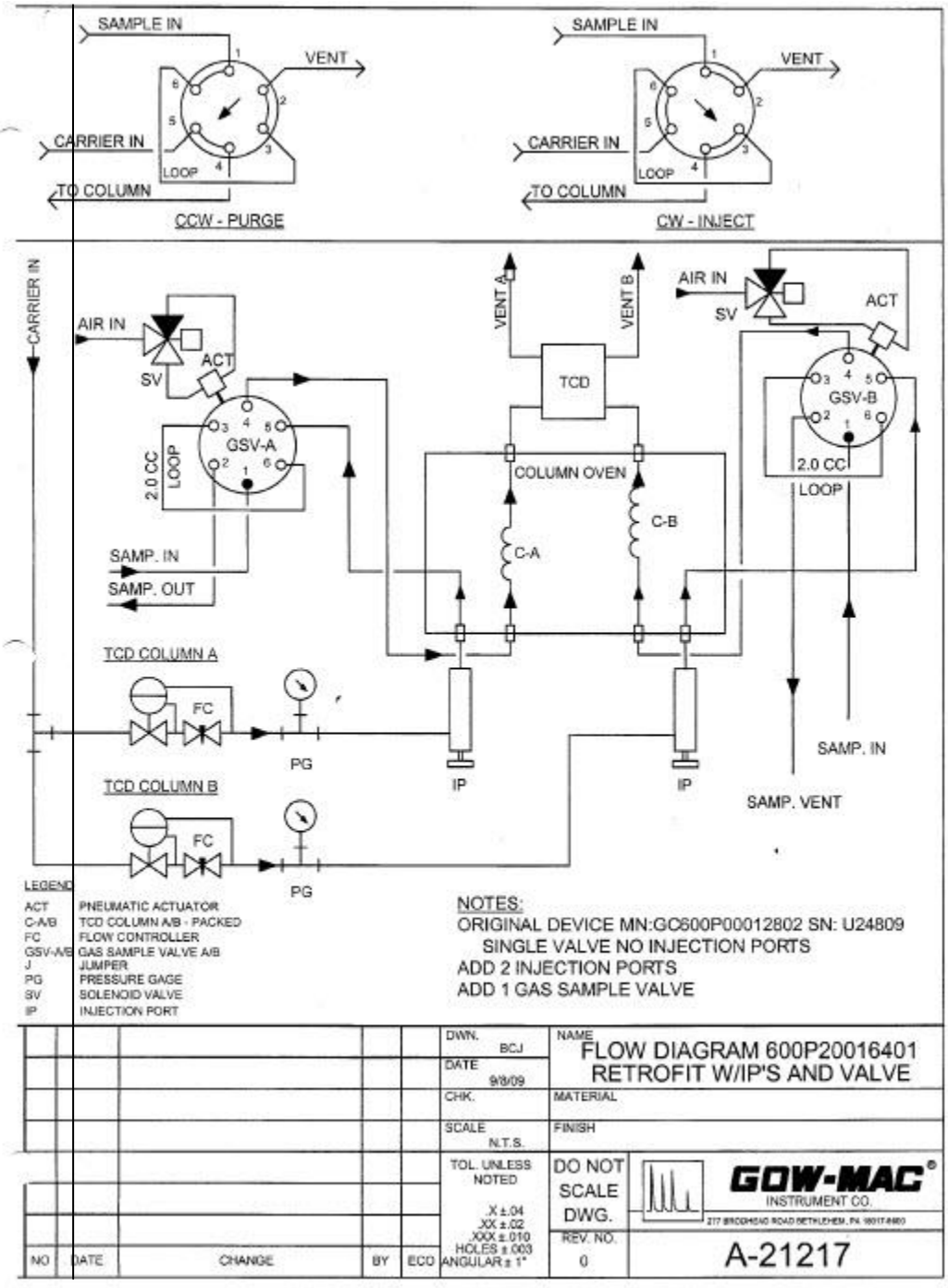

Figure 2.10: GC Flow Diagram (GOW-MAC Instrument, Co.

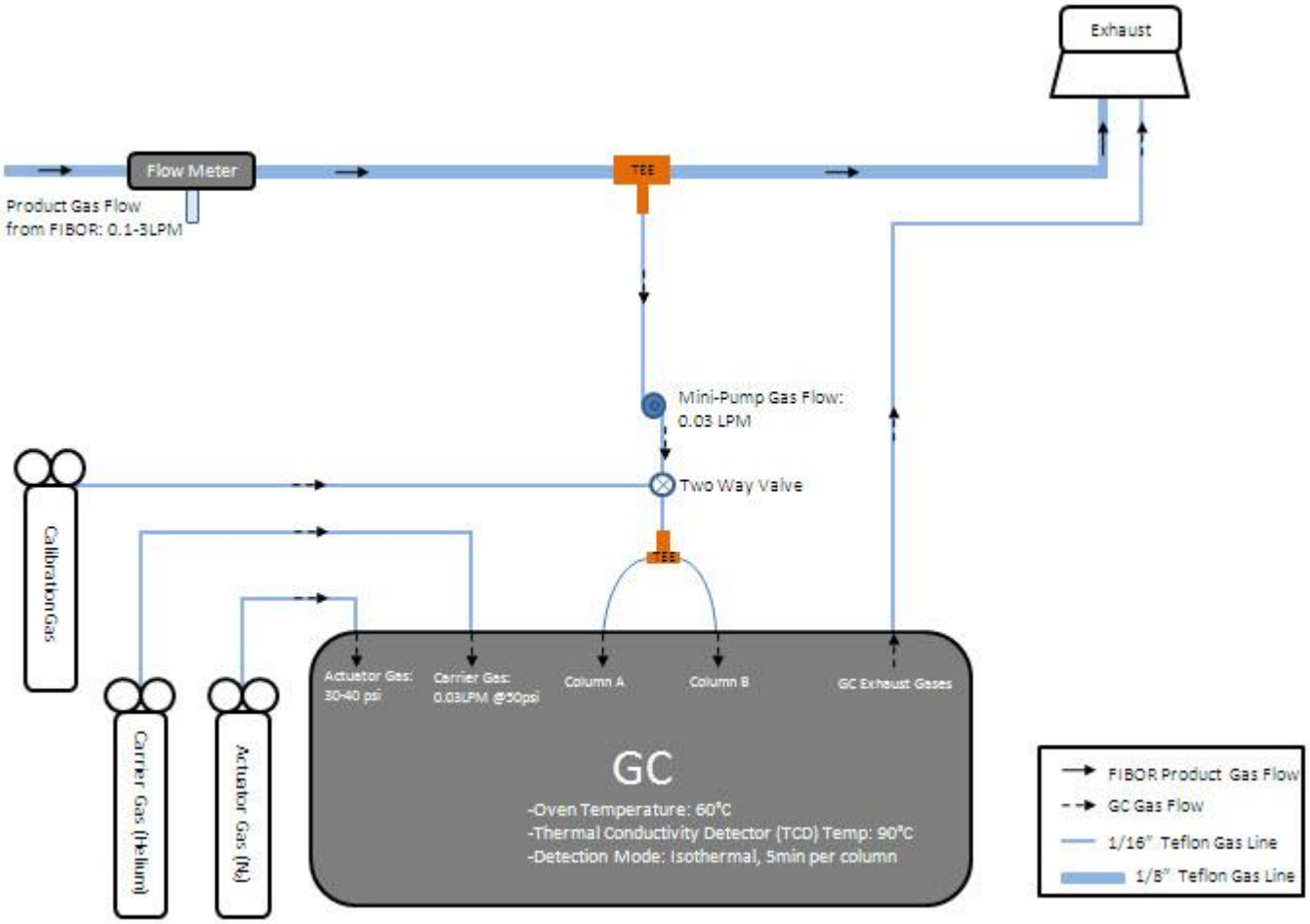

Figure 2.11: GC Configuration

between 0.1-3.0 liters/min (LPM) depending on the operating conditions of the FIBOR (mainly surface temperature and catalyst) that affect the rate of chemical reaction. Downstream of the flow meter, a product gas sample is extracted through a mini-pump set at 0.03 LPM. The relatively small rate of flow induced by the mini-pump prevents disturbance of the flow meter and also entrainment of air at the end of the exhaust line.

The GC is interfaced with data acquisition software (ChromPerfect, version 5.5.4) that is programmed to allow for an automated gas sample injection initiated under control of the user first into Column A, followed by an automatic injection into column B. The injections are timed to precisely correspond with starting the respective gas chromatograms for accurate and repeatable retention times. The actuator gas is compressed nitrogen set at 30-40 psi which provides pneumatic pressure (on a solenoid valve) to activate the gas sample injector valve. The carrier gas is compressed helium with a regulated pressure of 50 psi and a flow rate of 0.03LPM. The standard isothermal GC detection mode is used with a retention time of 5 minutes for each column which is sufficient to detect the species of interest when the column oven temperature is set at 90°C and the filament, or thermal conductivity detector (TCD) is set to 60°C. Although detection of individual species is possible by retention times alone found by reading experimental chromatograms, determining the actual concentration of the product species requires use of a calibration gas of a known composition.

A calibration gas with 50% CO, 35% H_2, 5% CH_4, 4% C_2H_4, 2% C_2H_6, 2% CO_2 and 2% C_2H_2 (Airgas Co.) is used as a comparison to determine the actual concentration of the FIBOR product gas. The chosen mixture concentration is somewhat arbitrary in that only serves as a known reference for analysis. The important aspect is at a minimum to ensure all anticipated species of interest are included. This concentration was chosen as a guess of the actual composition based

on ethylene glycol steam reforming studies (Kechagiopoulos 2007) and preliminary experiments in which relative chromatogram peak signal heights were compared for a rough estimate of relative concentration.

2.3.6 Data Acquisition

Operating parameters include the bulk liquid temperature, immersion heater power supply setting to the bulk liquid, heater tube temperature, power supply settings to the heater tube and product gas flow rates. The bulk liquid temperature is controlled by the manual power setting of the immersion heaters. The immersion heater power setting is manually controlled through an adjustable AC/DC transformer and therefore not an automated setting programmed into the Labview interface. Bulk liquid temperature data are monitored and digitally stored. The heater temperature is user-controlled in the Labview interface by adjusting the voltage difference across the heater tube and thereby the power input from the programmable DC power supply.

Figure 2.12 is a depiction of the Labview interface to show how thermocouple temperature readings, power, voltage, current, and product flow-rates are graphically monitored by the user. Respective column data that is automatically digitally stored includes time, temperature (4 heater tube thermocouples, 1 bulk liquid thermocouple), current, voltage, power and flow rates. The Labview program was modified from the work of Huang (2006) and Appendix C.3 provides further details of the Labview program used in this study.

2.3.7 Catalyst

Two transition metal based catalysts are used in this study, both utilizing an alumina (Al_2O_3) washcoat for adhesion. Applying a consistent and effective coating requires professional techniques and Catacel Corporation (Garrettsville, Ohio)

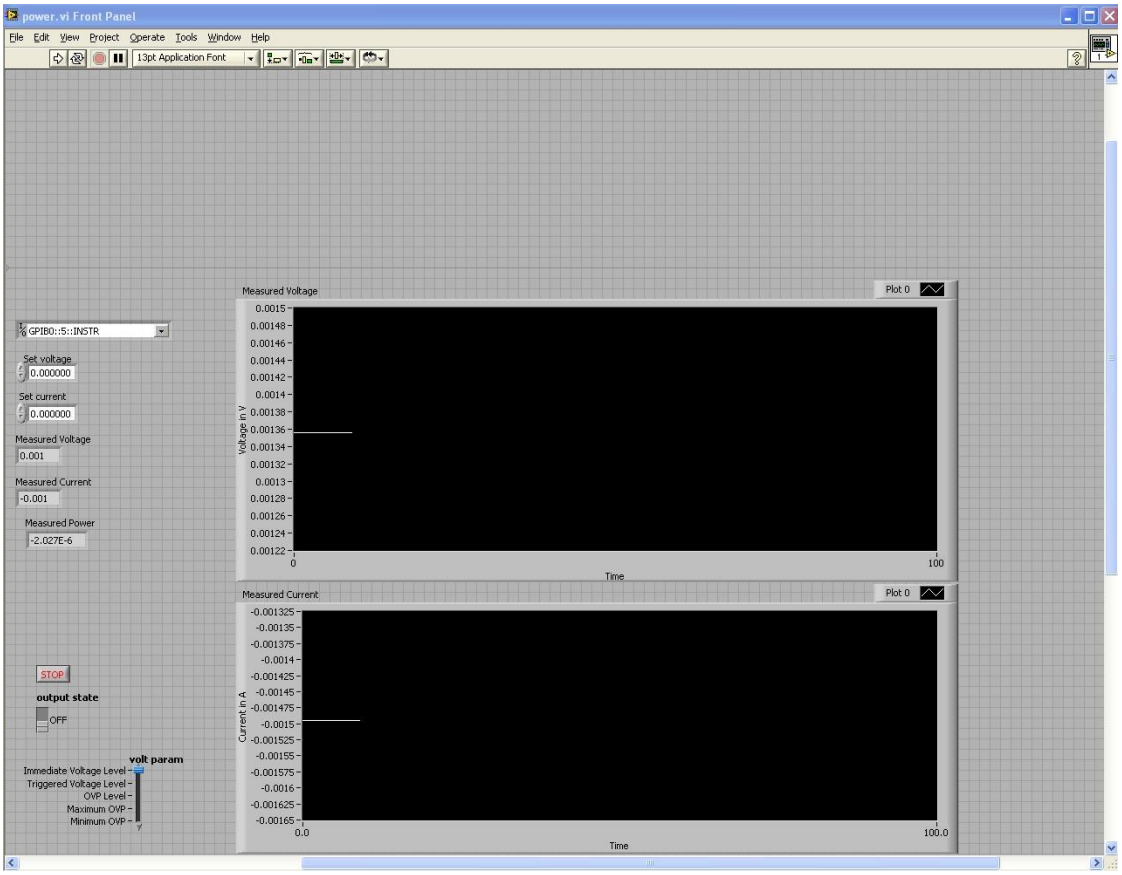

Figure 2.12a: Labview Power Initiation Interface (Power.vi)

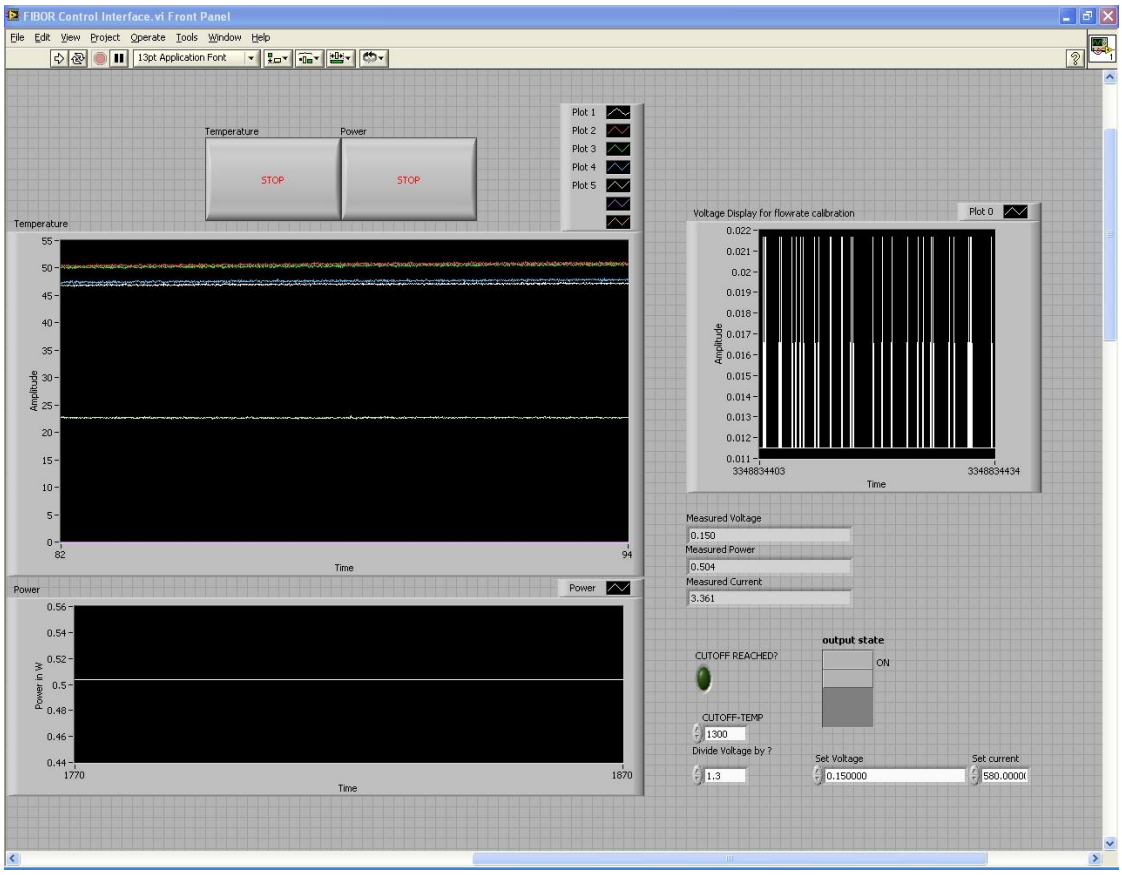

Figure 2.12b: Labview FIBOR User Control Interface (FIBOR Control Interface.vi)

applied the coatings. The general coating procedure includes the following steps:

a) Weigh and record bare heater tube weight. (at a minimum use a 3 place analytical scale)

b) Apply 3 coats of standard 34-08 alumina washcoat calcining each coating at 500°C. Weigh and record weight after each applied coating of alumina.

c) Apply 10 coats of tetraammine platinum hydroxide, or as much that will yield a jet black appearance, calcining between each applied coating at 500°C. Weigh and record weight after each coating of platinum.

d) Repeat same procedure as above for the nickel coated tube, except use nickel nitrate instead of tetraammine platinum hydroxide.

e) The final weight fraction of catalyst/alumina should be approximately 50%.

Table 2.3 provides actual specifications for the catalyst coated heater tubes used in this study (Pt-Tube, Ni-Tube).

2.4 Preliminary Testing

Initial tests are often required to validate a final design based on modeling with possibly over-simplifying assumptions. The purpose of the first preliminary test was

Table 2.3: Catalyst Coating Specifications

Pt Tube			Ni Tube		
	Material	Weight [g]		Material	Weight [g]
Bare Tube	NA	1.1142	Bare Tube	NA	1.1197
Coating-1	Al_2O_3	1.1205	Coating-1	Al_2O_3	1.1300
Coating-2	Al_2O_3	1.1290	Coating-2	Al_2O_3	1.1404
Coating-3	Al_2O_3	1.1404	Coating-3	Al_2O_3	1.1507
Coating-1	Pt	1.1418	Coating-1	Ni	1.1522
Coating-2	Pt	1.1431	Coating-2	Ni	1.1538
Coating-3	Pt	1.1448	Coating-3	Ni	1.1555
Coating-4	Pt	1.1467	Coating-4	Ni	1.1569
Coating-5	Pt	1.1483	Coating-5	Ni	1.1584
Coating-6	Pt	1.1499	Coating-6	Ni	1.1599
Coating-7	Pt	1.1511	Coating-7	Ni	1.1615
Coating-8	Pt	1.1525	Coating-8	Ni	1.1630
Coating-9	Pt	1.1543	Coating-9	Ni	1.1646
Coating-10	Pt	1.1654	Coating-10	Ni	1.1660
Weight Fraction Pt/Al_2O_3		49%	Weight Fraction Ni/Al_2O_3		33%

to check the design results determined in Sections 2.3.1-2.3.3 (Heater Tube Size, Reflux Condensing and Power Supply Requirements). Specific objectives of preliminary testing of mixtures in the FIBOR included the following:

- Achieve film boiling with the heater geometry developed in Section 2.3.1

- Estimate boiling curve data for an aqueous mixture of ethylene glycol (80%EG/20%Water by volume) and compare to pure ethylene glycol. Verify the assumption used in Sections 2.3.2 and 2.3.3 that boiling curve data for pure ethylene glycol can be used to model condensing and power requirements for aqueous mixtures

- Test reflux condensing design to ensure adequate surface area and temperature (Section 2.3.2)

- Check Estimated Power Supply Requirements (Section 2.3.3)

Specifics of this test will not be explained in detail because the final and repeatable experimental procedure was subsequently refined and will be covered in detail in Chapter 3 and Appendix B. Nonetheless, this preliminary test provided surprisingly reliable results despite the somewhat hasty and imprecise approach.

The ethylene glycol aqueous mixture (80%EG/20%Water by volume) was prepared with graduated flasks to +/- 5% accuracy using ethylene glycol (J.T. Baker, 9300-33) and distilled water (Mallinckrodt Chemicals, 6795-10). A bare Inconel 600 heater tube (no catalyst coating) (See Table 2.2) was secured to the electrode buses in a rudimentary fashion since the electrode clamp design had not yet been developed.

No. 8 AWG copper grounding wire and self fastening copper grounding wire clamps, secured the heater tube to existing copper electrode buses (depicted in Figure 2.2(m)). Two thermocouples [Omega, KMQXL-010G-18] were inserted into one side of the heater tube. The first was placed approximately 30 mm from the end (middle of tube) while the second was placed approximately 15mm from the end. Thermocouples were insulated from the inside wall of the electrically conducting heater surface using a ceramic insert. (Omega,ORX-132116) A "cold finger" condenser (Aldrich, Z164038) was utilized to provide for reflux of condensate back into the bulk liquid chamber. A dry-ice/acetone bath was used as a coolant occupying an available cold finger space of 250mm x 80mm (Length x Diameter). A cold trap (Aldrich, Z256870) was placed downstream of the condenser to check for accumulation of condensate which would suggest that the condensing surface area and/or temperature are insufficient.

Figure 2.13 is a photograph taken with a hand-held digital camera of the heater tube arrangement while immersed in the film boiling state. The grounding wire clamps secured the heater tube in place. Although the picture quality is rather poor, closer examination of the bubbling shape around the heater tube provides the first evidence of successful film boiling in the FIBOR for an aqueous mixture of ethylene glycol. The tube is also visibly bent as a result of the high operating temperatures and crude mounting technique.

Figure 2.14 depicts the boiling curve data collected from this preliminary experiment overlaid with the boiling curve of pure ethylene glycol (Choi 2010). The boiling curve of pure ethylene glycol is noticeably higher than that of the mixture. This observation is consistent with literature (Van Stralen et al. 1972; Yue and Weber 1973) that reports the effect of enhanced heat transfer in binary mixtures when

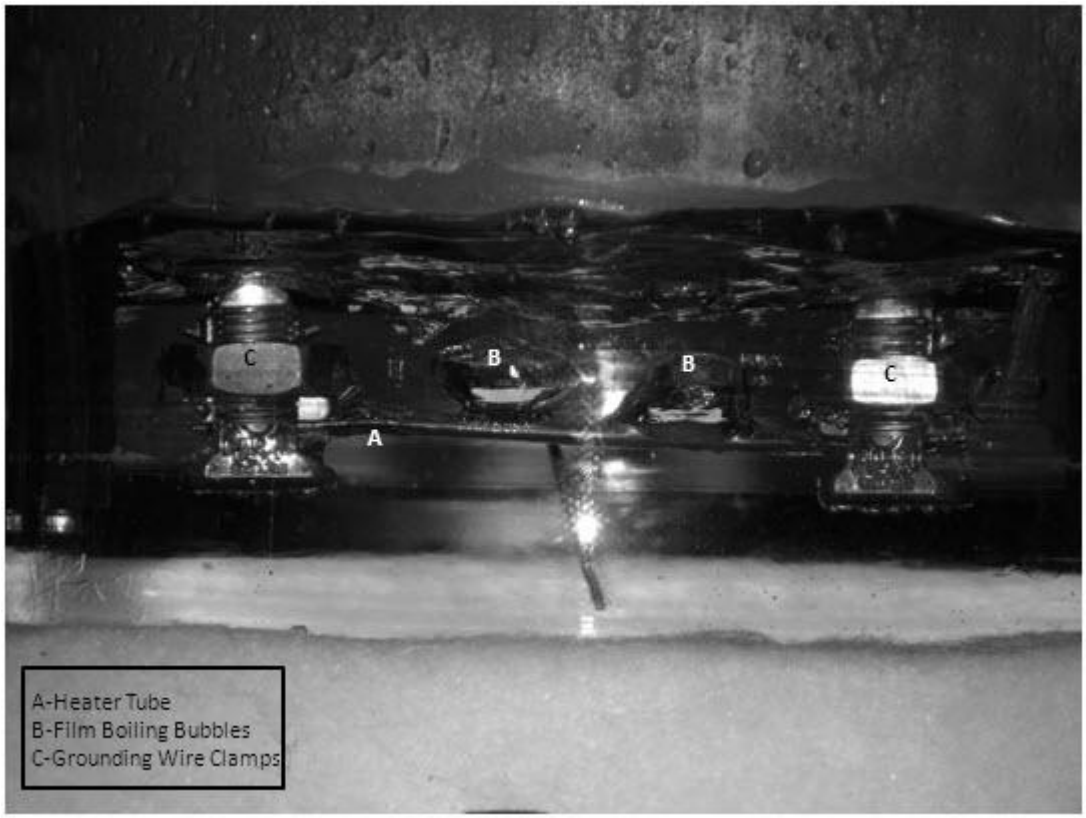

Figure 2.13: FIBOR Preliminary Test, 80/20% EG/Water

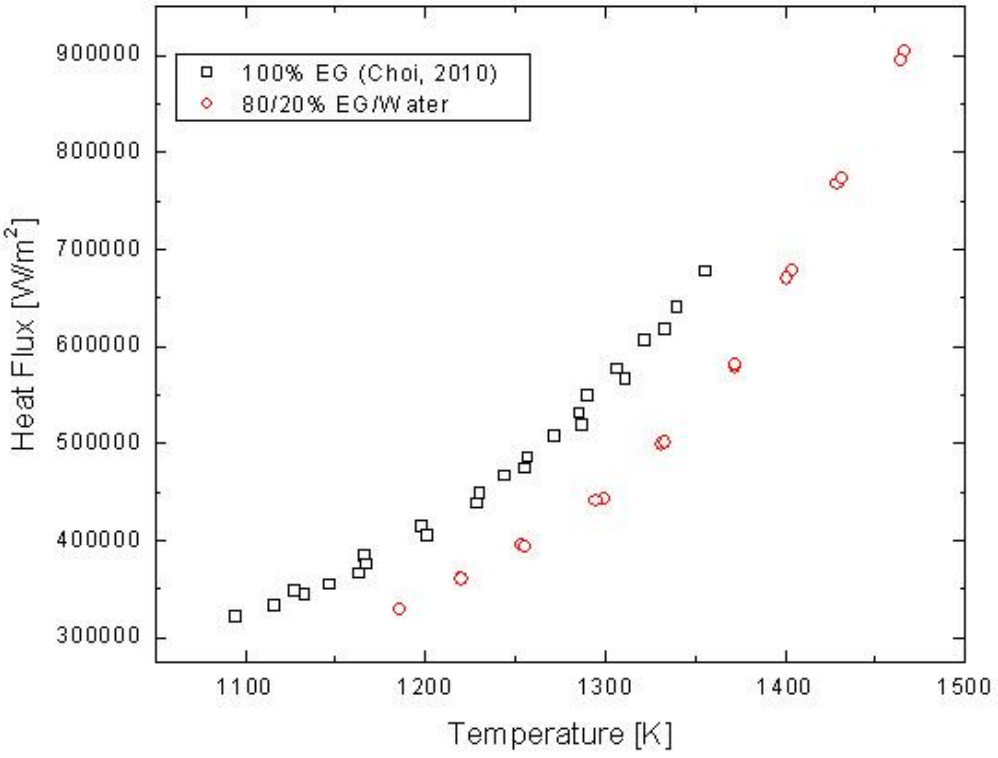

Figure 2.14: Boiling Curve-FIBOR Preliminary Test Results

compared to film boiling the pure, less volatile component (in this case being pure ethylene glycol) alone. Several factors influence this effect, namely local preferential vaporization of the volatile species increases the vapor-liquid interface temperature, which effects the vapor properties and causes conduction heat transfer (and thus reduced overall vaporization into the film) into the bulk. The vapor properties, reduced vaporization and conduction into the bulk all act to enhance the overall heat transfer from the cylinder, thus causing the boiling curve for the binary mixture to be lower than that of the pure, less volatile component.

The boiling curve results in Figure 2.13 show that the assumption used in Sections 3.2.2 and 3.2.3 to model condenser and power supply requirements based on boiling curve data for pure ethylene glycol is both conservative and valid. Specific observations to validate the design included the following: 1) achieving a maximum heater wall temperature of 1473K by applying 3.5V/80A which is well within the available power supply requirements (580A/8V) input power; 2) the bulk liquid temperature remaining at a constant 390K through the length of the experiment (approximately one hour) which is significant because it is consistent with vapor-liquid equilibrium data (Figure 1.2) for an 80% EG/20% Water mixture. It further suggests no composition change as result of preferential vaporization (depletion of water) and no composition change due to chemical reaction; and 3) no condensate forming in the cold trap proving that the chosen condenser size and coolant are sufficient.

2.4 Final Design

The results of the preliminary tests validated the design. Final details will be covered in the next chapter and Appendix B. Table 2.4 provides a component by

Table 2.4: Final Design Material List

Figure 2.2	Description	Brand	Model Name	Vendor	Part Number
a	Bulk Feedstock Reservoir	Nalgene	Nalgene Round Carboy with Spigot, 10L	Sigma-Aldrich	C6692
b	Feedstock Liquid Mixture	J.T. Baker	Ethylene Glycol, 4L	Clarke Hall Chemical Stock Room	9300-33
b	Feedstock Liquid Mixture	Mallinckrodt	Distilled Water, 4L	Clarke Hall Chemical Stock Room	6795-10
c	In-line Peristaltic Pump	Omega	Peristaltic Pump, 750 ml/min, 1/4" Tube	Omega Engineering	FPU-124
d	Pump Mount	Custom Design	Custom Design	Custom Design	Custom Design
e	Feedstock Line	Tygon	Tygon 2075 Tubing (1/4in-ID-3/8in-OD)	Sigma-Aldrich	Z279846
f	2-way Valve	Swagelok	Brass Integral Bonnet Needle Valve	Swagelok	B-1ks6
g,i	Copper Tubing	Bulk	Copper Tubing (3/8in)	Clarke Hall LASSP Machine Shop	TCS10050
g	Heating Tape	Omega	Heating Tape With Adjustable Thermostat	Omega Engineering	HTWAT101-010
h	3-way Valve	Swagelok	Brass 1-Piece 40 Series 3-Way Ball Valve	Swagelok	B-43XS4
j	Immersion Heaters (x4)	Wattco	Immersion Heaters (1/4inx3in-300W)	Wattco	WC20303001
k	Bulk Liquid Reactant Chamber	Custom Design	Custom Design	Custom Design	Custom Design
k	Chamber O-Ring	Viton	Viton O-Ring, Size 362	sealingdevices.com	Viton, Size 362
l	Heater Tube	Inconel 600	See Table 2.2	Microgroup	600F10093X010SL
m	Copper Electrode Buses	Custom Design	Copper Alloy 145, 1/2"-#20 Thread	Tim Brock, Hollister Hall, Cornell	NA
n	Heater Tube Thermocouples (x4)	Omega	Sub-Mini T/C W/Molded Connector	Omega Engineering	KMQXL-010G-18
o	Bulk Liquid Thermocouple	Omega	Sub-Mini T/C W/Molded Connector	Omega Engineering	KMQXL-040E-12
p	Packing Gland	Conax	Feed Through Packing Gland	Conax Technologies	PG2-125-A-T
p	Packing Gland Replacement Seal	Conax	Teflon Packing Gland Seal	Conax Technologies	RS-PG2-125-G
q	Compressed Nitrogen	AirGas	Compressed Nitrogen	AirGas	NA
r	Pressure Gauge w/ Release Valve	USG	30 psi Gauge/6 psi Safety Release Valve	USG	C-PT1X750
s	Redundant Coil Condenser	Aldrich	Aldrich Jacketed Friedrichs Coil Condenser	Sigma-Aldrich	Z517232
s	Cold Finger Condenser	Aldrich	Cold Finger Dry Ice Condenser	Sigma-Aldrich	Z164038
t	Dry-Ice/Acetone Coolant	Mallinckrodt	Acetone, 4L	Clarke Hall Chemical Stock Room	2440-16
t	Dry-Ice/Acetone Coolant	Bulk	Dry Ice, Grinded	Clarke Hall Chemical Stock Room	Bulk
u	Cold Trap	Ace	Ace Vacuum Trap w/ Threaded Inlet/Outlet	Sigma-Aldrich	Z256870
v	Digital Flow Meter	Omega	Mass flow meter with Integral Display	Omega Engineering	FMA-A2309
w	Mini-Pump	Virtual Industries	Mini-Pump, 6 VDC	Virtual Industries, Inc.	VMP1624MM-6-60
x	GC	GOW-MAC	Series 600 GC	GOW-MAC Instrument Co.	600P20015401
y	Carrier/Actuator Gas	AirGas	Carrier-He; Actuator-N (Compressed)	AirGas	NA
y	Calibration Gas	AirGas	50% CO, 35% H_2, 5% CH_4, 4% C_2H_4, 2% C_2H_6, 2% CO_2 and 2% C_2H_2	AirGas	NA
z	Data Acquisition	National Instruments	High Accuracy M Series Multifunction DAQ	National Instruments	NI PCI-6281
z.1	Digital Power Supply	Agilent	System DC Power Supply (580A/8V)	Agilent	34980A
z.2	PC Workstation	Hewlett Packard	HP Compaq w/Microsoft Office, Labview	Hewlett Packard	DC 5000-MT

component listing and description of all materials used for the final design. The numbering of each component corresponds to Figure 2.2 for reference.

CHAPTER 3

EXPERIMENTAL SETUP AND PROCEDURE

3.1 Introduction

In the broadest sense, the underlying purpose of every experiment is to demonstrate the extent that a FIBOR can promote chemical conversion. Even for the case of testing pure water (reported in Appendix F) where no chemical reaction occurs, the overall purpose of conducting the experiment remains unchanged since the boiling curve data are used as a reference for chemical conversion of other liquids or aqueous mixtures. The objectives are a set of more specific tasks to be carried out during the experiment. They provide the building blocks, or data sets, for further analysis. Critical data include: 1) flow rates with respect to wall temperature to give the simplest proof of chemical reaction and its sensitivity to temperature; 2) GC analysis to provide more detailed evidence of individual product species and their concentrations; 3) boiling curve data to reveal the heat required to support the endothermic nature of the chemical reaction mechanism postulated in Chapter 1; 4) high resolution digital photographs to provide further evidence of the film boiling characteristics around a heater tube such as film thickness and bubbling dynamics; and 5) Scanning Electron Microscope (SEM) images and Energy Dispersion X-Ray Spectroscopy (EDS) scans of the coating to illustrate the morphology of the heater surface before and after use, particularly to help characterize the integrity of catalyst coatings.

3.2 Heater Tube and Bulk Liquid Reactant Chamber Assembly

Preparation for an experiment starts with the heater tube. When using a catalyst coated tube, the surface is first characterized through SEM images and EDS

scans. A Leica 440 SEM allows the entire heater tube to be inserted inside as a specimen. At 10KeV, sufficient resolution (~10μm) is achieved to observe the catalyst structure. A special feature of this instrument also allows for electron backscatter (EBS) diffraction to provide information about the surface composition. In this mode, the image's relative contrast relates to the material's average atomic number and provides a qualitative analysis of different elements present at the surface. In order to detect specific elements, a Kevex EDS Detector (7.5μm Beryllium Window) is able to X-ray the surface and produce spectra (Evex Data Acquisition Software) with signals that correspond to specific elements. Again, this instrument provides only a qualitative analysis and is not intended to provide precise surface composition results. Unfortunately this instrument is incapable of detecting carbon.

Following SEM and EDS characterization, four thermocouples (Omega, KMQXL-010G-18) are inserted inside of the heater tube through a ceramic insert (Omega, ORX-132116) that provides electrical insulation between the thermocouples and electrically conducting Inconel surface, while also enhancing axial thermal conduction (thermocouple responsiveness) and preventing the tube from deforming at high operating temperatures. Heater tubes (Microgroup, 600F10093X010SL) are manufactured and cut to length by Microgroup, Inc. (See Table 2.2). Thermocouples are spaced equidistantly between the electrode clamps to verify an axially symmetric temperature profile. Figure 3.1 shows the proper spacing of thermocouples and also a typical temperature distribution during film boiling showing that the surface temperature is nearly constant. The temperature however decreases sharply at the ends of the heater clamps due to conduction heat losses to the electrode clamps.

Silicone sealant is used at the ends of the heater tube (Dow Corning, RTV 736) and on the electrode clamps to prevent liquid penetration. The bulk liquid reactant chamber is assembled with an air-tight seal through use of packing gland (Conax,

PG2-125-AT) feedthroughs for thermocouples and an o-ring (Viton, no. 362) between the glass chamber and heater tube mount. Figure 3.2 is a depiction of the heater tube properly mounted in the bulk liquid reactant chamber. See Appendix B for further details regarding heater tube and bulk liquid reactant chamber assembly.

3.3 Condenser Assembly

Two condensers and one cold trap are installed to ensure all reactant vapors are separated from the product gas flow and returned into the bulk liquid mixture. The condensers mount directly on top of the assembly depicted in Figure 3.2 between the electrode bus terminals. Based on the modeling results of Section 2.3.2 and preliminary testing summarized in Section 2.4, one cold-finger condenser (Sigma-Aldrich, Z164038) with dry-ice/acetone used as a coolant is sufficient to condense all of the anticipated reactant vapors. However at this stage of the FIBOR's design, ensuring complete condensation is more important than optimizing condensing capacity. Therefore a redundant condenser (Sigma-Aldrich, Z517232) that utilizes cold running tap water through its coil design is used in addition to the primary cold finger condenser. The chosen condenser design allows for reflux of all condensate back into the bulk liquid reactant chamber. Sealant [DuPont, Krytox] is used at all condenser fittings to ensure a proper vacuum seal is achieved and to also allow for ease of disassembly.

A cold trap is installed downstream of the condensers in order to visibly verify that all reactant vapors are condensed. The cold trap (Ace Vacuum Trap, Sigma Aldrich Z256870) utilizes ice water as a coolant. Figure 3.3 shows the condenser assembly. When the heater tube is not submerged in the bulk liquid reactant, nitrogen (dotted arrows in Figure 3.3) is passed through the system (0.1 LPM) to eliminate the

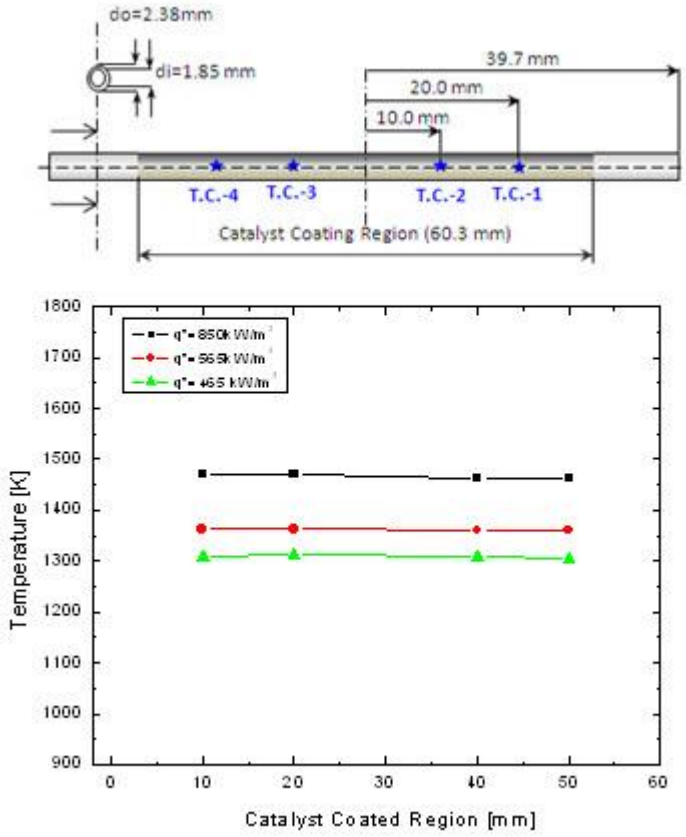

Figure 3.1: Thermocouple Spacing and Temperature Profile

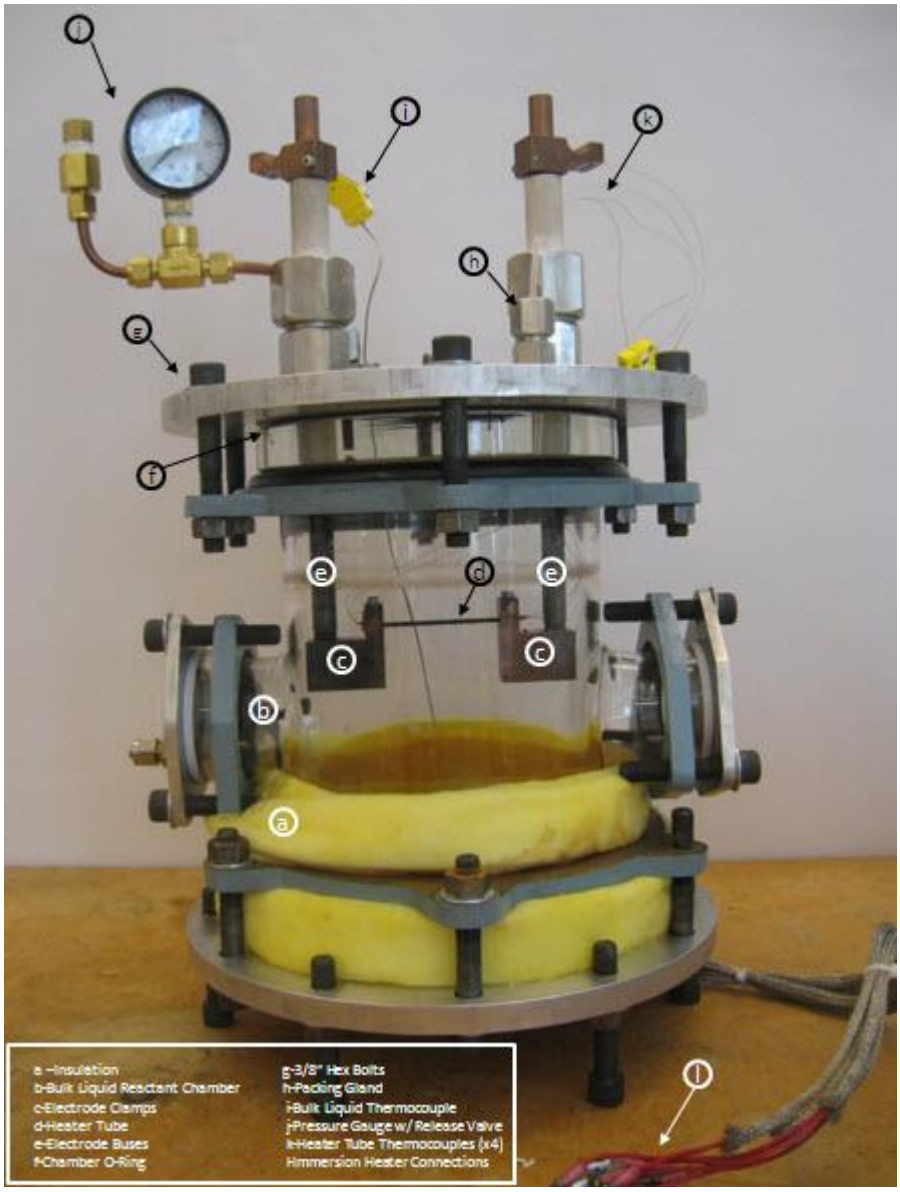

Figure 3.2: Heater Tube Mounted in FIBOR Chamber

possibility of ignition as electrical current passes through the terminals (shown in Figure 3.3-with fixed connection leading to DC power supply). Once the heater tube is submerged and film boiling ensues, the nitrogen is turned off so that the gas flow (dashed arrows) only consists of product species as a result of chemical reaction in the FIBOR. Reactants are condensed (thick arrows) and returned to the bulk liquid reactant as a result of the redundant coil condenser (a) which utilizes cold tap water flow as a coolant depicted by solid arrows and the primary cold finger condenser (b) that utilizes a dry ice/acetone bath coolant. Only product species flow through the cold trap (c) which is submerged in an ice-water bath coolant. Any accumulation of condensate in the cold trap (c) signals insufficient total reflux condensation through (a) and (b) and thus possible bulk liquid reactant composition change as a result of evaporation enriched with steam due to vapor-liquid equilibrium.

The condensing system (Figure 3.3) is checked thoroughly for leaks before each experiment by inspecting each connection as nitrogen flows (10-20psi, ~0.1LPM) through the system. An initial leak check includes comparing the output flow regulator at the compressed cylinder to the digital flow meter, they should match within 0.05 LPM. For a thorough check, each connection is inspected with Snoop Liquid Leak Detector (Swagelok).

3.4 Data Acquisition Testing and GC Setup

Before proceeding further with an experiment, the data acquisition system is first tested. The purpose of this test is to ensure thermocouples work properly, proper electrical contact between the heater tube and electrode clamps and that the data acquisition software in Labview functions properly. A more detailed step by step procedure is given in Appendix B for setting up and launching the Labview program that controls the operating parameters of an experiment. The general steps include the

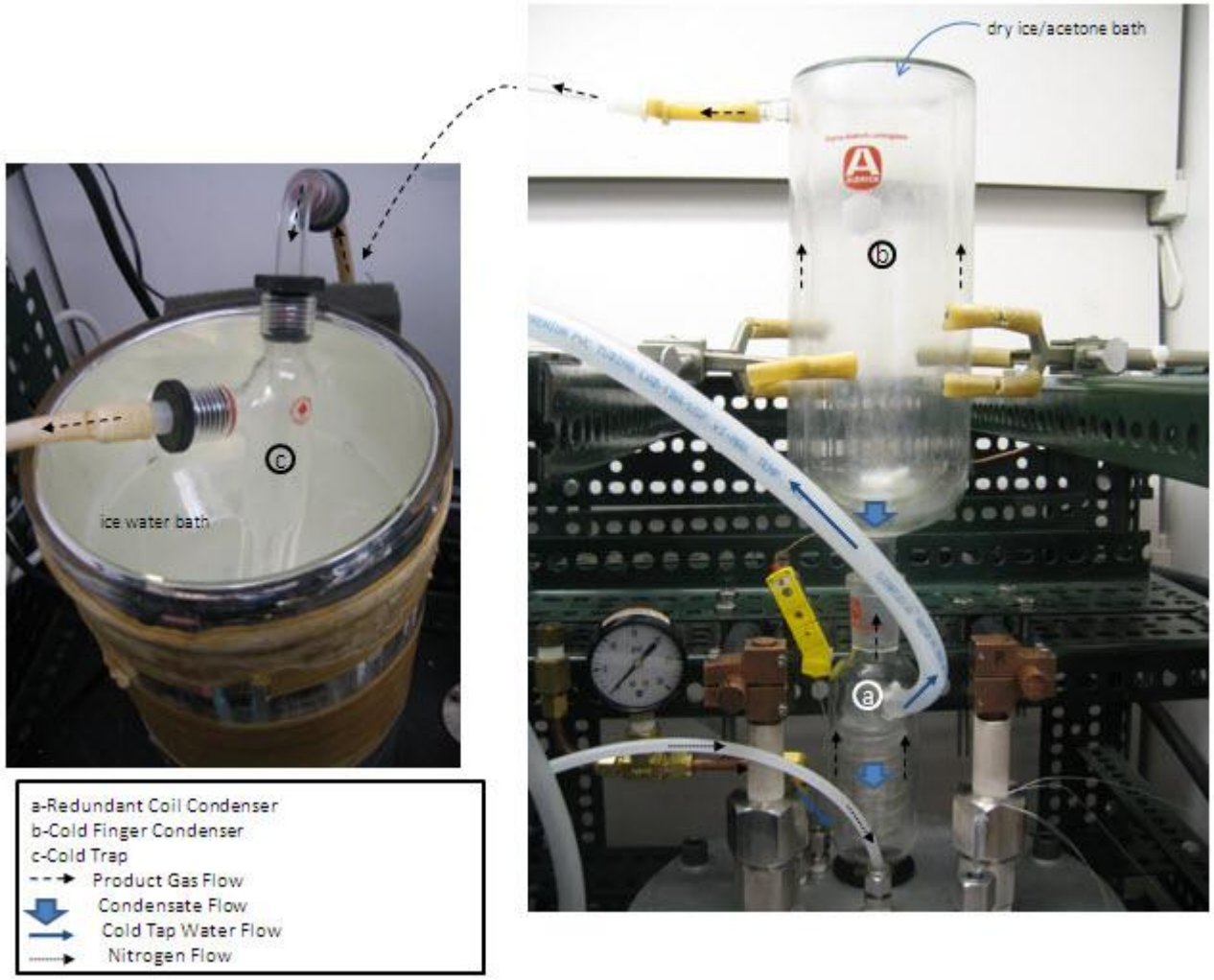

Figure 3.3: Condenser Assembly

following:

- Connect all thermocouples (4 heater tube TC's and 1 bulk liquid TC)
- Power on the Data Acquisition (DAQ) (National Instruments, NI PCI-6281)
- Power on Power Supply (Agilent, 34980A)
- Open Agilent Connection Software in PC, refresh all connections
- Open, start and stop Power Initiation Labview Program (Power.vi; see Figure 2.10)
- Open User Interface Labview Program (FIBOR Control Interface.vi; see Figure 2.10)
- Set "cutoff temperature" to 1300, set "divide voltage by" to 1.3 and set "current" to 580
- Start program by clicking arrow on main toolbar at top of screen
- The time should begin to scroll by giving 5 TC readings. The bulk liquid TC should be slightly lower (1-2 degrees) than the four heater TC readings that are enclosed inside of the tube.
- Apply a small voltage (.1-.2V) to observe heater TC response

If thermocouples are mounted according to Figure 3.1, a symmetrical temperature profile should be displayed. The temperatures of TC#1 and #4 should be within 1-2 degrees, while the temperatures of TC#3 and #4 should also be within 1-2 degrees. Due to conductions losses to the electrode clamps, the temperature reading of TC#1 and #4 should be lower than TC#3 and #4. Figure 3.4 is a typical temperature profile used to validate the data acquisition system before starting an experiment. Data for a bare tube and the platinum coated tube used in this study are provided for reference. A voltage of approximately 0.15V is sufficient to raise the temperature of

the tube and test for a symmetrical profile. The power supplied to the bare tube is slightly higher in Figure 3.1 resulting in a higher temperature for each thermocouple. The catalyst coating also slightly alters the properties of the tube that affect the heat transfer; the electrical resistivity and overall thermal resistance can result in a slightly different temperature profile. A temperature profile similar to that found in Figure 3.4 validates that the DAQ system is working properly and subsequent experimental preparation steps can continue.

The GC is pre-programmed and configured to minimize setup time during an experiment. Details regarding additional capabilities of the GC can be found in the Series 600 Gas Chromatograph User's Manual (GOW-MAC, 2006). Three separate gas flows must first be connected to the GC (see Figures 2.9 and B.9 for additional details). The actuator gas (compressed Nitrogen, 20-30psi) serves to pressurize the solenoid inside of the GC which physically controls the injection of the sample gas into the column(s). The carrier gas (compressed Helium, 40-50psi, 30CCM) provides a constant flow through the column(s) and carries the product species of interest with it. The sample gas consists of either the actual FIBOR product gas or a calibration gas. The FIBOR gas sample is extracted from the actual product gas flow during an experiment through a mini-pump (Virtual Industries, VMP1624MM-6-60) set at 30CCM (See Figure 2.9 and B.7). After the experiment is complete, the direction of the two-way valve (Figure 2.9 and B.9) is changed so that a calibration gas (10psi/30CCM) with a known composition can be analyzed for comparative analysis. Once all three gas lines are connected, the GC is powered on.

The GC's settings are adjusted from the keypad on the front of the instrument. Figure 3.5 is a depiction of the "Home Page" that the GC displays by default after it powers on and also from which all commands start from. The GC automatically heats

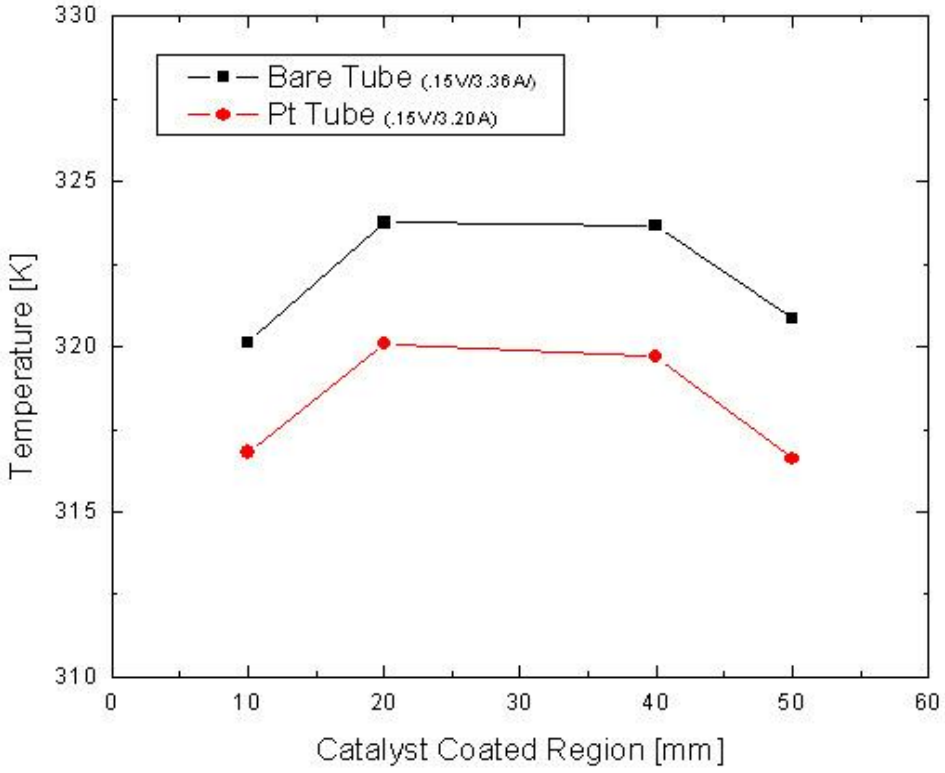

Figure 3.4: DAQ Testing

the column oven to 70°C and the TCD to 110°C which is programmed into a "method file" and is activated from the keypad. Detailed steps are included in Appendix B.3.4. The GC is also equipped with ChromPerfect data acquisition software that provides automated user control of the GC during experiments along with chromatogram retrieval and analysis tools. Detailed steps for opening and setting up the software are included in Appendix B.3.4. Once the column oven and TCD are heated to the temperatures specified in the method file, the GC is ready to inject and analyze a sample. Samples are injected on command by the user through the ChromPerfect Software. The first sample is injected into Column A. After five minutes, a second sample is injected automatically into column B. The chromatogram is automatically displayed and saved to the hard drive once the run is complete (after ~10min).

3.5 Quenching Method to Attain Film Boiling (FIBOR) and Data Collection

The quenching method developed by Choi (2010) and further refined in this study is perhaps the most critical step to a successful FIBOR experiment. Transition from nucleate boiling directly to film boiling (Figure 1.1) is difficult to traverse since the film boiling temperature that corresponds with the CHF is often close to or higher than the heater tube material's melting point. It is especially important to minimize liquid contact on the catalyst tube (this is not an issue for a bare tube) as such contact could deactivate the catalyst. These challenges motivated the development of a quenching method which minimizes liquid contact with the heater surface. Although possible with one user, this step is much easier and performed safer with two.

Before entraining any mixture into the bulk liquid reactant chamber, for safety nitrogen flow is activated through the system (10-20psi, ~0.1LPM) as noted previously. The heater tube's temperature is then raised 50-100K above ethylene glycol's boiling point (470K).

Figure 3.5: GOW-MAC Series 600 GC Key Pad

This prevents unintentional liquid/surface contact from inadvertent bubbling/splashing due to air pockets in the feedstock line as the mixture enters.

Figure 3.6 shows the steps during the quenching procedure. The liquid level is first brought to approximately 15mm (Figure 3.5a) below the heater tube by ensuring appropriate valves are manually opened and controlled (Figure 2.2a-h). The immersion heaters are then turned on to full power until the bulk liquid temperature reaches saturation according to Figure 1.2. (Quenching below the saturation point (sub cooled liquid) requires additional heat input due to conduction losses to the bulk liquid and thus possible collapse of film boiling) As the bulk liquid reaches its saturation point, the heater tube temperature is raised to approximately 1100K. This temperature is chosen based on several trial and error attempts until a high enough temperature is found. Theoretically, the initial heater temperature should only need to be above the Leidenfrost point, or minimum film boiling temperature (point C, Figure 1.1). The liquid level is then raised (Figure 3.5b) by opening the two way valve (Figure 2.2f). Once the liquid level reaches the heater surface, or as soon as the user sees an abrupt decrease in heater temperature (Labview User Interface), the voltage is doubled (power increased by a factor of 4) for a bare tube or tripled (power increased by a factor of 9) for a catalyst coated tube. As the liquid level rises and film boiling develops around the tube, all thermocouple temperature readings abruptly increase approximately 200K and reach a steady, uniform temperature along the length of the tube. The liquid level is then increased to approximately 25mm above the heater surface (Figure 3.5c) and experimental data can now be collected. Data is now collected for the film boiling curve by either increasing or decreasing the power input in small increments from the initial increase (4x for bare tube or 9x for catalyst) which

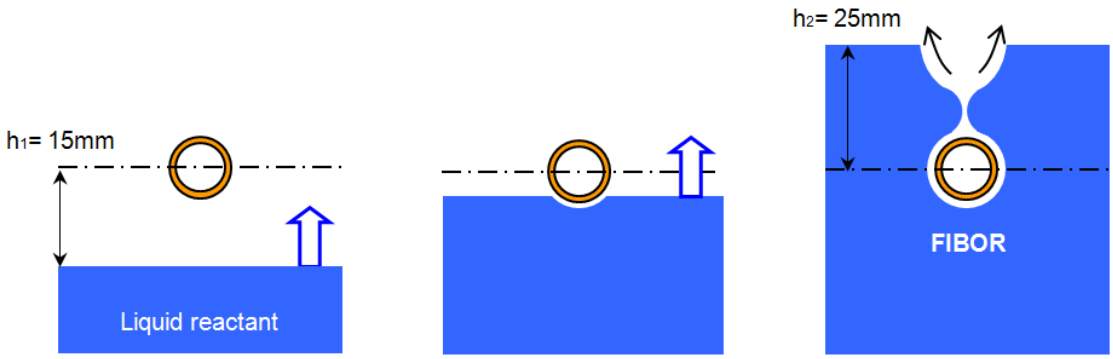

Figure 3.6: Quenching Method

also increases/decreases the wall temperature. This method has proven to be an effective and consistent means to achieve film boiling.

Data are collected by traversing the film boiling curve (C-D in Figure 1.1) by adjusting the power input into the tube. Data (thermocouple temperatures, flow rates, current, voltage, power and time are displayed on the Labview interface) are automatically stored as individual column data files. After immersion, the initial tube temperature is approximately 1300K. Power input is then changed by increments of 0.02V or approximately 0.5W, allowing sufficient time (2-3 minutes) for the heater temperature to reach steady state. This method is followed until a wall temperature of approximately 1500K is reached.

For a bare heater tube, the same method is used to decrease the wall temperature in a reverse manner until film boiling collapses corresponding to the Leidenfrost temperature. For a catalyst coated tube, film boiling collapse should be avoided to prevent liquid contact which could degrade the catalyst coating. Another consideration for catalytic testing is to conduct endurance tests in order to characterize the catalyst. Power input is fixed for a prolonged period of time. Endurance tests for this study are conducted for three hours while holding a constant power input to maintain wall temperatures of approximately 1370K and 1470K respectively. Product flow rates-evidence of chemical reaction, can be visually observed by the digital display on the flow meter and are automatically stored for later analysis. At a given temperature, a sample is injected for analysis into the GC by following the steps in Appendix B.3.4.

CHAPTER 4

DATA ORGANIZATION AND ANALYSIS

The objective of organizing raw data collected during experiments is to generate three important figures that with further analysis can measure the extent of chemical conversion in the FIBOR: 1) the volumetric flow rate of product species with respect to wall temperature, or the "flow rate curve;" 2) the applied heat flux with respect to wall temperature, or the boiling curve, and; 3) the chromatogram, showing product compositions. The chromatogram's peaks reveal individual chemical species. The integrated areas under the peaks relate to concentration.

Chromatograms generated from analyzing a FIBOR gas sample are compared to chromatograms from a calibration gas sample. This analysis serves to verify both the presence and concentration of individual species in the FIBOR gas stream. The organization and analysis of raw data require significant computation in Matlab and Excel, advanced data plotting and statistical analysis in OriginPro, and chromatogram analysis with ChromPerfect software. The remainder of this chapter describes the detailed steps of organizing raw data and analyzing the extent that the FIBOR can promote chemical conversion.

4.1 Data Organization

The time intervals at which acquired temperature data, flow rate data and power setting data obtained is different. Temperature and flow rate data are acquired and stored simultaneously approximately every 0.03 seconds. Power data (voltage, current and power) are stored at a different time interval of approximately every 0.13 seconds. A common time scale must be developed to synchronize the large volumes of temperature, flow rate and power setting data.

4.1.1 Correlating Temperature and Power Time Scales

Raw column data files (TEMPERATURES.lvm, time.lvm, flowrates.lvm, voltage.lvm, POWER.lvm and current.lvm) are stored on the workstation PC and saved to a separate folder after an experiment. (See Appendix B.3.6) Data files are first opened with Notepad++ software then copied into OriginPro 7. Notepad++ is useful because of its capability to handle large volumes of data that can be conveniently selected, copied and pasted. OriginPro is also used because of its ability to handle large volumes of data yet also provides advanced plotting and statistical analysis tools.

Data organization starts with plotting raw temperature (TEMPERATURES.lvm) data versus time (time.lvm) data and power data vs. row number. The following steps cover inserting row number data along with steps to create general plots in OriginPro :

- right click raw data (.lvm) file and select “edit with Notepad++”
- right click column, select “select all,” right click again and select “copy”
- open OriginPro, right click the first cell of desired column to place data in, and select “paste”
- to create a new column, right click the top of the column (gray cell) and select “insert.” A new column is created to the right of the column selected.
- before plotting data, ensure the respective column is designated as “X” for x-axis and “Y” for y-axis by double clicking the top of the column (gray cell)

- select the columns by clicking the top of the column (gray cell), right click, then select plot (several options are given e.g. line, scatter etc.)

- to create row number data, select the cell after the last corresponding data point, right click and select "Set as End"

- select the entire column, right click and select "Fill Column with Row Numbers"

Figure 4.1 is a sample data set that shows raw temperature data plotted against time and power versus row number. In order to create a corresponding time scale for the power data, known reference points (x_1, y_1, x_2, y_2) must be identified. These points are selected because they are distinguishable points in the experiment that occurred simultaneously. The first points (1-subscript) are known to occur simultaneously because this is when the heater tube is first quenched into the liquid reactant. At this moment during the experiment, the power is instantaneously surged with a corresponding abrupt increase in temperature. The second points (2-subscript) are known to occur simultaneously just before the maximum power input, along with corresponding maximum temperature, is decreased. (Another option for selecting a known point is the final data point in the experiment.) With the four known points depicted in Figure 4.1, the following two equations can be readily solved for the linear parameters, a and b, which further allows time data to be created from linear interpolation.

$$y_1 = ax_1 + b \qquad 4.1$$

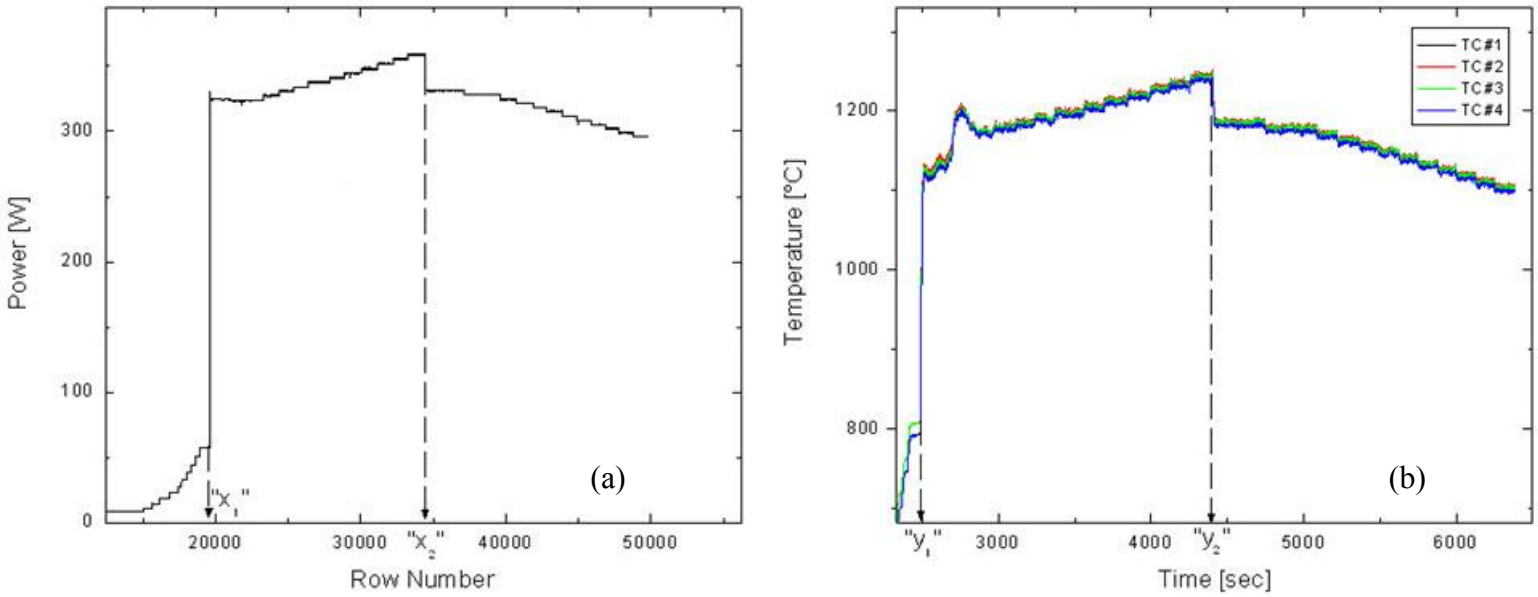

Figure 4.1: Correlating Temperature and Power Time Scales

$$y_2 = ax_2 + b \tag{4.2}$$

With a and b solved, time data are created through the computational Matlab code found in Appendix C.4.1 and further used to plot corresponding power setting data (power, current and voltage).

4.1.2 Flow Rate vs. Wall Temperature (Flow Rate Curve)

The acquired raw data requires a calibration factor to represent the actual flow rate. Raw flow rate data voltage outputs acquired from the digital flow meter must be converted to the actual volumetric flow rate value. This is accomplished by calibrating the digital flow meter with a DryCal flow meter (Definer 220) that obtains volumetric readings as a result of its frictionless piston technology. The work of Hsueh (2007) for a 66.6%-H_2, 33.3%-CO gas mixture verified a linear trend of the following form:

$$F(V) = 2352.85V - 169.96 \tag{4.3}$$

with F representing the actual volumetric flow rate (mL/min) and V representing the voltage (V) reading from the digital flow meter (Omega FMA-A2309) used in the experimental apparatus.

This result was verified (Figure 4.2) for a 66.6%-H_2, 33.3%-CO gas mixture (Calibration Gas #1), along with a second calibration mixture containing 35%-H_2, 50%- CO, 5%-CH_4, 2%- CO_2, 2%-C_2H_2, 4%-C_2H_4 and 2%-C_2H_6 (Calibration Gas #2). Results for N_2 are also presented for reference. Although repeatable results for Calibration Gas #1 (66.6%-H_2, 33.3%-CO) and Hsueh's (2007) data were achieved,

the Calibration Gas #2 showed a distinctly lower linear trend as a result of a different density. In order to report results as accurately as possible, raw flow rate data that most closely matches the composition of the first calibration mixture is converted to a volumetric basis using Equation 4.3. This applies to all catalytic conversion data (See Table 5.2). The remainder of the data, which includes results for thermal decomposition using a bare tube, uses the following correlation (determined from Calibration Gas #2) to convert voltage readings from the digital flow meter to an actual volumetric flow rate:

$$F(V) = 1939.93V + 81.15 \qquad 4.4$$

The flow rate curves reported in this study depict representative results across the FIBOR's operational domain. The most precise technique however would be to first determine the product composition after each experiment using gas chromatography techniques covered in Section 4.3. Based on these results, a separate gas mixture should then be prepared/ordered that matches the exact composition for a given experiment. The digital flow meter results would then be calibrated with the exact measured composition after each experiment to yield the most accurate results. Disadvantages of this technique however would be the significant addition of time, added cost to the experiment and likely overall negligible differences in terms of the resulting flow rate curves.

With a flow rate calibration correlation known, raw data is organized resulting in the flow rate curve. Raw data files (TEMPERATURES.lvm, flowrates.lvm and time.lvm) are first transferred (copy, paste) into the Matlab working directory. The Matlab code (Appendix C.4.2) is then run to retrieve the actual flow rate data normalized by the heater surface area. It is convenient to first plot the flow rate versus

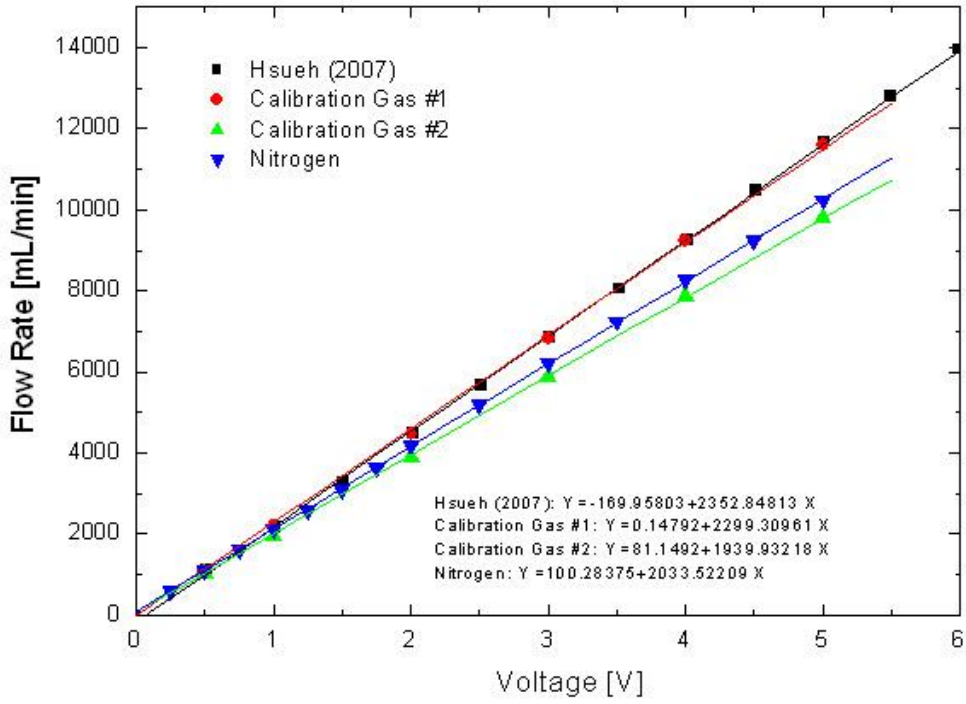

Figure 4.2: Digital Flow Meter Calibration

time in order to easily identify the portion of data to be analyzed. For example, data that is recorded before immersion and when the nitrogen supply is turned on should be neglected. Temperature data is averaged based on the assumption of a constant axial temperature (See Figure 3.1) and converted to Kelvin with the Matlab code in Appendix C.4.3. The resulting exported flow rate and average temperature data is then plotted to generate the flow rate curve.

Noticeable noise is generated during collection of flow rate data. This is likely due to both the bubbling dynamics as gases are expelled from the bulk liquid as well as the flow meter's error (+/- 0.1LPM). Statistical averaging assists with reducing noise for easier analysis. This motivated the development of a program (See Appendix C.4.5) that determines the mean values for a given temperature interval. Figure 4.3 is a sample analyzed data set. The left figure (4.3a) is the raw data of ethylene glycol thermal decomposition. Figure 4.3b shows the mean data for a 1 degree temperature interval, along with a polynomial fit to show the flow rate's dependence on temperature. The polynomial fit is applied to the raw data and overlaid with the mean data to validate the accuracy of the program (Appendix C.4.5).

Also shown are the standard deviations for all raw data points for a 1 degree interval to provide insight into the overall data dispersion (or fluctuations). All data sets are presented in this manner in Appendix E.

4.2 Applied Heat Flux vs. Wall Temperature (Boiling Curve)

The boiling curve captures the physics (boiling heat transfer) of the FIBOR. Boiling curve data is useful because it can be used to estimate how much heat (power) is required to achieve film boiling for a given application. It is also useful to isolate the heat for chemical reaction. Boiling curves with little or no chemical reaction (bare tube, thermal decomposition) are compared to boiling curves with significant chemical

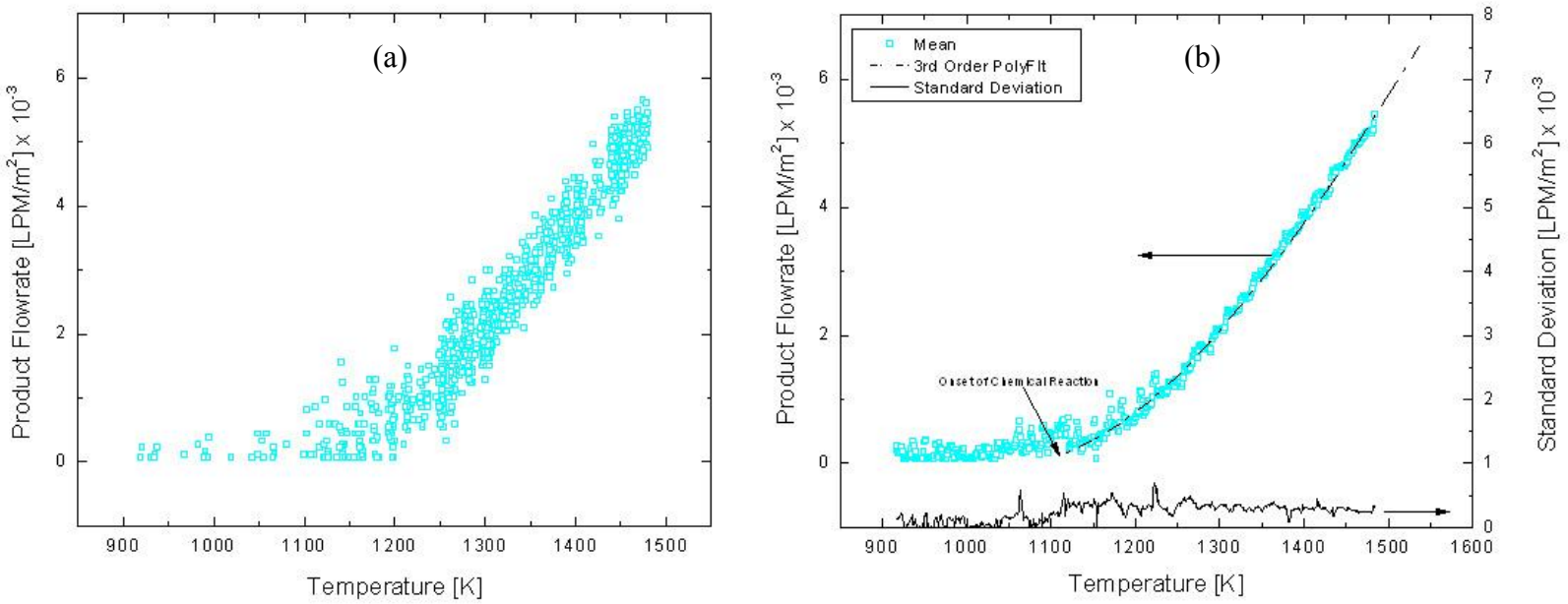

Figure 4.3: (a) Example raw data product flow rate curve plot and (b) corresponding mean and standard deviation for all measurements within a 1 degree [K] interval. A curve fit (3rd order polynomial) is extended to zero to estimate the onset of chemical reaction.

reaction (catalyst coated tube). The difference between the curves at a given temperature is representative of the additional heat required to support the chemical reaction (proportional to the heat of reaction, $\Delta h°$). The heat of reaction can readily be determined by the difference in tabulated enthalpy between the products and reactants at a given reference temperature for any chemical reaction.

Relatively little is known regarding the FIBOR's complete set of chemical reactions, or chemical mechanism. Numerous reactions are likely to occur simultaneously inside of the FIBOR, with one dominant reaction pathway and numerous secondary reactions. The heat consumed by the dominant endothermic reaction is also likely to be large compared to the heat consumed by secondary reactions. Thus the boiling curve can provide an indication of whether the overall chemical mechanism is endothermic (or exothermic), how much heat is consumed due to chemical reactions alone and finally suggest a dominant chemical reaction pathway.

4.2.1 Proof that Axial Conduction is Negligible

By inspection, the nearly constant axial temperature profile in Figure 3.1 suggests minimal axial conduction heat loss. A derivation follows that solves for the radial conduction heat flux while also accounting for axial conduction. Substituting experimental data reveals that axial conduction can in fact be neglected.

The heat flux depicted by the boiling curve for the case of a cylindrical FIBOR represents heat transfer via radial conduction from the heater surface into the vapor film/bulk liquid. Figure 4.3 is a drawing (not to scale) that shows the modes of heat transfer for the case of an electrically heated (joule heating) Inconel 600 tube. The red dotted lines, bounding the inside surface of the Inconel heater material and the outside of the vapor film, represents the control volume used for an energy balance

analysis. The side view (left) shows the spacing of thermocouples along with the heat which is transported in three directions-the outward radial direction (thick red arrow, $q_r^{"}$), and also axially out each end of the tube (small red arrows, $q_{left}^{"}, q_{right}^{"}$). Also shown is the cross section view (right) that shows the dimensions of the heater tube assembly along with the direction of the radial heat flux (axial heat flux is directed into and out of the page). Below each drawing is a qualitative sketch of the temperature profile. The left shows how the temperature varies in the axial direction (also depicted in Figure 3.1 by actual data), while the right shows the radial direction.

An energy balance on the heater reveals that the generated heat flux (I^2R) must balance with the sum of the radial and axial heat fluxes. Symbolically, this can be represented as,

$$q_{gen} = q_r^{"}\pi d_i 2L + \frac{\pi d_i^2}{4}\left(q_{x,left}^{"} + q_{x,right}^{"}\right) \tag{4.5}$$

where,

$$q_{gen} = I^2 R \tag{4.6}$$

and from Equation 2.1

$$R = \frac{8\rho L}{\pi\left(d_i^2 - d_c^2\right)} \tag{4.7}$$

since,

$$q_x^{"} = -k\frac{dT}{dx} \quad \text{and} \quad q_r^{"} = -k\frac{dT}{dr} \tag{4.8}$$

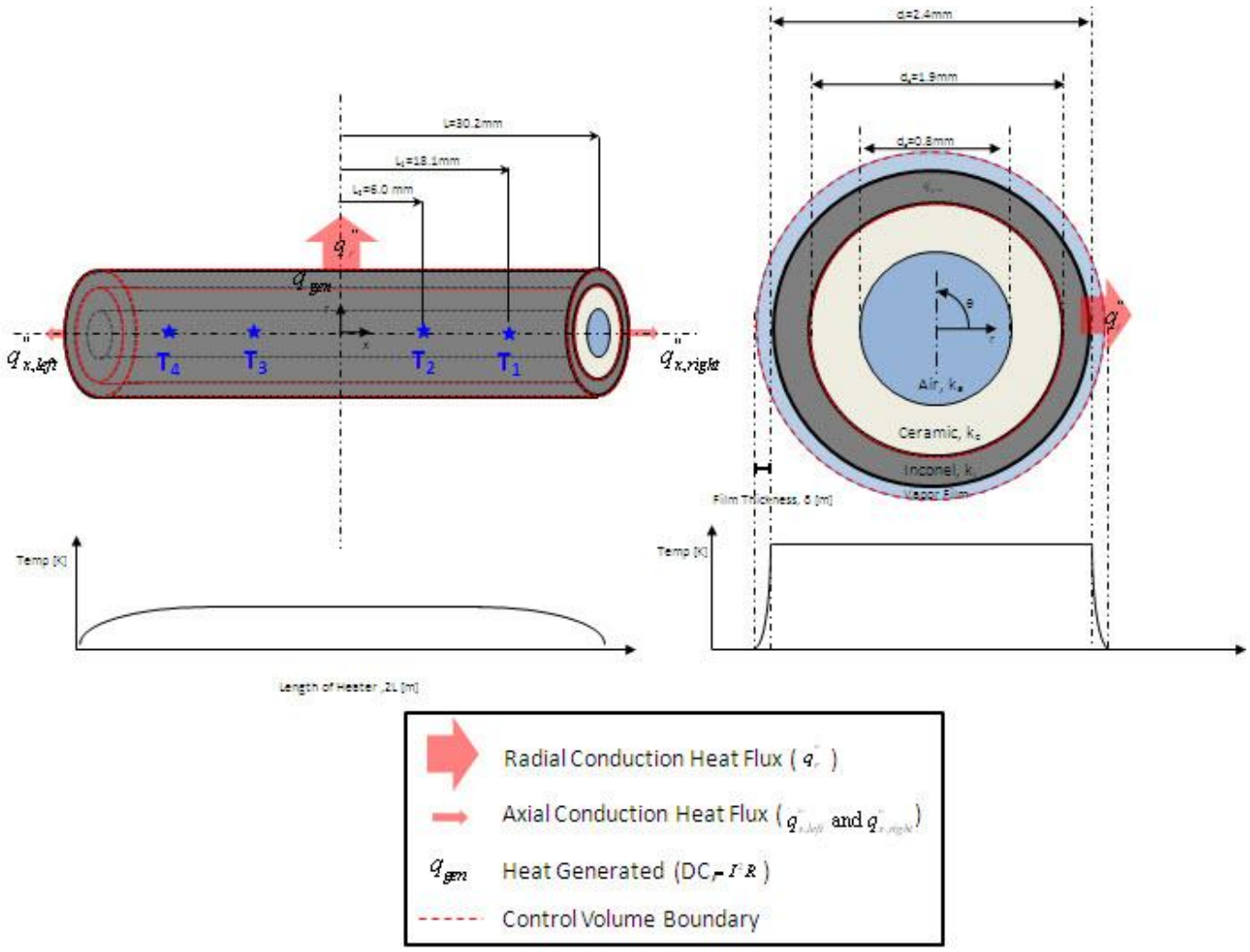

Figure 4.4: Heater Tube Energy Balance Analysis

$$q''_{x,left} = k\frac{dT}{dx} = k\left(\frac{\frac{T_3+T_2}{2}-T_4}{L_1}\right) \quad 4.9$$

$$q''_{x,right} = k\frac{dT}{dx} = k\left(\frac{\frac{T_3+T_2}{2}-T_1}{L_1}\right) \quad 4.10$$

Equations 4.6-4.10 allow Equation 4.5 to be re-written as,

$$\left(\frac{8\rho L}{\pi\left(d_i^2-d_c^2\right)}\right)I^2 = q''_r\pi d_i 2L + \pi\left[k_i\left(d_i^2-d_c^2\right)+k_c\left(d_c^2-d_a^2\right)+k_a d_a^2\right]\left[\left(\frac{\frac{T_3+T_2}{2}-T_1}{4L_1}\right)+\left(\frac{\frac{T_3+T_2}{2}-T_4}{4L_1}\right)\right] \quad 4.11$$

Rearranging Equation 4.11 and solving for q''_r,

$$q''_r = \underbrace{\frac{4\rho I^2}{\pi^2 d_i\left(d_i^2-d_c^2\right)}}_{\text{Heat Generation Contribution}} - \underbrace{\frac{\left(k_i\left(d_i^2-d_c^2\right)+k_c\left(d_c^2-d_a^2\right)+k_a d_a^2\right)\left(T_3+T_2-T_1-T_4\right)}{8d_i L L_1}}_{\text{Heat Loss Due to Axial Conduction}} \quad 4.12$$

The heat flux for the boiling curve can now be solved. All information on the right hand side of Equation 4.12 is known. The current (I) and corresponding temperatures (T_1-T_4) are raw data outputs retrieved from the experiment (See Section 4.1.1, TEMPERATURES.lvm and current.lvm). The geometry (d_i, d_c, d_a, L, L_1) is of course known and remains unchanged for each experiment. The resistivity (ρ) is determined from Equation 2.2 using a 6th order polynomial where the temperature (T) is the average of the 4 temperatures measured by thermocouples (T_1-T_4).

It turns out that the axial conduction term in Equation 4.12 contributes a very small amount, or just under 0.1% of the total heat flux (See Appendix C.4.4) for

experimental measurements. This value however is likely slightly higher since the temperature is known to drop at the ends of the heater tube and thermocouples are not placed there to verify. Appendix G provides an additional proof that axial conduction is negligible for the worst case scenario such that the ends of the heater tube (Figure 4.4) are at the liquid saturation temperature as a result of partial nucleate boiling.

In order to create boiling curves, the heat flux (Equation 4.12) is plotted versus the average wall temperature (T_1-T_4). Appendix C.4.4 provides details regarding the computation of the boiling curve using Excel software and Figure F.1 depicts the complete boiling curves for pure ethylene glycol, aqueous mixtures and pure water.

4.2.2 Correction for Thermocouple Measurements

At steady state, the temperature within the heater assembly (r < 0.95mm, ceramic insert, air) is constant. This can be readily shown by solving the heat diffusion equation. For steady state, uniform generation and constant properties, the heat diffusion equation considering the axial and radial directions is,

$$\frac{\partial^2 T}{\partial X^2}+\frac{1}{r}\frac{\partial}{\partial r}\left(r\frac{\partial T}{\partial r}\right)+\frac{\dot{q}}{k}=0 \qquad 4.13$$

We showed in the previous section that axial conduction is negligible ($\frac{\partial^2 T}{\partial X^2}=0$). Within the center region of the tube that occupies the space for the ceramic insert and thermocouples, no heat is generated ($\dot{q}=0$). Therefore Equation 4.13 can be simplified to,

$$\frac{1}{r}\frac{\partial}{\partial r}\left(r\frac{\partial T}{\partial r}\right)=0 \qquad 4.14$$

Integrating Equation 4.14 twice, the general solution is

$$T(r) = C_1 \ln r + C_2 \tag{4.15}$$

At r = 0, the solution must be bounded. Therefore $C_1 = 0$ and the temperature in the radial direction inside of the heater tube is shown to be uniform.

The temperature across the heater surface in the radial direction is also assumed to be constant and thus equal to the temperature monitored by thermocouples inserted within the air space inside of the heater assembly. Since the heater wall thickness is so small relative to its length in addition to Inconel's thermal conductivity (27.5 W/m·K), this assumption is reasonable by inspection. However this is verified by also solving the heat diffusion equation with respect to a control volume bounding the cross section of the heater material. However in this case a source terms exists since there is heat generation due to joule heating,

$$\frac{1}{r}\frac{d}{dr}\left(r\frac{dT}{dr}\right) + \frac{\dot{q}}{k} = 0 \tag{4.16}$$

Integrating twice, the general solution is,

$$T(r) = \frac{-\dot{q}r^2}{4k} + C_1 \ln r + C_2 \tag{4.17}$$

In order to test the assumption that the temperature drop across the heater wall thickness is negligible, typical experimental data is used to identify the needed boundary conditions to solve for the constants of integration for Equation 4.17. For example, typical boiling curve data for pure ethylene glycol reveals a wall temperature equal to 1280K at a corresponding applied heat flux of 511,194 W/m^2 (See Appendix

F). The problem is now fully defined assuming no radiation effects, uniform heat generation (1.38×10^8 W/m^3) and steady state conditions. The thermal conductivity for Inconel 600 is assumed constant (27.5 W/m·K). The first boundary condition is that the heat flux is zero (insulated) on the inside of the heater tube (r_1=0.95mm) and the second boundary condition also occurs on the inside of the heater tube where the temperature is known ($T(r_1)$=1280K).

The constants of integration in Equation 4.17 are solved with boundary conditions above giving the following particular solution,

$$T(r) = \frac{\dot{q}}{2k}\left(\frac{r_1^2}{2} - r^2 + r_1^2 \ln\frac{r}{r_1}\right) + T(r_1) \qquad 4.18$$

Substituting appropriate values and solving Equation 4.18 for $T(r_2)$ (outside of heater tube) shows that the temperature on the surface of the heater is approximately 1278K, or just 2 degrees less than the temperature on the inside surface which was also proven to be the same temperature monitored by the thermocouples placed inside of the heater assembly (Equations 4.14, 4.15). This therefore proves the assumption that the temperature reading monitored by the thermocouple inside of the heater assembly is a reasonable measurement of the actual surface temperature.

4.3 Chromatogram Analysis

Chromatograms are analyzed using Chrom Perfect software. In order to verify chemical species and their concentrations, a calibration gas mixture is required. The following gas mixture is used with the following nominal concentration:

Acetylene (C_2H_2)-2.0%

Carbon Dioxide (CO_2)-2.0%

Ethane (C_2H_6)-2.0%

Ethylene (C_2H_4)-4.0%

Methane (CH_4)-5.0%

Hydrogen (H_2)-25.0%

Carbon Monoxide (CO)-50.0%

This mixture was prepared by Airgas Inc. and verified by direct comparison to calibration standards traceable to National Institute of Standards and Technology (NIST) gas mixture reference materials. The analytical uncertainty is +/- 2.0%. The gas mixture composition is somewhat arbitrary in that it only serves as a known reference for confirming all species of interest and their concentrations. See Section 2.3.5 for a more complete explanation.

ChromPerfect software compares experimental chromatograms with a calibration chromatogram in order to determine the actual species and their concentrations. The residence time for each specie is proportional to its molecular weight so that peaks appear in the order from lightest to heaviest. Since the composition of the calibration is known, each species can be readily identified based on the order they appear and their respective molecular weight. When comparing to experimental chromatograms, overlapping peaks allows the identification of individual species. Determining the specie concentrations however is more complex since integration of the peaks is required. ChromPerfect software however performs this integration and reports composition results.

4.3.1 Detailed Steps to Create a Calibration File and Determine Product Gas Concentration

- Acquire a chromatogram by analyzing a calibration gas sample in the same manner as analyzing an experimental sample (See Section 3.4)
- Open raw data file created in the previous step with the ChromPerfect software and select "Analysis" button (See Figure 4.5)
- Open a separate window by selecting the "File Editor" button (See Figure 4.5)
- Select "New Calibration File" and the blank file will appear as shown in Figure 4.6
- Activate the "Analysis" window and right click on the GC trace. Select "peak properties." Click anywhere on the first peak (H_2) and a window will appear with information related to the peak (See Figure 4.7)
- Activate the "New Calibration File" window and fill in the name (e.g. H2), retention time ("retention time" value from peak properties), window width ("width" from peak properties), level 1 amount (actual concentration), and level 1 response ("area" from peak properties).
- Repeat the previous step for each peak by selecting "insert comp." The final result for the calibration file should look like Figure 4.8. Name and save the file.
- Open an experimental chromatogram of interest by selecting "Analysis" (See Figure 4.5) and open the raw data file of interest.

Figure 4.5: Chrom Perfect Software

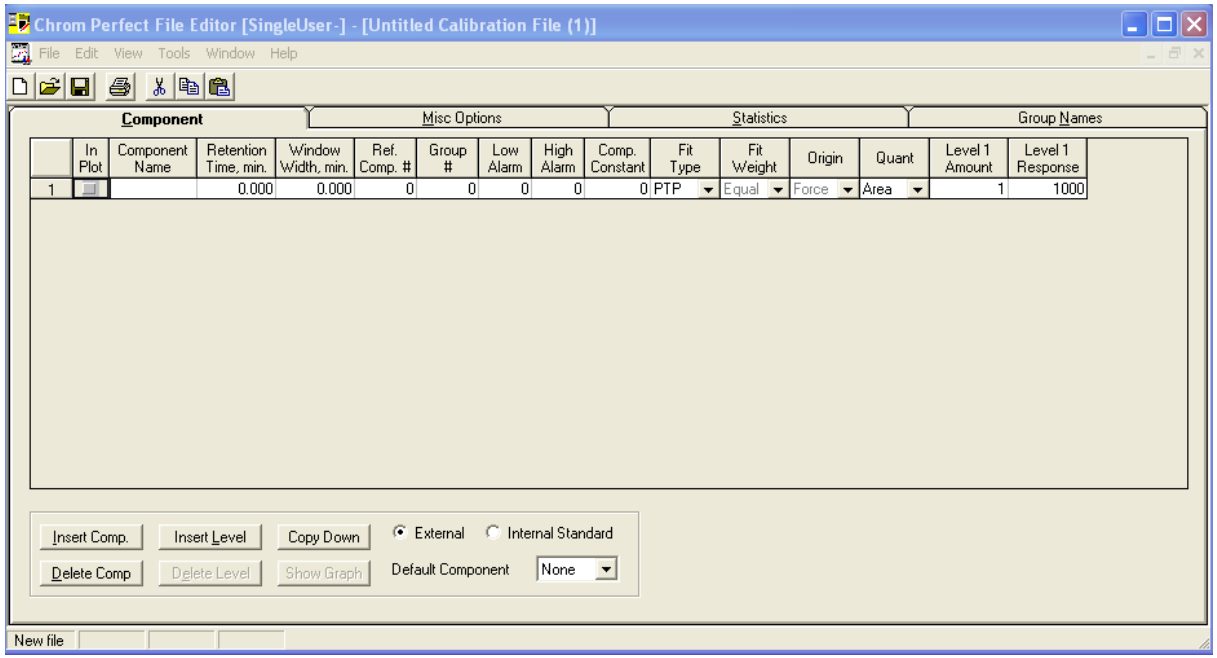

Figure 4.6: New Calibration File

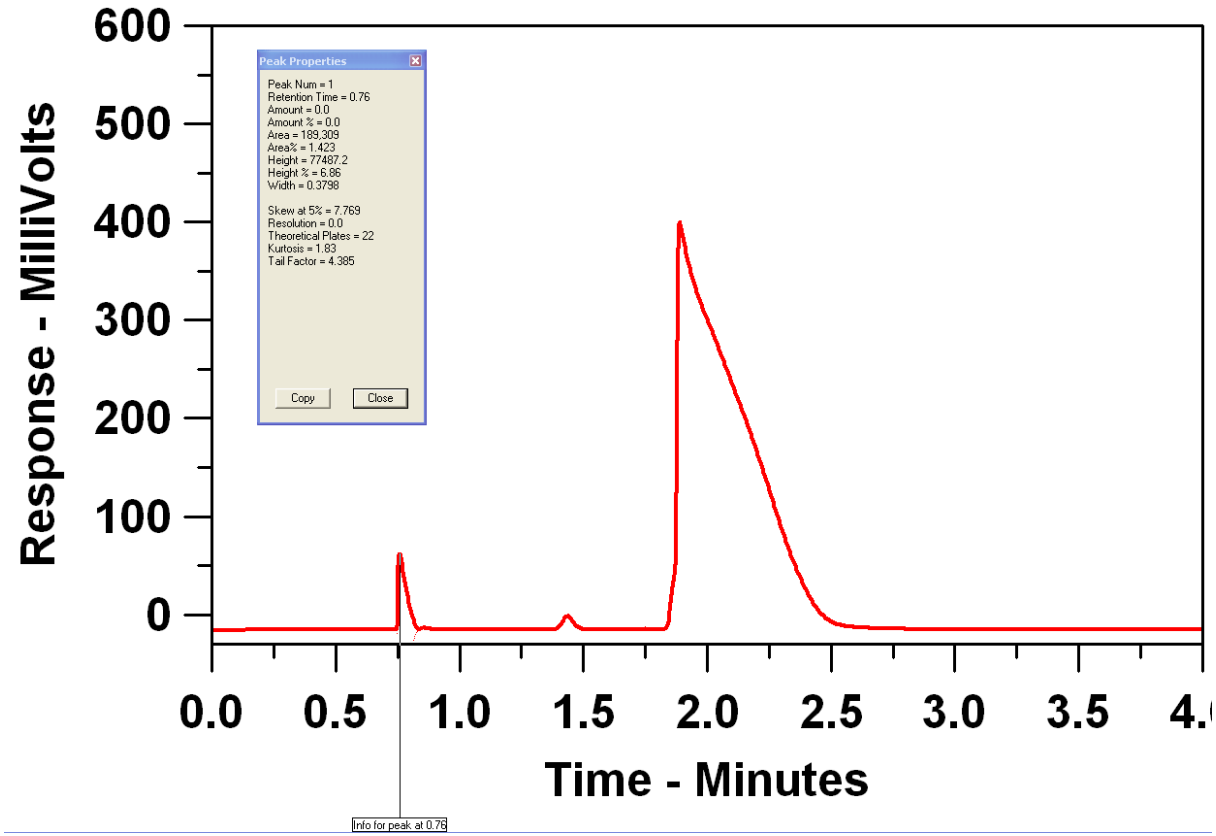

Figure 4.7: Peak Properties

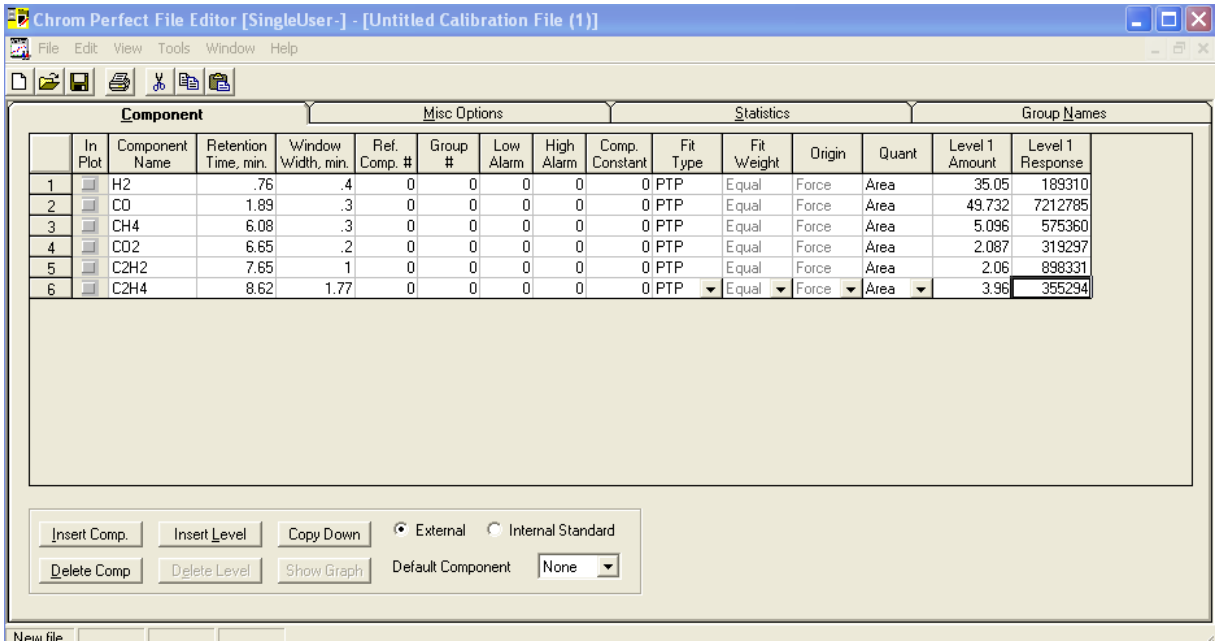

Figure 4.8: Final Calibration File

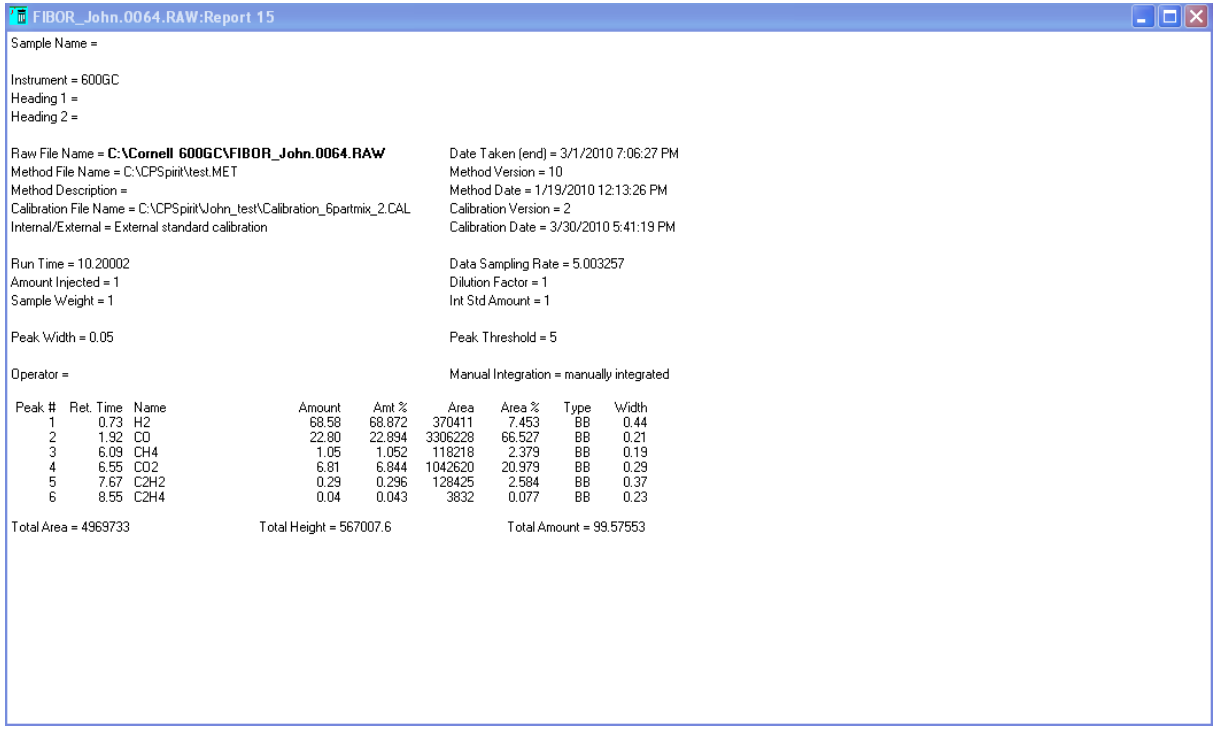

FIBOR_John.0064.RAW:Report 15

Sample Name =

Instrument = 600GC
Heading 1 =
Heading 2 =

Raw File Name = **C:\Cornell 600GC\FIBOR_John.0064.RAW**
Method File Name = C:\CPSpirit\test.MET
Method Description =
Calibration File Name = C:\CPSpirit\John_test\Calibration_6partmix_2.CAL
Internal/External = External standard calibration

Date Taken (end) = 3/1/2010 7:06:27 PM
Method Version = 10
Method Date = 1/19/2010 12:13:26 PM
Calibration Version = 2
Calibration Date = 3/30/2010 5:41:19 PM

Run Time = 10.20002
Amount Injected = 1
Sample Weight = 1

Data Sampling Rate = 5.003257
Dilution Factor = 1
Int Std Amount = 1

Peak Width = 0.05

Peak Threshold = 5

Operator =

Manual Integration = manually integrated

Peak #	Ret. Time	Name	Amount	Amt %	Area	Area %	Type	Width
1	0.73	H2	68.58	68.872	370411	7.453	BB	0.44
2	1.92	CO	22.80	22.894	3306228	66.527	BB	0.21
3	6.09	CH4	1.05	1.052	118218	2.379	BB	0.19
4	6.55	CO2	6.81	6.844	1042620	20.979	BB	0.29
5	7.67	C2H2	0.29	0.296	128425	2.584	BB	0.37
6	8.55	C2H4	0.04	0.043	3832	0.077	BB	0.23

Total Area = 4969733 Total Height = 567007.6 Total Amount = 99.57553

Figure 4.9: Sample Composition Results Using a Calibration File

- Select file>Calibration. Navigate to the calibration file created in the previous step.
- Select Report>Fixed Long Form. Concentrations are displayed for each specie (See example in Figure 4.9) under the "Amt %" column.

CHAPTER 5

RESULTS AND DISCUSSION

This chapter summarizes the results of experiments carried out for converting pure ethylene glycol and its aqueous mixtures through both thermal decomposition and catalytic means. Thermal decomposition of pure ethylene glycol is considered first and compared to previously reported results to examine the effect of heater tube diameter. Results are then presented for aqueous mixtures consisting of 10% and 20% (by volume) water, where the suspected effect of carbonaceous layering on the heater surface is investigated. Final results include catalytic conversion of a 20% (by volume) water mixture to demonstrate the possibility of using a FIBOR to promote ethylene glycol steam reforming (Equation 1.2). For ease of referencing general specifications and results for each heater tube, Table 5.1 provides a summary of results which are presented in further detail throughout this chapter.

5.1 Pure Ethylene Glycol Thermal Decomposition

Figure 5.1 shows photographs of pure ethylene glycol film boiling at 3 wall temperatures. The distinct bubbling shape and pattern is representative of film boiling (Lienhard 2008). At lower temperatures, a pattern of bubbles are periodically emitted from the vapor film. At higher temperatures, the heat flux is so intense that a complete vapor film clearly surrounds the entire heater surface. Although beyond the scope of this study, the bubbling pattern is useful for theoretical analysis using Raleigh-Taylor Instability Theory and is qualitatively similar to results reported in the literature (Arias 2010). The liquid that surrounds the percolating bubbles (ethylene glycol or aqueous mixture) is maintained at its saturation point through use of immersion heaters installed in the bottom of the bulk liquid reactant chamber.

Table 5.1: Summary of Experimental Results

Tube Name	Outside Diameter [mm]	Coating	Reacant (%EG/%H_2O)	Film Boiling Wall Temperature Range [K]	Product Flow Rate Range [LPM/m^2x10^{-3}]	Avg. Bulk Temperature (subcooling in parentheses) [K]	
						Trial #1	Trial #2
Choi (2010)	4.76	NA	Pure EG	900-1350	0.0-4.3	425 (45)	NA
Bare Tube #1	2.38	NA	Pure EG	900-1475	0.0-6.3	440 (30)	430 (40)
Bare Tube #2	2.38	NA	90/10	1150-1475	0.0-2.0	407 (11)	407 (11)
Bare Tube #3	2.38	NA	90/10	1150-1475	0.0-2.0	408 (10)	NA
Bare Tube #4	2.38	NA	80/20	1050-1475	0.0-0.9	397 (0)	395 (1)
Pt Tube	2.38	49%-Pt/51%-Al_2O_3	80/20	1360-1525	2.8-3.3	393 (3)	393 (3)
Ni Tube	2.38	33%-Ni/67%-Al_2O_3	80/20	1300-1540	2.1-3.0	393 (3)	393 (3)

*Saturation Temperatures: Pure EG= 470K; 90%/10%=418K; 80%/20%=396K

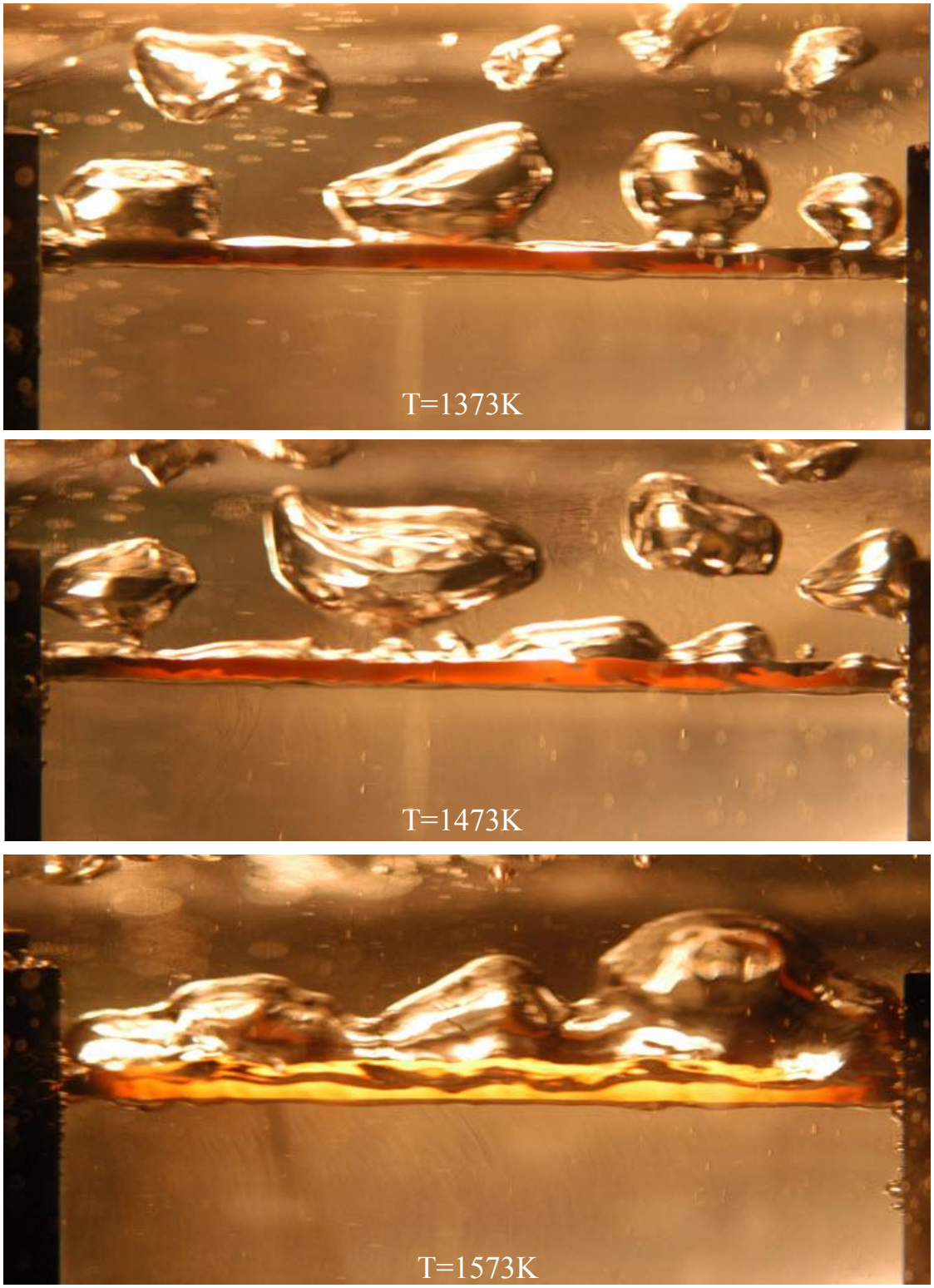

Figure 5.1: High Resolution Film Boiling Images

5.1.1 Product Flow Rates and Boiling Curves

Figure 5.2 compares product flow rates as obtained previously for a 4.76mm (Choi 2010) and a 2.38 mm diameter tube as examined here. The data in Figure 5.2, along with all subsequent flow rate figures in this chapter, are mean values. The dotted lines are polynomial fits of the raw data. Further analysis of individual data sets as explained in Section 4.1.2 (Figure 4.3), to include raw data can be found in Appendix E. The onset of chemical reaction for both heater tube sizes appear to coincide at approximately 1100K. As expected, the smaller tube diameter achieves lower product yields. This result is consistent with the theoretical prediction (Urban et al. 2006). Overall reactor performance however would likely reach a peak value if the tube diameter continued to increase as a result of other factors such as chemical conversion efficiency, cost and size constraints. (Urban et al. 2006)

In order to further demonstrate FIBOR performance presented in Figure 5.2, a repeatability test was conducted under identical conditions for the case of converting pure ethylene glycol through thermal decomposition using the same 2.38mm bare tube (Bare Tube #1). Figure 5.3 compares the flow rate curves (a) and boiling curves (b) of the first trial (also shown in Figure 5.2) and a second trial where now the tube is blackened, likely by carbon deposits. The onset of chemical reaction during the second trial was similar to the first at approximately 1100K, however noticeably lower product flow rates were observed (Figure 5.3a), despite using the same tube. The operating temperature domain for film boiling was also significantly limited for the second trial, with a collapse of film boiling at approximately 1275K while the first trial was able to sustain film boiling at temperatures well below 1100K. The film boiling curve is also noticeably lower for the second trial than the first (Figure 5.3b). The difference between the film boiling curves is likely caused by the lower product flow rate for the second trial (Figure 5.3a), and thus less heat is consumed by

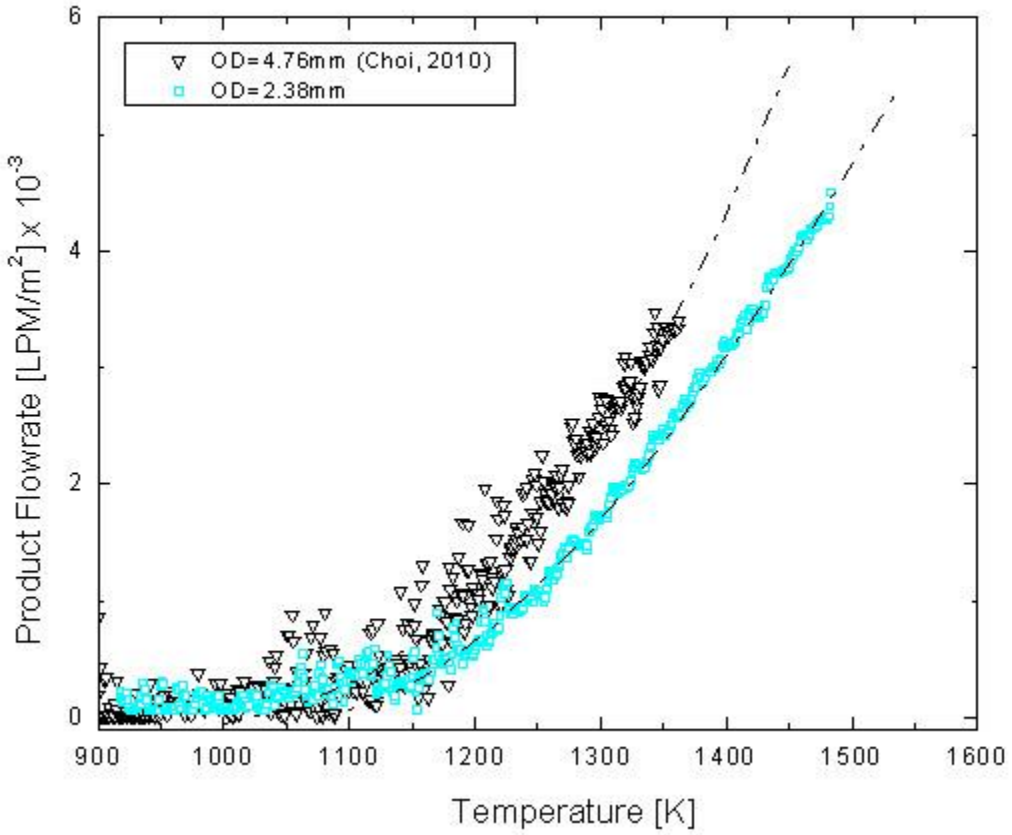

Figure 5.2: Effect of Heater Tube Diameter on Pure Ethylene Glycol Thermal Decomposition

the endothermic chemical reaction for ethylene glycol thermal decomposition (Equation 1.1). The carbon deposits may also create thermal resistance on the outside of the tube, which would raise the heater temperature for a given heat flux, also contributing to a shift in the boiling curve.

It appears that the occurrence of black (likely carbon) deposits may coincide with lowering the FIBOR's performance in terms of product yields. The exact mechanism, however, is not clear as to why carbon inhibits chemical reactivity. This interesting phenomena will be investigated further for the case of 90%(EG)/10%(H_2O) and ultimately proven as the cause/effect for deteriorating performance.

5.1.2 Liquid Contamination During Operation

A liquid contamination effect of the bulk liquid reactant was observed during prolonged operation for pure ethylene glycol thermal decomposition. Data collected for the bulk liquid temperature over the course of the second trial (Figure 5.3) reveals that the temperature of the bulk liquid reactant noticeably changed with time (Figure 5.4a) implying a changing concentration. The exact nature of the temperature change involves complex vapor-liquid equilibrium phenomena owing to the unsteady development of a multi-component reactant mixture. This is verified by GC-MS analysis (Agilent Technologies 6890N/5973 High Performance Combination) of a liquid sample after the experiment (Figure 5.4b) that showed the bulk liquid includes nearly 17% contaminants (various alcohols, ketone, and heterocyclic acetals).

Figure 5.4c depicts likely transport paths for the various species produced by the FIBOR which causes liquid contamination. Separate bubbles form at the heater surface where vapor ligaments are pinched and bubbles are released and eventually expelled at the surface under the action of buoyancy. The bubble contains reactants, products (Equations 1.1-1.7) and various contaminants (e.g Equation 1.8). Some of

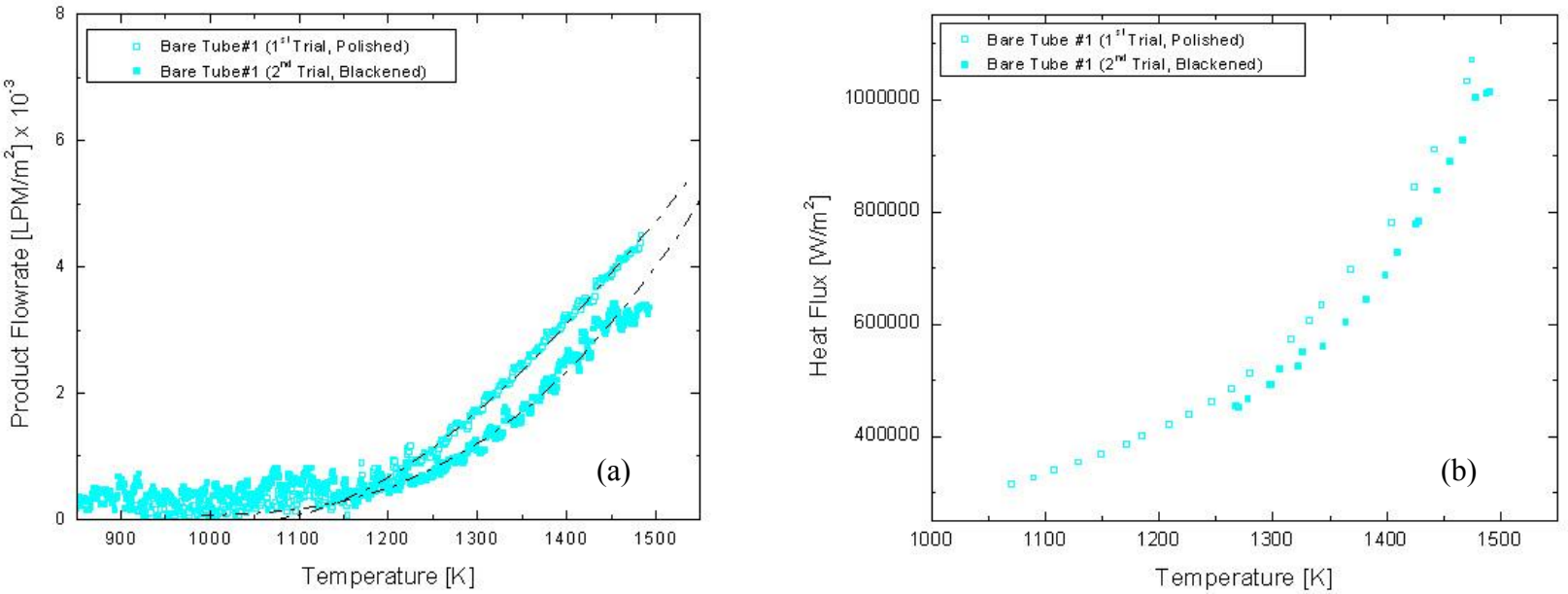

Figure 5.3: Pure Ethylene Glycol Thermal Decomposition (a) Flow Rate Curves and (b) Boiling Curves

the reactants and contaminants condense and diffuse into the bulk liquid as the bubble approaches the liquid surface. The remaining reactants and contaminants are returned to the bulk in liquid form as result of the reflux condensing system. Non-condensable products continue on through the system for flow rate and GC analysis.

If secondary chemical reactions (such as Equation 1.11) produce condensable by-products with comparatively lower boiling temperatures than the reactant (e.g. ethanol), the bulk liquid temperature decreases over the course of an experiment as a result of composition changes. Closer analysis of the individual contaminant boiling temperatures (Figure 5.4) suggests that the decreasing temperature trend could be the result of an azeotropic mixture. However, the exact nature of the multi-component vapor-liquid equilibrium, as well as the underlying chemistry that forms each contaminant is beyond the scope of this study. In addition, liquid contamination had no obvious effect on overall product yields suggesting that products could continue to be produced while the bulk liquid composition is changing. Interestingly, aqueous mixtures which will be covered in the remaining sections held a constant bulk liquid temperature ($\Delta T_{bulk} \approx 2K$) during all experiments suggesting minimal or no contamination.

5.2 Aqueous Mixture (90% EG/10%H_2O) Thermal Decomposition

The first aqueous mixture examined consists of 90% (by vol) ethylene glycol and 10% (by vol) water. This mixture is chosen based on assuming vapor-liquid equilibrium (Figure 1.2) within the film around the heater; reactants are significantly enriched with steam (approximately 70%) yet still contain an appreciable amount of ethylene glycol (30%) to offer the possibility of chemical reaction. A bare tube is used to establish a baseline comparison. Although steam reforming of ethylene glycol

	Methanol	Ethanol	Acetone	1,3-dioxolane	2-methyl-1,3-dioxolane	Ethylene glycol	2,2'-oxybis-Ethanol	Triethylene glycol
Chemical structure						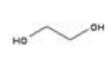	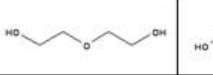	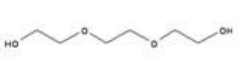
Boling point [°C]	64.8	78.5	56.3	75	81.7	197.5	246	267
Molecular wt. [g/mol]	32.04	46.07	58.08	74.1	88.11	62.07	106.12	150.17
Molar %	0.12	0.28	1.65	0.32	7.65	83.23	3.14	3.61

10.02 %

6.75 %

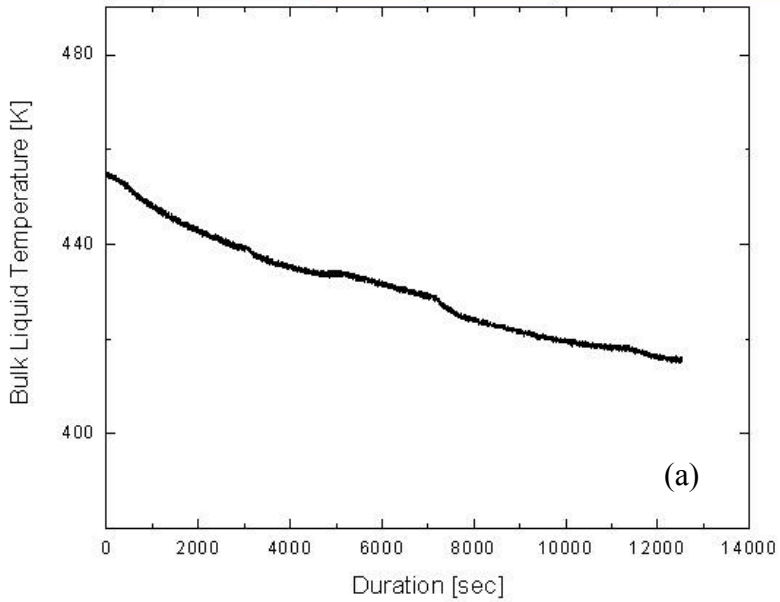

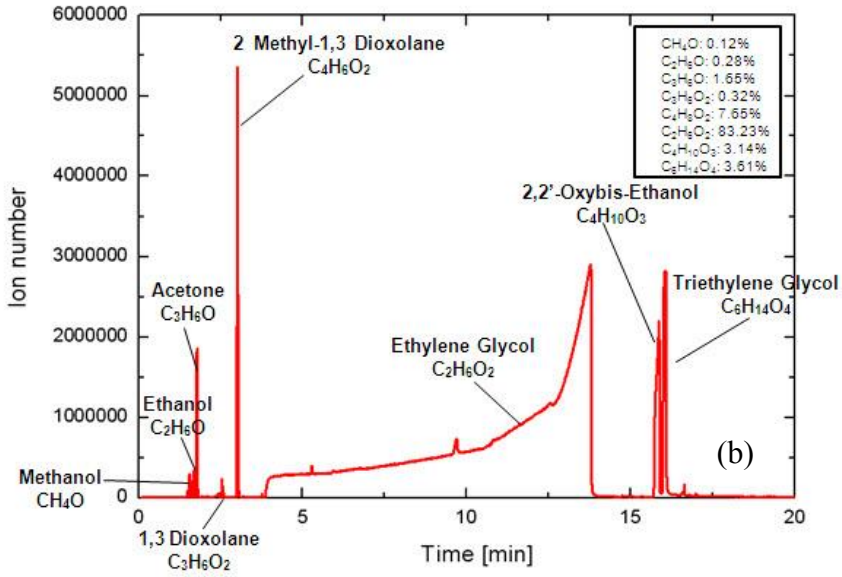

Figure 5.4: Liquid contaminants (table) and the (a) decrease in bulk liquid temperature during thermal decomposition of pure ethylene glycol (Bare Tube #1, 2nd Trial) with (b) results of a liquid sample analyzed with a GC-MS.

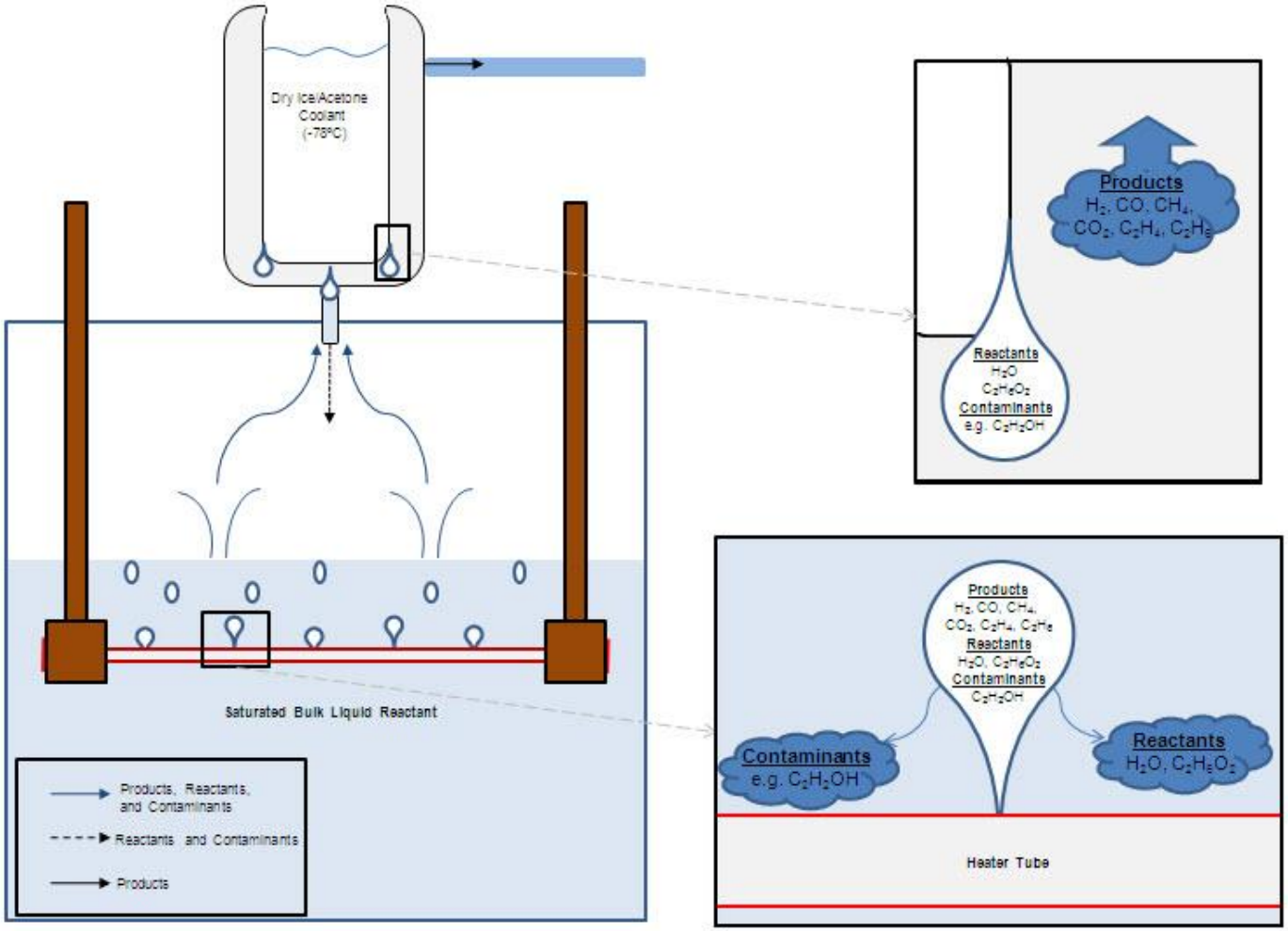

Figure 5.4c: Transport of Species in the FIBOR

is not possible without an active catalyst surface (Kechagiopoulos 2007; Hu 2009), any chemical reaction detected is likely a result of thermal decomposition (Equation 1.1) of ethylene glycol within the vapor.

5.2.1 Product Flow Rates and Boiling Curves

Figure 5.5 shows product yields and boiling curves for a bare 2.38mm heater tube (Bare Tube #2, cf. Table 5.1)) converting an ethylene glycol aqueous mixture (90% EG/10% H_2O). The first trial utilized a new, polished tube. The second trial utilized the same tube. However, the surface was noticeably blackened from carbon formation during the first trial. Comparing these results (Figure 5.5a) to pure ethylene glycol (Figure 5.3a), the second trial (blackened tube) similarly achieved lower product yields than the first trial (polished tube). However the aqueous mixture (90%/10%) achieved much lower product yields than pure ethylene glycol (cf. Figure 5.3). At peak operating temperatures of approximately 1475K, pure ethylene glycol yielded close to 6 LPM/m^2 x 10^{-3} while the aqueous mixture only produced close to 2 LPM/m^2 x 10^{-3}.

The boiling curves for both pure ethylene glycol (Figure 5.3b) and a 90%/10% aqueous mixture (Figure 5.5b) show similar results in that both cover similar operating domains (power, wall temperature). The boiling curve for the second trial (blackened) is noticeably lower than the first trial (polished). This may be the result of the carbon layering creating thermal resistance, and therefore a higher temperature for a given heat flux or possibly cause reduced chemical reactivity from the existence of a carbon coating.

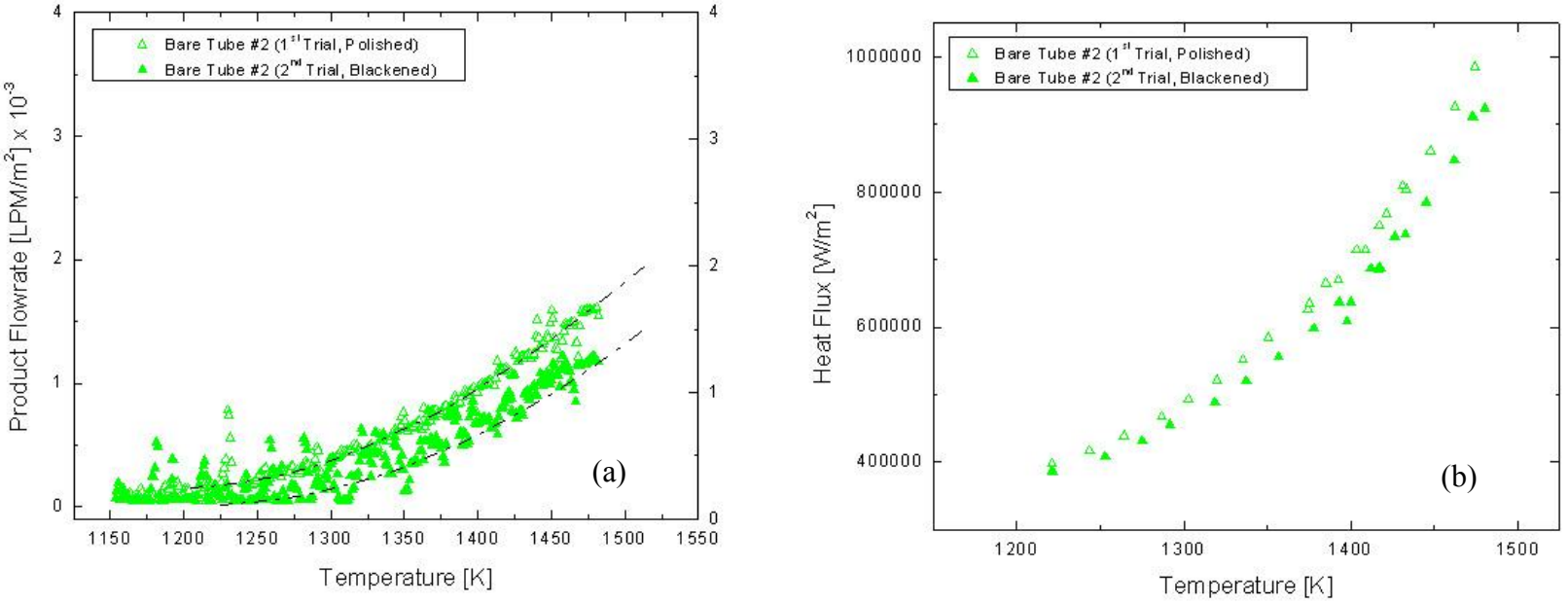

Figure 5.5: Ethylene Glycol (90% vol)/water (10% vol) thermal decomposition (a) flow rate curves and (b) film boiling curves

5.2.2 Gas Chromatography Analysis

Samples of product gas from Figure 5.5a were analyzed through gas chromatography in order identify individual species and their concentrations. Figure 5.6 shows the results of a sample extracted at 1473K. Relative concentrations of H_2 (43.7%) and CO (40.3%) suggest that thermal decomposition (Equation 1.1) is likely the dominant reaction pathway. The appreciable amount of CH_4 (11.4%) also suggests the presence of the secondary methanation reaction (Equation 1.4) which also in turn prevents hydrogen production from reaching stoichiometric ratios (H_2/CO=3/2) predicted by Equation 1.1. Small traces of carbon dioxide may be the result of some steam reforming (Equation 1.2) activity, the water-gas shift reaction (1.3) and/or the result of carbon formation (Equation 1.5). Small traces of C_2H_2 and C_2H_4 suggest the presence of secondary chemical reactions though with small yields. The tiny trace of air (N_2 and O_2), was found to be entrained in the gas line configuration downstream of the flow meter and before entering the GC (Figure B.9). This was determined to be the cause through tedious leak inspections throughout the system and also several trial tests which revealed that as the flow rate is increased by the mini-pump (Figure B.7), the amount of air injected and also detected by other GC traces decreases. The small amounts of air are therefore neglected when determining the product concentrations and also do not account of any of the product flow rate curves since air enters the product sample downstream of the flow meter.

5.2.3 Repeatability Test to Investigate Heater Surface Blackening

In order to further investigate the nature of the heater surface blackening, as well as isolate its role with respect to how it impacts the FIBOR's performance, a

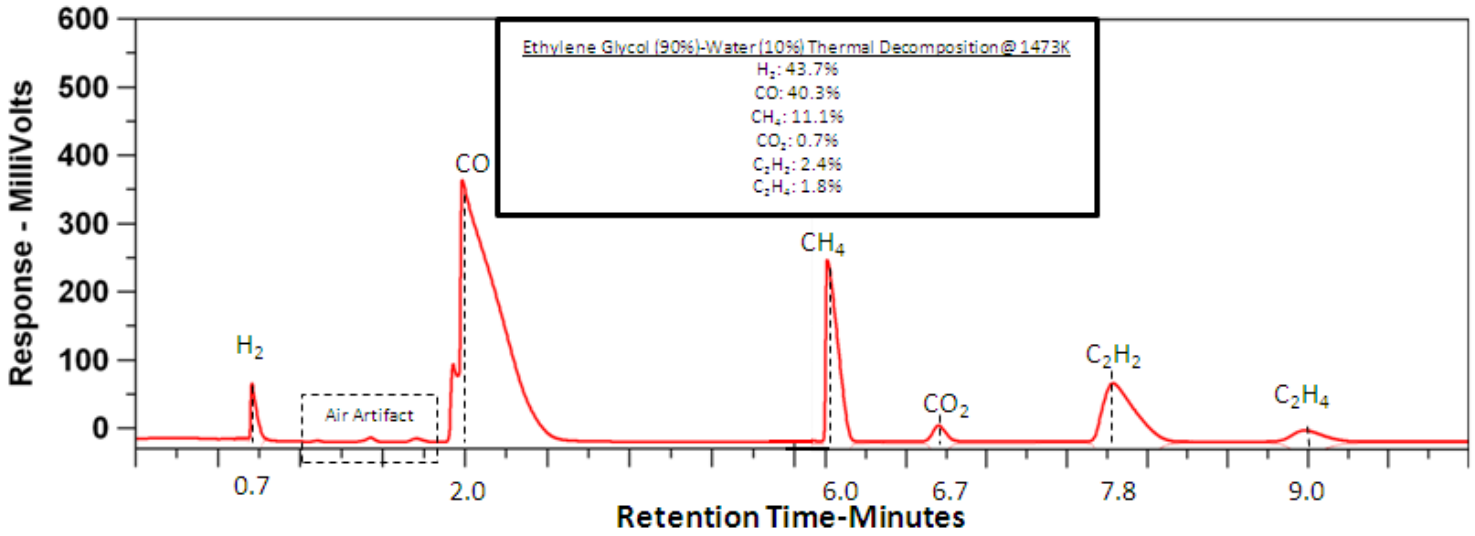

Figure 5.6: GC Trace for thermal decomposition of ethylene glycol (90% vol)/water (10% vol) at 1473K

separate repeatability test was conducted with a new bare tube (Bare Tube #3, cf. Table 5.1). The objective of this experiment was to closely observe how the heater surface changed with respect to operating conditions and time.

Film boiling was achieved with a new, polished bare tube and the power was increased in a step wise manner for approximately the first 30 minutes of the experiment. Power was then held constant for the next 30 minutes. Figure 5.7 shows that despite the power being held constant, the temperature of the heater continued to slowly rise. The slow blackening of the heater surface could also be seen with the naked eye during this time when it became the most evident after approximately 105 minutes where flakes of black material could be seen detaching from the heater surface as a result of boiling induced agitation. Around this time coincidentally the temperature also increased significantly which suggests the blackening may create an outer thermal resistance layer on the heater causing the measured centerline temperature to increase.

The repeatability data set was divided into two parts: 1) data taken during the initial half of the experiment when the tube was polished; and 2) data taken during the latter half when the heater was blackened. Figure 5.8 compares the data for the first 90% EG / 10% H_2O experiment (Bare Tube #2) for a new and polished tube, and the initial half of the repeatability experiment when the heater tube (Bare Tube #3) was also new and polished. Both the flow rate and boiling curves closely coincide. Similarly in Figure 5.9, separate data sets for Bare Tube #2 and #3 after being blackened during exposure in the FIBOR are compared. Again, flow rate and boiling curves closely match which provides convincing evidence that the lowering of reactor performance is likely a result of the heater surface blackening. This result is therefore significant because it suggests that although a bare tube was previously thought to

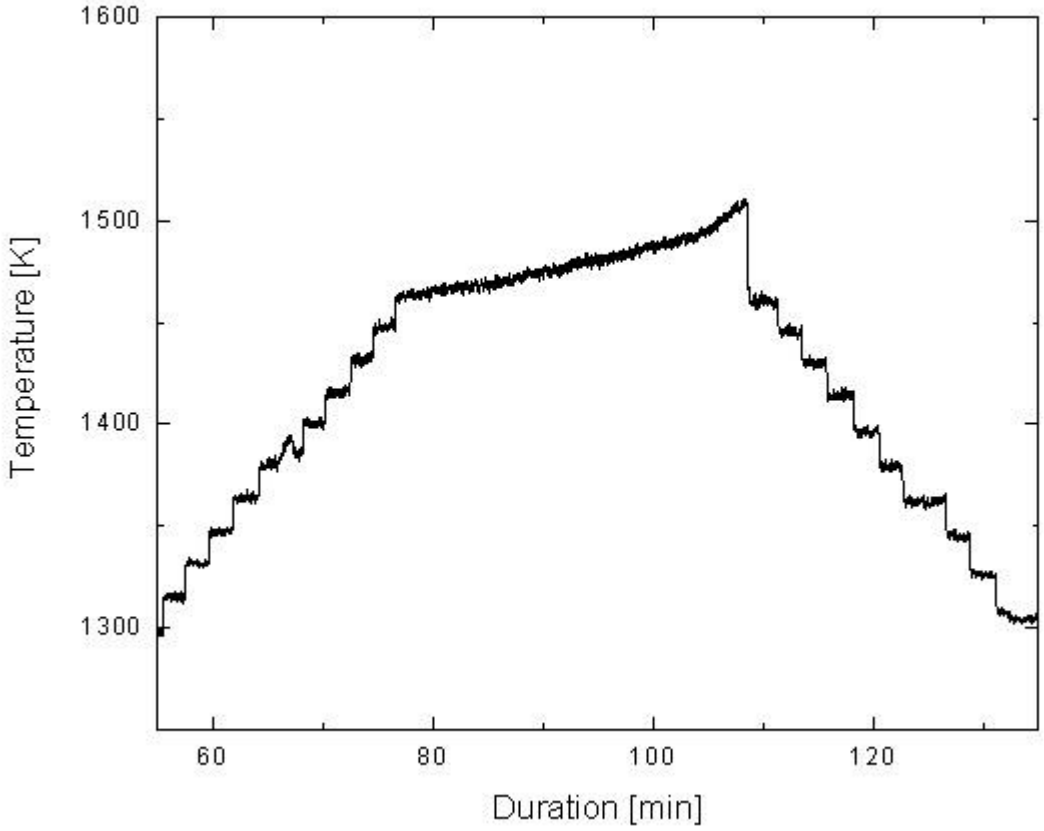

Figure 5.7: Ethylene Glycol (90% vol)/Water (10% vol) Repeatability Test

promote as a purely homogeneous reaction within the vapor film, there must in fact be a heterogeneous reaction component on the surface of the Inconel tube. As the tube is coated with carbon, the surface reaction component is likely diminished (or removed), causing lower product yields. An explanation of the shift in the boiling curve can be attributed to adding a thermal resistance layer to the tube (carbon layer) therefore causing increased temperature for a given heat flux.

This result is also consistent with Choi's (2010) work which showed repeatable results for thermal decomposition of methanol using a polished tube for both tests. Additionally, Choi (2010) determined that bulk sub-cooling can lower reactor yields and shift the boiling curve to higher temperatures, however this is not the case here since sub-coolings are nearly constant for all 90%/10% tests as shown in Table 5.1.

5.2.4 Scanning Electron Microscope (SEM) and X-Ray Dispersion Spectroscopy (EDS) Analysis

For closer examination and analysis of the heater surface, images of Bare Tube #2 were taken before and after use (Figure 5.5) with an SEM (Leica 440). Figure 5.10 shows before and after images at 100x and 300x magnifications respectively. These images clearly show a layering effect which grows on the heater surface over time (Figure 5.10c, d). The substance is dark black in color and appears to have a botryoidal like texture. It is postulated that these layers consist of a carbonaceous material due to its dark black appearance, supporting chemistry (Equations 1.5-1.7) and Zhukov's (2003) similar observation. Additionally, standard chemical reactors are often inhibited by "coking" or the deposition of carbon on reactor materials further suggesting that the black layering on the heater surface captured in Figures 5.10c and 5.10d is in fact carbon.

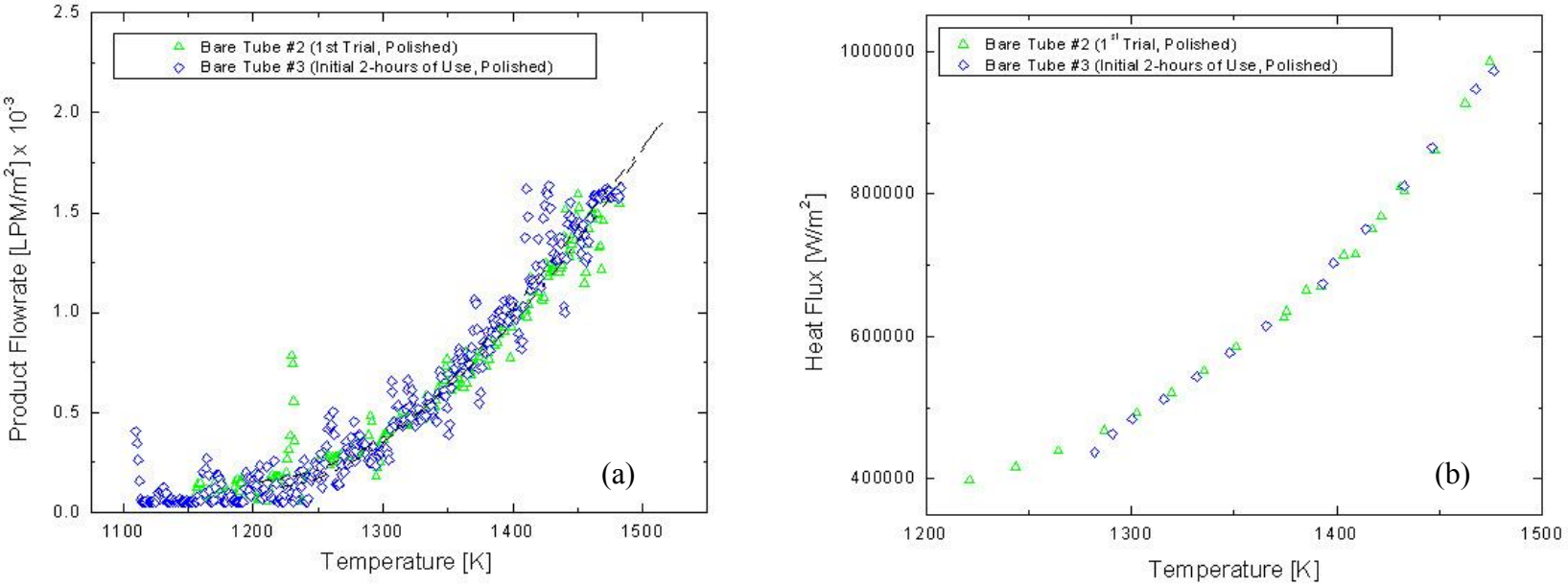

Figure 5.8: Ethylene glycol (90% vol)/water (10% vol) flow rate curves (a) and film boiling curves (b) from repeatability test before blackening of heater surface

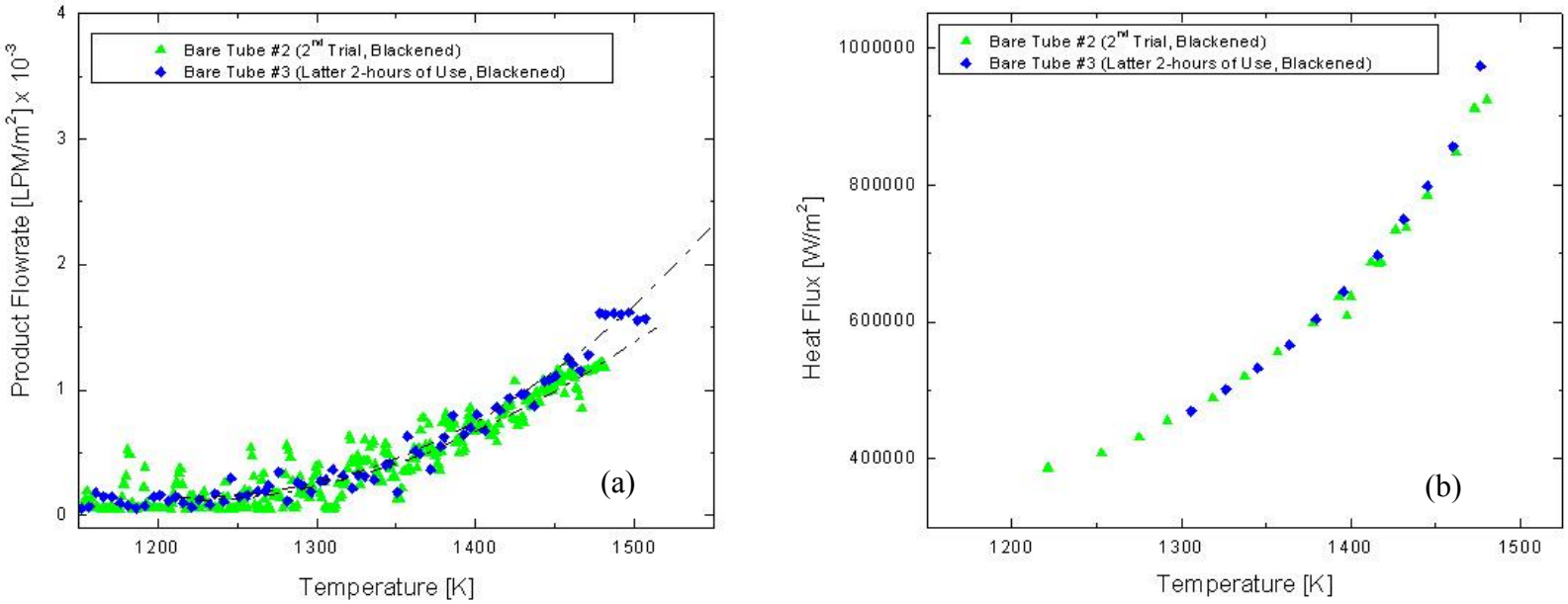

Figure 5.9: Ethylene glycol (90% vol)/water (10% vol) flow rate curves (a) and film boiling curves (b) from repeatability test after blackening of heater surface

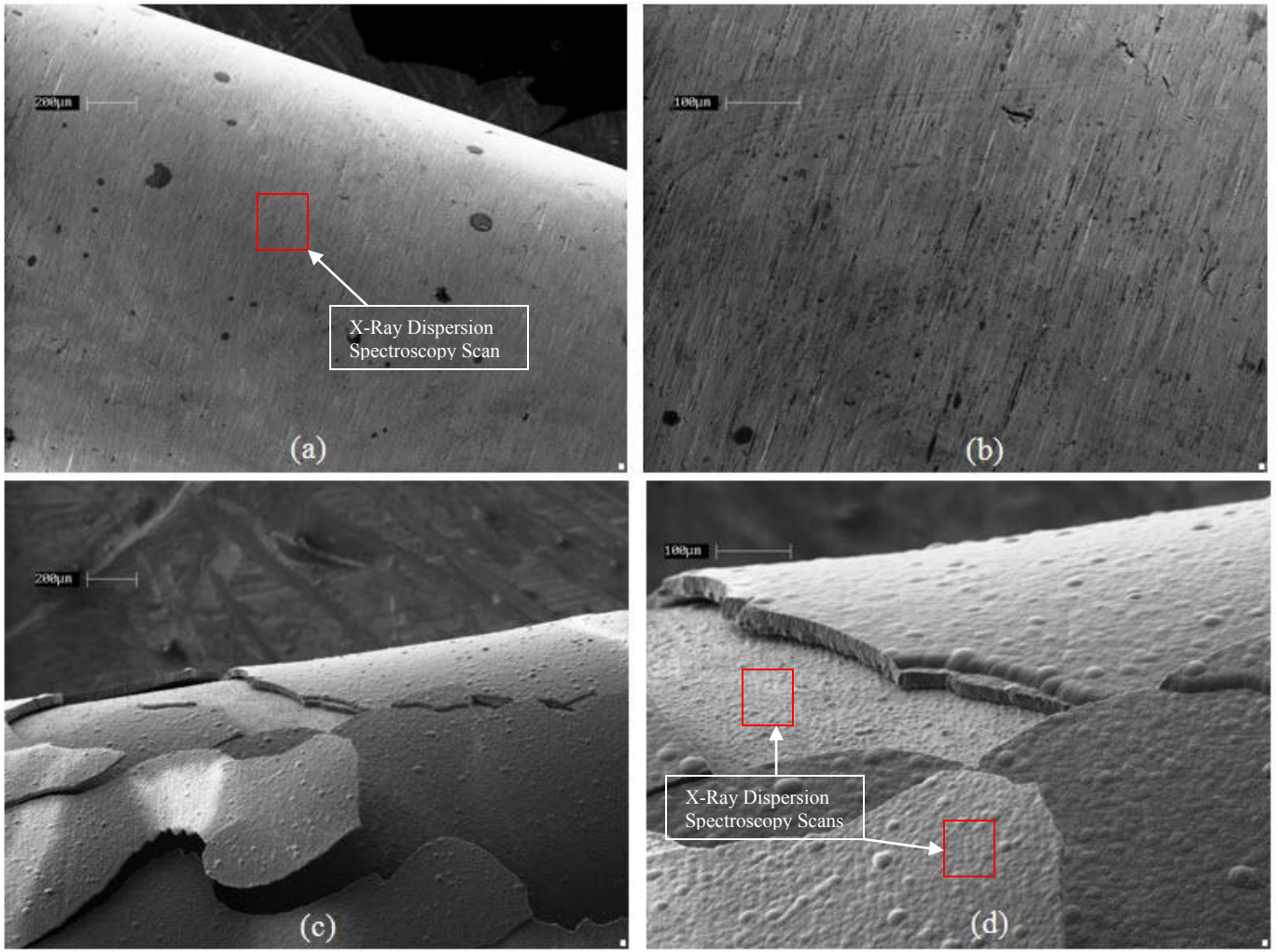

Figure 5.10: SEM Images of Bare Tube #2 surface at (a) 100x (b) 300x and blackened surface at (c) 100x (d) 300x

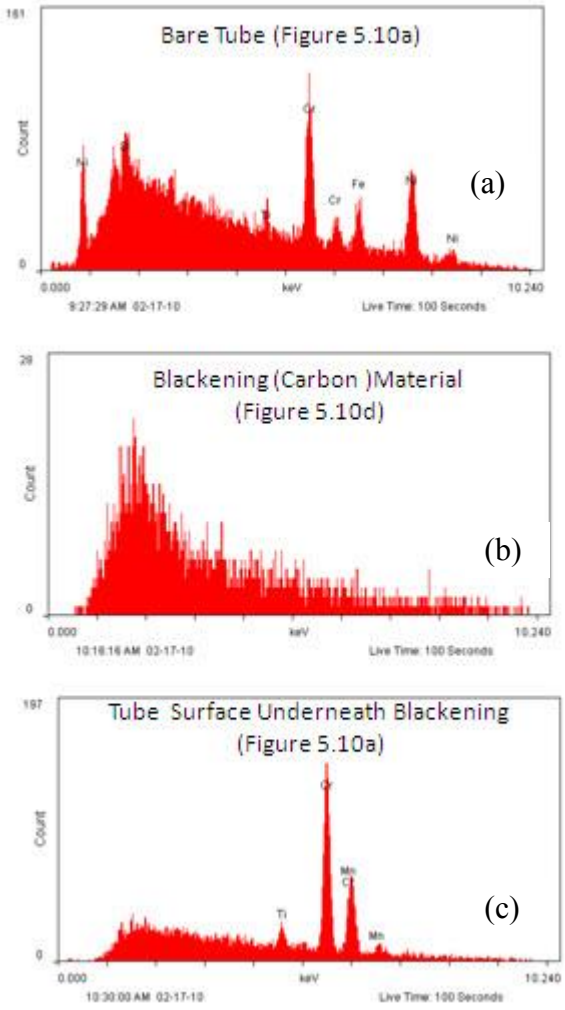

Figure 5.11: X-Ray Dispersion Spectroscopy Scans of Bare Tube #2 polished surface before use (a), blackening (carbon) material (b), and tube surface underneath (c).

In order to provide further evidence that the blackening is carbon (as opposed to another effect such as the removal of Inconel material) X-ray Dispersion Spectroscopy (EDS) scans were taken of the bare surface (Figure 5.10a), along with the top surface of the carbon material and the surface underneath (Figure 5.10d). EDS provides for identifying individual elements present on a surface. Elements are depicted by individual "peaks" across an EDS spectrum. Figure 5.11 shows the EDS results for the locations of scans depicted in Figure 5.10. The main elements of Inconel 600 Alloy (Iron, Nickel, Chromium) are identified in Figure 5.11a for the bare tube surface. The scan of the blackening material (Figure 5.11b) however shows no identifiable peaks, while the surface underneath identifies again reveals the elements of Inconel 600. (Although Figure 5.11b appears to have one peak, this is in fact a "baseline peak" and does not represent an element) This proves that the blackening material does not contain any metals (therefore disproving the possibility that Inconel Material may be detaching). Unfortunately, the EDS used for this thesis (Kevex EDS Detector-7.5µm Beryllium Window) is unable to detect just a handful of elements, with one of the elements it is not able to detect being carbon.

5.3 Aqueous Mixture (80% EG/20%H_2O) Thermal Decomposition

Identical experiments were conducted for 80% (by vol) ethylene glycol and 20% (by vol) water mixtures using a bare tube (Bare Tube #4) to establish a baseline comparison for future catalytic tests as well as to compare product yield performance to previously discussed 90%/10% mixtures. Since the vapor concentration contains just 10% (vol) ethylene glycol as a result of vapor-liquid equilibrium (Figure 1.2), a liquid mixture at higher water loading would likely result in minimal chemical reaction since the vapor consists almost entirely of steam. The presence of steam

however can provide some advantages, particularly in reducing carbon deposits or coking. (Hu 2009)

5.3.1 Product Flow Rates and Boiling Curves

Results for thermal decomposition of an 80%/20% mixture are presented in Figure 5.12. The first trial and the second trial show good agreement with respect to product flow rates (Figure 5.12a) and film boiling curves (Figure 5.12b). The surface blackening effect that was examined previously for pure ethylene glycol and 90%/10% aqueous mixtures was not observed for an 80%/20% mixture which suggests the presence of steam in the FIBOR may have a similar effect in preventing carbon deposition as it does in traditional reactors. Although repeatable results were achieved, an 80%/20% mixture gave minimum product yields. At a maximum operating temperature of 1475K, product flow rates were approximately half that of 90%/10% and over six times lower than pure ethylene glycol reaching just 0.9 $LPM/m^2 \times 10^{-3}$. This is likely due to very low concentrations of ethylene glycol in the vapor phase (~10%), however, reactions still occur. An additional repeatability test was not necessary as it was with a 90%/10% mixture since the effect of heater surface blackening or carbon deposits was not observed.

5.3.2 Gas Chromatography Analysis

Despite low chemical reactivity, product gas samples were successfully extracted for GC Analysis. Figure 5.13 is a GC Trace which confirms the presence of individual species and their concentrations. The results are quite similar to the GC analysis of products from a 90%/10% mixture. Concentrations of H_2 (44.8%) and CO (40.0%) are quite similar, as well as the presence of CH_4 (9.0%) and small traces of CO_2, C_2H_2 and C_2H_4. This result suggests similar chemistry for an 80%/20% mixture

that was also postulated for a 90%/10% mixture, namely thermal decomposition dominating (Equation 1.1), along with a strong presence of the methanation reaction (Equation 1.4) and several secondary reactions which create small traces of other species (CO_2, C_2H_2, C_2H_4).

5.4 Aqueous Mixture (80% EG / 20% H_2O) Catalytic Conversion (Steam Reforming)

The chemical reactivity detected for bare heater tubes is the result of mainly thermal decomposition (Equation 1.1). Steam reforming of ethylene glycol (Equation 1.2) is promoted by platinum and nickel based catalysts; specifications for each coated tube can be found in Table 2.3. An 80%/20% mixture is tested since it achieved the lowest product yields with a bare heater and provides the best opportunity to isolate the effect of the catalyst. Although catalytic conversion of 90%/10% mixtures is not conducted, results are likely to be similar to that of catalytic conversion of 80%/20% mixtures when compared to bare heater results.

An initial experiment was conducted for each tube in which the power was varied in order to traverse the film boiling operating domain. A second, separate repeatability trial was then conducted under the same operating conditions as the first in order to detect any possible catalyst deactivation. Finally a third "endurance test" was conducted with the power held constant for approximately two, three hour intervals to further characterize the catalyst's integrity.

5.4.1 Platinum (Pt Tube) Catalyst Performance

Results for a heater tube coated with a platinum catalyst (Pt Tube) converting an 80%/20% ethylene glycol aqueous mixture are presented in Figure 5.14. Open circles denote the initial experiment while solid circles denote the second. Results from Figure 5.12 of an 80%/20% aqueous mixture converted using a bare heater tube

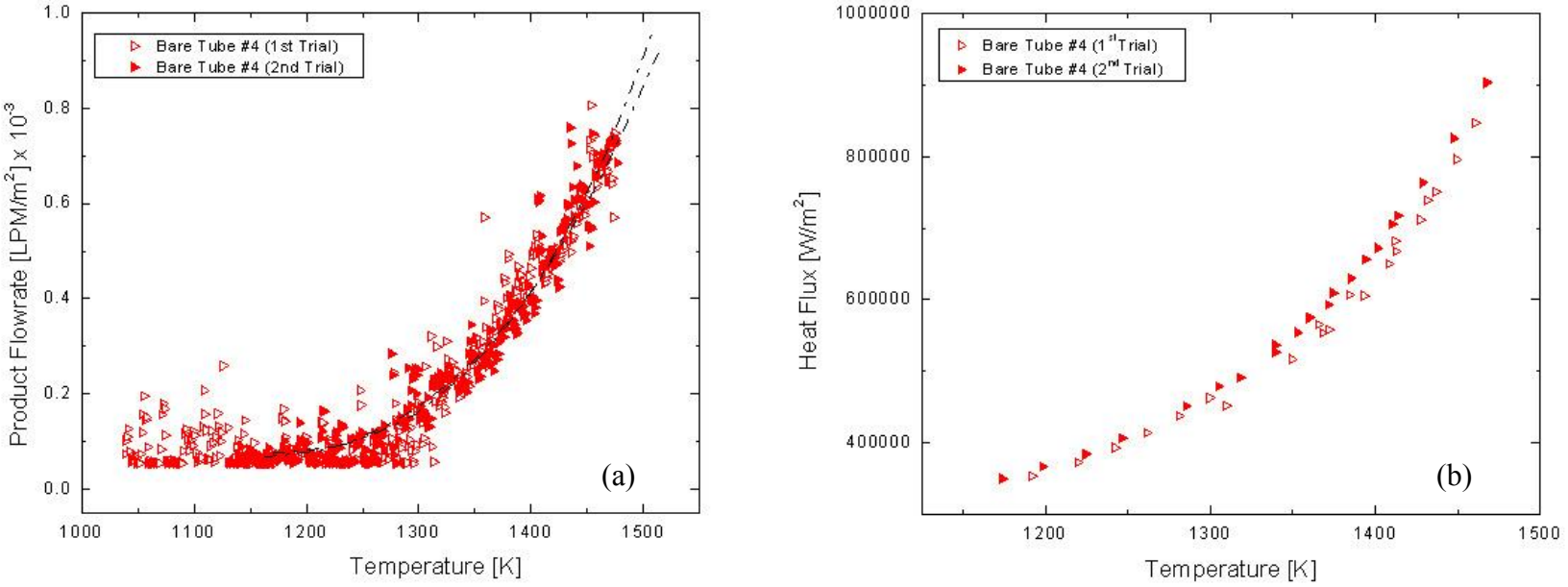

Figure 5.12: Ethylene glycol (80% vol)/water (20% vol) thermal decomposition (a) flow rate curves and (b) film boiling curve

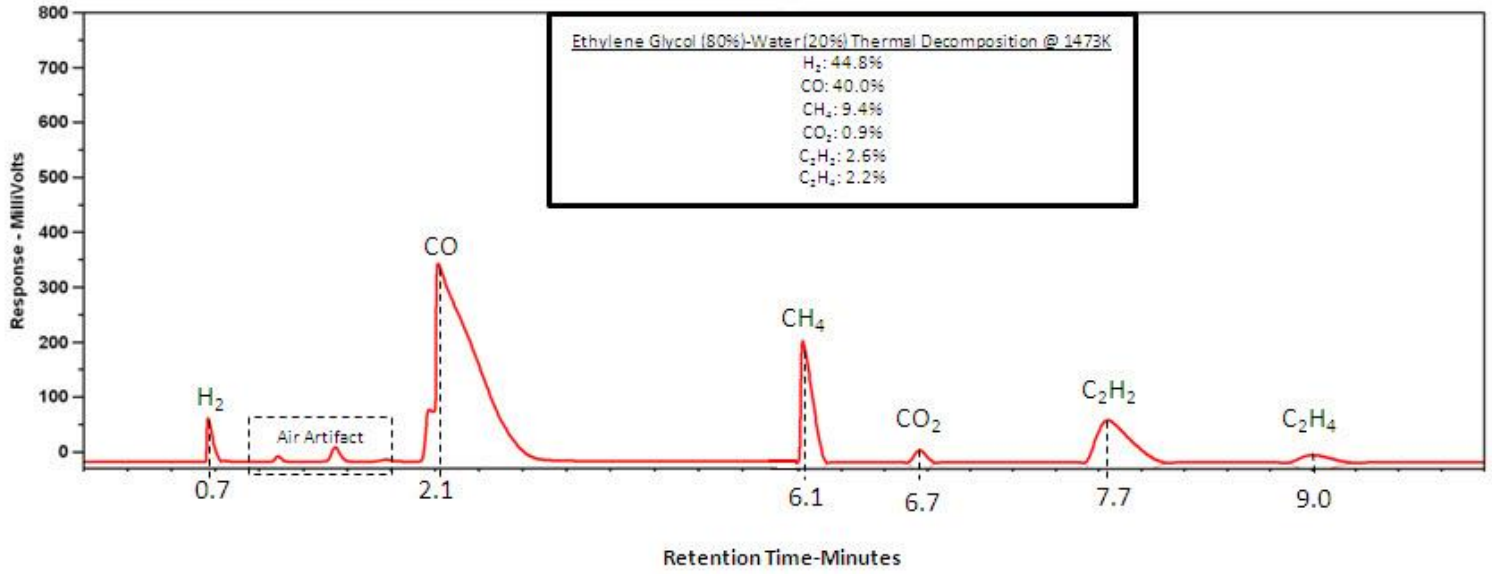

Figure 5.13: GC Trace for thermal decomposition of ethylene glycol (80% vol)/water (20% vol) at 1473K

(thermal decomposition) are also provided for comparison. The catalyst's effect is clearly evident, achieving nearly four times the product yield to that of the bare heater tube (Figure 5.14a). The second trial however shows noticeably lower yields which suggests possible catalyst deactivation. The boiling curves (Figure 5.14b) also provide further insight into the FIBOR's performance using a platinum catalyst. Although the second Pt Tube trial is slightly lower than the first, the overall thermal effect is negligible on the boiling curves. The catalytic boiling curves however are significantly higher than the bare heater tube which is likely due to the increase in endothermic chemical reactivity.

In order to better evaluate the catalyst's deactivation over time, an endurance test was conducted with the power held constant for two separate intervals (1,100 kW/m^2 and 720 kW/m^2), each lasting approximately three hours. Figure 5.14 summarizes the results showing the variation of heater temperature with respect to time (top) and the corresponding flow rates (bottom). Despite the power being held constant at 1,100 kW/m^2 for the first half of the endurance test, the temperature gradually rises from approximately 1460K to 1500K (Figure 5.14-top). The corresponding flow rate also decreases sharply during this interval dropping nearly 0.4 $LPM/m^2 \times 10^{-3}$. For the second interval however, both the temperature and flow rate remain relatively constant at 1390K and 2.0 $LPM/m^2 \times 10^{-3}$ respectively. These results can be explained as follows.

Over time, the catalyst is constantly changing, or deactivating. Deactivation can be a result of several modes-all of which reduce the catalyst's active surface area to promote chemical reaction. Examples include the fusion of the catalyst's crystal structure at high temperatures otherwise known as "sintering," carbon deposits fouling the catalyst or "coking," or differential thermal expansion of the catalyst material

causing it to crack, break apart or delaminate. Higher operating temperatures (1460-1500K) for the first interval seemed to accelerate the catalyst's deactivation while lower operating temperatures (1390K) prevented further deactivation. This is likely a result of the different catalyst deactivation modes sensitivity to temperature.

The catalyst's deactivation is also related to an increase in wall temperature as shown in Figure 5.14 despite the applied heat flux being held constant. This can be explained by examining the modes of heat transfer depicted in Figure 5.15. An energy balance results in the following expression:

$$q''_{app} = q''_r + q''_{fb} + q''_{sub} \tag{5.1}$$

Assuming that the liquid is at saturation (no sub-cooling), and considering conduction across the vapor film, Equation 5.1 can be expressed,

$$q''_{app} = q''_r + \frac{k(T_w - T_{sat})}{\delta} \tag{5.2}$$

Rearranging Equation 5.2 to solve for the change in temperature across the vapor film,

$$(T_w - T_{sat}) = q''_{app}\left(1 - \frac{q''_r}{q''_{app}}\right)\frac{\delta}{k} \tag{5.3}$$

And finally expressing Equation 5.3 in non-dimensional form,

$$\frac{(T_w - T_{sat})k}{q''_{app}\delta} = 1 - \frac{q''_r}{q''_{app}} \tag{5.4}$$

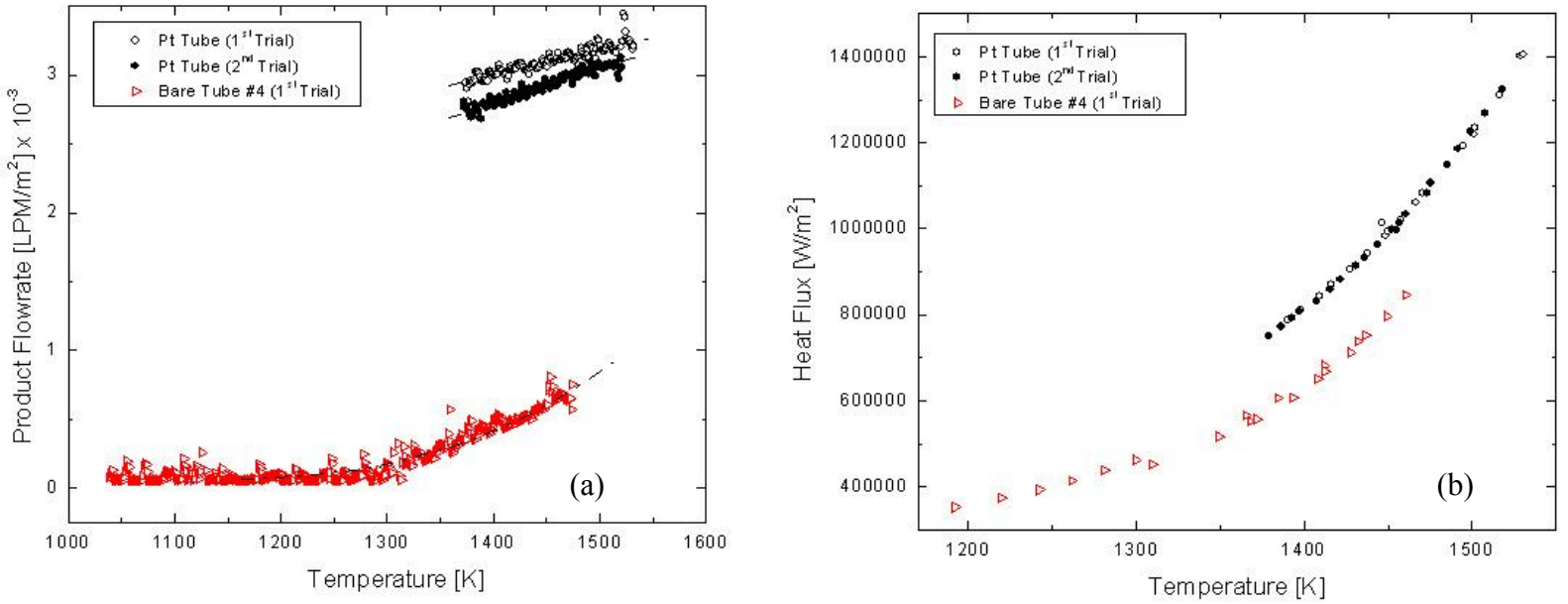

Figure 5.14: Ethylene glycol (80% vol)/water (20% vol) catalytic (Pt) conversion (a) flow rate curves and (b) film boiling curves. Thermal decomposition data (red) is also shown for comparison.

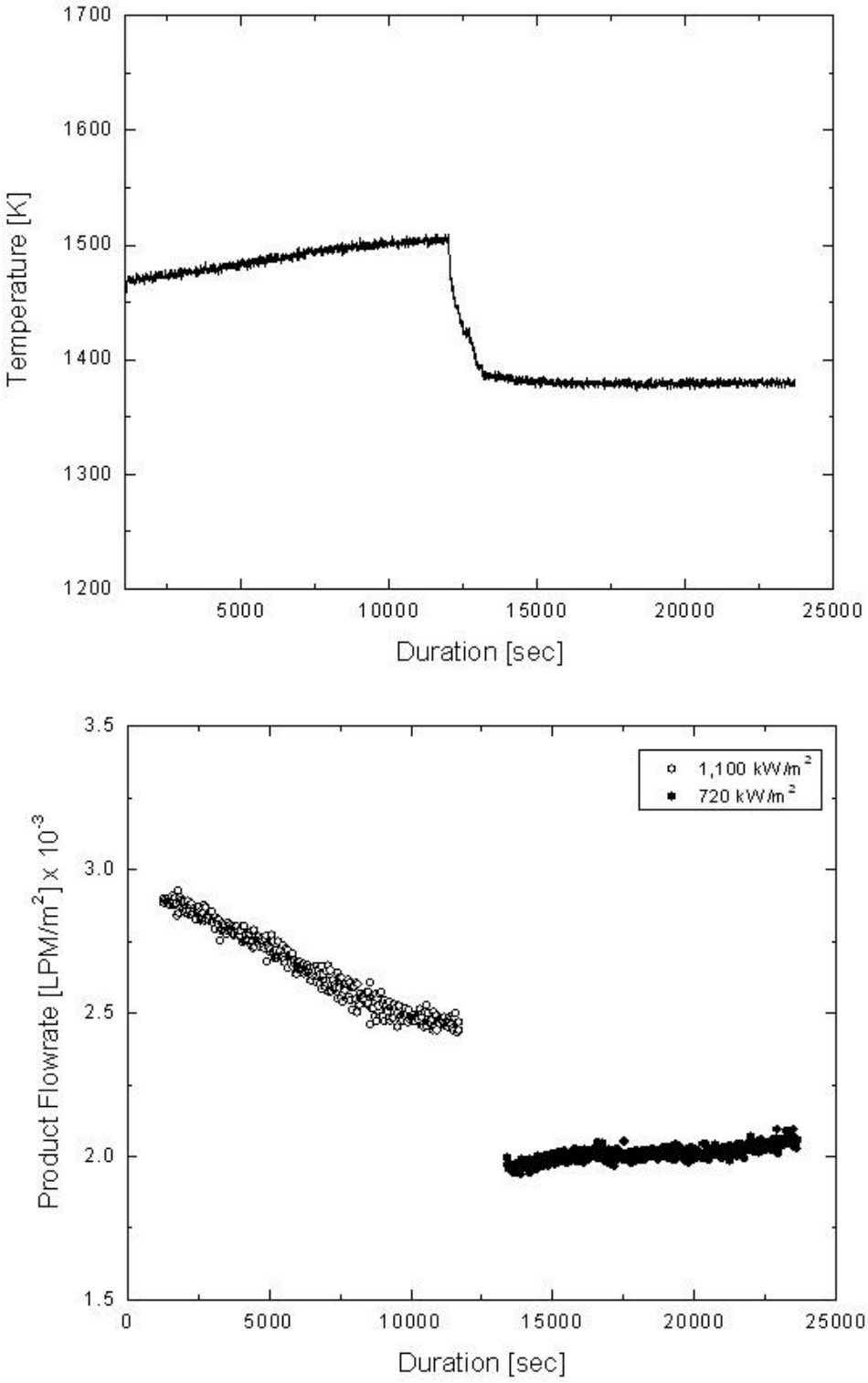

Figure 5.15: Catalytic (Pt) Conversion Constant Power Endurance Test

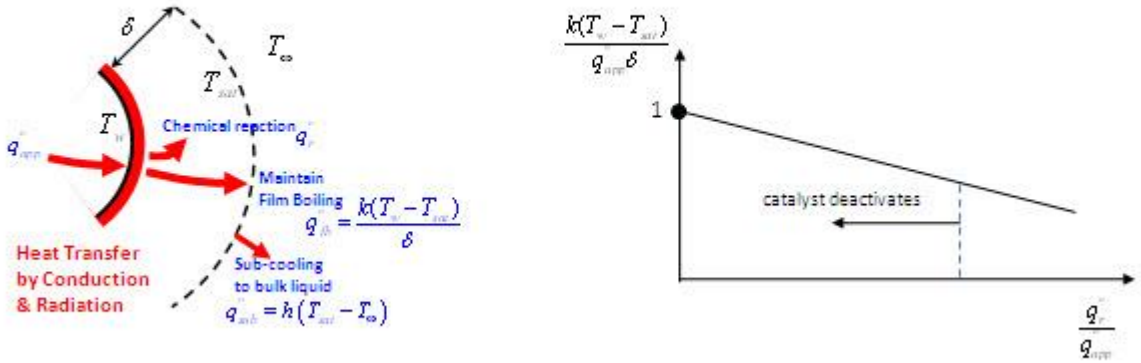

Figure 5.16: Heat transfer paths in the FIBOR for a saturated bulk liquid

This result (Equation 5.4) can be plotted as shown in Figure 5.15 (not to scale). As the catalyst deactivates, the heat for chemical reaction decreases evidenced by reduced product yields and the wall temperature must increase if the applied heat flux is held constant.

Scanning Electron Microscope (SEM) images were taken before and after use (Pt Tube) to further characterize the catalyst. Figure 5.17 shows images before testing (a, b, e) at magnifications of 100x, 300x, and 600x and after operation in the FIBOR (c, d, f). The most evident feature of these images is the cracking of the catalyst coating which supports the deactivation mode of differential thermal expansion during operation at high temperatures. The sections of catalyst material between the cracks (Figure 5.17f) also appear less porous when compared to the images shown before an experiment (Figure 5.17e), suggesting that the material may have undergone some sintering deactivation at high temperatures. Images at 300x (b, d) utilize a special feature of the SEM called Electronic Back Scattering (EBS). This provides contrast to the image relative to the average atomic number of elements on the surface: low atomic number elements (e.g. carbon) as well as void spaces appear darker than higher atomic number elements (e.g. metals). Figure 5.17b shows very light images, appearing white which is likely due to the strong presence of platinum on the surface. The EBS feature picks up the dark voided cracks in the surface in Figure 5.17d which are also apparent in the other images; however darker areas around the cracks may possibly be carbon material as a result of coking.

5.4.2 Nickel (Ni Tube) Catalyst Performance

Results for a nickel catalyst (Ni Tube) are presented in Figure 5.18. Overall, results are very similar to platinum. The first experiment trial achieved the highest

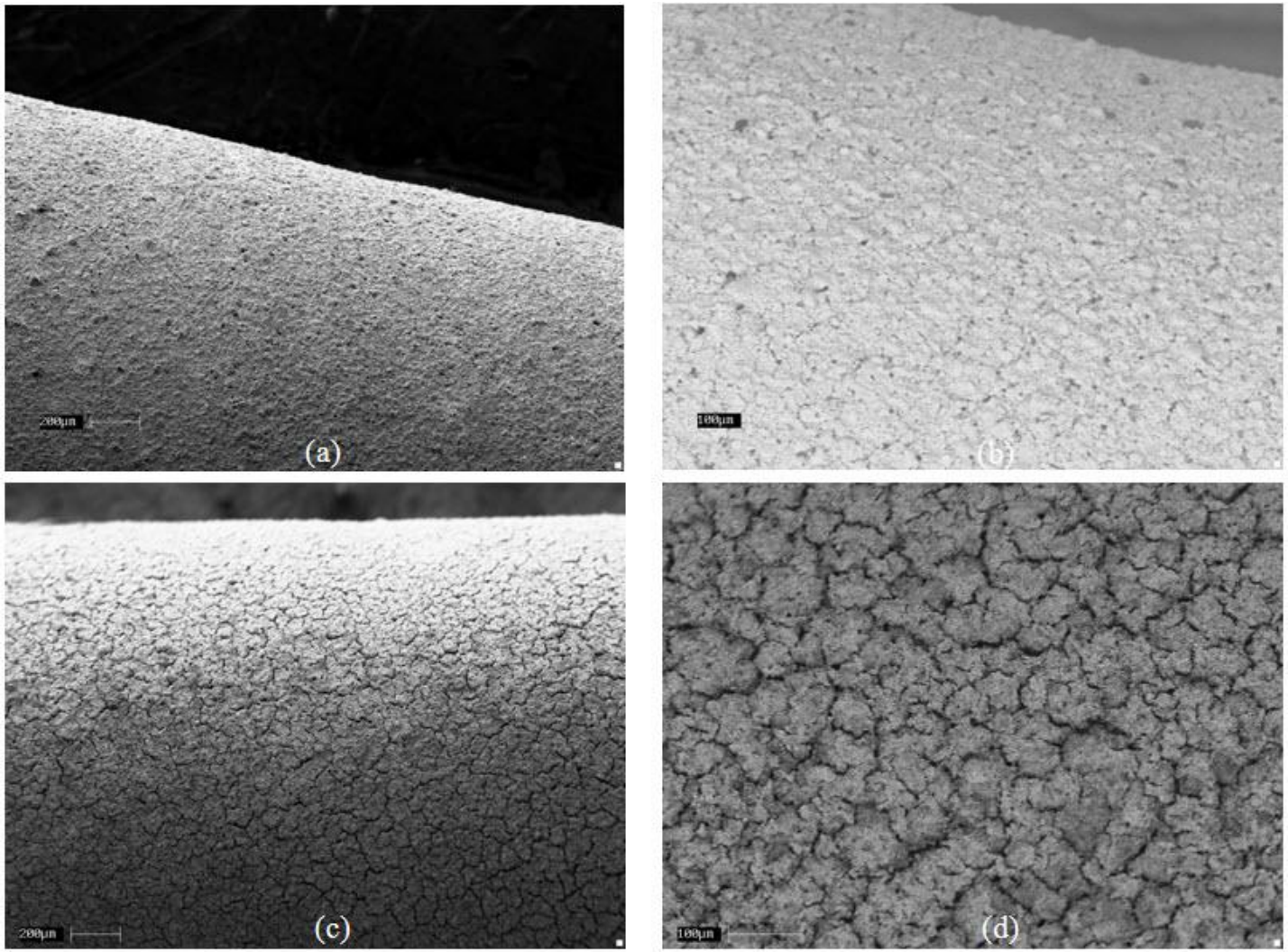

Figure 5.17a-d: SEM images of Pt heater surface before use at (a) 100x (b) 300x-EBS and after at (c) 100x (d) 300x-EBS

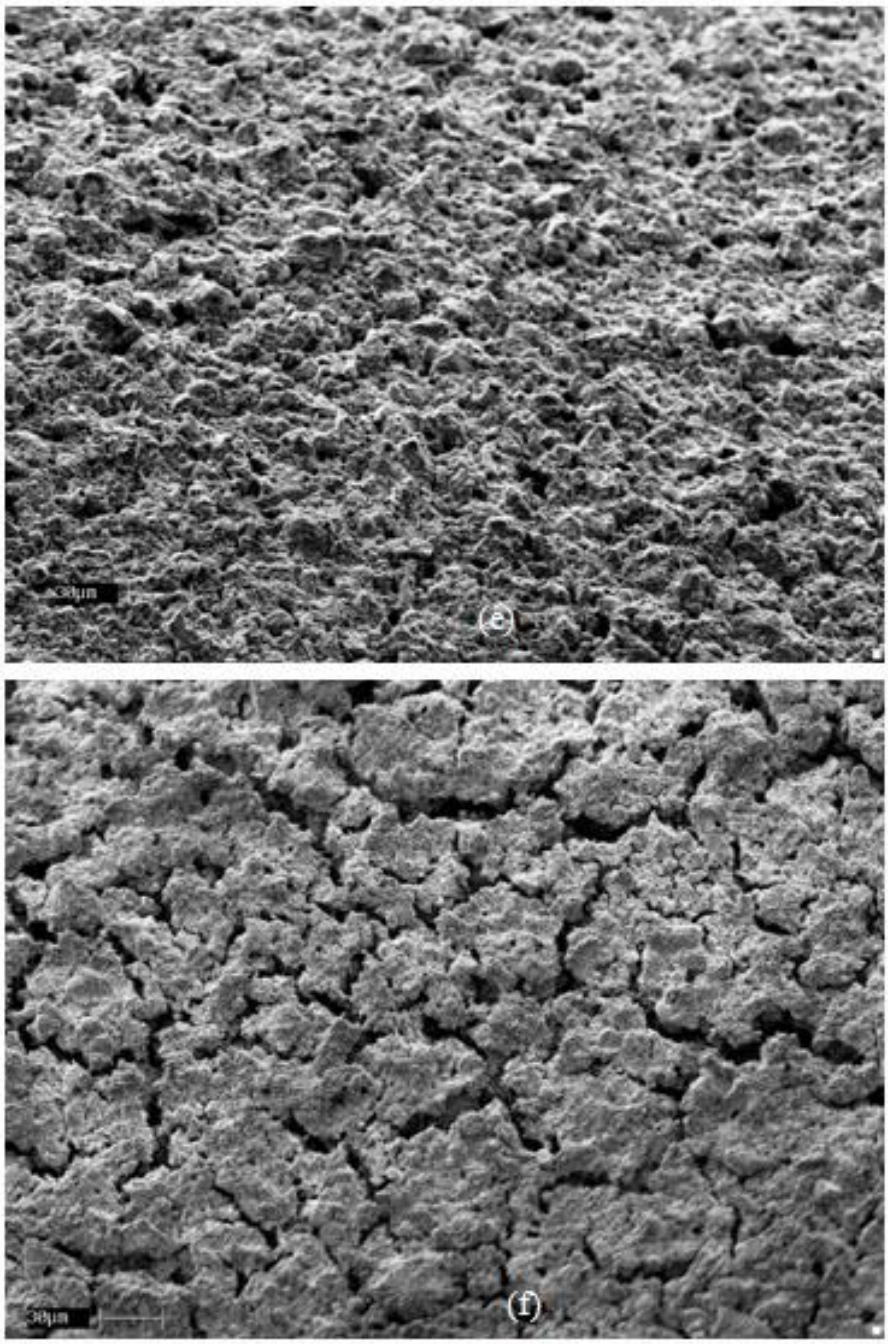

Figure 5.17e-f: SEM Images of Pt heater surface before (e) and after (f) use at 600

product yields, while the second trial achieved noticeably lower yields likely, as a result of catalyst deactivation. Results from Figure 5.12 for an 80%/20% aqueous mixture thermal decomposition are again shown for comparison. The nickel catalyst achieves significantly higher product yields (2-3 times higher) when compared to thermal decomposition. Closer comparison of the results for platinum and nickel however reveal some differences.

The second trial for nickel seems to show a more abrupt decrease in flow rate when compared to the second trial for a platinum catalyst. The difference is significant enough to have a slight thermal effect on the catalytic boiling curves as evidenced by the second trial being slightly lower than the first trial (Figure 5.18b). As shown in Figure 5.16a, product yields on average for nickel are also slightly less than that of platinum. (Figure 5.14a)

The results of the endurance test for nickel (Figure 5.19) shows that corresponding flow rates also decrease during the initial time interval by approximately 0.5 LPM/m^2 x 10^{-3}, which is slightly higher than the case for the platinum catalyst. At a lower heat flux (660 kW/m^2) however, both the temperature and flow rate remain relatively stable at approximately 1370K and 1.4 LPM/m^2 x 10^{-3} respectively. The modes of catalyst deactivation for the nickel catalyst are likely similar to that of platinum which include sintering, coking and/or delaminating as a result of differential thermal expansion.

Results for both platinum and nickel are presented together in Figure 5.20. Figure 5.20a compares results with thermal decomposition. Platinum clearly achieves higher yields than nickel. However, both show a similar trend with respect to heater temperature. Results of the endurance test are also provided in Figure 5.20b. Again, platinum achieves higher product yields than nickel, though both show very similar

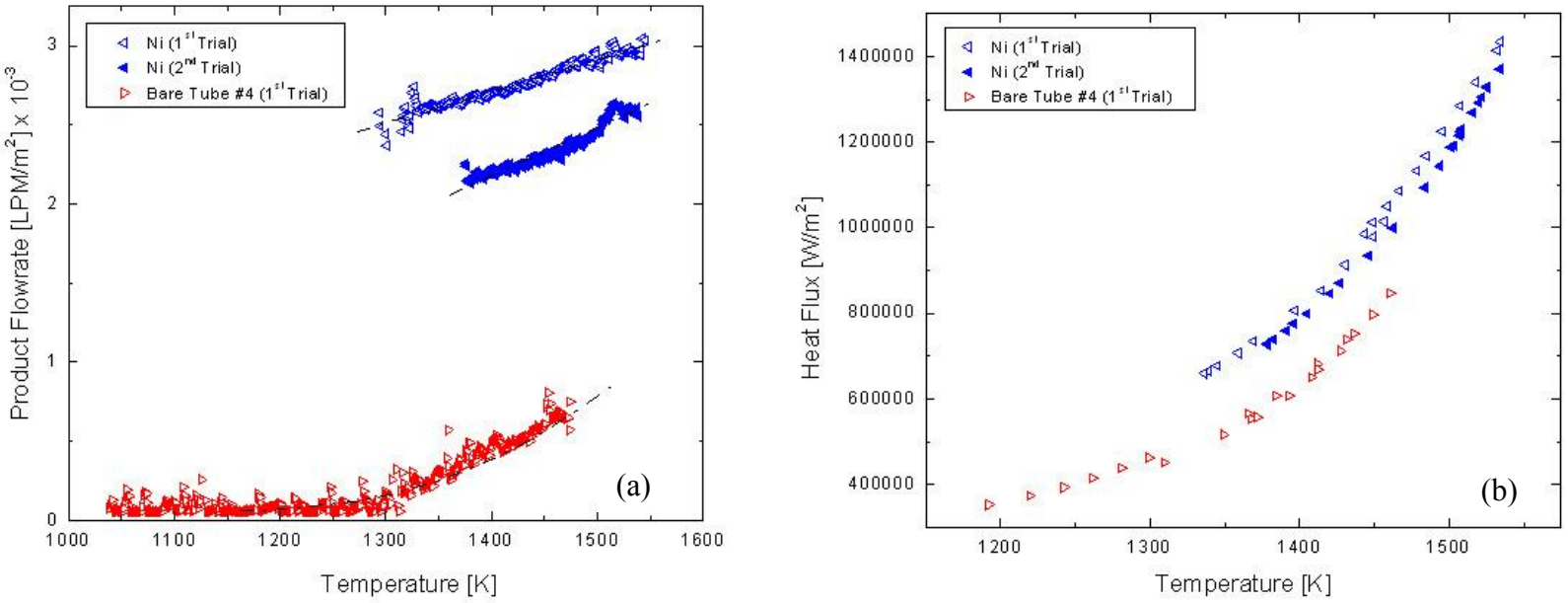

Figure 5.18: Ethylene glycol (80% vol)/water (20% vol) catalytic (Ni) conversion (a) flow rate curves and (b) film boiling curves. Thermal decomposition data (red) is also shown for comparison.

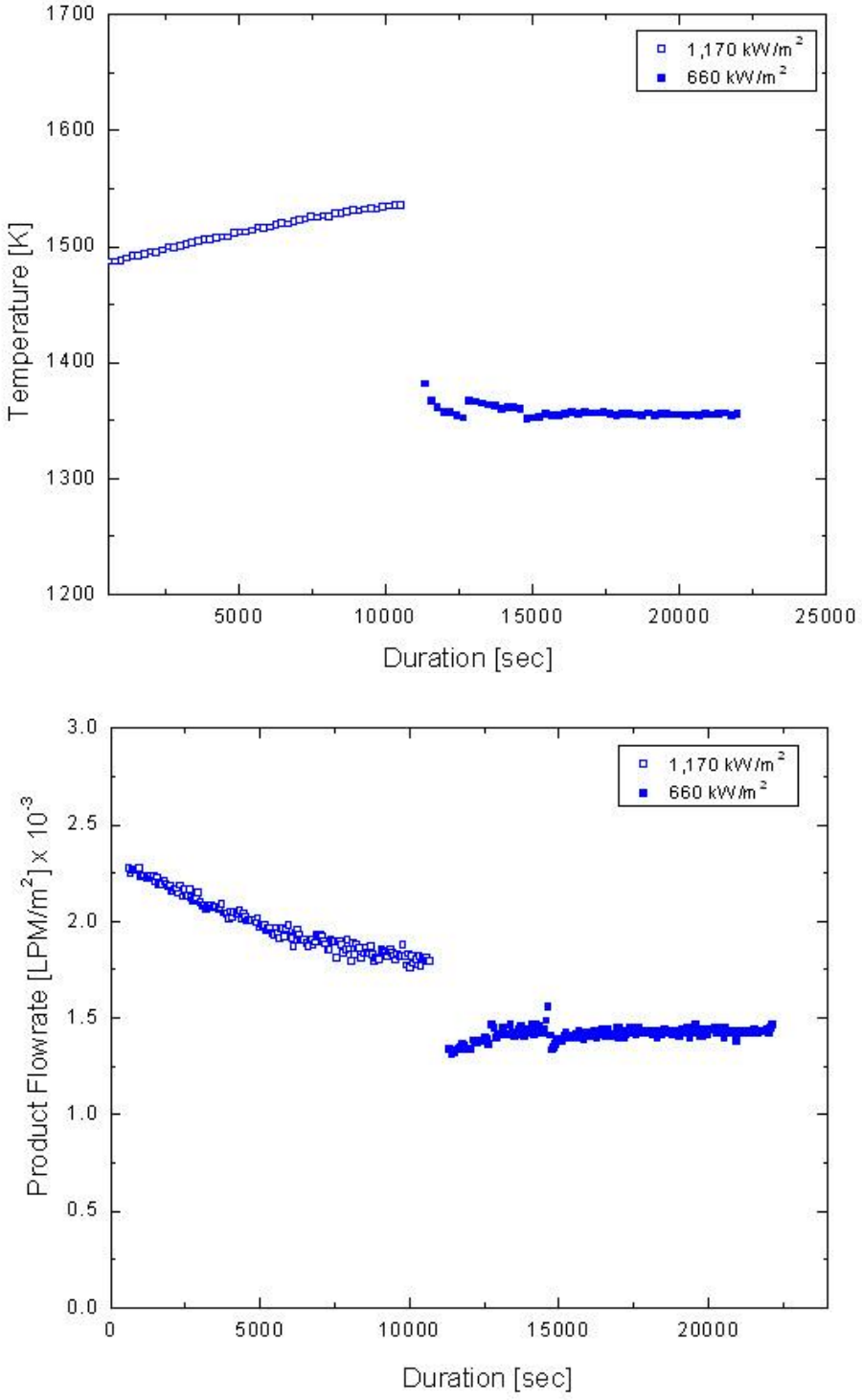

Figure 5.19: Catalytic (Pt) Conversion Constant Power Endurance Test

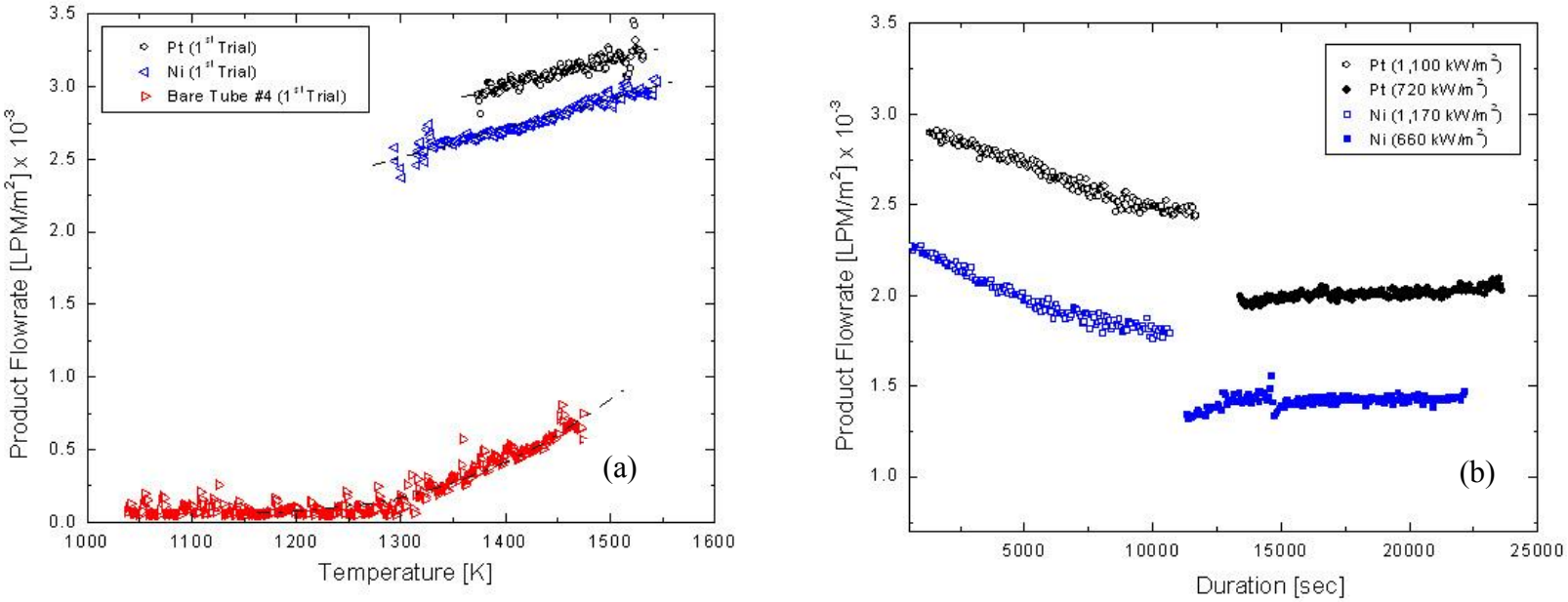

Figure 5.20: Pt vs. Ni performance comparison (a) flow rate curves and (b) endurance test

trends in terms of deactivation at higher power settings as well as stabilization in product flow rates at lower settings.

Images taken from an SEM before and after use with the nickel coated tube (Ni Tube) are presented in Figure 5.21. The images are organized in an identical manner as Figure 5.17 "before" use (a, b, e) at magnifications of 100x, 300x, and 600x compared to respective "after" use (c, d, f). An additional image at a higher magnification, Figure 5.21g, (1800x) however is provided to better examine the catalyst structure after use. Nickel crystals are clearly seen by their distinct geometric shapes. The other material surrounding the crystals may either be carbon or alumina. The most evident feature from these images is the surface cracking which again makes a strong case for differential thermal expansion as a result of high operating temperatures. The EBS feature shows noticeably different images than the platinum case. While the image before use (Figure 5.21b) is similar, showing a high contrast surface which is likely caused by the abundance of nickel on the surface, the EBS after image (d) shows a darker image speckled with lighter contrast likely representing nickel crystals. This may be the result of carbon (coking) layering over the surface covering the nickel or possibly some sort of surface restructuring.

Catalysts (Pt Tube and Ni Tube) were further characterized by EDS scans before and after use. Figure 5.22 shows results for the Pt Tube (a) and Ni Tube (b). Scans confirm the presence of both catalyst metals (platinum and nickel) as well as aluminum which comes from the alumina (Al_2O_3) adhesion layer in the form of peaks along the EDS spectra. Scans were taken after but not presented because they depict no noticeable changes than the scans in Figure 5.22. These results (Figure 5.22) therefore serve to only confirm the reported composition of the catalyst layer, yet does not provide any sort of chemical analysis regarding catalyst degradation.

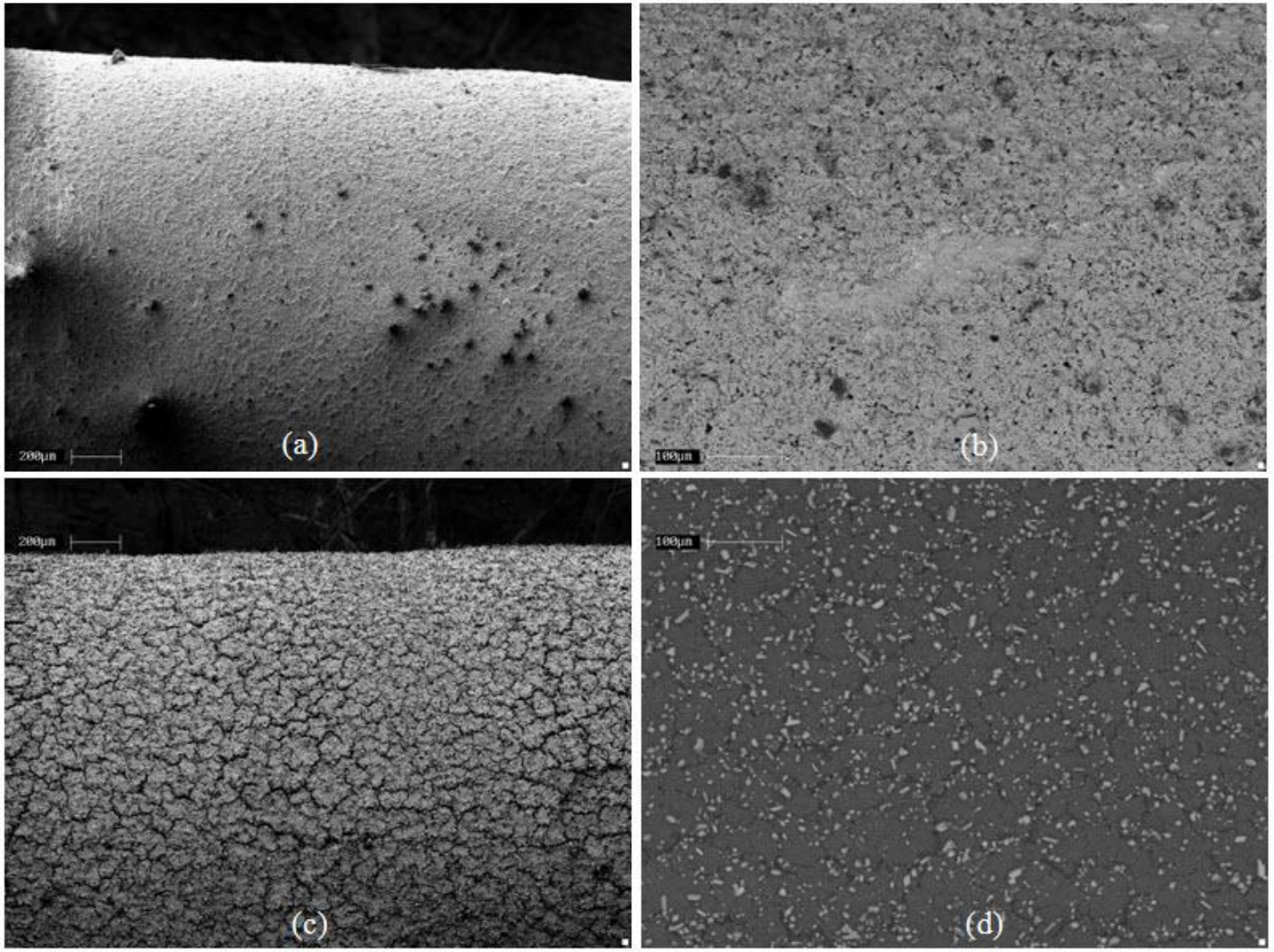

Figure 5.21a-d: SEM Images of Ni heater surface before use at (a) 100x (b) 300x-EBS and after at (c) 100x (d) 300x-EBS

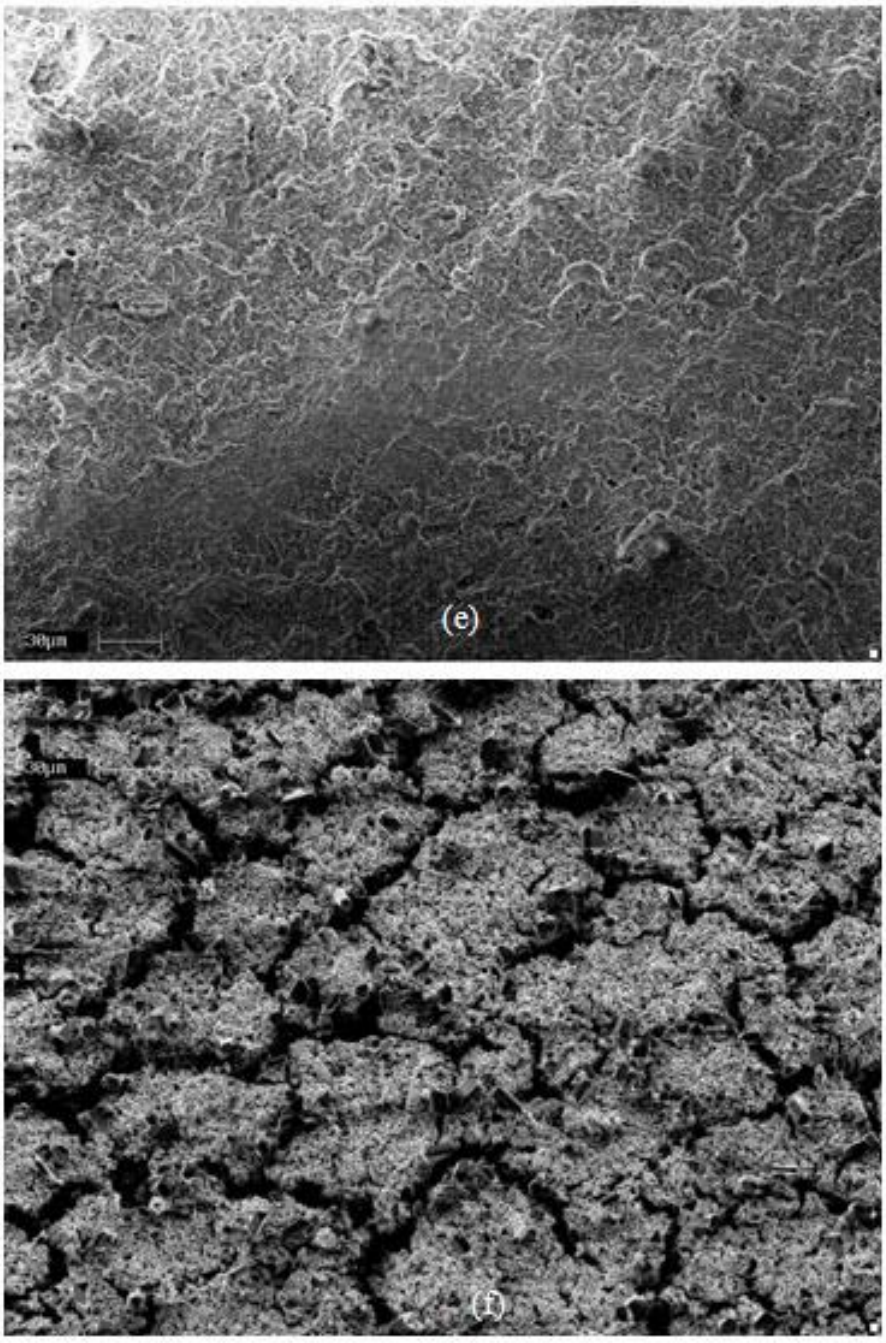

Figure 5.21e-f: SEM Images of Ni heater surface before (e) and after (f) use at 600x

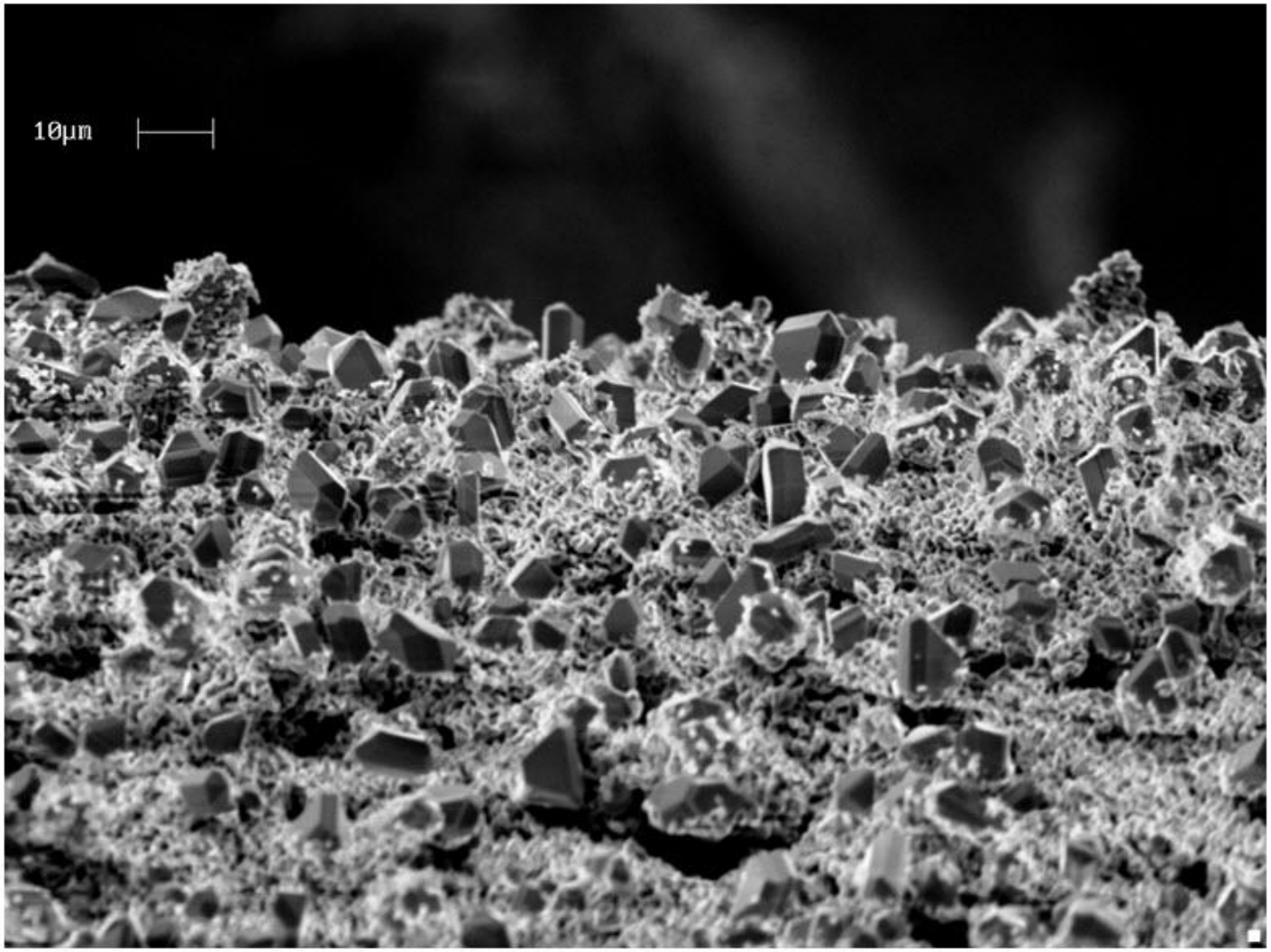

Figure 5.21g: SEM image of Ni heater surface after use taken at 1800x to observe unique crystal structure

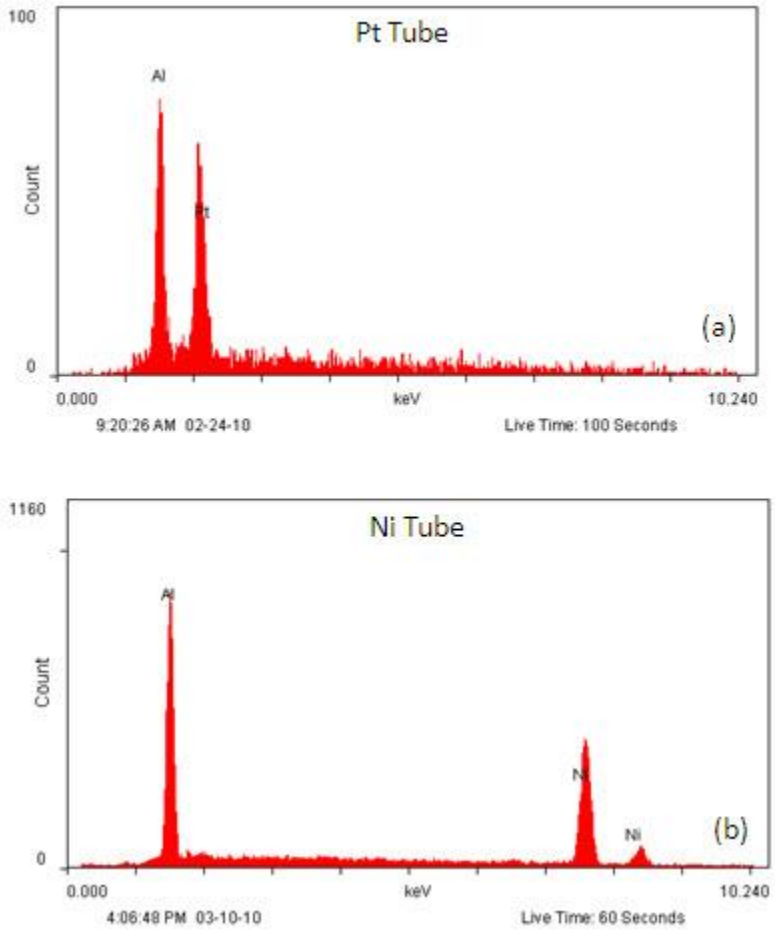

Figure 5.22: EDS scan of Pt Tube (a) and Ni Tube (b)

5.4.3 Steam Reforming Chemistry

Two approaches are used to present a better understanding of the FIBOR's chemistry. The first assumes that the difference in boiling curves for thermal decomposition (bare tube) and catalytic conversion (Ni and Pt tubes) is a result of chemical reaction alone as a result of the endothermic reactions (Equations 5.1-5.4) to estimate the heat required to support chemical reaction. The second approach compares species concentrations determined from GC analysis with soichiometric ratios for a bare tube. Although neither approach provides a definitive chemical analysis, results suggest that a catalyst coated tube can promote steam reforming in a FIBOR.

Choi (2010) demonstrated for the case of methanol that the difference between boiling curves for a tube supporting catalytic conversion and a tube with no reaction was approximately equal to the heat of reaction for methanol decomposition. This was a result of a simple chemical mechanism with one reaction dominating (methanol decomposition). This simplified approach leads to erroneous results with pure ethylene glycol (Choi 2010) and ethylene glycol aqueous mixtures because of a much more complex chemical mechanism. For example, numerous secondary reactions exist as evidenced by the previously discussed tendency for carbon deposits to form, liquid contamination and the existence of several product species for thermal decomposition (Figures 5.6, 5.13) and catalytic reaction (to be discussed in Figures 5.23.) To further complicate matters, the experimental data for catalytic reaction is also within the temperature range for thermal decomposition to exist. Therefore, the difference in boiling curves in Figures 5.14 and 5.18 cannot be attributed to one dominant reaction (steam reforming, Equation 1.2) alone.

Table 5.2 nonetheless summarizes the performance of the FIBOR for a bare and catalytic tube. Results indicate that the chemical mechanism is indeed endothermic. The heat

Table 5.2: Extracted Data from Flow Rate and Boiling Curves to Estimate Heat for Chemical Reaction

Wall Temp (K)	Heat Flux Applied (W/m^2)			Product Flow Rate (LPM/m^2)			Estimated Heat Flux for Chemical Reaction (W/m^2)/ (Percentage of Applied Heat Flux in Parentheses)	
	Bare Tube	Pt Tube	Ni Tube	Bare Tube	Pt Tube	Ni Tube	Pt	Ni
1390	599,493	787,513	787,941	440	2,960	2,690	188,020 (23.9%)	188,448 (23.9%)
1430	738,392	920,000	912,514	562	3,035	2,756	181,608 (19.7%)	174,122 (19.1%)
1450	797,057	994,257	980,000	600	3,100	2,800	197,200(19.8%)	182,943 (18.7%)

flux attributed to catalytic chemical reaction is shown in the far right column and although it increases for higher temperatures, the overall percentage of the total heat flux that supports catalytic chemical reaction decreases. This can be explained by the fact that as the temperature increases, the contribution from thermal decomposition increases which also consumes a portion of the applied heat flux.

Detecting the product species and their concentrations through GC analysis provides the clearest evidence for the underlying chemistry that supports converting aqueous mixtures in a FIBOR. Figure 5.23 shows the GC traces for catalytic reaction in the FIBOR at a temperature of 1373K (a) and 1473K (b). Table 5.3 summarizes results for all GC analysis by comparing the results discussed in Figures 5.6 and 5.13 for bare tubes to that of the catalytic tubes in Figure 5.23. Although the same species are detected, their concentrations are noticeably different for a catalytic tube. The product gas for catalytic reforming is enriched significantly more with hydrogen at approximately 68% compared to just 44% for a bare tube. The concentrations of CO_2 also increase from just under 1% for a bare tube to approximately 7% for a catalyst coated tube. The concentration of CH_4 decreases significantly from approximately 10% for a bare tube to just over 1% for catalytic, while other higher hydrocarbons such as C_2H_2 and C_2H_4 are also significantly decreased by approximately a factor of 10. The increase in hydrogen and carbon dioxide respectively is evidence of the steam reforming reaction (Equation 1.2). The water gas shift reaction is also likely present which reduces CO_2 concentrations below the stoichiometric ratio of Equation 1.2 ($H_2/CO_2=5/2$) and in turn creates appreciable amounts of carbon monoxide (approximately 20%). These amounts however remain significantly lower than thermal decomposition alone (approximately 40%). The methanation reaction is likely limited since its reactants are not direct products of the primary reaction as is the case for thermal decomposition.

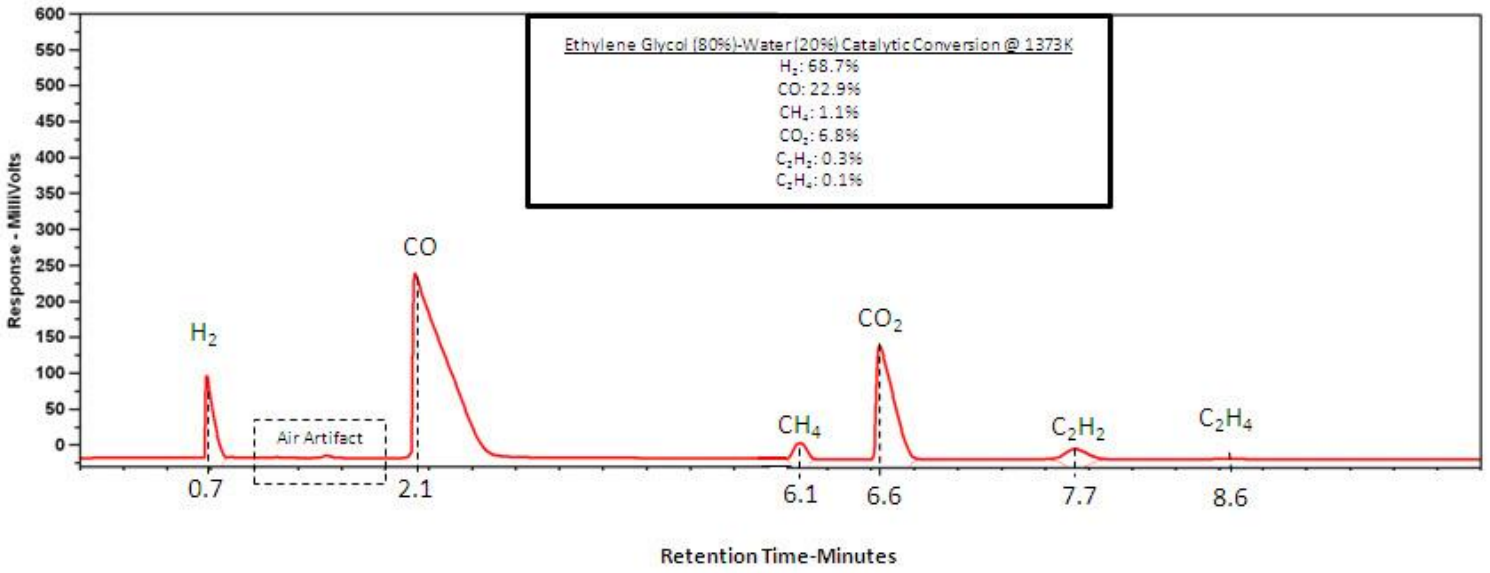

Figure 5.23a: GC Trace for catalytic conversion of ethylene glycol (80% vol)/water (20% vol) at 1373K

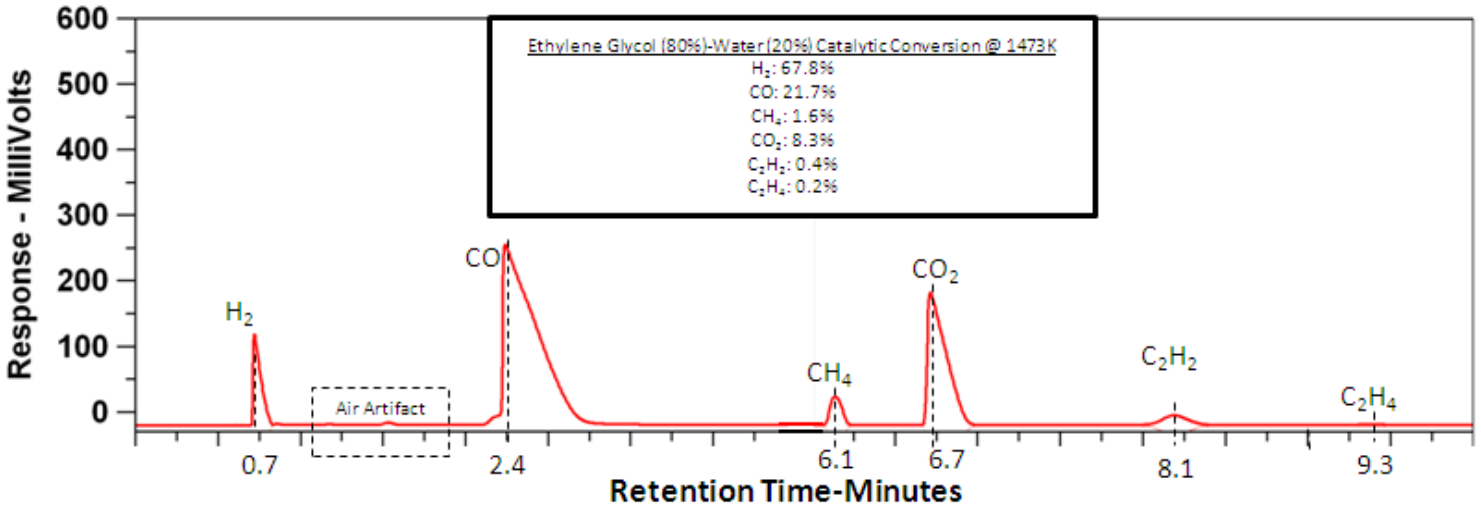

Figure 5.23b: GC Trace for catalytic conversion of ethylene glycol (80% vol)/water (20% vol) at 1473K

Table 5.3: Summary of GC Analysis

Reacant (%EG/%H_2O)	Heater Surface	Temperature (K)	H_2 (%)	CO (%)	CH_4 (%)	CO_2 (%)	C_2H_2 (%)	C_2H_4 (%)
90/10	Bare	1473	43.7	40.3	11.1	0.7	2.4	1.8
80/20	Bare	1473	44.8	40	9.4	0.9	2.6	2.2
80/20	Catalytic	1373	68.7	22.9	1.1	6.8	0.3	0.1
80/20	Catalytic	1473	67.8	21.7	1.6	8.3	0.4	0.2

For catalytic conversion, the temperature seems to have little effect on the concentrations of product species. The operating domain however was limited to a range of approximately 200K which provides a limited assessment of the temperature's effect on products. This temperature range however can likely be extended to lower temperatures with design modifications to the heater tube assembly.

\

CHAPTER 6

CONCLUSIONS AND RECOMMENDATIONS FOR FUTURE RESEARCH

6.1 Conclusions

- A FIBOR experimental apparatus has been designed, fabricated and tested which is capable of chemically converting liquid organic aqueous mixtures into gas products consisting mainly of hydrogen and carbon monoxide, or syngas.
- A smaller heater diameter lowers the FIBOR's performance, however overall power supply and condensing requirements are minimized. Additionally, a smaller heater diameter allows for better observation of bubbling dynamics.
- For the case of a bare heater, a black carbonaceous layer forms around the heater surface which lowers reactor performance. This phenomenon is observed for pure ethylene glycol reactant and a 90% (EG) / 10% (H_2O) reactant mixture. This effect however was not observed for 80% (EG) / 20% (H_2O) which suggests the presence of steam within the reactor volume may diminish the formation of carbon.
- The bulk liquid reactant is contaminated with various species as a result of condensable products formed from secondary chemical reactions for the case of pure ethylene glycol reactant. The bulk was not observed to be contaminated for aqueous mixtures.
- Chemical conversion is possible with a bare heater, however product flow rates diminish considerably as the reactant mixture is enriched with water. This is likely the result of only ethylene glycol thermal decomposition occurring within the vapor film for the case of a bare heater tube.

- Catalytic conversion of aqueous organic mixtures can be promoted through steam reforming in a FIBOR. This is demonstrated with platinum and nickel based catalysts converting an 80% ethylene glycol / 20 % water mixture where both achieve significantly higher product yields than a bare heater tube. Measured yields are approximately three to four times higher for a catalyst coated tube compared to a bare tube. This is attributed to enhanced chemical reactivity at the catalyst coated surface.
- Platinum demonstrates slightly better performance than nickel in terms of overall product yield and resistance to deactivation. Nickel however could be more attractive at larger scales due to its low cost compared to platinum. The rate of deactivation is limited when operating at lower temperatures.
- Products (syngas) are significantly enriched with hydrogen for catalytic conversion (H_2/CO=68%/22%) compared to thermal decomposition (H_2/CO=44%/40%). Methane (CH_4) is significantly reduced for catalytic conversion (1.3%) compared to thermal decomposition (10%) while the concentration of carbon dioxide (CO_2) shows the opposite trend with products for catalytic conversion containing approximately 7% compared to just 0.8% for thermal decomposition. Small traces of acetylene (C_2H_2) and ethylene (C_2H_4) are detected for both means of conversion with slightly higher amounts detected for thermal decomposition.
- Thermochemical and gas chromatography analysis provides evidence that ethylene glycol can be converted in a FIBOR via steam reforming (Equation 1.2), in order to enrich the products with hydrogen. Additional species are created in small amounts through several secondary chemical reactions.
- Adding water to ethylene glycol reduces overall product yield as a result of vapor-liquid equilibrium. Catalytic performance of an 80%/20% mixture is

able to match the performance of converting pure ethylene glycol at an operating temperature of approximately 1300K, however with less sensitivity to temperature. Although higher yields can be achieved with pure ethylene glycol reactant, it may be more beneficial to convert an aqueous mixture reactant in order to promote steam reforming to limit the formation of carbon and enrich the products with hydrogen. A compilation of flow rate and boiling curves is provided in Figure 6.1. Further details to include raw data and analysis of flow rate curves can be found in Appendix E. Boiling Curve data, to include experiments conducted with water, can be found in Appendix F.

6.2 Recommendations for Future Research

- **Heater Design.** Figure 4.3 shows the axial temperature profile across the heater tube. The decrease in temperature at the ends of the heater tube as a result of axial conduction heat losses to the electrode clamps causes destabilization of film boiling. As a result, nucleate boiling commonly formed at the ends, often around 1373K, and would subsequently spread quickly across the tube unless power was quickly increased. Design considerations should be made to minimize this effect. Possible modifications could include: 1) modifying the electrode clamp design to minimize the surface contact between the electrode clamps and heater tube to reduce conduction losses; 2) reduce the diameter of at the end of the heater tube as well as remove catalyst coating material to create a "surge" in heat flux as well as limit thermochemical losses to prevent the spread of nucleate boiling; and 3) consider a smaller heater (e.g. platinum wire under tension) such that the electrode clamp connection minimizes conduction losses and is not submerged in the bulk liquid.

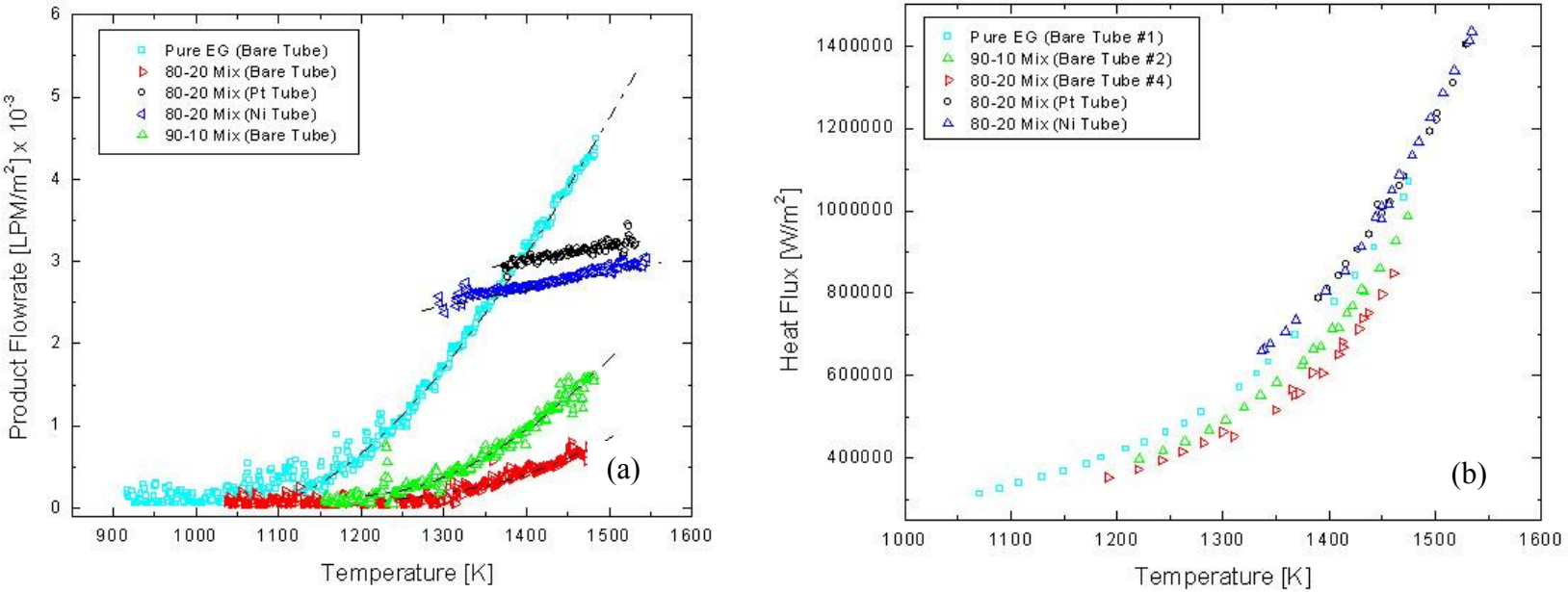

Figure 6.1: Compilation of (a) flow rate curves and (b) film boiling curves for Ethylene Glycol and its Aqueous Mixtures

- **SEM Images.** Characterizing the heater surface through SEM imaging should be sustained, however taking before/after images at a higher magnification and better orientation should be followed. The magnification and orientation shown in Figure 5.19g provides the best results.
- **X-Ray Dispersion Spectroscopy (EDS).** The black coating substance which should be verified through EDS testing that is capable of detecting carbon.
- **Air Artifact in GC Trace.** The gas line configuration shown in Figure B.9 should be modified to prevent air from contaminating product samples sent through the GC.
- **Additional Mixture Testing.** Testing of several additional aqueous mixtures should be conducted. Efforts should focus on closer examination of the limits at which no chemical reaction is possible as well as the role that different mixtures (or steam to ethylene glycol ratios) have with respect to hydrogen production, resistance to deactivation and overall product yield.
- **Catalyst Coating Technique.** Results of this work are largely attributed to the expertise of Catacel Corp. in fabricating suitable catalyst coatings that can endure the FIBOR's operating conditions. Further collaboration is needed to better understand this coating procedure and to ultimately refine and develop a repeatable technique.
- **Modeling.** Theoretical work is needed to model the two phase boundary layer problem for film boiling mixtures with chemical reaction. Such work will provide a better understanding of the physics and operating parameters for converting mixtures in a FIBOR. Particularly the role of vapor-liquid equilibrium, mass diffusion and steam reforming chemistry should be investigated.

APPENDIX A

Heater Assembly Detailed Technical Drawings

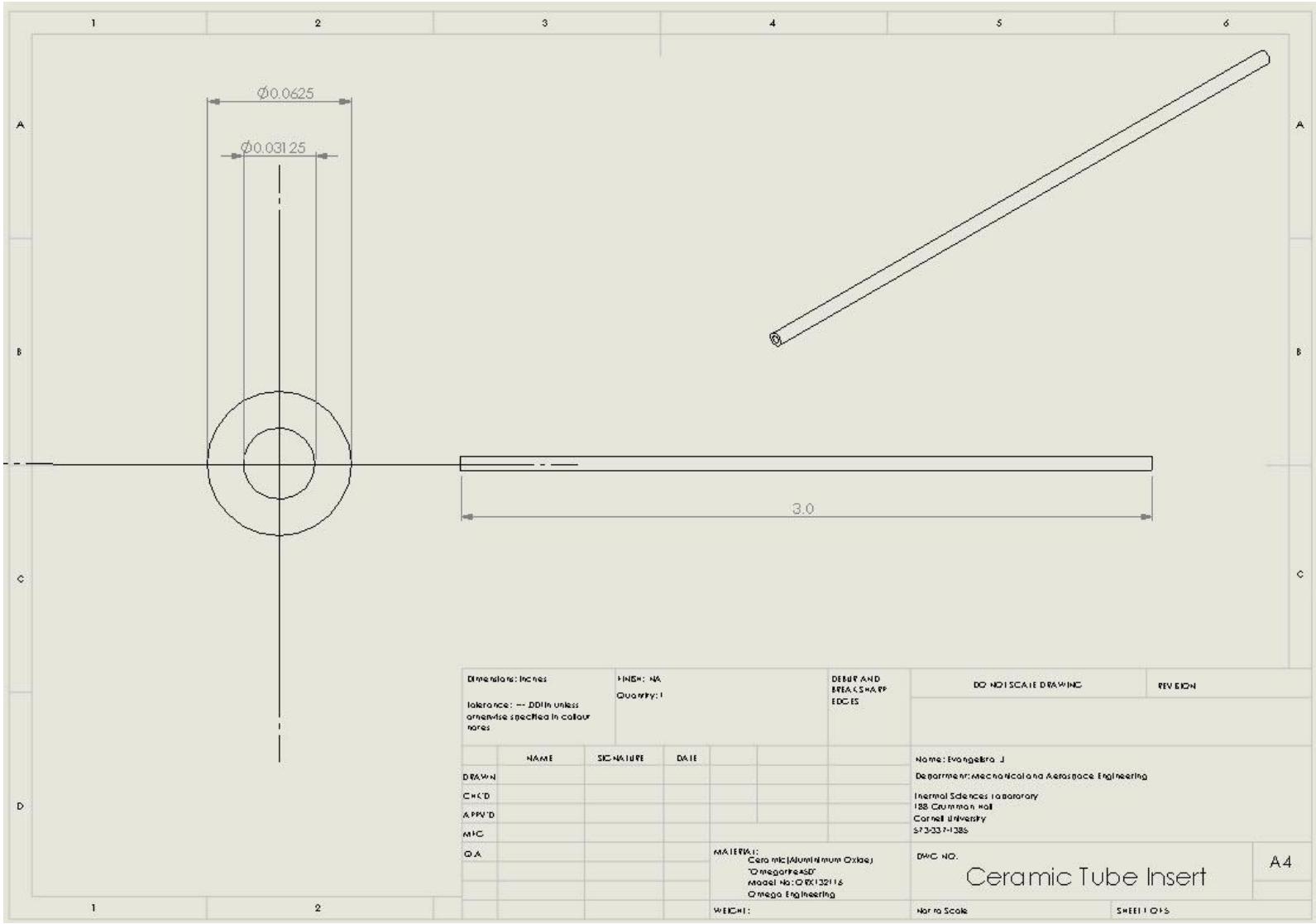
Ø0.0625
Ø0.03125
3.0
Dimensions: Inches
Tolerance: -- .001in unless otherwise specified in colour notes
FINISH: NA
Quantity: 1
DEBUR AND BREAK SHARP EDGES
DO NOT SCALE DRAWING
REVISION
NAME
SIGNATURE
DATE
DRAWN
CHK'D
APPV'D
MFG
Q.A
MATERIAL:
Ceramic (Aluminum Oxide)
"Omegaforce 650"
Model No: CRX13216
Omega Engineering
WEIGHT:
Name: Evangelos J
Department: Mechanical and Aerospace Engineering
Thermal Sciences Laboratory
188 Grumman Hall
Cornell University
973-337-1385
DWG NO.
Ceramic Tube Insert
A4
Not to Scale
SHEET 1 OF 1

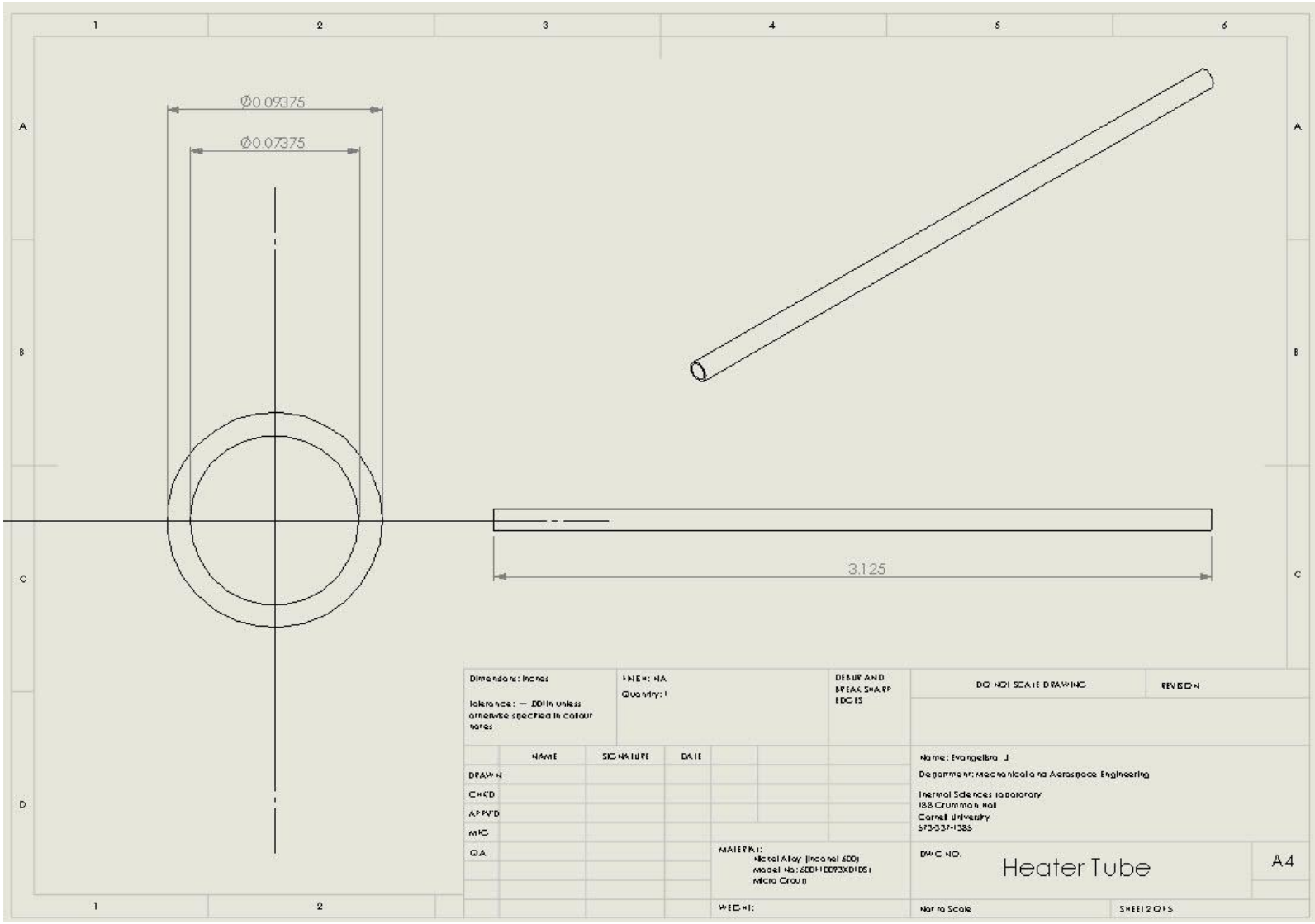
Ø0.09375
Ø0.07375
3.125
Dimensions: Inches
tolerance: ± .001in unless otherwise specified in callout notes
FINISH: NA
Quantity: 1
DEBUR AND BREAK SHARP EDGES
DO NOT SCALE DRAWING
REVISION
NAME
SIGNATURE
DATE
DRAWN
CHK'D
APP'D
MFG
Q.A
Name: Evangelos J
Department: Mechanical and Aerospace Engineering
Thermal Sciences Laboratory
188 Grumman Hall
Cornell University
MATERIAL:
Nickel Alloy (Inconel 600)
Model No: 600-1.0093X0.0751
Micro Group
DWG NO.
Heater Tube
A4
WEIGHT:
Norma Scale
SHEET 2 OF 5

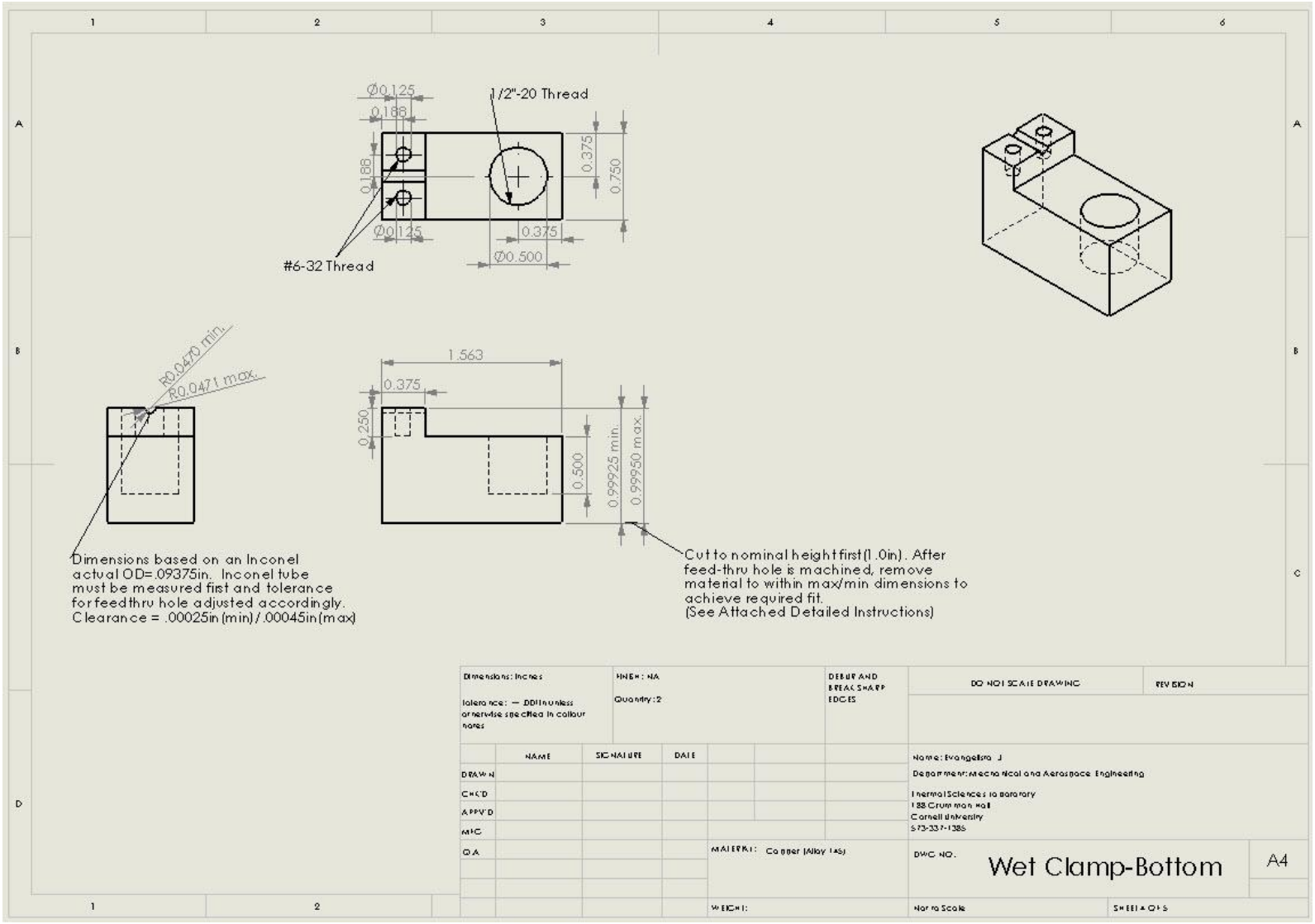
Ø0.125
0.188
1/2"-20 Thread
0.188
0.375
0.750
Ø0.125
0.375
Ø0.500
#6-32 Thread
R0.0470 min.
R0.0471 max.
1.563
0.375
0.250
0.500
0.99925 min.
0.99950 max.
Dimensions based on an Inconel actual OD=.09375in. Inconel tube must be measured first and tolerance for feedthru hole adjusted accordingly. Clearance = .00025in (min) / .00045in (max)
Cut to nominal height first (1.0in). After feed-thru hole is machined, remove material to within max/min dimensions to achieve required fit. (See Attached Detailed Instructions)
Dimensions: Inches
Tolerance: +/- .001in unless otherwise specified in callout notes
FINISH: NA
Quantity: 2
DEBUR AND BREAK SHARP EDGES
DO NOT SCALE DRAWING
REVISION
NAME
SIGNATURE
DATE
DRAWN
CHK'D
APPV'D
MFG
Q.A
MATERIAL: Copper (Alloy 145)
WEIGHT:
Name: Evangelos J
Department: Mechanical and Aerospace Engineering
Thermal Sciences Laboratory
188 Crumman Hall
Cornell University
573-337-1385
DWG NO.
Wet Clamp-Bottom
A4
Not to Scale
SHEET 1 OF 1

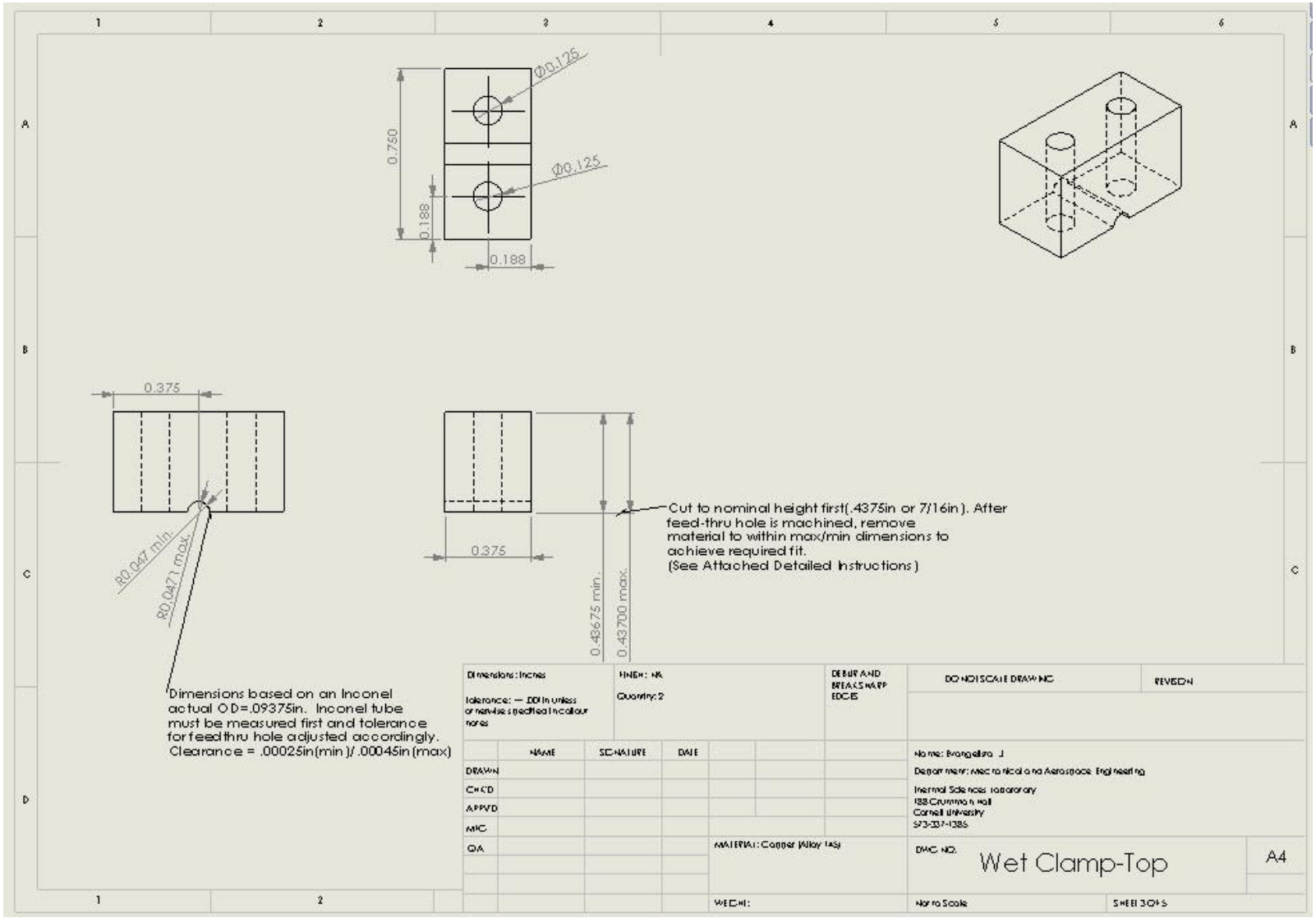
Ø0.126
Ø0.125
0.750
0.188
0.188
0.375
R0.047 min.
R0.0471 max.
0.375
0.49675 min.
0.49700 max.
Cut to nominal height first(.4375in or 7/16in). After feed-thru hole is machined, remove material to within max/min dimensions to achieve required fit.
(See Attached Detailed Instructions)
Dimensions based on an Inconel actual OD=.09375in. Inconel tube must be measured first and tolerance for feedthru hole adjusted accordingly. Clearance = .00025in(min)/.00045in(max)
Dimensions: Inches
Tolerance: ± .005 in unless otherwise specified Inch&our notes
FINISH: NA
Quantity: 2
DEBUR AND BREAK SHARP EDGES
DO NOT SCALE DRAWING
REVISION
NAME
SIGNATURE
DATE
DRAWN
CHK'D
APPV'D
MFG
QA
MATERIAL: Copper Alloy 145
WEIGHT:
Name: Evangelista J
Department: Mechanical and Aerospace Engineering
Thermal Sciences Laboratory
188 Grumman Hall
Cornell University
973-337-1386
DWG NO.
Wet Clamp-Top
A4
Name Scale
SHEET 3 OF 5

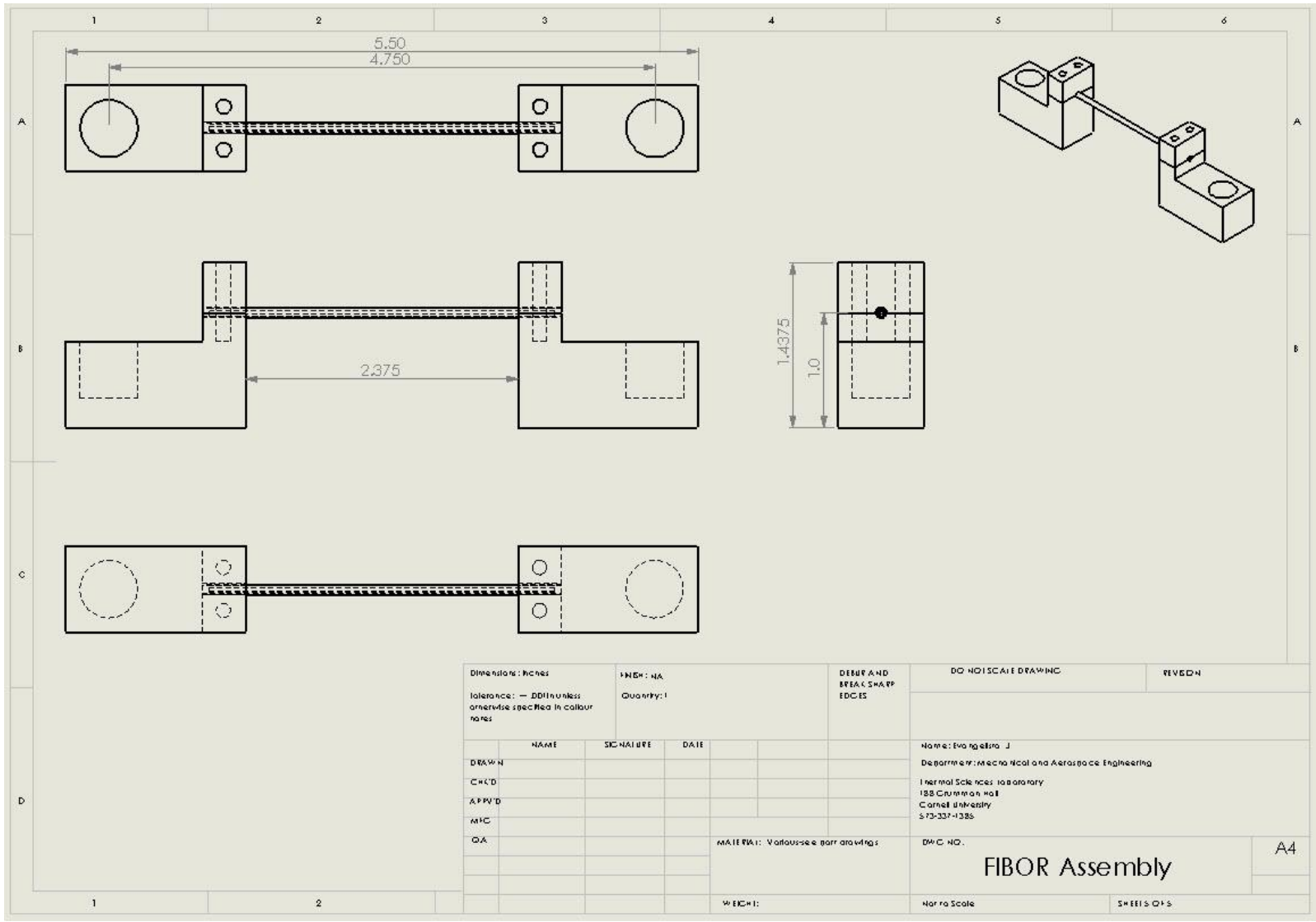
5.50
4.750
2.375
1.4375
1.0
Dimensions : Inches
Tolerance : ± .001in unless otherwise specified in callout notes
FINISH : NA
Quantity: 1
DEBUR AND BREAK SHARP EDGES
DO NOT SCALE DRAWING
REVISION
NAME
SIGNATURE
DATE
DRAWN
CHK'D
APPV'D
MFG
QA
MATERIAL: Various-see part drawings
WEIGHT:
Name: Evangelista J
Department: Mechanical and Aerospace Engineering
Thermal Sciences laboratory
188 Grumman Hall
Cornell University
573-337-1386
DWG NO.
FIBOR Assembly
A4
Not to Scale
SHEET 1 OF 1

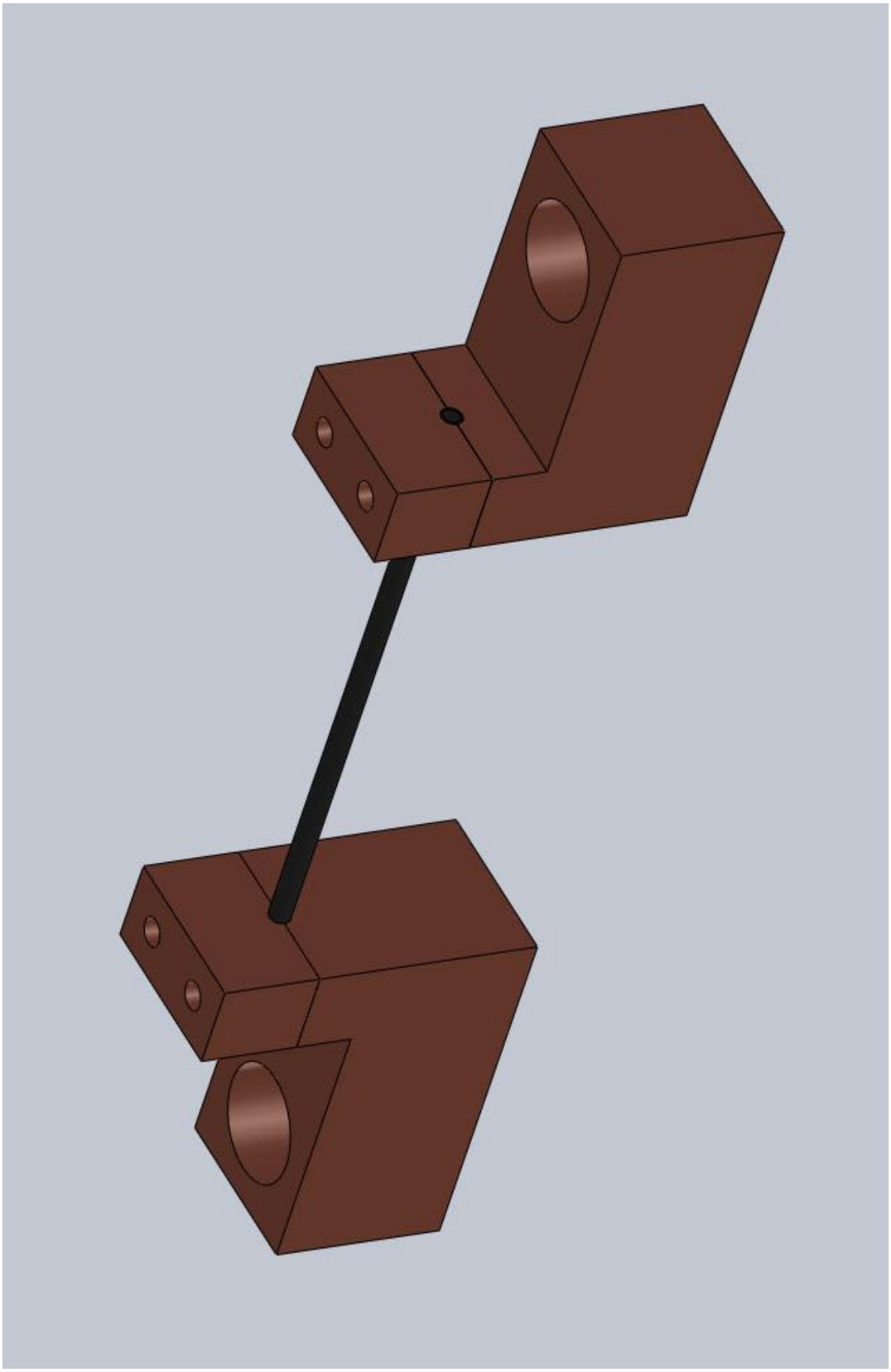

APPENDIX B

DETAILED STEPS FOR EXPERIMENTAL SETUP AND PROCEDURE

Setting up for an experiment using a new heater tube requires at least two days for proper mounting and time for sealants to cure. The end-state is shown in Figure B.1 that depicts the bulk liquid reactant chamber top mount. The heater tube is properly mounted with installed thermocouples. The actual experiment occupies the third and final day. A detailed, step-by-step description follows that is organized first by each set-up day, followed by the actual experimental procedure on the third day.

B.1 Installing Thermocouples into Heater Assembly (Day 1)

a. If using a bare heater tube, rinse the inside and outside with ethanol and allow to dry. Plastic gloves are recommended whenever handling the heater tube, especially if coated with a catalyst.

b. If a catalyst coated heater tube is used, the surface should first be characterized with Scanning Electron Microscope (SEM) images and/or Energy Dispersive X-ray Spectroscopy (EDS). Analysis in this study uses a Leica 440 SEM and Kevex EDS Detector. (Bard Hall, SB 56-contact John Hunt, 5-3789)

c. Remove the bulk liquid reactant chamber top mount and secure on a workbench as shown in Figure B.2. Thoroughly clean the contact surfaces of the copper electrode clamp components (Figure B.2a/B.3a) to remove any built up oxidation residue. Brake cleaner (CRC Brakleen) works sufficiently well, evaporates quickly and does

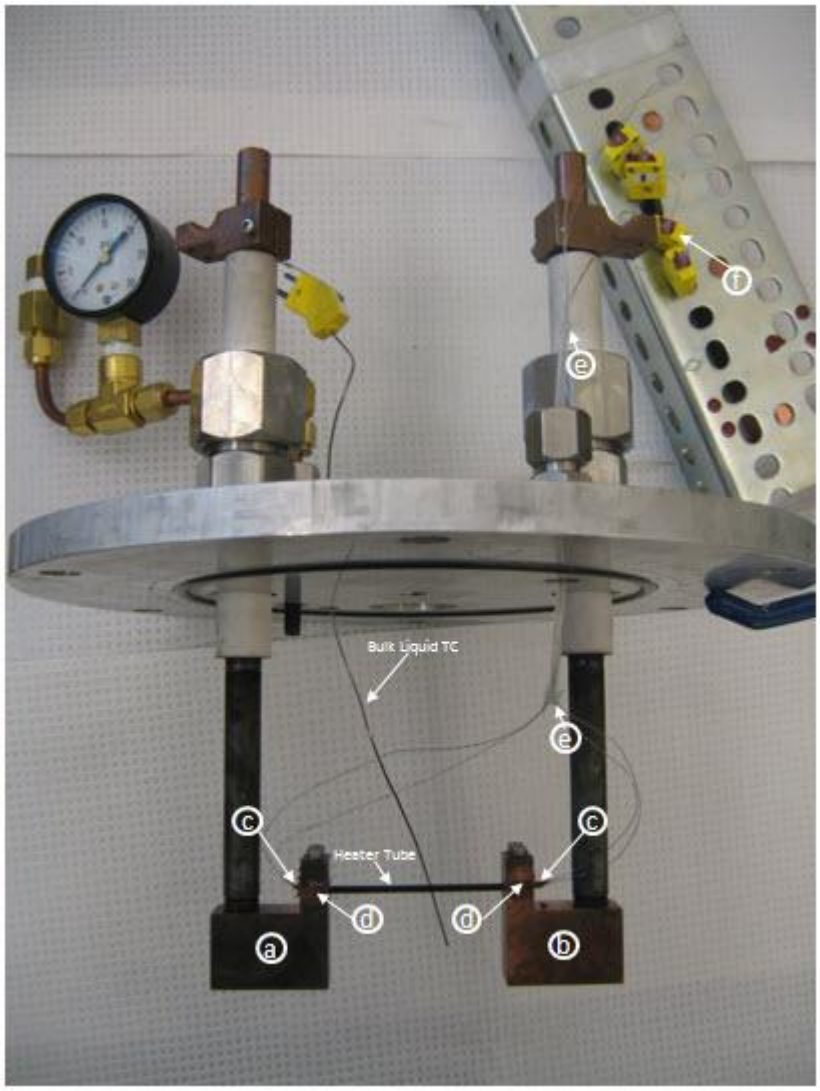

Figure B.1: Chamber Top with Mounted Heater Assembly

Figure B.2: Chamber Top Mounted on Work Bench

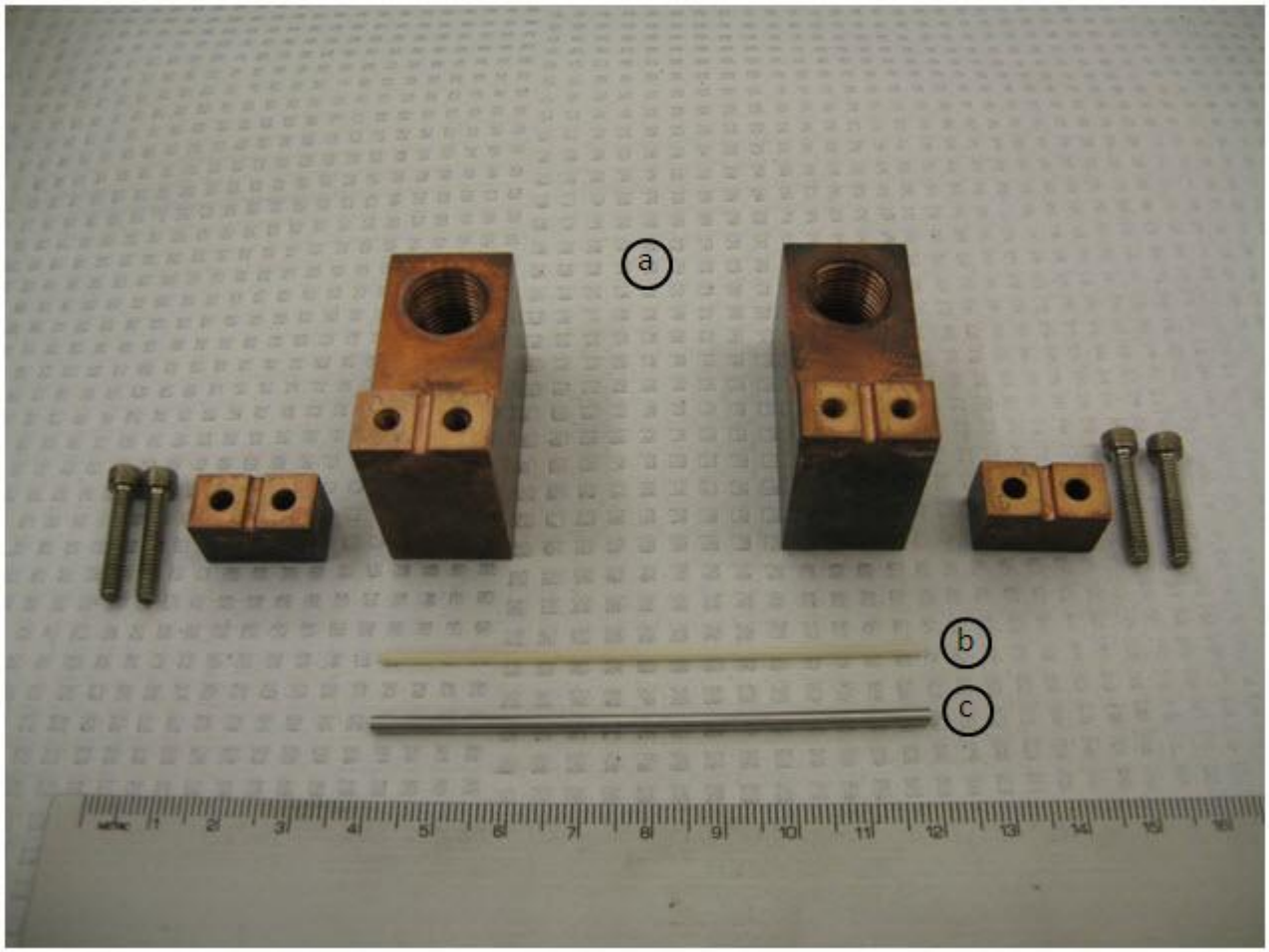

Figure B.3: Diassembled Electrode Wet Clamps and Heater Tube Component

not leave a residue. Battery terminal cleaner (Lynx Battery Cleaner) can be used to remove more difficult residue build up.

d. Figure B.3 shows cleaned, disassembled electrode clamps that include two top wet-clamps, two bottom wet-clamps and four 1/8" (#6-32 thread) hex screws (a), ceramic tube insert (b) and the heater tube (c). Heater tubes are manufactured and cut to length by Microgroup, Inc. (Microgroup, 600F10093X010SL) Details of the heater tube to include dimensions and material characteristics are listed in Table 2.2.

e. Cut a ceramic insert tube (Omega,ORX-132116) to 79.5mm (Figure B.3b) using a Dremel Tool with a specialty blade designed for cutting ceramics (Dremel 545 Diamond Wheel).

f. Cut a 4 inch piece of Teflon tubing (Sigma-Aldrich, Z515337-1PAK, Chemflour Tubing, PTFE, I.D. 1/16in., O.D. 1/8in.)

g. Insert Teflon tubing through packing gland (CONAX, PG2-125-AT) using a Teflon packing gland seal (CONAX, RS-PG2-125-T). Assemble gland components but do not tighten. See Figure B.2b.

h. Insert 4 thermocouples (Omega, KMQXL-010G-18) through Teflon tubing as shown in Figure B.2c.

i. If new thermocouples are being used, label the thermocouples (TC) #1-4.

j. From the end of TC#1, measure 21.6mm and place a mark on the TC wire using a black permanent marker. In the same manner, from the end of TC#2, measure and mark 39.7mm. For TC#3, measure and mark 39.7mm and for TC#4 measure and mark 21.6mm. Accurate measurements and markings are critical as they will affect the assumption of a symmetrical temperature profile across the length of the heater tube.

k. Create a heater tube assembly by inserting the ceramic insert (Figure B.3b) into the heater tube (Figure B.3c).

l. Insert TC's #1 and #2 into the left hand side of the heater tube assembly. Insert TC's #3 and #4 into the right hand side of the heater tube assembly.

m. Ensure the markings on the TC's align exactly with the end of the ceramic insert/heater tube. Figure 3.1 depicts the proper spacing of thermocouples inside of the heater tube/ceramic insert assembly.

n. Apply a coating of heat resistant silicon sealant (Dow Corning, RTV 736) on the ends of the heater tube to secure the TC's and ceramic insert inside of the heater tube. Using the top wet clamp components to hold the heater tube is useful. See Figure B.4.

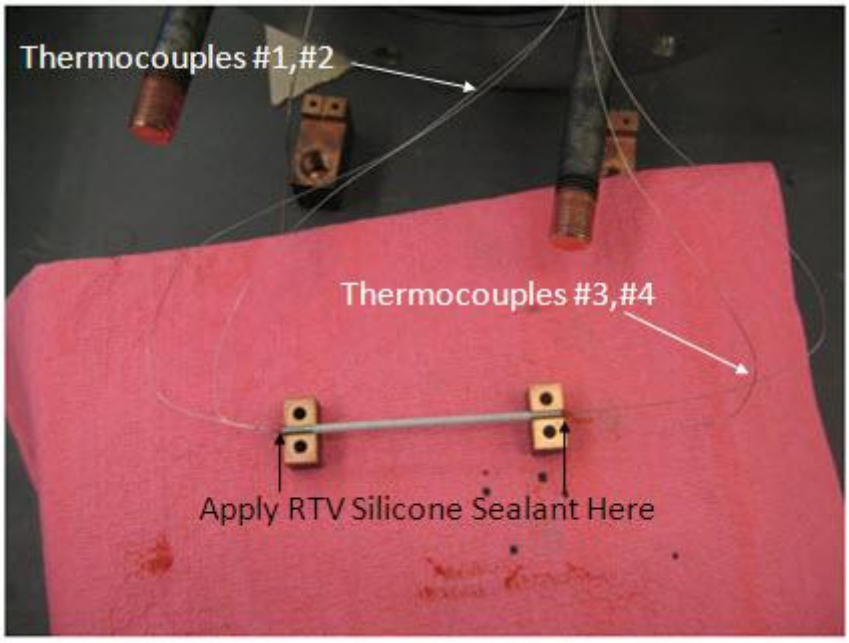

Figure B.4: Installation of Thermocouples into Heater Tube Assembly

o. If using new thermocouples, apply a coat of varnish (GC Electronics, 10-9002) at the junction of the TC wire and the yellow electrical connector. This will strengthen this connection as it is easy to break over the course of experiments. Allow to dry for 24 hours.

B.2 Mount and Seal Heater Assembly into Electrode Wet-Clamps (Day 2)

a. The top and bottom electrode wet-clamps (Figure B.1a/b) have an "A" or "B" stamped into the side. Ensure the "A" top wet-clamp is mated with the "A" bottom clamp and is placed on the left hand side electrode bus as you look at the front of the chamber (Figure B.2a). Assemble in the same manner on the right hand side electrode bus using the wet-clamps labeled "B" (Figure B.2b). Useful labeling is also on the chamber mount in permanent marker.

b. Ensure the bottom electrode wet-clamps are centered and square.

c. Gently raise and place the heater tube into the machined grooves of the bottom electrode clamps while adjusting the TC's through the Teflon tube and packing gland.

d. Fasten the left hand side top wet-clamp (Figure B.1a) and fasten the hex screws hand-tight.

e. Fasten the right hand side top electrode clamp (Figure B.1b) and fasten the hex screws hand-tight.

f. Using an Allen Wrench, fasten the hex screws in an opposite manner to ensure even pressure so achieve optimum electrical and thermal contact between the wet-clamp components and heater tube. (Caution: Fastening too tight can easily bend the tube or crack the ceramic insert-apply a “finger-tight” torque with the Allen Wrench)

g. Apply a second coat of heat resistant silicon sealant (Dow Corning, RTV 736) on the ends of the heater assembly. Apply a generous coat to prevent liquid penetration inside of the tube or between the electrode clamps. See Figure B.1c.

h. Apply a coat of clear silicon sealant (GE, RTV 108) around the adjoining wet-clamps to prevent liquid penetration. See Figure B.1d.

i. Apply a coat of clear silicon sealant (GE, RTV 108) to the top and bottom of the Teflon tube to prevent escape of vapors/product gases. See Figure B.1e.

j. If using new thermocouples, apply a coat of clear silicon sealant (GE, RTV 108) at the junction of the TC wire and the yellow electrical connector. This will strengthen this connection as it is easy to break over the course of experiments. See figure B.1f.

k. Allow to dry for 24 hours.

B.3 Experiment (Day 3)

Once the sealants on the heater tube have cured, one or multiple experiments can be run with the same heater tube. On the day of an experiment, the following supplies must be acquired and readily available before proceeding to further steps:

- Feedstock (e.g. ethylene glycol and water mixture) prepared/mixed
- Ground dry ice (fill 3-gallon cooler)
- 1 L Acetone
- Crushed Ice (fill 3-gallon cooler)
- Ensure adequate compressed nitrogen on-hand for both safety feed (Figure 2.2(q)) and GC actuator gas (Figure 2.9)
- Ensure adequate compressed helium on-hand for GC carrier gas (Figure 2.9)

B.3.1 Mount FIBOR into Fume Hood

a. Figure B.1 (Mounted Heater Tube) is inserted inside of the bulk liquid reactant chamber and fastened forming an air tight seal. Tighten six hex bolts in an opposite manner while ensuring that the top of the bulk liquid reactant chamber is centered on the chamber o-ring for a proper sealing. See Figure 3.2.

b. Insert the bulk liquid reactant chamber with mounted heater tube into the hood. Align and fasten copper electrode terminals (Figure B.5a) and chemical waste line (Figure B.5b).

c. Connect immersion heater power terminals. When connecting, ensure a positive (red) and ground (black) is connected to each immersion heater line. See Figure B.5c.

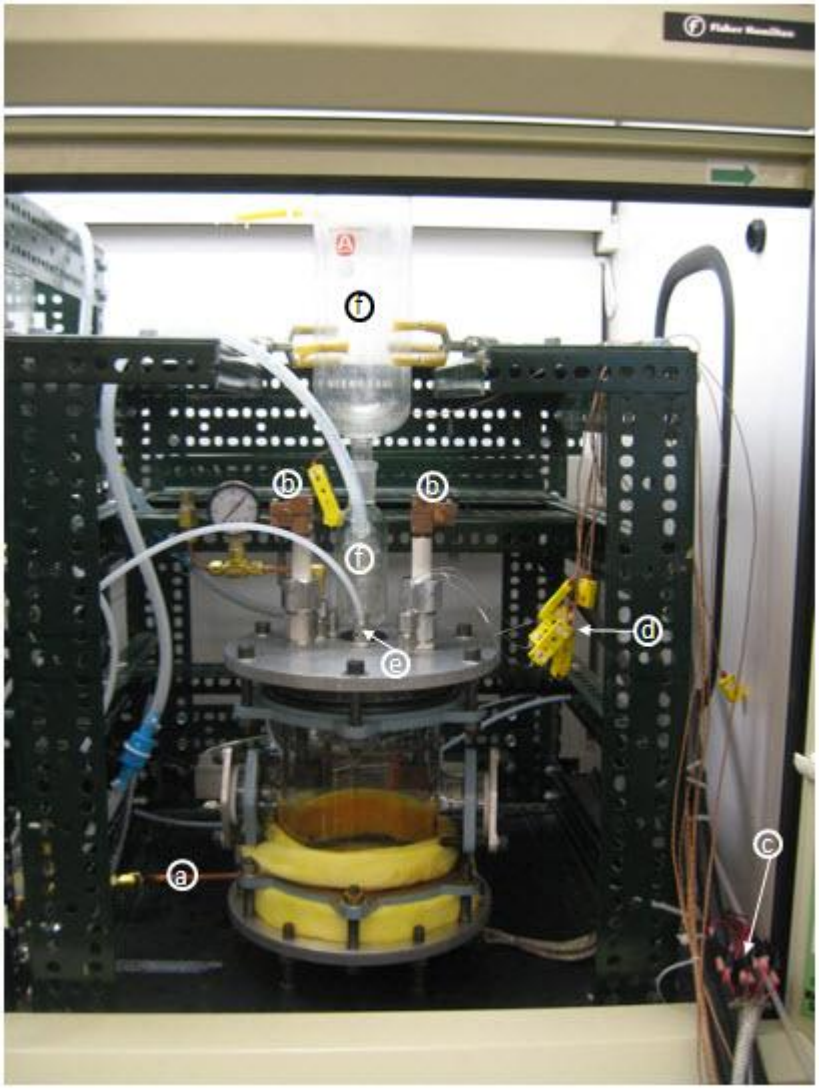

Figure B.5: FIBOR Chamber Mounted in Fume Hood

Figure B.6: DAQ, Power Supply, PC Workstation and GC

d. Connect thermocouples, ensuring proper connections for respective numbering. See Figure B.5d.

e. Connect Nitrogen gas line; fasten fitting tightly to prevent any leakage. See Figure B.5e.

f. Before going further, it is recommended to test thermocouples in Labview to ensure all data acquisition is working properly.

B.3.2 Data Acquisition Testing

a. Turn on the DAQ (National Instruments, NI PCI-6281). See Figure B.6a.

b. Turn on Power Supply (Agilent, 34980A). See Figure B.6b.

c. Open Agilent Connection Software in PC (Figure B.6c), refresh all connections.

d. Establish a new folder on the hard drive (c-drive). Establish a sub-folder containing the Labview programs (Power.vi, FIBOR Control Interface.vi). If more or less heater thermocouples are used, the block diagrams (Appendix C) for these programs must be modified. Also establish necessary subfolders to place copies of column data and Chromatograms.

e. Open "Power.vi". Select GPIBO::5::INSTR under the I/O control selector. Click the "run" arrow button at the top of the screen. Once a power reading is observed, click the red "stop" button. A captured view of this software program is provided in Figure 2.10.

f. Open “FIBOR Control Interface.vi”. Set “CUTOFF-TEMP” to 1300, set “Divide Voltage by?” to 1.3 and set “Set current” to 580. Click the “run” arrow button at the top of the screen. A captured view of this software program is provided in Figure 2.10a.

g. Three plots are provided. The first depicts a scrolling time reading of the 5 TC’s. The second is a scrolling time reading of the power output from the power supply. The third display is a scrolling flow reading from the flow meter. Additionally the actual numerical values of the voltage (V), power (W) and current (A) are digitally displayed. See Figure 2.10b.

h. The experiment is controlled by the user inputting the voltage under “Set Voltage.” The corresponding power and current are automatically adjusted. In order to apply power to the tube, click “output state” to “on.” Apply a small voltage (.1-.2V) to observe heater TC response. See Figure 2.10b for a depiction of the Labview program and Section 3.4 for further discussion regarding a typical TC response during DAQ testing.

B.3.3 Condenser Assembly and Leak Test

a. Two condensers and one cold-trap are required. The assembled condensers are shown in Figure B.5f and also Figure 3.3. Install the first condenser (Sigma-Aldrich, Z517232) by first applying sealant (DuPont, Krytox) to both the male and female connections. Insert the female end into the rubber fitting at the top of the FIBOR. Insert fully to ensure an adequate seal. Connect the water lines and slowly pressurize with running cold tap water which runs through its coil design.

b. Install the second and primary condenser (Sigma-Aldrich, Z164038) by applying necessary sealant (DuPont, Krytox) and inserting the male fitting into the female fitting of the first condenser. Fill the dry finger (inside portion of condenser) ¾ full with dry ice. Slowly poor acetone until a boiling slurry is made. Continue to slowly combine dry ice and acetone until the cold finger is full. CAUTION: Always wear gloves when handling dry ice to avoid freezer burns. Also ensure acetone is added slowly as it is easy to boil over.

c. Connect gas line from the second condenser to the cold trap (Ace Vacuum Trap, Sigma Aldrich Z256870). Place the cold trap in an insulated container immersed in ice water. See Figure 3.3.

d. Connect gas line from the cold trap to the flow meter.

e. Connect safety Nitrogen feed (Figure B.5e) and pressurize the system to test for leaks. The system should be sealed from outside air if all components are installed properly. To check for leaks, the first step is to set the flow of the Nitrogen and turn on the flow meter. The flow rates should be within +/- 0.05 LPM. Next, use liquid leak detector (Snoop, Swagelok) at each fitting in the system. The presence of tiny bubbles forming indicates a leak. Fix leaks as necessary by adjusting or tightening fittings.

B.3.4 GC Setup

The last step before filling the bulk liquid reactant chamber and establishing a FIBOR is to configure the GC so that product gas samples can be extracted and

analyzed once chemical reaction is detected by a flow reading on the flow meter. The GC is pre-programmed and configured to minimize setup time during an experiment. Once all three gas lines are connected according to Figure 2.9, the following steps are executed in order before powering on the GC:

a. Open carrier gas flow-compressed Helium, 40-50psi, ~30CCM. (Figure B.6d)

b. Open actuator gas-compressed Nitrogen, 20-30psi. (Figure B.6e)

c. On the back of the GC, turn the power switch to "on" (Figure B.6f)

Figure 3.5 is a depiction of the "Home Page" that the GC displays by default after it powers on and also from which all commands start from. Pressing the "Home" button on the key pad always returns to this display. The first step to program the GC for use during an experiment involves retrieving a pre-programmed "method." This requires pressing the following keys:

d. Edit>Retrieve>QCTEST1>Return

e. "Method Retrieved Successfully" should be displayed

f. Press "Home"

The GC is equipped with Chrom Perfect data acquisition software that provides automated user control of the GC during experiments along with

chromatogram retrieval and analysis tools. The software is opened through the following steps:

g. Open Chrom Perfect Software

h. Click Data Acquisition Button

i. Click the yellow “Claim” button under the Selection Tab

j. The Instrument Control Button should be highlighted in color under the Status Tab and the word “Ready” should be displayed next to it

The remaining steps conclude setting up the GC for an experiment since all control after is from the Chrom Perfect Software. Going back to the key pad on the front of the GC, press:

k. Action>Heat On

l. Press “Home”

As the GC heats, the words “Not Ready” will be displayed on the Home Page in the upper left corner. The actual temperature of the column oven and TCD can be viewed by pressing “Status.” Once the word “Ready” appears in the top left corner, press:

m. Control>Filament>On

n. The GC is now ready to detect a sample. During an experiment, ensure the mini-pump (Figure B.7) is turned on and the flow reads approximately 30CCM. For a calibration gas, set the gas regulator on top of the cylinder to 10psi and the flow regulator to 30CCM (Figure B.8). Figure B.9 is an actual picture of the gas line configuration on the back of the GC that is drawn in Figure 2.9. In order to inject a sample, change the direction of the two-way valve (Figure B.9) to either the FIBOR gas (during an experiment) or the calibration gas.

o. Click the colored "Instrument Control" button in the Chrom Perfect status window. Press "Start Run" when ready to inject a sample. The first sample is injected into Column A. After five minutes, a second sample is injected automatically into column B. The chromatogram is automatically displayed and saved to the hard drive once the run is complete (after ~10min). It is important to not change any of the settings (power input) during an injection so that the conditions for the sample entering Column A are identical to the conditions for the sample entering Column B

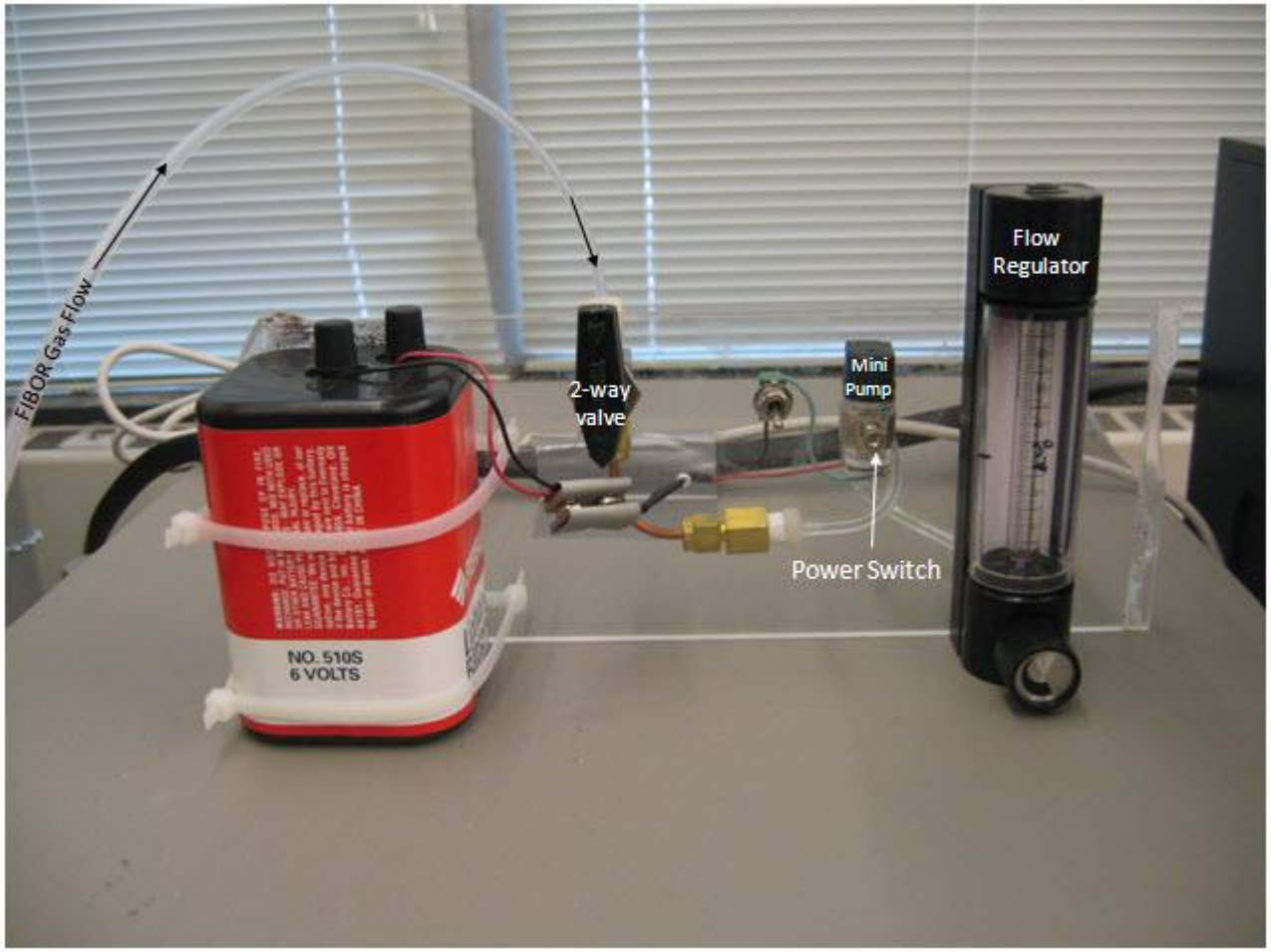

Figure B.7: Mini Pump

Figure B.8: Calibration Gas Setup

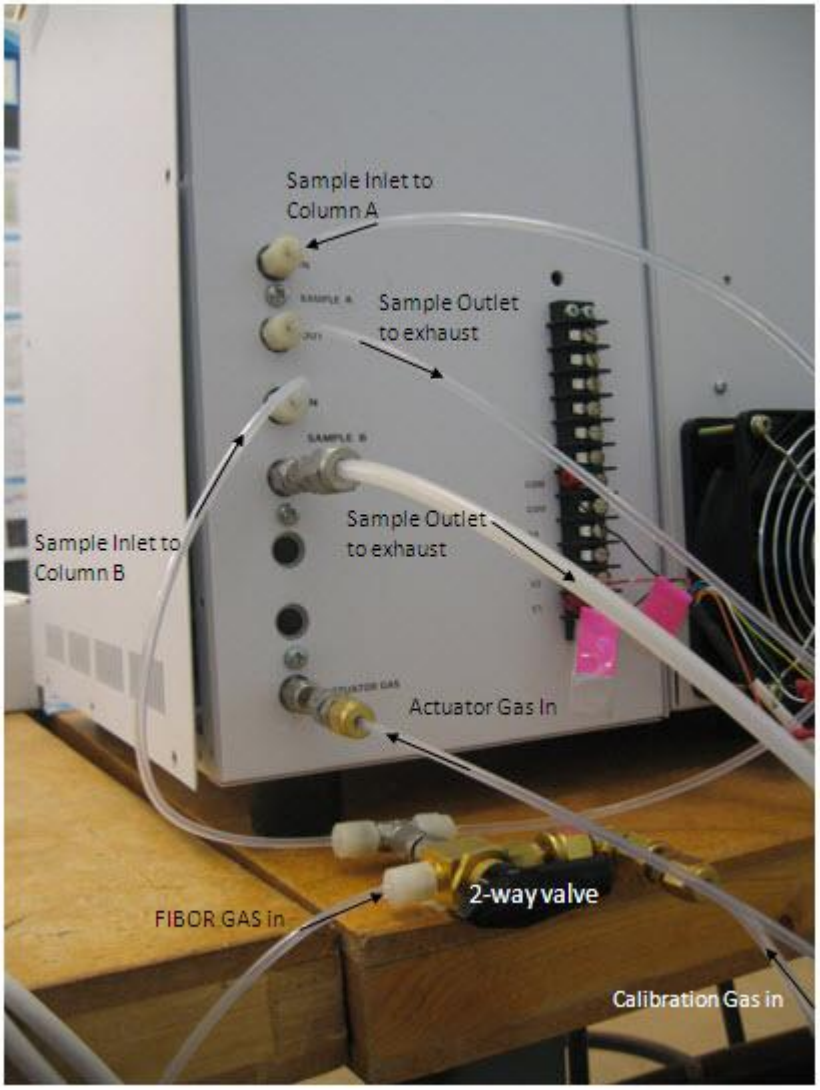

Figure B.9: Back View of GC; Gas Line Configuration

OPTIONAL

The GC automatically heats the column oven to 70°C and the TCD to 110°C which is programmed into the method file. There may be conditions where these settings should be changed such as overlapping detection peaks or insufficient retention time to detect a certain species. The general rule of thumb is that increasing the column temperature speeds up the retention time. However the TCD temperature must always be higher than the oven temperature. The Series 600 Gas Chromatograph User's Manual (GOW-MAC, 2006) should always be reviewed prior to changing any settings on the GC or call GOW-MAC Technical Support (610-954-9000). To modify settings of the GC method press:

- Edit>Chromatography Method 1>Do This
- Select either Detector 1 or Column Oven by pressing the arrow key until it is next to it
- Press "Do This"
- Manually raise or lower the respective temperatures with up/down buttons
- Press "Accept"
- Press "Home"

B.3.5 Quenching Method and Data Collection

At this point in the experiment, an assistant is recommended. The heater temperature should first be raised to the less volatile component's saturation temperature. For the case of ethylene glycol and water, the tube should be raised to approximately 473K (200ºC) or the saturation temperature of pure ethylene glycol. For safety reasons, the first step is activating Nitrogen flow through the system:

a. Set Nitrogen flow to 10-20psi and ~0.1LPM

b. To start the data acquisition, follow the same steps in B.3.2

c. Electrically heat the tube to at least 473K by increasing the voltage in increments of 0.1V

d. Open the bulk feedstock reservoir valve (Figure 2.2b and B.10). The peristaltic pump is not necessary when using ethylene glycol (and aqueous mixtures) because the viscosity is low enough to allow sufficient flow as a result of gravity alone. Processing more viscous liquids however such as glycerol require additional pumping.

e. Figure B.11 is picture of liquid lines and valves that control flow in and out of the FIBOR chamber. Heating tape is installed yet is unnecessary for ethylene glycol (and aqueous mixtures). This component is intended to enhance the flow of liquids with a sensitive viscosity dependence on temperature (e.g. glycerol). Ensure the 3-way valve (Figure 2.2h and B.11) is set to the appropriate direction. The two-way valve (Figure 2.2f and B.11) is now the means to control the level of the bulk liquid reactant. Ensure it is open.

f. Visually inspect as the bulk liquid reactant chamber is filled. Fill to the bottom of the wet-clamps and close the two way valve.

g. Turn on immersion heaters to maximum power.

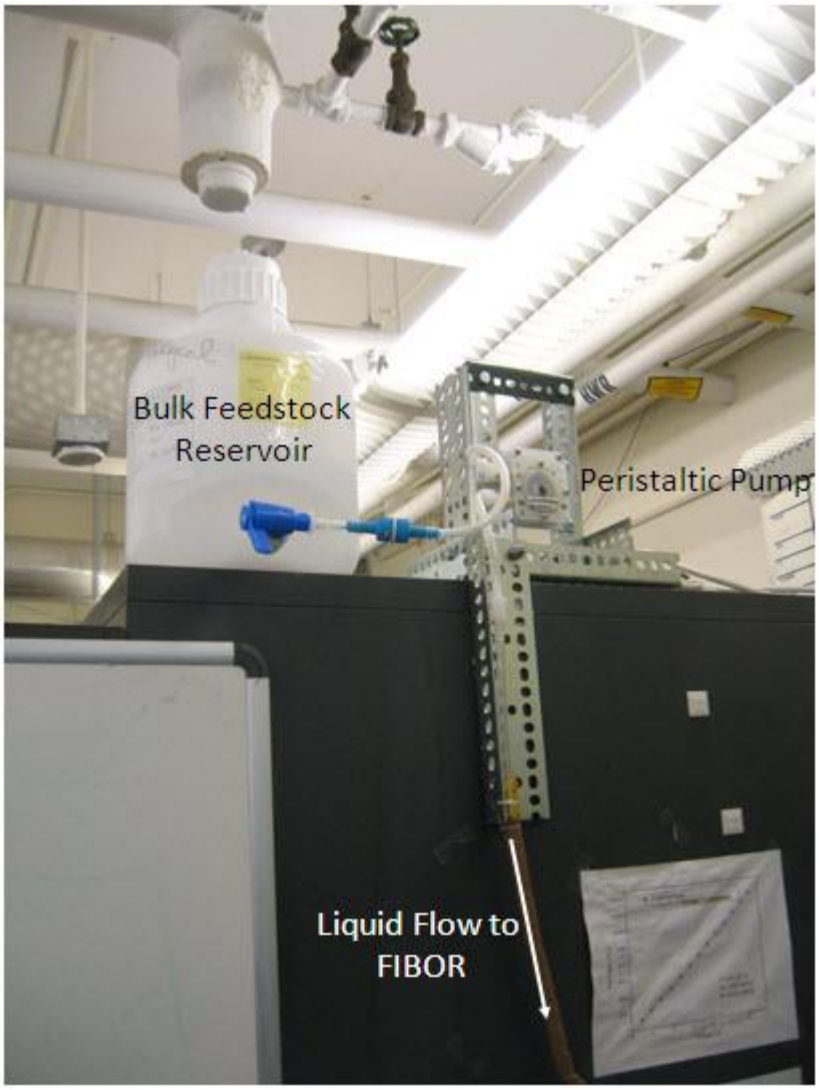

Figure B.10: Bulk Feedstock Reservoir

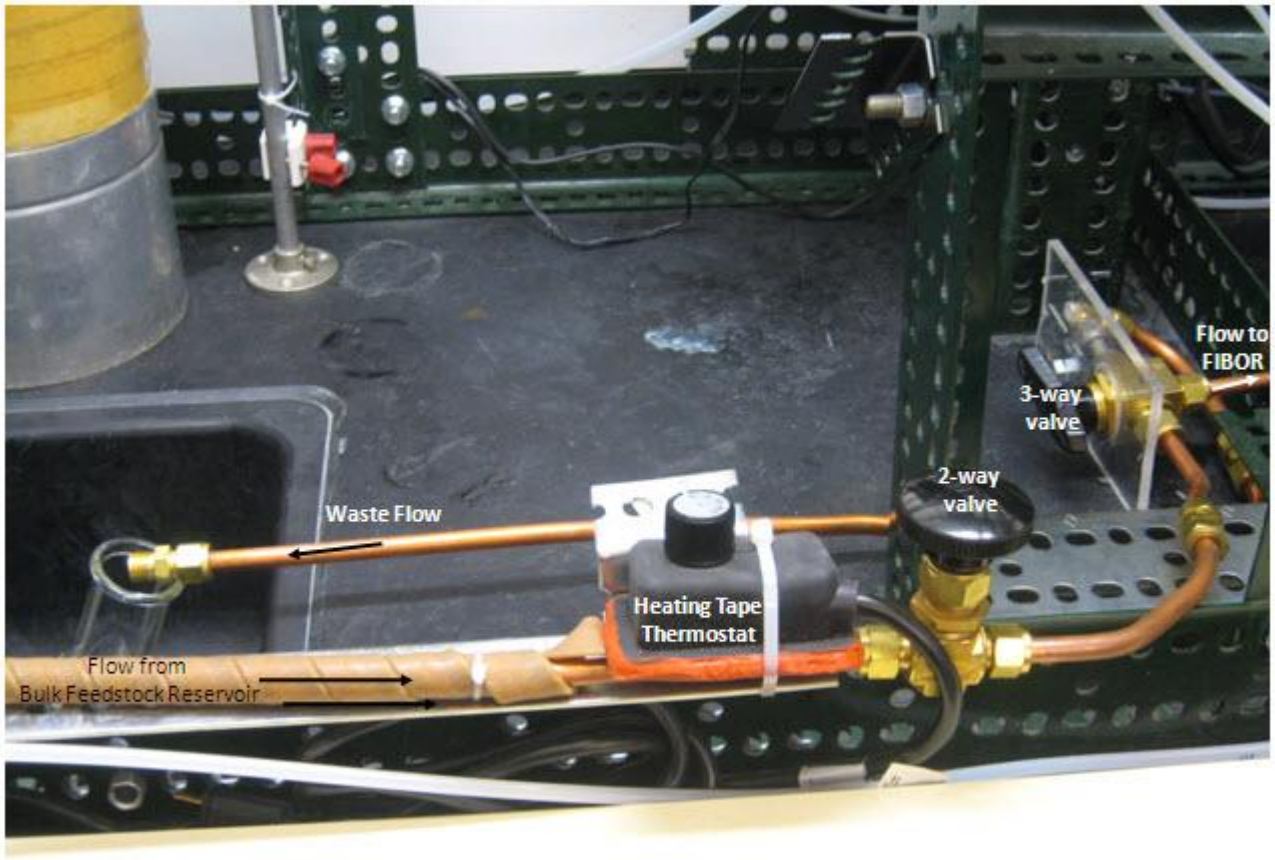

Figure B.11: Liquid Line Configuration

h. Wait until liquid temperature reaches saturation point. The bulk liquid reactant TC is the lowest on the Labview TC display (Figure 2.10b). The saturation point is determined by vapor-liquid equilibrium (Figure 1.2). The liquid should be visibly boiling when quenching the heater tube to prevent any heat losses to sub-cooling and stable achieve film boiling.

i. Heat the tube to a minimum of 973K (700ºC)

j. Bring the liquid level approximately 15mm below the heater tube (See Figure 3.6). Allow the bulk to reach saturation.

k. For a bare tube, take voltage in step i and double it. For a catalyst coated tube, triple the voltage. Enter this voltage into Labview, however DO NOT PRESS ENTER.

l. It is best to have the assistant control the two way valve. Slowly open the two way valve and closely monitor the temperature of the tube in Labview. As soon as the temperature begins to drop (the liquid level is reaching the tube) the ENTER button is simultaneously pressed to either double the voltage (4x power) for the bare tube or triple the voltage for the catalyst tube (9x power). This technique has been experimentally proven to provide the necessary surge in heat to support film boiling yet is not high enough to melt the tube. The additional heat for the catalyst coated tube is necessary to offset the heat that is consumed by the endothermic chemical reaction.

m. Once film boiling is achieved, traverse the film boiling curve by increasing/decreasing the voltage in increments of 0.02V. Between each increment

allow approximately two minutes for the tube's temperature to reach steady state. A change of 0.02V changes the tube's temperature by approximately 10 degrees. Ensure the Nitrogen is TURNED OFF once film boiling is achieved to prevent erroneous (over-estimate) flow rate results.

B.3.6 Saving Data and Removing Heater From Liquid

Once the necessary amount of data has been acquired from the film boiling curve, the data must first be saved. The tube is then removed from the liquid in the reverse fashion of the quenching method. It is also recommended to have an assistant during this part of the experiment.

a. Stop the experiment at a temperature that is not at risk of film boiling collapsing. A temperature of 1373K (1100ºC) is suitable. Press the two "stop" buttons on the Labview interface (See Figure 2.10b). This temporarily stops data from being stored however the power settings remain on.

b. Navigate to the hard drive (c:\experiment)

c. Locate six relevant data files: current.lvm, flowrates.lvm, POWER.lvm, TEMPERATURES.lvm, time.lvm and voltage.lvm. One at a time, right click, select "open with," select "notepad," and save files into the folder created in step B.3.2.d above.

d. Once all files are saved, click the "run" arrow button in Labview. The Labview program resumes yet also erases all data in the files from the previous step (c:\experiment) and begins storing new data. It is therefore crucial that all data is

verified to have saved properly in the separate folder established in B.3.2.d since it could easily be lost once the Labview program resumes.

e. Enter a voltage of 1V into Labview, however DO NOT PRESS "ENTER."

f. Have the assistant place a waste beaker at the end of the waste line and change the direction of the 3-way valve so that the bulk liquid in the chamber begins to empty. CAUTION: This liquid is scolding hot and protective gloves should be worn.

g. As soon as the bulk liquid level reaches the level of the heater tube, the temperature in Labview will begin to rapidly rise. The temperature increases rapidly because the heat transfer coefficient is abruptly decreased in quiescent air compared to the conditions of film boiling. Simultaneously press "ENTER." This lowers the power input, and therefore the temperature of the heater tube. This prevents liquid from contacting the surface and also inadvertently melting the tube.

h. Gradually continue to decrease the temperature of the tube and safely dispose the waste liquid.

g. Safely shut down the experiment by following these remaining steps:

- Shut Down Labview/PC
- Turn off power supply
- Turn off DAQ

- Turn off immersion heaters

- Shut down the GC by pressing Action>Shutdown on the keypad. The GC column oven must cool before safely turning the power off. The word "OFF" will be displayed in the top left corner of the keypad display when it is safe to power off. See Figure 3.5.

- Turn off all gas flow (Nitrogen, Carrier, Actuator)

- Allow dry ice to evaporate before removing condensers (allow 24 hours)

- Ensure bulk feedstock reservoir valve is closed.

APPENDIX C

Computational Programs (Code) for Design Modeling, Data Acquisition and Data Analysis

C.1 Heater Design- Bulk Liquid Composition Change as a Result of Chemical Reaction

```
%Matlab Code Written by John Evangelista, Cornell University 2010

%Computes:
%rate of bulk liquid composition change in FIBOR as a result of
%chemical reaction

clear
%Convert starting volume fractions to mole fractions
Vfe=.8;  %Volume fraction of ethylene glycol (eg), 80%
Vfw=.2;  %Volume fraction of water (w), 20%
Vtot=3;  %Assume starting bulk liquid supply in FIBOR is 3 Liters
Ve=Vtot*Vfe;  %Volume ethylene glycol, liters
Vw=Vfw*Vtot;  %Volume water, liters
roe_e=1113;  %density of ethylene glycol, kg/m^3
roe_w=1000;  %density of water, kg/m^3
MWe=62.07;  %Molecular weight ethylene glycol, kg/kmol
MWw=18.02;  %Molecular weight water, kg/kmol
Nw=Vw*(1/1000)*roe_w*(1/MWw)*1000;  %moles of water
Ne=Ve*(1/1000)*roe_e*(1/MWe)*1000;  %moles of ethylene glycol
Nt=Nw+Ne;  %total number of moles
Xw=Nw/Nt;  %mole fraction of water
Xe=Ne/Nt;  %mole fraction of ethylene glycol

%Convert product flow rate from L/min to mol/min
Flowperarea=7267;  %Assumed flowrate of L/min*m^2 based on
Experimental Data
d=.00238;  %**Design Parameter** Tube diameter, meters
L=.060;  %**Design Parameter** Tube length, meters
Flow=Flowperarea*pi*d*L; %product flow rate, L/min
mol_vol=22.4; %1 mole of products is approximately 22.4L
Ndot=Flow/mol_vol; %molar flowrate, mol/min

%Chemistry
stop=240;  %Time of typical experiment, 240 min
t=0;  %Initialize time
i=1;  %Initialize column data

for t=0:4:stop  %start at time=0, end at 240min in increments of 1min
Ne_1=Xe*Nt-(1/7)*Ndot*t; %remaining ethylene glycol as a function of
time
Nw_1=Xw*Nt-(2/7)*Ndot*t; %remaining water as a function of time
Ve_1=Ne_1*MWe*(1/1000)*(1/roe_e)*1000; %Convert to volume of eg
Vw_1=Nw_1*MWw*(1/1000)*(1/roe_w)*1000; %convert to volume water
Vfe_1=(Ve_1/(Ve_1+Vw_1))*100; %volume fraction of ethylene glycol
```

```
Vfw_1=(Vw_1/(Ve_1+Vw_1))*100; %Volume fraction of water
water(i,1)=Vfw_1; %Fill column data for water volume fraction
time(i,1)=t; %Fill colum data for time
i=i+1; %Update row number
end
water; %water volume fraction column data
time;  %time column data
dlmwrite('water.xls',water); %export data to excel file
dlmwrite('time.xls',time); %export data to excel file
cutoff=15; %Water fraction cannot fall below this line (5% decrease)
plot(time,water,time,cutoff) %plot results
xlabel('time [min]'); %label x-axis
ylabel('Water Volume Fraction [%]'); %label y-axis
```

C.2 Condenser Design

```
%Matlab Code Written by John Evangelista, Cornell University 2010

%Computes:
%necessary condenser surface area and required coolant

%Calculation for condensing steam
%Condenser Dimensions
i=1; %initialize column data
D=.08; %Condenser Diameter, meters
for L=.05:.01:.3 %Vary Condenser length, meters
A=pi*D*L; %Condenser surface area
Ts=-78; %0 for Ice Bath, -78 for Dry Ice, Celsius

%Liquid Properties evaluated at film temperature ((Ts+Tsat)/2)
roe=1000; %Density, kg//m^3, 987.2 for ice bath, 1000 for Dry Ice
cp=4189; %Heat Capacity, J/kg-K, 4182 for ice bath, 4189 for Dry Ice
mue=1225E-6; %Viscosity, N*s/m^2, 528E-6 for ice bath, 1225E-6 for
Dry Ice
k=.59; %Thermal Cond, W/mk, .645 for ice bath, .590 for Dry Ice
hfg=2473000; %Heat of Vap, J/kg, 2378000 for ice, 2473000 for dry ice
v=mue/roe; %kinematic viscosity, m^2/s
Pr=8.81; %Prandtl Number, 3.42 for ice bath, 8.81 for Dry Ice

%Saturated vapor properties
roe_v=.596; %Steam density
Tsat=100; %Saturation Temperature, Celsius

%Find Heat Transfer Coefficient, H
Ja=cp*(Tsat-Ts)/hfg; %Jacob Number
hfg_1=hfg*(1+.68*Ja); %Modified Heat of Vap for condensation
g=9.8; %Acceleration due to gravity, m/s^2

%Calculate Reynolds # for laminar, laminar-wavy and turbulent region
Re_lam=3.78*(((k*L*(Tsat-Ts))/(mue*hfg_1*(v^2/g)^(1/3)))^.75);
Re_wavy=((((3.7*k*L*(Tsat-Ts))/(mue*hfg_1*(v^2/g)^(1/3)))+4.8)^.82);
Re_turb=(((.069*k*L*(Tsat-Ts))/(mue*hfg_1*(v^2/g)^(1/3)))*Pr^.5-
151*Pr^.5+253)^(4/3);
```

```
%Select appropriate Reynolds #
if Re_lam < 30
    Re=Re_lam;
elseif 30 <= Re_wavy < 1800
    Re=Re_wavy;
else
    Re=Re_turb;
end

%Eqn 10.31 (Incroprera, 2006)
h=(Re*mue*hfg_1)/(4*L*(Tsat-Ts));

h_1=h/10; %Heat transfer rate reduced by a factor of 10 due to non-
%condensible gases (Rhosenhow,1998)

q=h_1*A*(Tsat-Ts); %Heat Transfer into condenser coolant
heatxfer(i,1)=q; %Fill column
Area(i,1)=A; %Fill column
heatreq(i,1)=2000; %Baseline heat required to balance heat input from
FIBOR
%and immersion heaters
i=i+1; %Update column data counter
end

%Export data to excel files in working directory
dlmwrite('heatxfer.xls',heatxfer);
dlmwrite('Area.xls',Area);
dlmwrite('heatreq.xls',heatreq);

%Plot results
plot(Area,heatxfer,Area,heatreq)
xlabel('Condenser Surface Area [m^2]');
ylabel('Heat Transfer Rate to Coolant [W]');
```

C.3 Data Acquisition

C.3.1 Power.vi Labview Block Diagram

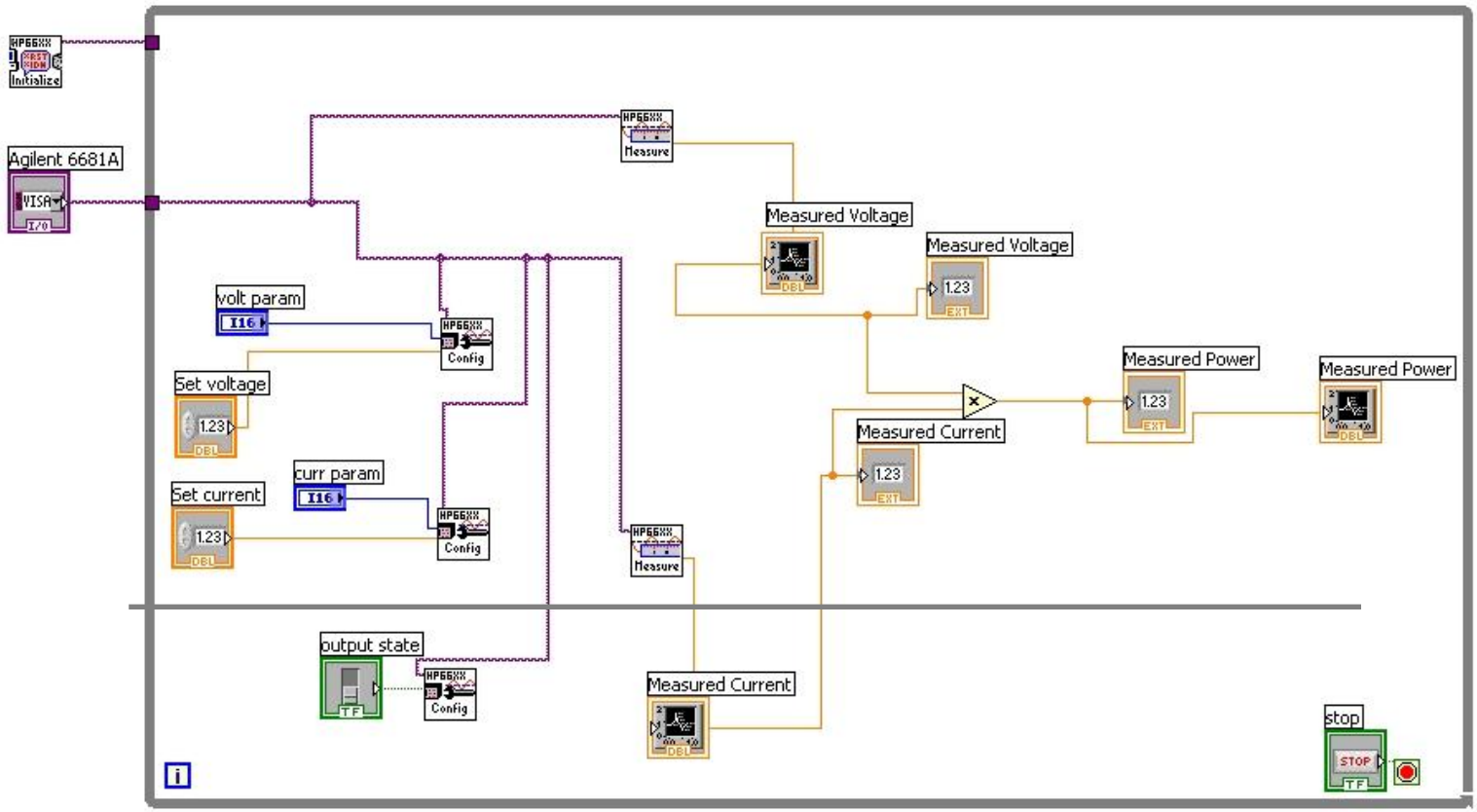

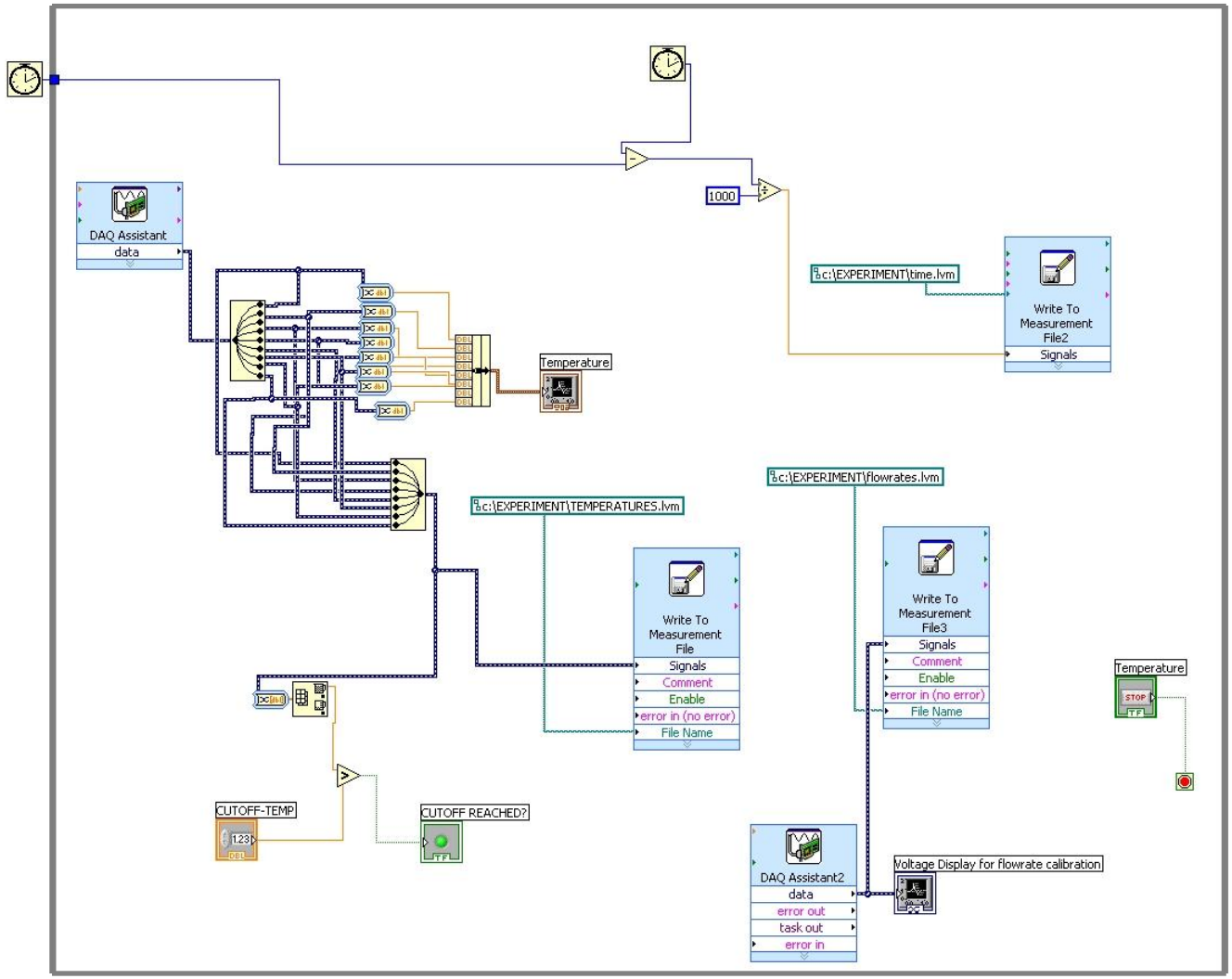
DAQ Assistant
data
1000
c:\EXPERIMENT\time.lvm
Write To Measurement File2
Signals
Temperature
c:\EXPERIMENT\TEMPERATURES.lvm
c:\EXPERIMENT\flowrates.lvm
Write To Measurement File
Signals
Comment
Enable
error in (no error)
File Name
Write To Measurement File3
Signals
Comment
Enable
error in (no error)
File Name
Temperature
STOP
TF
CUTOFF-TEMP
CUTOFF REACHED?
DAQ Assistant2
data
error out
task out
error in
Voltage Display for flowrate calibration

C.3.3 FIBOR Control Interface.vi Labview Block Diagram (page 2)

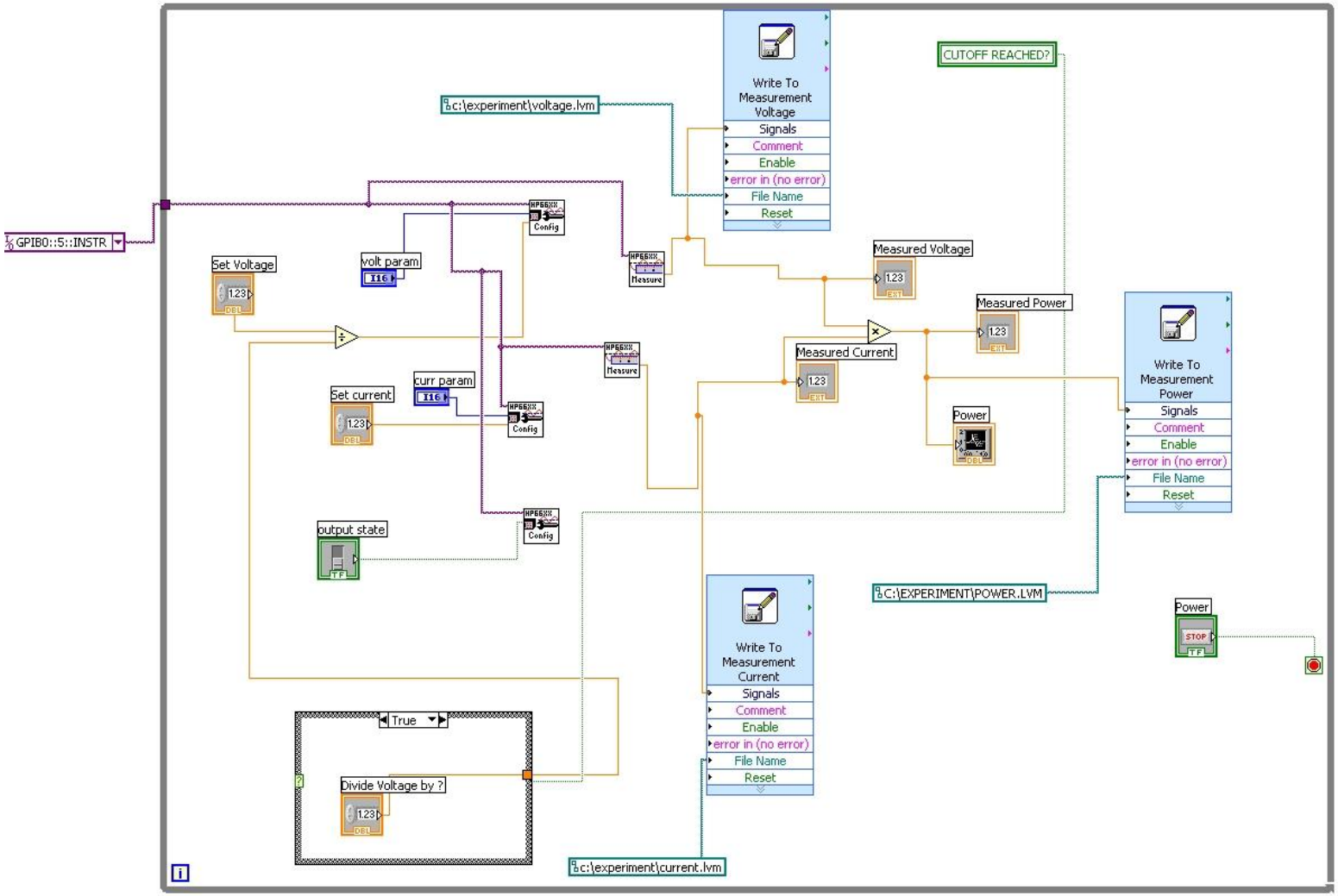

C.4 Data Organization and Analysis

C.4.1 Synchronizing Temperature and Power Data

```
%Orignal Matlab Code Written by Choi (2010),
%Modified by John Evangelista, Cornell University 2010

%Computes:
%time data for corresponding power data points through linear
interpolation

i=1; %initialize counter
a=0.1284; %linear parameter solved by Equations 4.1 and 4.2
b=117.48; %linear parameter solved by Equations 4.1 and 4.2

%Establish empty column, number of rows must match the rows of power
data
TimeG = zeros(183535,1);
%Fill column with linearly interpolated time data
while i <= 183535
    TimeG(i,1) = a*i+b;
    i = i + 1;
end
TimeG;

%Write column data to file in working directory to be retrieved for
%plotting power setting data (power, current, voltage)
dlmwrite('TimeG.txt',TimeG)
```

C.4.2 Calibrate and Normalize Flow Rate Data

```
%Orignal Matlab Code Written by Choi (2010),
%Modified by John Evangelista, Cornell University 2010

%Computes:
%actual flow rate normalized by heater surface area

TEMP = dlmread('TEMPERATURES.lvm','\t'); %read in raw temp column
data
flowrates = dlmread('flowrates.lvm'); %read in raw flowrate column
data
time = dlmread('time.lvm'); %read in time data
d=.00237617; %Heater tube outside diameter, meters
l=.060325; %Heater tube length, where reaction occurs, meters
i=1; %initialize counter

%Establish empty column, number of rows must match the rows of time
data
CFR_real= zeros(720731,1);
%Fill column with actual flow rate normalized by heater surface area
while i <= 720731
    FS = flowrates(i,1);
```

```
    % calibration & compensation of omega flow meter L/min/m^2*10^-3
    CFR_real(i,1) = (2352.84813*FS-
169.95803+94)/(3.14159265*d*l*1000000);
    i = i + 1;
end
CFR_real;
%Write column data to file in working directory to be retrieved for
%plotting flow rate curve
dlmwrite('CFR_real.txt',CFR_real)
```

C.4.3 Average Thermocouple Temperature and Convert to Kelvin

```
%Orignal Matlab Code Written by Choi (2010)
%Modified by John Evangelista, Cornell University 2010

%Computes:
%average heater tube thermocouple temperature and converts to Kelvin
scale
TEMP = dlmread('TEMPERATURES.lvm','\t'); %read in raw temp column
data

i=1; %initialize counter

%Establish empty column, number of rows must match the rows of time
data
TEMP_AVG = zeros(720731,1);

%Fill column with average temperature, Kelvin
while i <= 720731
    TEMPERATURE =
((TEMP(i,2)+273.15)+(TEMP(i,3)+273.15)+(TEMP(i,4)+273.15)+(TEMP(i,5)+
273.15))/4;
    TEMP_AVG(i,1) = TEMPERATURE;
    i = i + 1;
end
TEMP_AVG;

%Write column data to file in working directory to be retrieved for
%plotting flow rate curve
dlmwrite('TEMP_AVG_Kelvin.txt',TEMP_AVG)
```

C.4.4 Boiling Curve

	A	B	C	D	E	F	G	H	I	J
1	**Boiling Curve Computation**									
2					Heater Outside Diameter, d_o [meters]:	0.00238				
3					Ceramic Insert Outside Diameter, d_c [meters]:	0.00185				
4					TC Insert Space Outside Diameter, Air, d_a [meters]:	0.0008				
5					Inconel 600 Thermal Conductivity, k_i [W/m·K]:	27				
6					Ceramic (Al_2O_3) Thermal Conductivity, k_c [W/m·K]:	18				
7					Air Thermal Conductivity, k_a [W/m·K]:	0.082				
8					Heater Tube Half Length, L [meters]:	0.0302				
9					TC #1/#4 Spacing From Center of Heater, L_c [meters]:	0.0181				
10	Current[A	Resistivity [m	T1 [°C]	T2[°C]	T3[°C]	T4[°C]	T_avg[°C]	Heat Flux-No Axial Conduction [W/m^2]	Heat Flux w/ Axial Conduction [W/m^2]	T_avg[K]
11	85.65	1.76640116	1183.78	1184.46	1181.64	1177.03	1181.7258	997682.496	997626.522	1454.88
12	86.1328	1.77465074	1185.34	1185.49	1183.73	1178.94	1183.3753	1013673.99	1013621.74	1456.53
13	86.453	1.79581473	1187.47	1188.51	1189.48	1184.69	1187.5383	1033403.54	1033341.81	1460.69
14	86.9333	1.86138037	1202.24	1202.57	1198.65	1195.97	1199.8565	1083068.04	1083036.19	1473.01
15	87.5737	1.87412135	1204	1204.34	1202.46	1197.83	1202.1567	1106606.92	1106554.32	1475.31
16	87.8939	1.93238895	1213.82	1214.34	1212.98	1208.16	1212.327	1149371.16	1149314.57	1485.48
17	88.3742	1.97039069	1219.64	1219.8	1220.13	1215.13	1218.6751	1184817.92	1184763.1	1491.83
18	88.8545	2.0155845	1227.46	1227.72	1226.52	1222.13	1225.9597	1225203.26	1225154	1499.11
19	89.1747	2.07144888	1236.18	1236.26	1235.32	1230.65	1234.601	1268252.74	1268202.37	1507.75
20	89.655	2.14019549	1245.98	1246.98	1245.84	1240.16	1244.7391	1324496.31	1324425.58	1517.89
21	85.9727	1.7542665	1181.68	1182.18	1178.65	1174.58	1179.2713	998308.984	998260.534	1452.42
22	85.4924	1.71181526	1171.96	1172.64	1170.89	1166.12	1170.4034	963296.961	963239.338	1443.55
23	85.0121	1.67700994	1164.05	1164.71	1163.77	1158.58	1162.7776	933136.983	933074.863	1435.93
24	84.6919	1.65569838	1159.16	1160.26	1158.1	1154.22	1157.934	914351.651	914298.892	1431.08
25	84.2116	1.61650935	1149.12	1150.22	1149.9	1145.33	1148.645	882613.033	882553.041	1421.79
26	83.7313	1.59238224	1143.61	1144.61	1143.26	1139.13	1142.655	859550.252	859495.91	1415.81
27	83.251	1.56021438	1135.18	1136.52	1135.35	1130.19	1134.3089	832552.196	832483.284	1407.46
28	82.9308	1.52350939	1124.95	1126.46	1125.39	1120.07	1124.2193	806724.268	806651.909	1397.37
29	82.6106	1.50709062	1121.06	1121.36	1120.29	1115.24	1119.4866	791879.675	791822.989	1392.64
30	82.1303	1.48629027	1114.42	1115.48	1113.82	1109.38	1113.2742	771895.893	771837.475	1386.42
31	81.65	1.46265566	1107.18	1107.98	1105.91	1102.5	1105.8923	750762.81	750718.179	1379.04

C11: Thermocouple #1, Raw Data from Experiment (TEMPERATURES.LVM)

D11: Thermocouple #2, Raw Data from Experiment (TEMPERATURES.LVM)

E11: Thermocouple #3, Raw Data from Experiment (TEMPERATURES.LVM)

F11: Thermocouple #4, Raw Data from Experiment (TEMPERATURES.LVM)

G11:=(D11+E11+C11+F11)/4

H11:=4*(A11)^2*B11*10^(-6)/(3.14159^2*0.002376*($F$2^2-$F$3^2))

I11:=((4*B11*A11^2*10^(-6))/(3.14159^2*($F$2^2-$F$3^2)*$F$2))-($F$5*($F$2^2-$F$3^2)+$F$6*($F$3^2-$F$4^2)+$F$7*$F$4^2)*(E11+D11-C11-F11)/(8*$F$2*$F$8*$F$9)

J11:=G11+273.15

Column I (Heat Flux, y-axis) is plotted with respect to Column J (Wall Temperature, x-axis) to attain the boiling curve.

C.4.5 Data Analysis

```
%Matlab Code Written by John Evangelista, Cornell University 2010

%Computes:
%mean flowrate and standard deviation for a given temperature
interval

clear
Traw = dlmread('TempRaw.txt'); %Read in column vector raw temperature
data
%which comes from data_organization_Kelvin.m (avg TC#1-4).
T_max=max(Traw); %Determine maximum temperature
T_min=min(Traw); %Determine minimum temperature
Tmax=round(T_max); %Round maximum temperature to nearest integer
Tmin=round(T_min); %Round minimum temperature to nearest integer
Trange=Tmax-Tmin; %Determine temp range of data to be analyzed
Tint=1; %Temperature increment that data is analyzed
Tindex=Trange/Tint; %Establish final index to insert into for-loop

Tlow=Tmin; %Initialize temp increment
Thigh=Tmin+Tint; %Initialize temp increment

for i=1:1:Tindex %Iterate
Tavg = dlmread('TempRaw.txt'); %Read/refresh raw temp data
Flow = dlmread('FlowRaw.txt'); %Read/refresh raw flow data


%Search temp data, find values less than temp increment and remove
index = find(Tlow > Tavg);
Tavg(index) = [];
%Also remove corresponding flow data points
Flow(index) = [];

%Search temp data, find values greater than temp increment and remove
index = find(Thigh < Tavg);
Tavg(index) = [];
%Also remove corresponding flow data points
Flow(index) = [];
%Resulting temp and flow column data vectors for given temp increment
Tavg;
Flow;
```

```
%Calculate mean and standard deviation
avgT=mean(Tavg);
avgF=mean(Flow);
sdT=std(Tavg);
sdF=std(Flow);
%Fill new mean temp and flow data vectors and standard deviation
T(i,1)=avgT;
F(i,1)=avgF;
ST(i,1)=sdT;
SF(i,1)=sdF;

%Update to next temp increment
Tlow=Tlow+Tint;
Thigh=Thigh+Tint;
end

%Write mean and standard deviation data to working directory
dlmwrite('AvgTemp.txt',T)
dlmwrite('AvgFlow.txt',F)
dlmwrite('SDFlow.txt',SF)
```

APPENDIX D

Net Energy Balance Analysis

D.1 Introduction and Literature Review

To evaluate the overall effectiveness of the Film Boiling Reactor (FIBOR) as a platform for chemical conversion, a suitable means to account for the net energy gain (or loss) should be defined within the context of its anticipated application. Conversion (Fogler 2006) is an appropriate assessment of the FIBOR's use solely as a chemical reactor. When comparing against other reactors, such as a packed bed reactor, considering the conversion per weight of catalyst can provide a suitable comparison. For this case, the FIBOR might be used as an intermediate platform to convert organic feedstocks into synthesis gas or syngas (mixture of hydrogen and carbon monoxide) which can then be combined with other chemical processes, such as the Fischer-Tropsch synthesis, to generate various chemicals and fuels. (Pagliaro, 2008)

Though appropriate from a chemical engineering perspective in terms of evaluating the FIBOR's ability to completely generate reactants to products, conversion however seems to lack a "bottom line" assessment. For example the FIBOR could be designed in a manner to raise the conversion (possibly even to 100%) by modifying the geometry alone such that the reactants are in contact longer with the catalyst surface, otherwise known as the residence time (Fogler 2006). Would this then suggest the FIBOR is preferable over other reactor designs with equivalent or even lower conversion? Other factors such as power requirements, cost, and the usefulness of the converted products are not addressed by conversion and should be considered by defining a method to assess the FIBOR's Net Energy Balance (NEB).

When combined with conversion, considering the NEB of the FIBOR can perhaps provide the broadest overall assessment since energy, environmental and economic impacts can be directly inferred. Within this context, the FIBOR could be envisioned as an onsite source of fuel (syngas) that is then combusted in a gas turbine as part of an integrated gasification combined cycle (IGCC) power plant. (DOE 2002) Within this context, the FIBOR might be compared to the IGCC's gasifier unit that converts coal to cleaner burning syngas. Other applications, often referred to as Advanced Thermal Technologies, employ pyrolysis or gasification in order to create energy from waste (e.g. municipal waste). Although these technologies are still in a state of development, several private companies throughout the world have developed large scale plants and claim promising results with energy efficiencies, or returns on energy invested (to be defined later) close to 1. (UC-Davis 2004) Systems that employ pyrolysis thermally degrade waste in the absence of air while gasification systems utilize small amounts of oxygen yet not enough to allow combustion to occur. These processes usually occur at temperatures above 800°C. These technologies rely on wastes such as paper, petroleum based products (e.g. plastics) and organic material such as food scraps. Syngas is created which can then be used as a fuel to generate electricity. The FIBOR could be integrated as a component to process liquid organic wastes similarly to these technologies.

Recent research provides an approach to assessing the FIBOR's conversion. (Choi 2010) This analysis is crucial to evaluating the FIBOR's overall feasibility as a chemical reactor. Results for catalytic conversion of methanol and ethylene glycol indicate that despite the simplistic geometric design (cylinder), the FIBOR's conversion is comparable to other chemical reactors and is a viable alternative for chemical processing. It also provides valuable insight into the effect of thermal decomposition on conversion by considering an integral energy balance around the

FIBOR, which will likely also play a similar role in its NEB. Conversion results are presented in Figure D.1 using Choi's (2010) approach for aqueous mixtures analyzed in this study. Results indicate that conversion estimates are quite low for this study (maximum approximately 10%). This is likely a result of the high steam content in the vapor phase along with using a small diameter than what Choi (2010) used. These results were computed using the following conversion formulation:

$$X = \left(\frac{\dot{N}_{P,out}}{\nu} \right) \frac{\int_{T_{sat}}^{T_{out}} C_{P,R}\, dT + h_{fg,R}}{\dot{Q} - A\bar{h}\left(T_{sat} - T_{\infty}\right) - h_{rxn,out}\left(\dot{N}_{P,out}/\nu\right)} \qquad \text{D.1}$$

Details regarding the derivation of Equation D.1 can be found in Choi (2010).

Urban (2006) also defined a "performance factor" which is the closest attempt to assess the FIBOR from an energy perspective. The ratio of hydrogen throughput to power input was considered. This approach however was based on theoretical modeling data and was not a non-dimensional quantity. This study seeks to consider the useful energy, or heating value of the products (SYNGAS) through a net energy balance analysis, resulting in a non-dimensional performance factor, otherwise known as the **E**nergy **R**eturn **O**n **E**nergy **I**nvested or EROEI.

D.2 Analysis

The extent that energy is converted from heat to work is the most common definition (Equation 1) of thermal efficiency, η. According to the Second Law of Thermodynamics, the

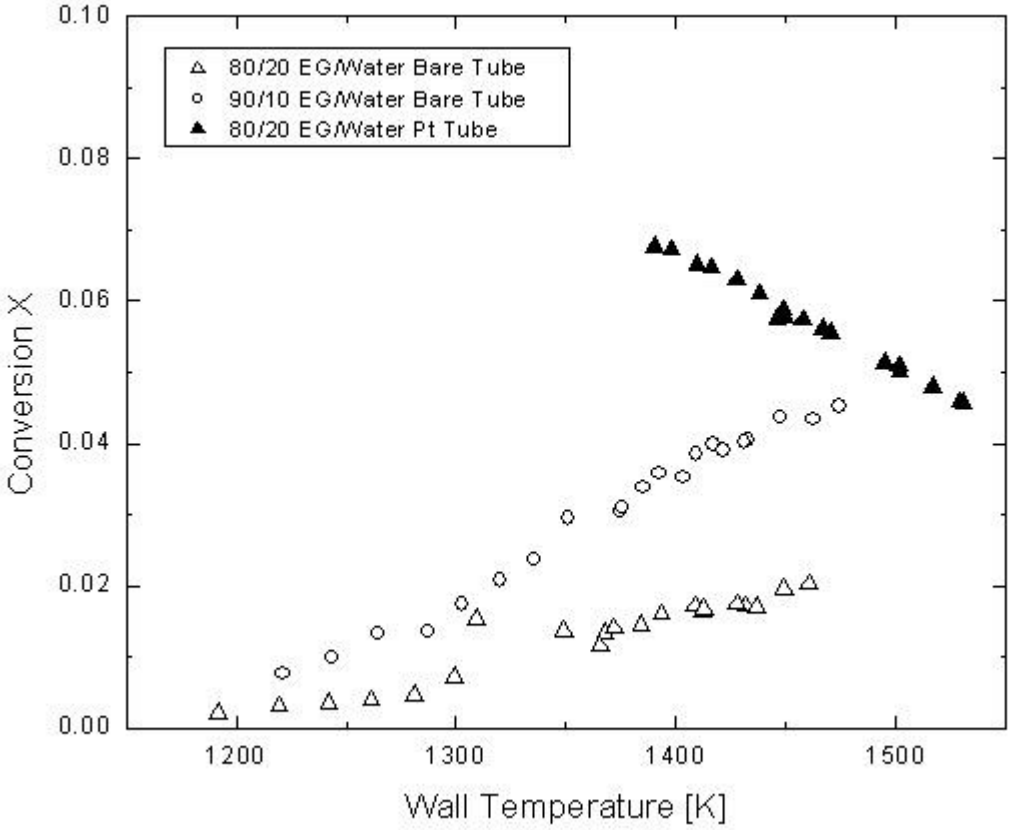

Figure D.1: Conversion Results

efficiency cannot exceed 100% and even the most efficient engine designs rarely reach 50%. (Moran 2008)

$$\eta = \frac{\dot{W}_{out}}{\dot{Q}_{in}} \quad \text{D.2}$$

Although the primary input parameter into the FIBOR is heat, useful work however is not performed on the surroundings as studied in common thermodynamic cycles (e.g. engines, power plants, etc.). Thus using the concept of thermodynamic efficiency for the FIBOR is inappropriate and cumbersome. A different definition of "energy efficiency," commonly used in literature to assess an intermediate process (e.g. Biofuels Industry) to produce sources of energy is the EROEI. (Cleveland 1984) In the most basic form, EROEI can be defined as:

$$\eta_{EROEI} = \frac{\text{Intrinsic Energy of Substance Produced}}{\text{Energy Required to Produce the Substance}} \quad \text{D.3}$$

If the EROEI is less than one, the process can be considered an energy sink, while if the EROEI is greater than one, a source of energy. A process that consumes more energy than is provided (EROEI<1) is something rarely considered to be useful and has an overall net energy loss. For example, many energy studies have been conducted on the biofuels industry to determine if extracting fuel (ethanol) from food sources, such as corn, is a viable alternative to fossil fuels. (Hill, 2006) In fact, Pimentel and Patzek (2005) found that ethanol produced from corn requires 29% more fossil fuel energy than the renewable ethanol fuel produced. These processes are evaluated based on considering all of the energy inputs (machinery for crop

harvesting, machinery to process and extract the fuel, transportation, etc.) to the energy value of the ethanol produced.

Estimates of EROEI are often the most compelling factor in terms of recommending whether resources should be invested in developing a certain process or technology. This definition should be used with caution and not confused with the thermodynamic concept of efficiency since the output is a source of energy (combustible product gases) rather than work or heat. In terms of applying this concept to the FIBOR, the following definition is proposed:

$$\eta_{EROEI} = \frac{(\text{Product Gas Heat of Combustion}) \cdot (\text{Product Flow Rate})}{\text{Power Applied to FIBOR}}$$

D.4

The product flow rate and power applied to the FIBOR are measured experimental quantities. A critical parameter in Equation D.4 is selecting an appropriate heat of combustion for products formed. This can be determined by first conducting a mass balance on the overall decomposition of ethylene glycol:

$$C_2H_6O_2 \rightarrow aCH_4 + bC_2H_2 + cC_2H_4 + dCO_2 + eCO + fH_2 + gH_2O + hC$$

D.5

In order to balance equation D.5, GC results in Table 5.3 are used in order to solve for the amounts of H_2O and Carbon (which are known to exist yet are not measured in our GC since H_2O is condensed back into the bulk and carbon is deposited as a solid on the heater tube). Once equation D.5 is balanced, the overall heat of reaction for decomposition of ethylene glycol (Equation D.5) can be

determined along with the heats of combustion (or heating values) of the combustible products (CH_4, C_2H_2, C_2H_4, and H_2). Results are given in Table D.1.

Table D.1: Products of Ethylene Glycol Decomposition and Corresponding Heats of Combustion

Reactant (%EG/%H_2O)	Heater Surface	Temperature [K]	Equation D.4 Coefficients								Products' Heat of Combustion [kJ/mol]
			a	b	c	d	e	f	g	h	
90/10	Bare	1473	0.370	0.080	0.060	0.020	1.330	1.450	0.620	0.000	824.00
80/20	Bare	1473	0.330	0.090	0.070	0.030	1.400	1.550	0.550	0.000	842.000
80/20	Catalytic	1373	0.030	0.009	0.003	0.195	0.656	1.969	0.954	1.095	523.000

D.3 Results

Figure D.1 shows the EROEI versus wall temperature for pure ethylene glycol and it's aqueous mixtures being converted into syngas by both catalytic reaction (Pt tube) and thermal decomposition (bare tube). These values were determined by analyzing the experimental data presented in Chapter 5 with Equation D.4. Power input values were determined from boiling curve data (Appendix F). The amount of heat required by the immersion heaters to maintain the liquid at saturation is not included since the design of the apparatus makes no attempt to prevent heat losses to the surroundings. The products flow rate is an experimentally measured quantity. The heat of combustion of the product gas was determined through a mass and energy balance of Equation D.5.

An interesting result is that EROEI increases for thermal decomposition (bare tube) however decreases with temperature for catalytic conversion (Pt tube). Choi (2010) also found a similar result for conversion decreasing with temperature for a platinum tube converting methanol, yet increased for cases with thermal decomposition present. This is also in fact the case for the results presented in Figure D.1 for aqueous mixtures analyzed in this thesis. Choi (2010) showed through an energy balance around the FIBOR's vapor film that the presence (or absence) of thermal decomposition determines the tendency for conversion to either increase or decrease with respect to temperature. This trend can be proven by recognizing that conversion is proportional to the ratio of heat transfer due to chemical reaction over the heat transfer due to evaporation at the vapor film:

Since,

$$X=\frac{\dot{N}_{P,out}/\nu}{\dot{N}_{R,in}} \qquad \text{D.6}$$

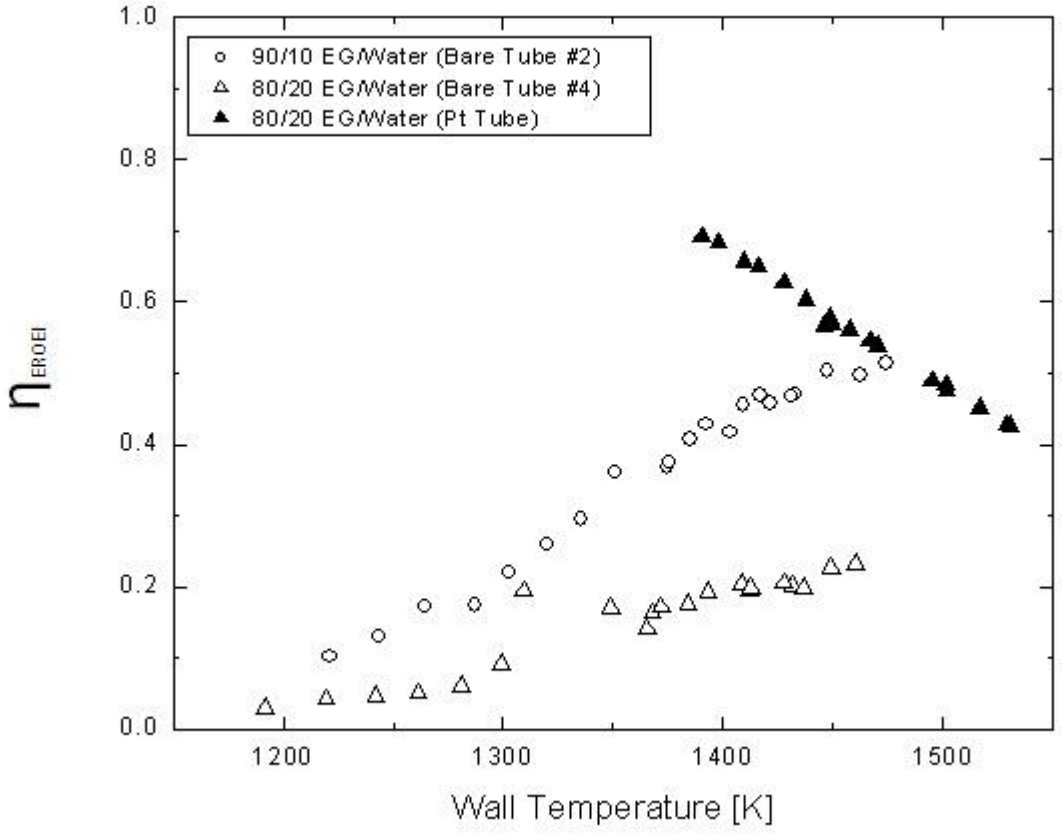

Figure D.2: Energy Return on Energy Invested (EROEI)

where X is conversion, $\dot{N}$ is the molar flow rate of products (P) and reactants (R) and ν is the stoichiometric amount of product (moles) with respect to the primary reaction pathway. The heat consumed by chemical reaction (q_{rxn}) and evaporation (q_{evap}) are

$$q_{rxn} = \Delta h_r^{\circ}\left(\dot{N}_P / \nu\right) \quad \text{D.7}$$

$$q_{evap} = \dot{N}_R h_{fg} \quad \text{D.8}$$

Combining D.4, D.5 and D.6 it follows that

$$\text{X} \propto \frac{q_{rxn}}{q_{evap}} \quad \text{D.9}$$

This explanation can also be extended to EROEI where,

$$\text{EROEI}_{FIBOR} = \frac{(\text{Products Heat of Combustion}) \cdot (\text{Product Flow Rate})}{\text{Power Applied to FIBOR}} = \frac{(\Delta h_c) \cdot \dot{N}_P}{I^2 R} \quad \text{D.10}$$

and since

$$q_{rxn} \propto \dot{N}_P \quad \text{D.11}$$

$$q_{evap} \propto q_{app} \quad \text{D.12}$$

$$\text{EROEI}_{FIBOR} \propto X \quad \text{D.13}$$

Comparing Equations D.7 and D.11 shows that the role of thermal decomposition has a similar effect on EROEI. Particularly, for catalytic reaction as

temperature increases, the rate of chemical reaction increases relatively less than the rate of evaporation (inflow of reactants) causing a decreasing trend in EROEI. For thermal decomposition however an opposite trend exists. The rate of chemical reaction is much more sensitive to temperature so that as the temperature increases, the rate of chemical reaction is higher relative to the rate of evaporation, causing an increasing trend in EROEI.

D.3 Conclusions

Considering both conversion and a net energy balance allows for a more complete assessment of the FIBOR's effectiveness as a platform to produce syngas. Results indicate that reforming aqueous solutions results in very modest returns on energy with a maximum of approximately 0.15. In terms of energy recovery, pure ethylene glycol showed the highest EROEI at maximum operating temperatures (approximately 0.4). Catalytic conversion for an aqueous mixture (80%/20%) showed the highest EROEI for aqueous mixtures of approximately 0.3 with a decreasing trend as temperature increased.

Despite these values being less than one indicating a net energy loss, adjusting the design of the heater and/or electrode clamps discussed in Chapter 6 in order to allow operation at lower temperatures could greatly enhance the EROEI of a catalyst coated tube. For example, Choi's (2010) results for catalytically converting methanol over a platinum catalyst results in an EROEI > 1 because of the appreciable yields at low operating temperatures. Minimizing the heat losses from the reactant chamber would also increase the EROEI. Catalytically reacting richer mixtures of ethylene glycol (e.g. 90%/10%) would also likely increase the product yields and thus EROEI.

Although all results for this study indicate EROEI values less than one, processing chemicals under these conditions may still be beneficial. For example in

the IGCC power plant scenario, syngas is generated in a gasification unit by pyrolysis of a coal slurry, however this syngas must be sent through other energy consuming systems to remove impurities (e.g. sulfur). (DOE 2002) Feedstocks processed in the FIBOR would likely bypass this requirement since the product feed does not contain such impurities. Additionally, there are cases when running a process with EROEI less than one makes practical sense. (Jones 2009) Common scenarios that can be envisioned from an economic perspective are when there are costs associated with otherwise disposing the feedstock (hazardous material), if use of a feedstock lowers overall CO_2 emissions and lastly if fuels can be generated onsite to avoid transportation costs. It seems that processing organic feedstocks with FIBOR technology could possibly exploit all three of these categories further suggesting that converting chemicals by means of film boiling could supplement or be a viable alternative to other processes, namely coal or waste gasification.

APPENDIX E

Flow Rate Curve Data

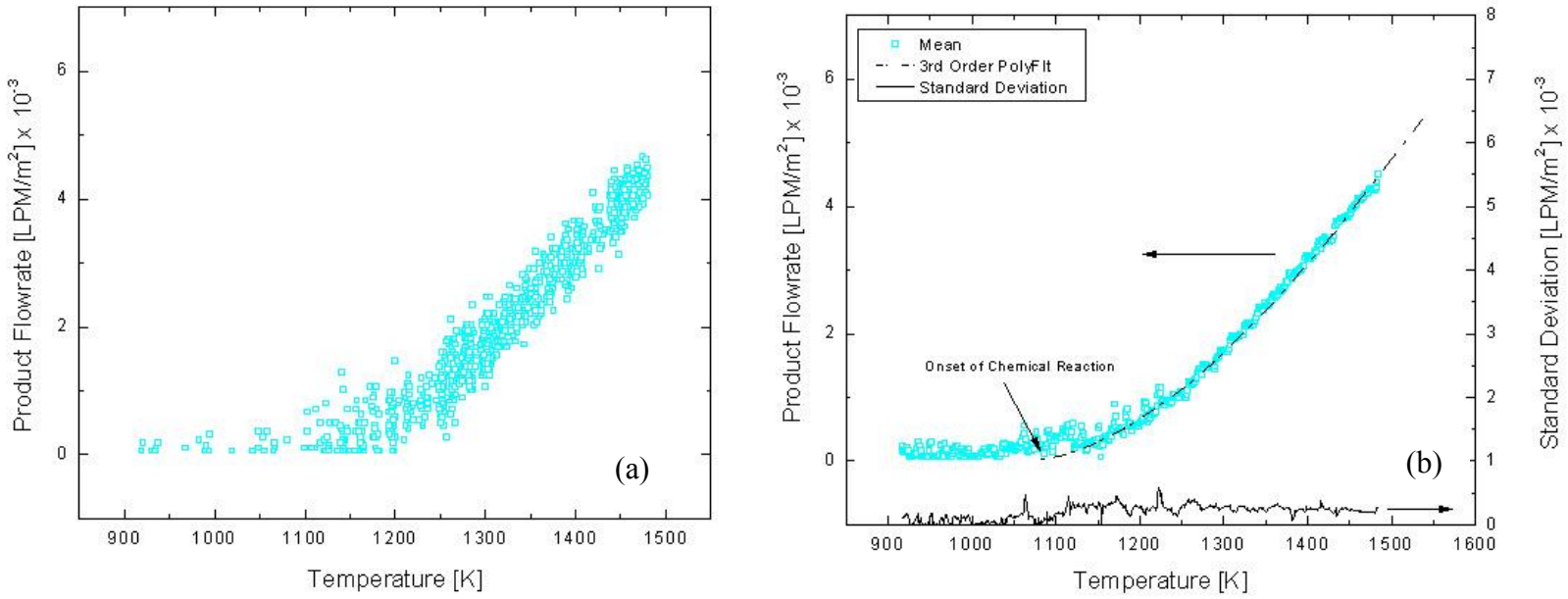

Figure E.1: Pure ethylene glycol converted with Bare Tube #1 (1st Trial, Polished) raw data product flow rate curve plot (a) and corresponding mean and standard deviation plot (b) for all measurements within a 1 degree [K] interval. A curve fit (3rd order polynomial) is extended to zero to estimate the onset of chemical reaction.

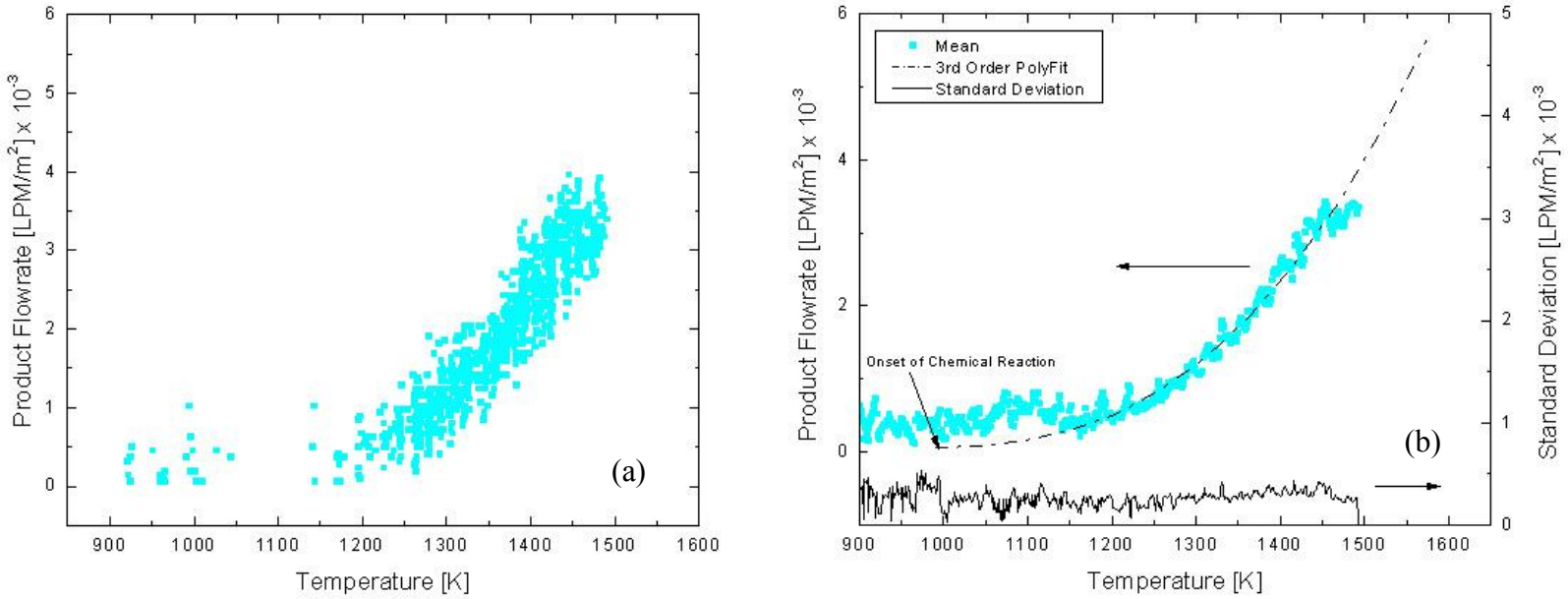

Figure E.2: Pure ethylene glycol converted with Bare Tube #1 (2nd Trial, Blackened) raw data product flow rate curve plot (a) and corresponding mean and standard deviation plot (b) for all measurements within a 1 degree [K] interval. A curve fit (3rd order polynomial) is extended to zero to estimate the onset of chemical reaction.

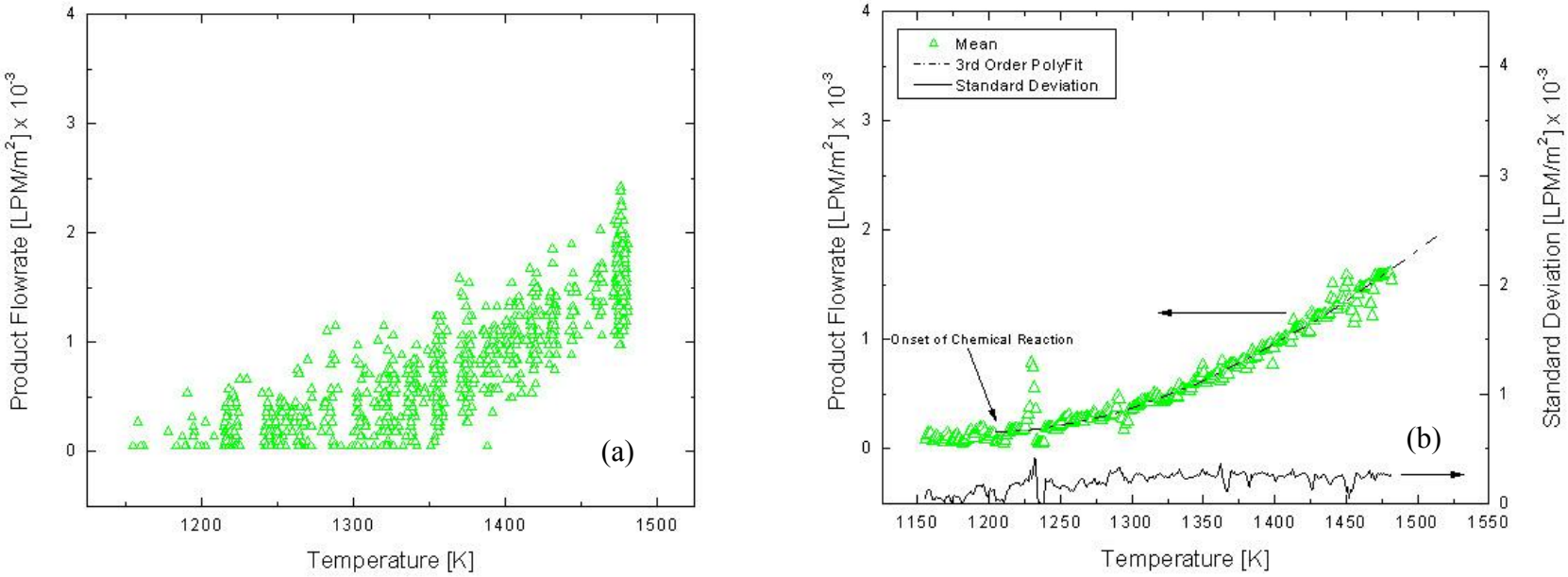

Figure E.3: Ethylene glycol aqueous mixture (90%/10% by vol) converted with Bare Tube #2 (1st Trial, Polished) raw data product flow rate curve plot (a) and corresponding mean and standard deviation plot (b) for all measurements within a 1 degree [K] interval. A curve fit (3rd order polynomial) is extended to zero to estimate the onset of chemical reaction.

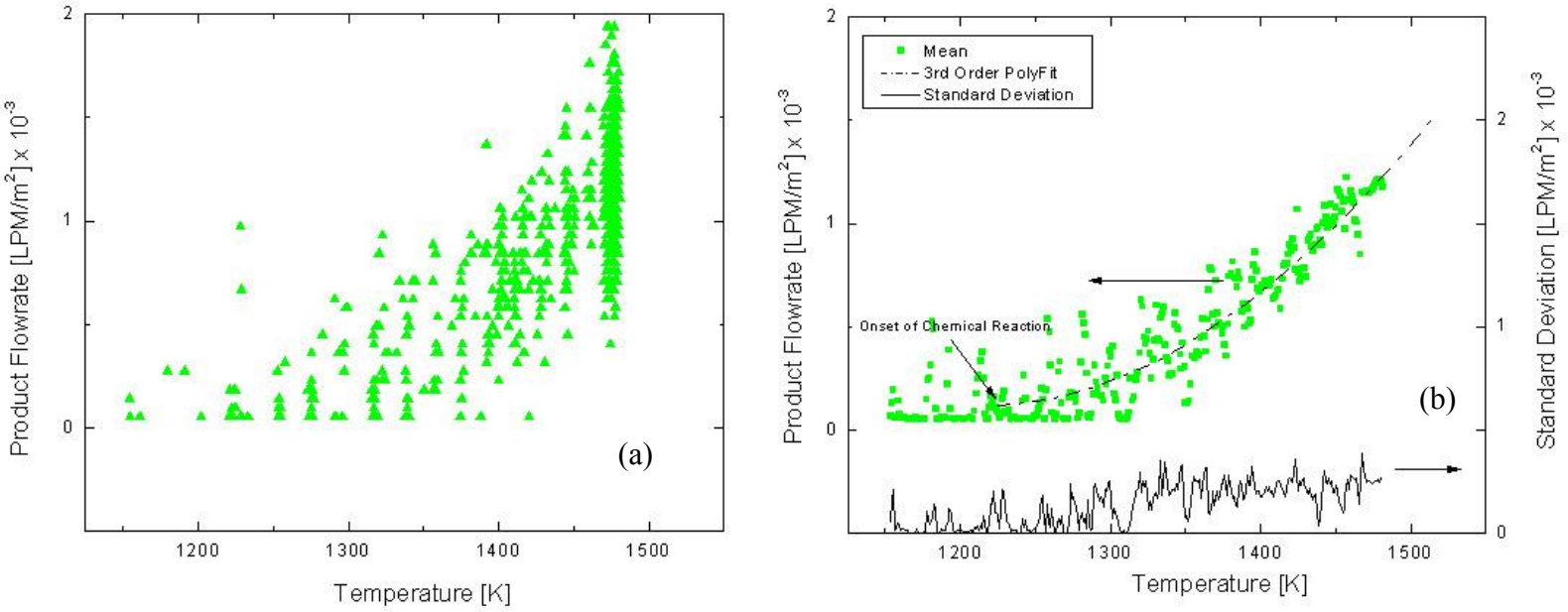

Figure E.4: Ethylene glycol aqueous mixture (90%/10% by vol) converted with Bare Tube #2 (2nd Trial, Blackened) raw data product flow rate curve plot (a) and corresponding mean and standard deviation plot (b) for all measurements within a 1 degree [K] interval. A curve fit (3rd order polynomial) is extended to zero to estimate the onset of chemical reaction.

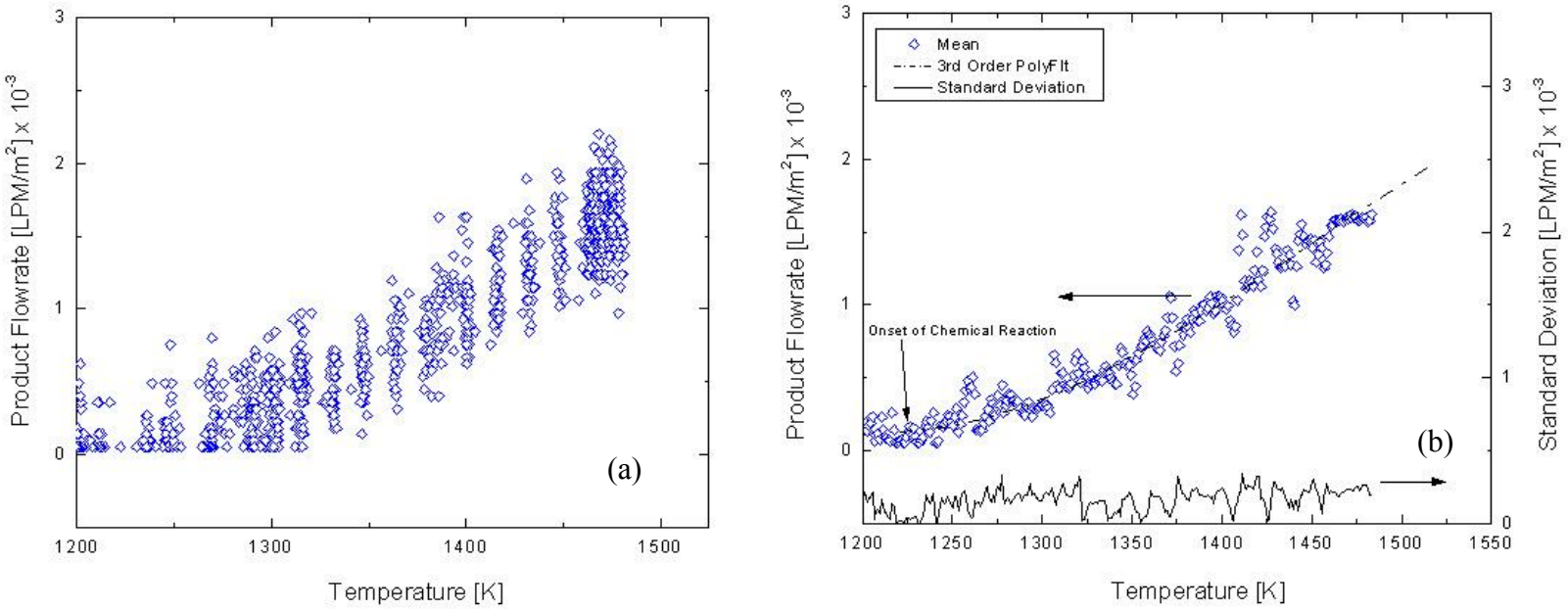

Figure E.5: Ethylene glycol aqueous mixture (90%/10% by vol) converted with Bare Tube #3 (Initial 2-hours of use, Polished) raw data product flow rate curve plot (a) and corresponding mean and standard deviation plot (b) for all measurements within a 1 degree [K] interval. A curve fit (3rd order polynomial) is extended to zero to estimate the onset of chemical reaction.

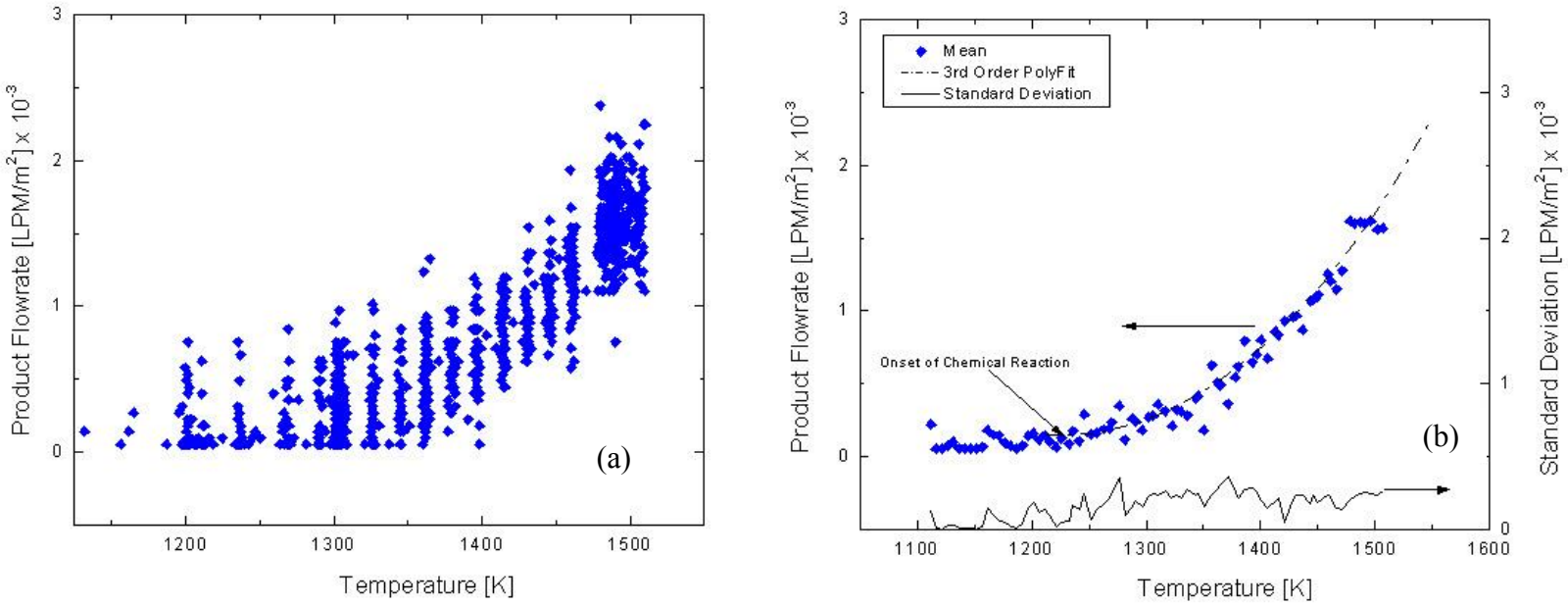

Figure E.6: Ethylene glycol aqueous mixture (90%/10% by vol) converted with Bare Tube #3 (Latter 2-hours of use, Blackened) raw data product flow rate curve plot (a) and corresponding mean and standard deviation plot (b) for all measurements within a 5 degree [K] interval. A curve fit (3rd order polynomial) is extended to zero to estimate the onset of chemical reaction.

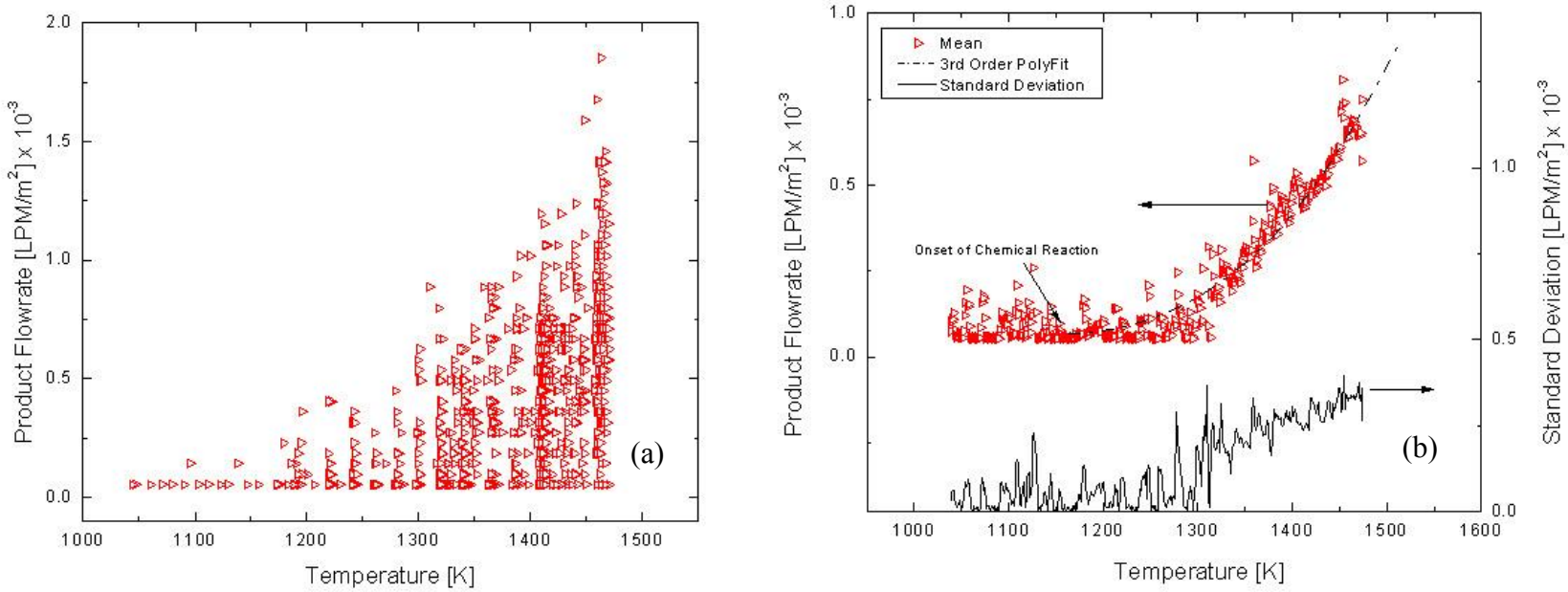

Figure E.7: Ethylene glycol aqueous mixture (80%/20% by vol) converted with Bare Tube #4 (1st Trial, Polished) raw data product flow rate curve plot (a) and corresponding mean and standard deviation plot (b) for all measurements within a 1 degree [K] interval. A curve fit (3rd order polynomial) is extended to zero to estimate the onset of chemical reaction.

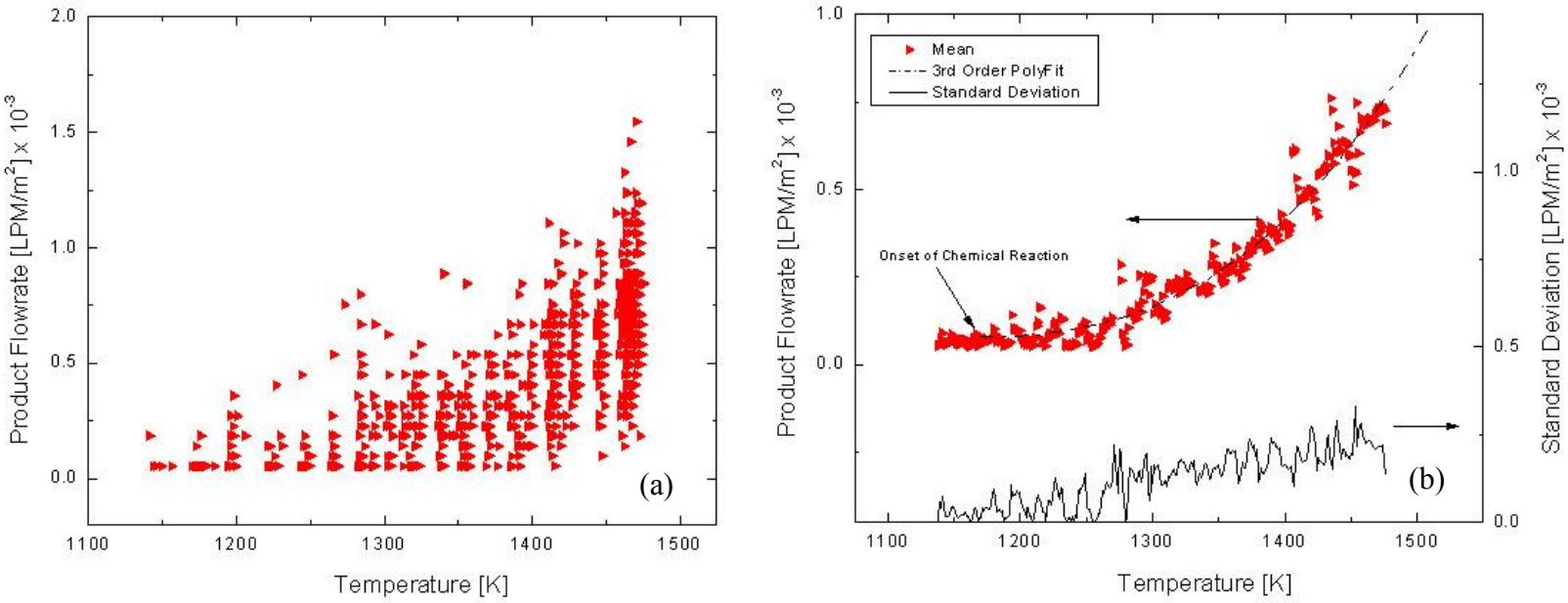

Figure E.8: Ethylene glycol aqueous mixture (80%/20% by vol) converted with Bare Tube #4 (2nd Trial) raw data product flow rate curve plot (a) and corresponding mean and standard deviation plot (b) for all measurements within a 1 degree [K] interval. A curve fit (3rd order polynomial) is extended to zero to estimate the onset of chemical reaction.

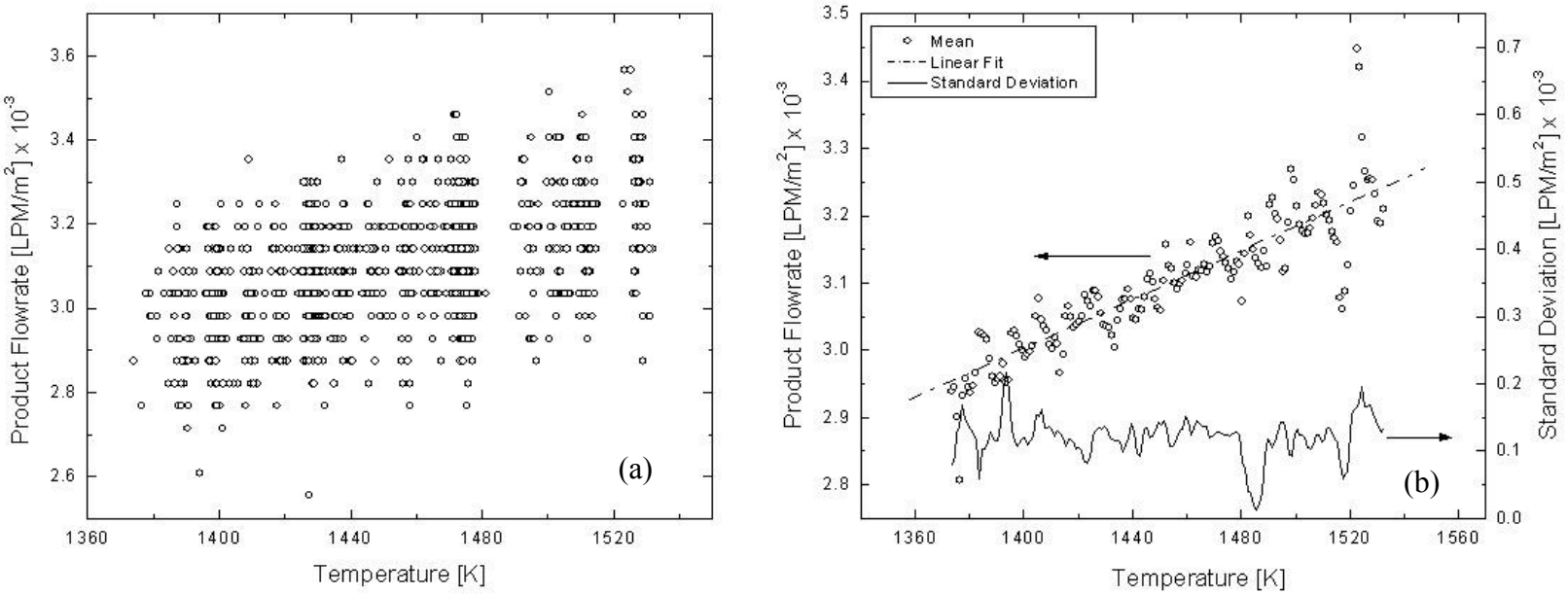

Figure E.9: Ethylene glycol aqueous mixture (80%/20% by vol) converted with a Platinum catalyst coating (1st Trial) raw data product flow rate curve plot (a) and corresponding mean and standard deviation plot (b) for all measurements within a 1 degree [K] interval. A linear curve-fit is shown to estimate the flow rate's dependence on temperature.

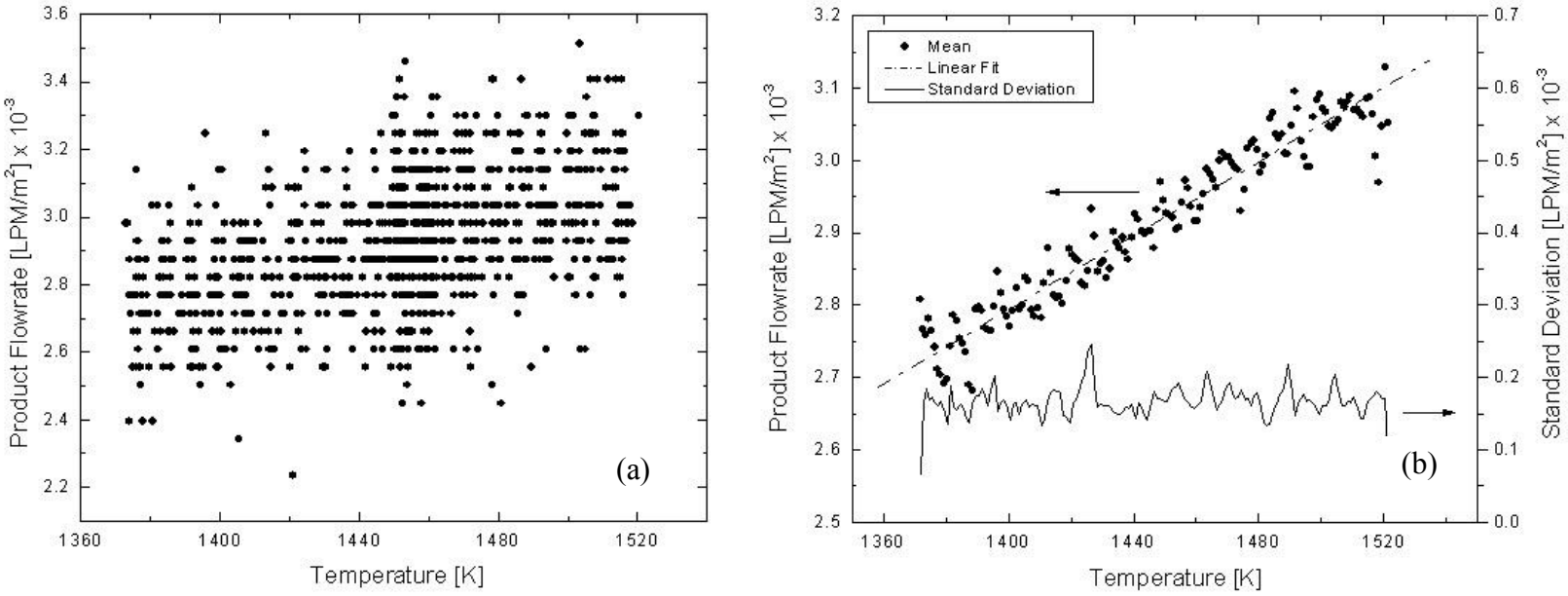

Figure E.10: Ethylene glycol aqueous mixture (80%/20% by vol) converted with a Platinum catalyst coating (2nd Trial) raw data product flow rate curve plot (a) and corresponding mean and standard deviation plot (b) for all measurements within a 1 degree [K] interval. A linear curve-fit is shown to estimate the flow rate's dependence on temperature.

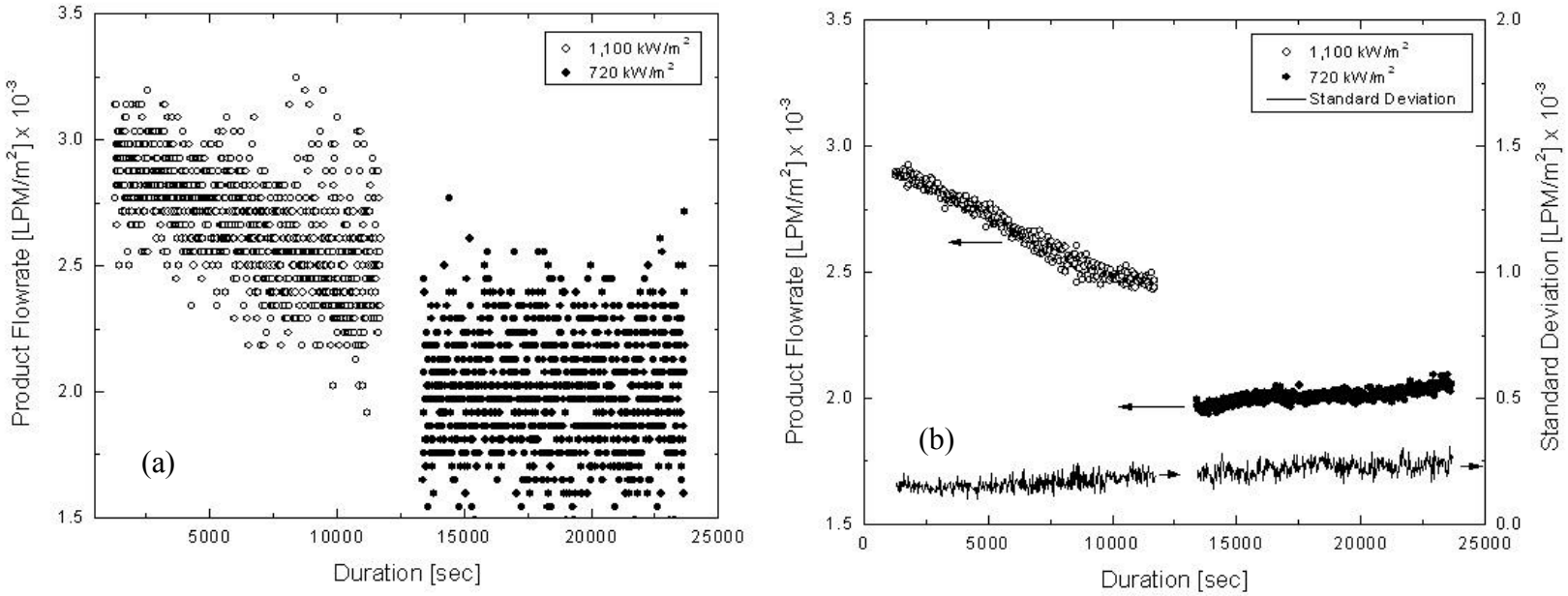

Figure E.11: Ethylene glycol aqueous mixture (80%/20% by vol) converted with a Platinum catalyst coating (Endurance Test) raw data product flow rate curve plot (a) and corresponding mean and standard deviation plot (b) for all measurements within a 1 degree [K] interval. A linear curve-fit is shown to estimate the flow rate's dependence on temperature.

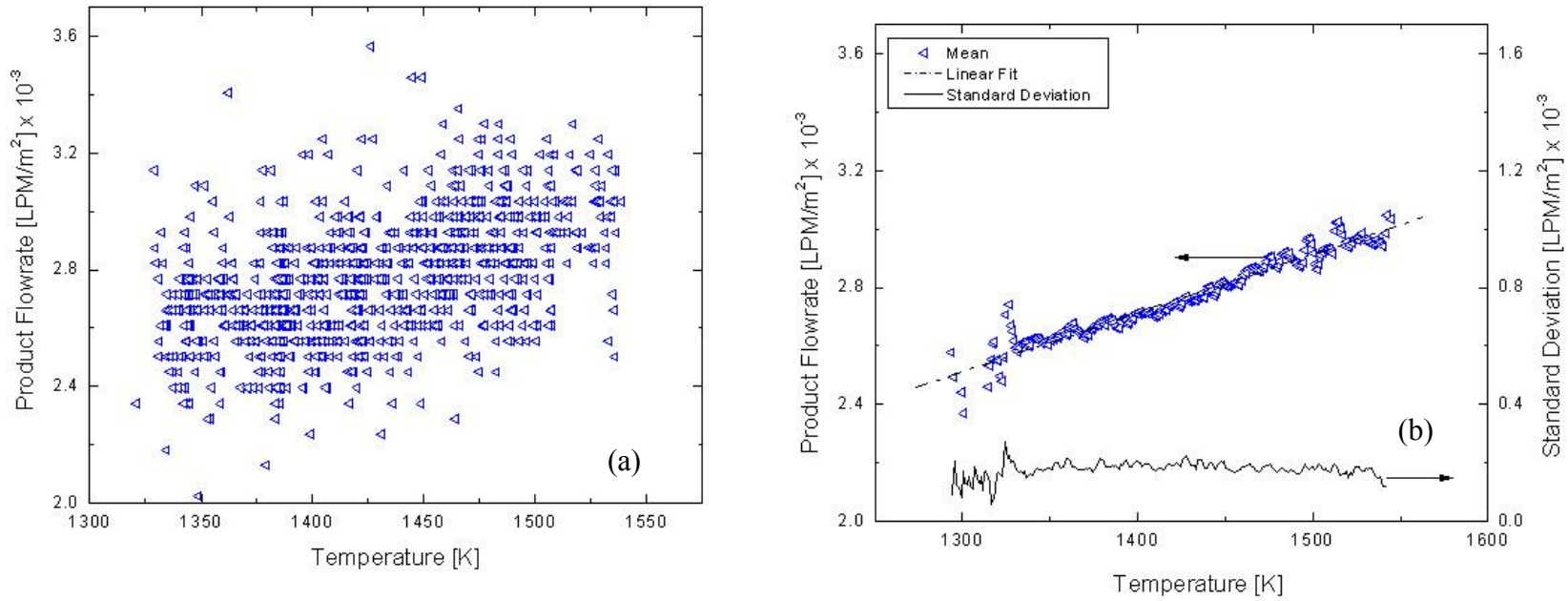

Figure E.12: Ethylene glycol aqueous mixture (80%/20% by vol) converted with a Nickel catalyst coating (1st Trial) raw data product flow rate curve plot (a) and corresponding mean and standard deviation plot (b) for all measurements within a 1 degree [K] interval. A linear curve-fit is shown to estimate the flow rate's dependence on temperature.

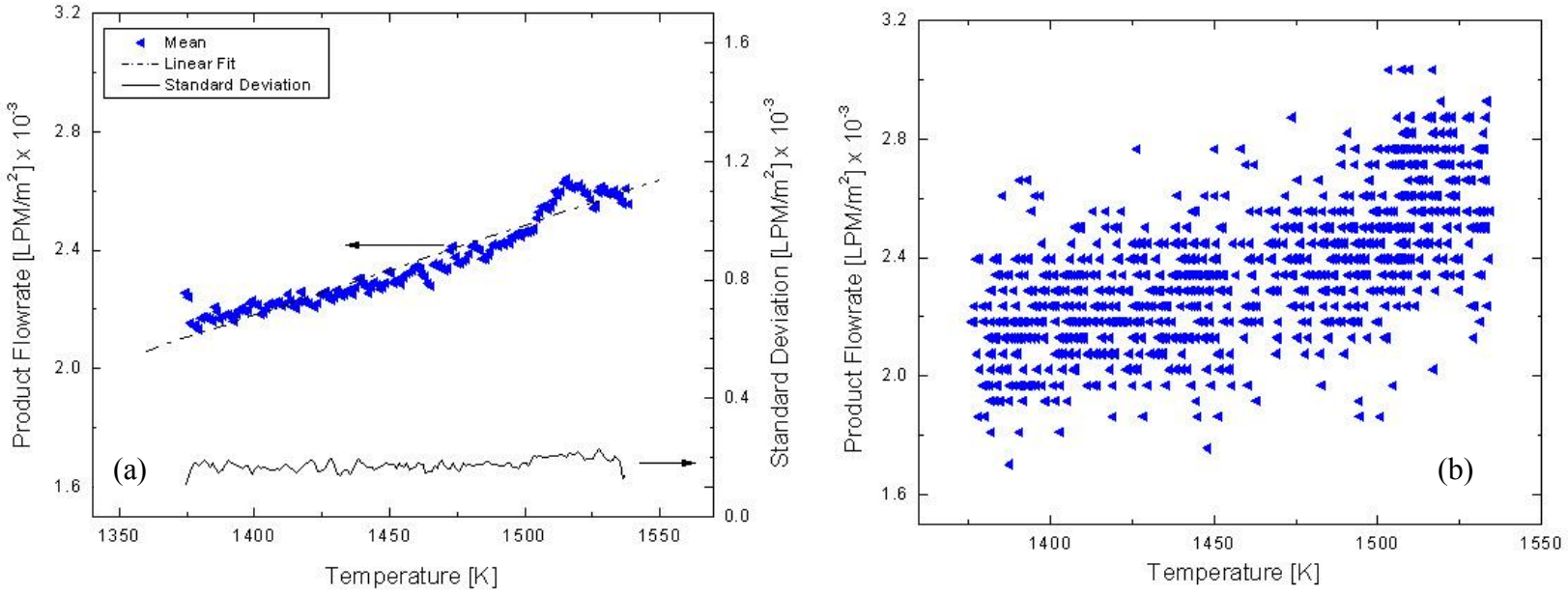

Figure E.13: Ethylene glycol aqueous mixture (80%/20% by vol) converted with a Nickel catalyst coating (2nd Trial) raw data product flow rate curve plot (a) and corresponding mean and standard deviation plot (b) for all measurements within a 1 degree [K] interval. A linear curve-fit is shown to estimate the flow rate's dependence on temperature.

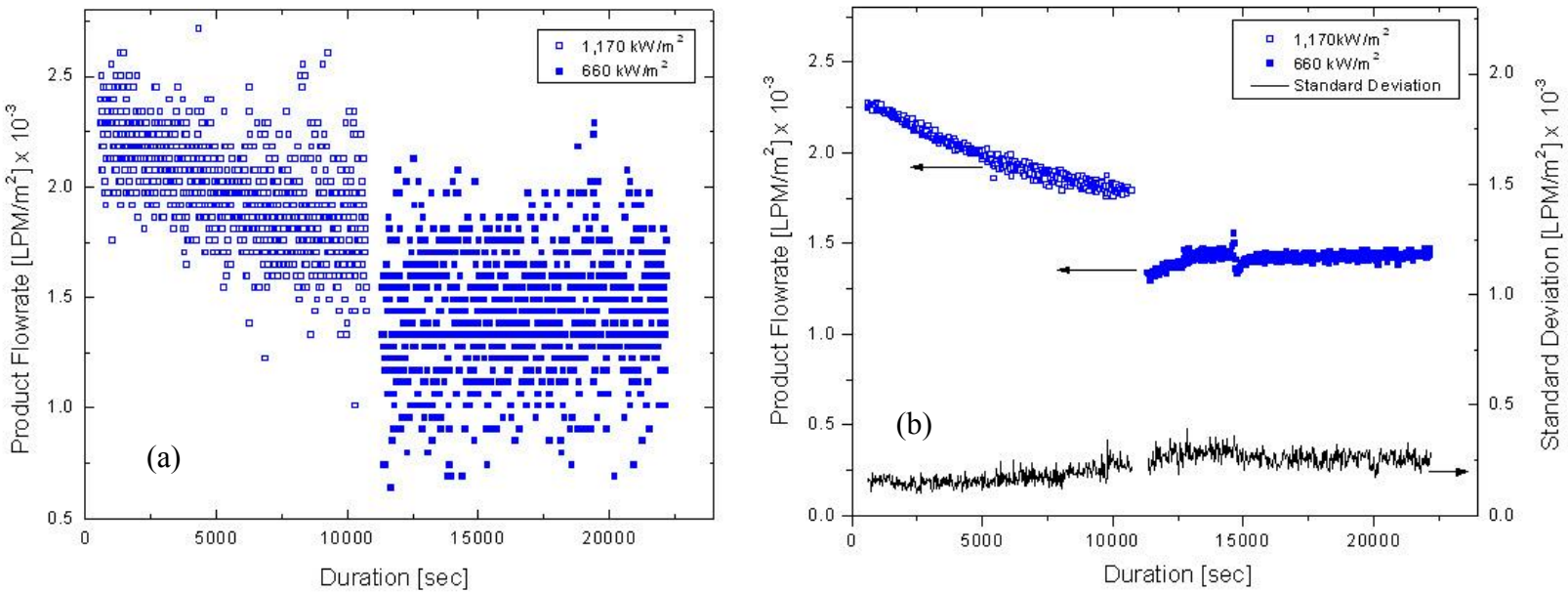

Figure E.14: Ethylene glycol aqueous mixture (80%/20% by vol) converted with a Nickel catalyst coating (Endurance Test) raw data product flow rate curve plot (a) and corresponding mean and standard deviation plot (b) for all measurements within a 1 degree [K] interval. A linear curve-fit is shown to estimate the flow rate's dependence on temperature.

APPENDIX F

Boiling Curve Data

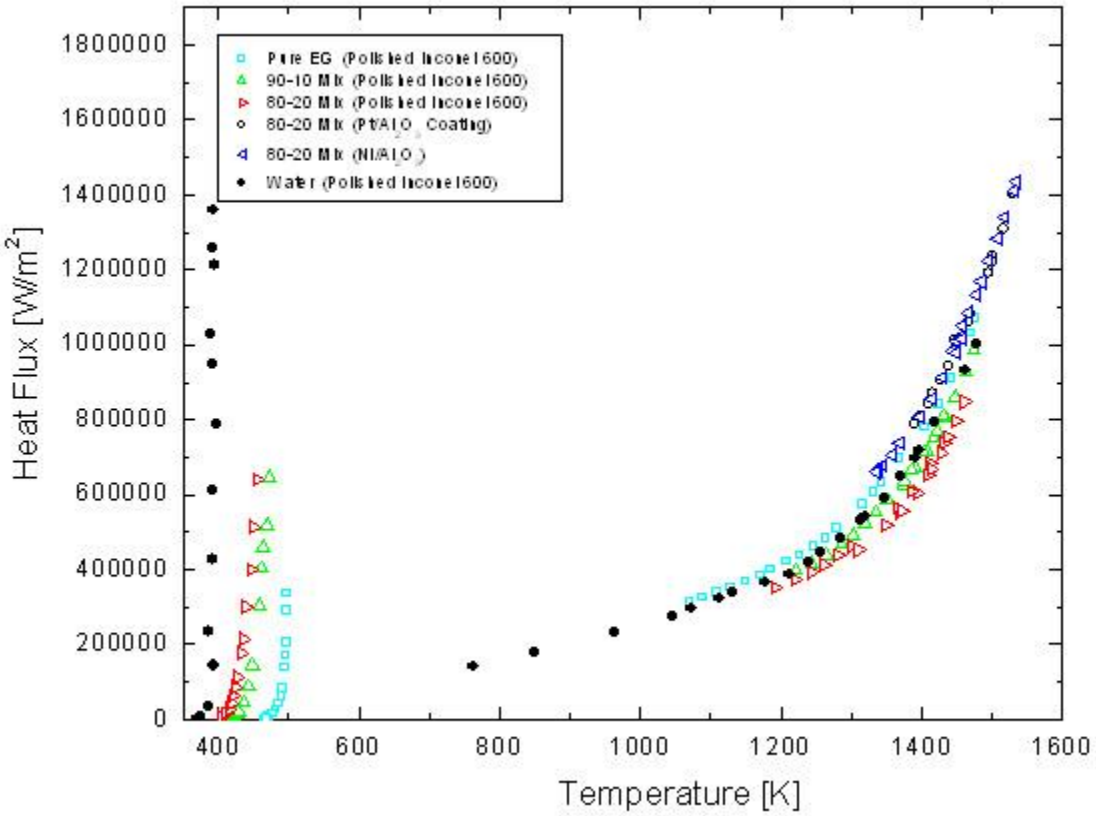

Figure F.1: Compilation of Complete Boiling Curves for Pure Ethylene Glycol, Aqueous Mixtures and Pure Water

Table F.1: Boiling Curve Data

Appendix F-Boiling Curve Data (Polished Inconel-600)							
Nucleate Boiling Curve							
Water (ρ-9980 kg/m^3)		Ethylene Glycol (ρ-1112 kg/m^3)		90% Ethylene Glycol/10%Water (ρ-1106 kg/m^3)		80% Ethylene Glycol/20%Water (ρ-1099 kg/m^3)	
Wall Temp [K]	Heat Flux [W/m^2]	Wall Temp [K]	Heat Flux [W/m^2]	Wall Temp [K]	Heat Flux [W/m^2]	Wall Temp [K]	Heat Flux [W/m^2]
370	420	464	411	415	3978	404	6924
375	8942	470	3820	419	7163	411	15924
386	35754	472	6711	421	10981	415	28151
386	144223	477	15307	426	15951	418	44445
390	234533	482	26902	429	21836	421	63742
391	427107	486	42353	436	44499	424	86483
393	610068	490	61319	443	87473	426	113715
393	787443	493	83262	449	144901	433	176862
393	947029	495	138092	459	302998	435	214994
393	1029504	496	169751	461	403684	440	299271
394	1211706	498	205970	464	458531	446	399379
394	1259424	498	288845	469	517081	449	513853
399	**1361147**	**498**	**335529**	**474**	**646684**	**455**	**640639**
Film Boiling Curve							
Water (ρ-9980 kg/m^3)		Ethylene Glycol (ρ-1112 kg/m^3)		90% Ethylene Glycol/10%Water (ρ-1106 kg/m^3)		80% Ethylene Glycol/20%Water (ρ-1099 kg/m^3)	
Wall Temp [K]	Heat Flux [W/m^2]	Wall Temp [K]	Heat Flux [W/m^2]	Wall Temp [K]	Heat Flux [W/m^2]	Wall Temp [K]	Heat Flux [W/m^2]
763	140714	1071	313312	1221	397800	1192	352293
850	179569	1090	325442	1244	416660	1219	372831
964	231506	1108	339803	1264	439292	1242	392705
1046	274560	1129	353255	1287	467800	1261	413667
1073	297077	1149	367549	1303	492889	1281	437065
1113	321326	1172	385041	1320	521723	1299	451593
1131	339340	1186	400621	1335	551902	1309	462382
1178	364114	1209	421143	1351	584717	1349	516935
1212	387424	1227	438322	1374	626022	1365	553306
1239	418720	1246	461887	1376	635655	1368	557848
1256	445581	1264	484245	1385	665481	1372	565526
1285	483558	1280	511194	1392	670714	1384	605792
1314	530787	1316	572565	1403	713976	1393	606843
1321	541140	1332	605027	1409	714876	1408	649896
1347	588363	1343	632342	1417	750654	1412	668222
1371	648331	1368	696675	1421	768460	1413	681836
1392	697845	1405	779499	1431	804595	1427	711902
1397	718543	1425	842235	1433	809828	1432	738393
1419	790966	1442	910284	1448	860783	1437	751192
1463	930887	1471	1031731	1463	926797	1449	797058
1479	1002825	1475	1069797	1474	985883	1460	846865
**Critical Heat Flux (CHF) in bold type							

APPENDIX G

Proof of Negligible Axial Conduction for Film Boiling on a Horizontal Cylinder

This appendix extends the discussion from Section 4.2 regarding the modes of heat transfer for a horizontal cylinder experiencing film boiling. It is proven that considering the contribution of conduction heat transfer in the radial direction only (and neglecting axial conduction) provides an accurate measurement of the total heat flux reported on the boiling curve. Even for the case of partial nucleate boiling on the ends of the tube, which would create the maximum amount of heat transfer in the axial direction for the experimental arrangement reported in this thesis, axial conduction remains negligible. Details regarding this claim follow.

Figure D.1 shows a schematic of the thermocouple placement (stars) and temperature profile (not to scale) across the length of the heater tube. Arrows also depict the heat transfer paths in the radial and axial directions.

Thermocouples are not placed at the ends of the tube (stars labeled T_{sat}). Since these temperatures are not known, heat transfer in the axial conduction could be greater than what was estimated in Section 4.2. To investigate further, we calculate the axial conduction for the case where the ends of the tube are at the lowest possible temperature-the liquid's saturation temperature. This condition would correspond to the maximum axial heat flux possible during a film boiling experiment.

The axial heat transfer for this condition can be expressed as,

$$q_{axial} = \frac{2(T_{1,4} - T_{sat})k\pi(D_o^2 - D_i^2)}{L - L_1} \qquad \text{G.1}$$

and from Equation 4.12,

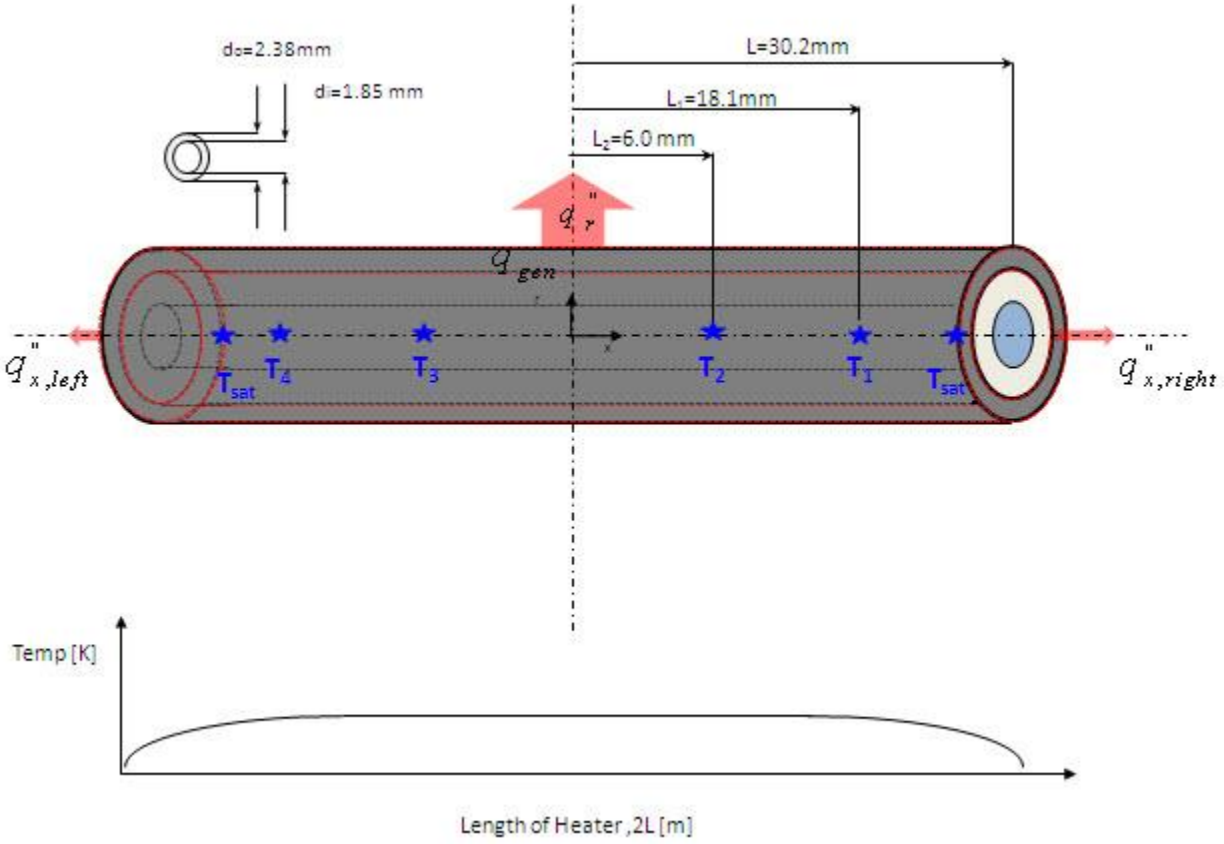

Figure G.1: Heat Transfer from Heater Tube

$$q_r = \frac{4\rho I^2 (2L)}{\pi (d_o^2 - d_i^2)} \qquad \text{D.2}$$

The following values are substituted into Equations D.1 and D.2,

a) k = 27.5 W/m·K (Special Metals 2008)

b) $T_1 = T_2 = T_3 = T_4 = 1405K$ (Appendix F, Pure Ethylene Glycol Film Boiling)

c) $T_{sat} = 470K$ (Pure Ethylene Glycol)

d) I=80.85 A (Measured for Pure Ethylene Glycol Film Boiling, Appendix F)

e) ρ = 1.85 μΩ-m (Equation 2.2)

Substituting values listed above in addition to geometric values provided in Figure G.1 it follows that,

$q_{axial} = 30W$

vs.

$q_r = 412W$

This therefore shows that even for the case of nucleate boiling at the ends of the tube which would cause the highest possible temperature gradient, the axial conduction would only account for just 7% of the total flux. The actual temperature at the ends was much higher however because film boiling was always maintained uniformly across the heater tube for all boiling curves reported in this thesis. Thus, the absence of thermocouples at the end of the tube to accurately account for axial conduction losses has a negligible effect on boiling curve measurements.

BIBLIOGRAPHY

Arias, F.J. 2010 *International Journal of Thermal Sciences* **49**, pp. 631-634.

Avedisian, C.T., Tsang, W., Davidovits, T., Allaben, J.R. 2008 *AIChE Journal,* **54** No. 2, (2)575-(2)581.

Breen, B.P., Westwater, J.W. 1962 *Chemical Engineering Progress,* **58** No. 7, (7)67-(7)72.

Bromley, L.A. 1950 *Chemical Engineering Progress,* **46** No. 5, (5)221-(5)227.

Choi, S. 2010 Ph.D. Thesis, Mechanical and Aerospace Engineering Department, Cornell University.

Cleveland, C., Costanza, R., Hall, C., Kaufman, R. 1984 *Science* **225**, pp. 890-897.

Cortright, R.D., Davda, R.R., Dumesic, J.A. 2002 *Nature,* **418**, pp. 964-967.

Dhir, V.K., Lienhard J.H. 1974 *Journal of Heat Transfer,* February, pp. 71-78.

Ede, A.J., Siviour, J.B. 1975 *Int. J. Heat Mass Transfer,* **18**, pp. 737-741.

Epstein, M., Leung, J.C., Hauser, G.M., Henry, R.E. 1984 *Int. J. Heat Mass Transfer,* **27**, pp. 1365-1378.

Fogler, H.S. 2006 *Elements of Chemical Reaction Engineering.* Pearson Publishing, pp. 37-40; 709-716.

Frea, W.J., Knapp, F.R., Taggart, T.D. 1977 *The Canadian Journal of Chemical Engineering*, **55,** pp 37-42.

General Electric (GE) Energy. Take from GE Integrated Gasification Combined Cycle(IGCC) website.(http://www.gepower.com/prod_serv/products/gas_turbines_cc/en/igcc/technology.htm.)

Hill, J., Nelson, E.,, Tillman, D., Polasky, S., Tiffany, D. 2006 *PNAS* **103**, pp 11206-11210.

Hsueh, M. 2007 Senior Design Project, Mechanical and Aerospace Engineering Department, Cornell University.

Hu, X., Lu, G. 2009 *Applied Catalysis B: Environmental,* **88**, pp. 367-385.

Huang, Z. 2006 Senior Design Project, Mechanical and Aerospace Engineering Department, Cornell University.

Incropera, F.P., Dewitt, D.P., Bergman, T.L., Lavine, A.S. 2007 *Fundamentals of Heat and Mass Transfer,* 6th Edition. John and Wiley Sons, pp. 620-655.

Jones, J.C. 2009 *Fuel*, **88**, pg. 584.

Katto, Y. 1994 *International Journal of Multiphase Flow,* **20,** pp. 53-90.

Kechagiopoulos, P.N., Voutetakis, S.S., Lemonidou, A.A., Vasalos, I.A. 2007 *Catalysis Today,* **127**, pp. 246-255.

Lee, D.J. 1998 *Int. J. Heat Mass Transfer,* **41**, pp. 2925-2928.

Lienhard, J.H., IV, Lienhard, J.H., V. 2008 *A Heat Transfer Textbook,* 3rd Edition. Phlogiston Press, pp. 487.

Liu, M.H., Yang, Y.M., Maa, J.R. 1996 *Numerical Heat Transfer, Part A,* **30**, pp. 815-834.

Liu, M.H., Yang, Y.M., Maa, J.R. 1997 *Heat and Mass Transfer,* **32**, pp. 261-269.

Marschall E., Moresco, L.L. 1977 *Int. J. Heat Mass Transfer,* **20**, pp. 1013-1018.

MEGlobal Group. 2008 *Ethylene Glycol Product Guide.* 001-00005-0508-CRCG (see http://www.meglobal.biz/literature/product_guides/MEGlobal_MEG.pdf).

Moran, M., Howard, S. 2008 *Fundamentals of Engineering Thermodynamics.* Wiley Publishing, pg. 66.

Nukiyama, S. 1934 *Journal Japan Soc. Mech. Engrs.*, **37**, pp. 367-374.

Oberg, E., Jones, F.D., Horton, H.L., Ryffel, H.H. 2008 *Machinery's Handbook,* 28th Edition, Industrial Press, pp. 627-647.

Okuyama K., Iida Y. 1994 *JSME International Journal* , **37**, No.1, pp. 123-131.

Othmer, D.F. 1943 *Industrial and Engineering Chemistry,* **35,** pp.614-620.

Pagliaro, M., Rossi, M. 2008 *The Future of Glycerol New Usages for a Versatile Raw Material*, RSC Publishing, pp. 18-29.

Pimentel, D., Patzek, T.W. 2005 *Natural Resources Research*, **14** No. 1, pp. 65-76.

Ruebsamen WC, Shon FJ, Chrisney JB. Chemical Reaction between Water and Rapidly Heated Metals. Report NAA-SR-197. Los Angeles, CA: North American Aviation; October 1952.

Rohsenow, W.M., Hartnett, J.P., Cho, Y.I. 1998 *Handbook of Heat Transfer*, 3rd Edition, McGraw-Hill, pp 14.13-14.14.

Satterfield, C.N., Audibert, F.P. 1963 *Industrial and Engineering Chemistry Fundamentals*, **2** No. 3, (3)200-(3)202.

Shabaker, J.W., Davda R.R., Huber, G.W., Cortright, R.D., Dumesic, J.A. 2003 *Journal of Catalysis,* **215**, pp. 344-352.

Shabaker, J.W., Huber, G.W., Davda, R.R., Cortright, R.D., Dumesic, J.A. 2003 *Catalysis Letters,* **88**, pp 1-8.

Special Metals Corp. 2008 *Inconel Alloy 600.* Publication Number SMC-027. (http://www.specialmetals.com/documents/Inconel%20alloy%20600%20(Sept%202008).pdf)

Turns, S.R. 2000 *An Introduction to Combustion,* 2nd Edition. McGraw Hill, p. 116.

Urban, B.J., Avedisian, C.T., Tsang, W. 2006 *AIChE Journal*, **52** No. 7, (7)2582-(7)2595.

U.S. Department of Energy (DOE). 2002 Pinion Pine IGCC Power Project a DOE Assessment. DOE/NETL-2003/1183. (www.netl.doe.gov)

University of California-Davis. 2004 Evaluation of Conversion Technology Processes and Products. (http://biomass.ucdavis.edu/materials/reports%20and%20publications/2004/2004_UC_CIWMB_ConversionTechnology_DraftFinal.pdf)

Van Stralen, S.J.D., Joosen C.J.J., Sluyter, W.M. 1972 *Int. J. Heat Mass Transfer,* **15**, pp. 2427-2445.

Yaws, C. L. 2003 *Yaws' Handbook of Thermodynamic and Physical Properties of Chemical Compounds*, online database available at: http://knovel.com.

Yue, P.L., Weber, M.E. 1973 *Int. J. Heat Mass Transfer,* **16**, pp. 1877-1888.

Zhukov, S.A., Rafeev, V.A., Afanas'ev, S.Y., Echmaev, S.B., Korsunskii, B.L. 2003 *Heat and Mass Transfer and Physical Gas Dynamics,* **41** No. 2, (2)243-(2)251.